

# Synthesis and Reactivity of Group 12 $\beta$ -Diketiminato Coordination Complexes

By

Dylan Webb

A thesis

Submitted to Victoria University of Wellington

in fulfilment of the requirements for the degree of

Masters of Science

In Chemistry



Victoria University of Wellington

2016

## Abstract

The variable  $\beta$ -diketiminato ligand poses as a suitable chemical environment to explore unknown reactivity and functionality of metal centres. Variants on the  $\beta$ -diketiminato ligand can provide appropriate steric and electronic stabilization to synthesize a range of  $\beta$ -diketiminato group 12 metal complexes. This project aimed to explore various  $\beta$ -diketiminato ligands as appropriate ancillary ligands to derivatise group 12 element complexes and investigate their reactivity.

A  $\beta$ -diketiminato-mercury(II) chloride,  $[o\text{-C}_6\text{H}_4\{\text{C}(\text{CH}_3)=\text{N-2,6-}^i\text{Pr}_2\text{C}_6\text{H}_3\}\{\text{NH}(2,6\text{-}^i\text{Pr}_2\text{C}_6\text{H}_3)\}]\text{HgCl}$ , was synthesized by addition of  $[o\text{-C}_6\text{H}_4\{\text{C}(\text{CH}_3)=\text{N-2,6-}^i\text{Pr}_2\text{C}_6\text{H}_3\}\{\text{NH}(2,6\text{-}^i\text{Pr}_2\text{C}_6\text{H}_3)\}]\text{Li}$  to mercury dichloride. Attempts to derivatise the  $\beta$ -diketiminato-mercury(II) chloride using salt metathesis reactions were unsuccessful with only  $\beta$ -diketiminato ligand degradation products being observed in the  $^1\text{H}$  NMR.

A  $\beta$ -diketiminato-cadmium chloride,  $[\text{CH}\{(\text{CH}_3)\text{CN-2,6-}^i\text{Pr}_2\text{C}_6\text{H}_3\}_2]\text{CdCl}$ , was derivatized to a  $\beta$ -diketiminato-cadmium phosphanide,  $[\text{CH}\{(\text{CH}_3)\text{CN-2,6-}^i\text{Pr}_2\text{C}_6\text{H}_3\}_2]\text{Cd P}(\text{C}_6\text{H}_{11})_2$ , via a lithium dicyclohexyl phosphanide and a novel  $\beta$ -diketiminato-cadmium hydride,  $[\text{CH}\{(\text{CH}_3)\text{CN-2,6-}^i\text{Pr}_2\text{C}_6\text{H}_3\}_2]\text{CdH}$ , via Super Hydride. Initial reactivity studies of the novel cadmium hydride with various carbodiimides yielded a  $\beta$ -diketiminato-homonuclear cadmium-cadmium dimer,  $[\text{CH}\{(\text{CH}_3)\text{CN-2,6-}^i\text{Pr}_2\text{C}_6\text{H}_3\}_2\text{Cd}]_2$ , which formed via catalytic reduction of the cadmium hydride. Attempts to synthesize an amidinate insertion product via a salt metathesis reaction or a ligand exchange reaction proved unsuccessful but a novel cadmium amidinate,  $[\{\text{CH}(\text{N-C}_6\text{H}_{11})_2\}_2\{\text{CH}(\text{N-C}_6\text{H}_{11})(\text{N}(\text{H})\text{-C}_6\text{H}_{11})\}]\text{Cd}$ , was synthesized from addition of dicyclohexyl formamidine to bis-hexamethyldisilazane cadmium.

A  $\beta$ -diketiminato-zinc(II) bromide,  $[o\text{-C}_6\text{H}_4\{\text{C}(\text{CH}_3)=\text{N-2,6-}^i\text{Pr}_2\text{C}_6\text{H}_3\}\{\text{NH}(2,6\text{-}^i\text{Pr}_2\text{C}_6\text{H}_3)\}]\text{ZnBr}$ , was synthesized by addition of  $[o\text{-C}_6\text{H}_4\{\text{C}(\text{CH}_3)=\text{N-2,6-}^i\text{Pr}_2\text{C}_6\text{H}_3\}\{\text{NH}(2,6\text{-}^i\text{Pr}_2\text{C}_6\text{H}_3)\}]\text{Li}$  to zinc dibromide. The  $\beta$ -diketiminato-zinc(II) bromide was derivatized to a variety of complexes (including amides and phosphanides) by a salt metathesis reaction. Chalcogen addition reactions were performed from  $[o\text{-C}_6\text{H}_4\{\text{C}(\text{CH}_3)=\text{N-2,6-}^i\text{Pr}_2\text{C}_6\text{H}_3\}\{\text{NH}(2,6\text{-}^i\text{Pr}_2\text{C}_6\text{H}_3)\}]\text{ZnP}(\text{C}_6\text{H}_{11})_2$  to produce double addition products from sulfur, selenium and

tellurium. Chalcogen addition reactions from  $[o\text{-C}_6\text{H}_4\{\text{C}(\text{CH}_3)=\text{N}-2,6\text{-}^i\text{Pr}_2\text{C}_6\text{H}_3\}\{\text{NH}(2,6\text{-}^i\text{Pr}_2\text{C}_6\text{H}_3)\}\text{ZnP}(\text{C}_6\text{H}_5)_2]$  produced a double addition product for selenium and a  $\beta$ -diketiminato-zinc(II) tellunoite bridged dimer,  $[o\text{-C}_6\text{H}_4\{\text{C}(\text{CH}_3)=\text{N}-2,6\text{-}^i\text{Pr}_2\text{C}_6\text{H}_3\}\{\text{NH}(2,6\text{-}^i\text{Pr}_2\text{C}_6\text{H}_3)\}\text{Zn}]\text{Te}$ , from tellurium. A total of 14 compounds were characterized via X-ray diffraction. Photoluminescence studies of the  $\beta$ -diketiminato-zinc(II) compounds were conducted where it was proposed that an electron transfer from the lone pair on the hetero-atom influenced the quantum yield and fluorescence intensities.

## Acknowledgements

Firstly, I would like to express my gratitude to my supervisor Dr. Robin Fulton for her continuous support of my research, her patience and consistent motivation. She constantly allowed this thesis to be my own work, but always steered me in the right the direction.

I would like to acknowledge the other academics who contributed to my research: Assoc Prof. Martyn Coles for his aid in crystallography and “unnecessary” input and technicians Jackie King and Ian Vorster for their patience with me and their machines.

I thank my fellow co-workers Struan, Putri, Loc, Grace, Peter, Cara and Ryan for the “stimulating” discussions, all the fun we have had in the last two years and for being my surrogate siblings, for better and for worse. A special thanks to Bradley White for his work during his undergraduate studies towards some of this research.

Over the past two years I have received funding from the Curtis-Gordon Research Scholarship in Chemistry for which I could not thank enough.

Last but not least, I must thank my parents for their constant support and words of encouragement, my loving girlfriend Danielle and the friends I have had the pleasure spending time with; in particular my flatmate Daniel, the other Masters students Jaime, Sarah and Matt and close friends Emma and Christoph.

## Table of Contents

Abstract.....	ii
Acknowledgements.....	iv
Glossary of Terms and Abbreviations.....	vii
Nomenclature .....	ix
List of Figures .....	xi
List of Schemes.....	xiii
List of Tables .....	xiv
Structural List of Newly Synthesized Compounds .....	xv
1 Background and Literature .....	1
1.1 Introduction.....	1
1.1.1 Group 12 Elements .....	1
1.1.2 The $\beta$ -Diketiminato Ligand .....	2
1.2 Project Aims .....	4
1.3 Important Chemical Reactions.....	4
1.4 Mercury Compounds.....	8
1.4.1 Background .....	8
1.4.2 Coordination Chemistry.....	9
1.5 Cadmium Compounds.....	14
1.5.1 Background .....	14
1.5.2 Coordination Chemistry.....	15
1.6 Zinc Compounds.....	20
1.6.1 Background .....	20
1.6.2 Coordination Chemistry.....	21
1.6.1 Research from 2014.....	25
1.7 Pre-Thesis Research Motive .....	37
1.7.1 Synthesis of [Ar-BDI <sub>Dipp</sub> -H] .....	37
2 Results and Discussion.....	38
2.1 Mercury.....	38
2.1.1 Synthesis of $\beta$ -Diketiminato-mercury Chloride .....	38
2.2 Cadmium .....	41
2.2.1 Alternative Synthesis of $\beta$ -Diketiminato-cadmium Chloride.....	41
2.2.2 Derivatization of $\beta$ -Diketiminato-cadmium Chloride .....	41

2.2.3	Reactivity of $\beta$ -Diketiminato-cadmium Hydride .....	45
2.3	Zinc .....	52
2.3.1	Synthesis of a Novel $\beta$ -Diketiminato-zinc Bromide .....	52
2.3.2	Derivatization of a Novel $\beta$ -Diketiminato-zinc Bromide.....	55
2.3.3	Photoluminescence of $\beta$ -Diketiminato-zinc Complexes.....	73
2.4	Summary of Results.....	78
3	Experimental.....	80
4	Appendices .....	96
4.1	Appendix A: NMR Spectra of Novel Compounds.....	96
4.2	Appendix B: Crystal Data Tables .....	115
4.3	Appendix C: Bibliography .....	129

## Glossary of Terms and Abbreviations

$\delta$	Chemical shift (ppm)
$\lambda$	Wavelength
$\lambda_{\text{Max}}$	Wavelength of maximum absorption
<b>NMR</b>	Nuclear magnetic resonance
$^1\text{H}$ NMR	Hydrogen nuclear magnetic resonance
$^{13}\text{C}$ NMR	Carbon nuclear magnetic resonance
$^{31}\text{P}$ NMR	Phosphorus nuclear magnetic resonance
$\text{\AA}$	Angstrom
<b>Ar (images)</b>	Commonly used aryl group 2,6-diisopropylphenyl (Dipp)
<b>Ar (characterization)</b>	Aryl or aromatic region
<b>Am</b>	Amidinate
<b>Approx.</b>	Approximately
<b>BDI</b>	$\beta$ -diketiminatate
<b>BDI<sub>Dipp</sub></b>	$\beta$ -diketiminatate ligand, $[\text{CH}\{(\text{CH}_3)\text{CN}-2,6\text{-}^i\text{Pr}_2\text{C}_6\text{H}_3\}_2]^-$
<b>Ar-BDI<sub>Dipp</sub></b>	Aryl incorporated $\beta$ -diketiminatate ligand, $[\text{o-C}_6\text{H}_4\{\text{C}(\text{CH}_3)=\text{N}-2,6\text{-}^i\text{Pr}_2\text{C}_6\text{H}_3\}\{\text{NH}(2,6\text{-}^i\text{Pr}_2\text{C}_6\text{H}_3)\}]^-$
<b>br</b>	Broad signal
<b>C<sub>6</sub>D<sub>6</sub></b>	Deuterated benzene
<b>Cy</b>	Cyclohexyl
<b>d</b>	Doublet
<b>dd</b>	Doublet of doublets
<b>ddd</b>	Doublet of doublet of doublets
<b>DCM</b>	Dichloromethane
<b>Dipp</b>	2,6-diisopropylphenyl
<b>E</b>	Chalcogen (sulfur, selenium or tellurium)
<b>eq</b>	Equation
<b>Eq.</b>	Equivalence
<b>Et</b>	Ethyl
<b>Et<sub>2</sub>O</b>	Diethyl ether
<b>Formamidine</b>	Fo
<b><sup>i</sup>Pr</b>	<i>iso</i> -propyl substituent
<b><i>i</i></b>	Ipso- position

<b>IR</b>	Infrared spectroscopy
<b>HMDS</b>	Hexamethyldisilazane
<b>Hex</b>	Hexane
<b>J</b>	Scalar coupling constant (Hz)
<b>LDA</b>	Lithium diisopropyl amide
<b>L<sub>n</sub></b>	An unspecified number of an unspecified ligand
<b>m</b>	Multiplet
<b><i>m</i></b>	Meta- position
<b>Me</b>	Methyl
<b>mes</b>	Mesitylene group
<b><sup>n</sup>Bu</b>	<i>n</i> -butyl substituent
<b><i>o</i></b>	Ortho- position
<b><i>p</i></b>	Para- position
<b>Ph</b>	Phenyl
<b>ppm</b>	Parts per million
<b>pz</b>	Pyrazole ring
<b>R</b>	An unspecified substituent
<b>s</b>	Singlet
<b>t</b>	Triplet
<b>td</b>	Triplet of doublets
<b>terp</b>	Terphenyl ligand
<b>tol</b>	Toluene
<b>THF</b>	Tetrahydrofuran
<b>TMS</b>	Trimethylsilyl
<b>TP</b>	Trispyrazol borate ligand
<b>UV/vis</b>	Ultraviolet-visible spectroscopy
<b><i>ν</i></b>	Wavenumbers (cm <sup>-1</sup> )



## Nomenclature

In this thesis, most of the compounds are supported by a bulky  $\beta$ -diketiminato ligand. Various  $\beta$ -diketiminato-group 12 metal complexes containing various substituents were synthesized. There are several ways of naming these compounds; the nomenclature generally used in this thesis is set out as below. Often the metal is omitted from the abbreviated name when clarification is not necessary.

**Table i: Nomenclature of the compounds synthesized in this thesis, where L = BDI<sub>Dipp</sub> or Ar-BDI<sub>Dipp</sub>, Metal = M = Zn, Cd or Hg.**

Structure	Nomenclature	Abbreviated name
[LMCl]	$\beta$ -diketiminato-metal(II) chloride	Metal chloride
[LMBr]	$\beta$ -diketiminato-metal(II) bromide	Metal bromide
[LMI]	$\beta$ -diketiminato-metal(II) iodide	Metal iodide
[LMBr <sub>2</sub> Li(S) <sub>n</sub> ]	$\beta$ -diketiminato-metal(II) dibromide lithium salt	Metal dibromide lithium salt
[LMHMDS]	$\beta$ -diketiminato-metal(II) hexamethyldisilazane	Metal HMDS
[LMN(H)Dipp]	$\beta$ -diketiminato-metal(II) 2,6-diisopropylphenyl amide	Metal anilido
[LMH]	$\beta$ -diketiminato-metal(II) hydride	Metal hydride
[LM] <sub>2</sub>	$\beta$ -diketiminato-homonuclear metal-metal dimer	Homonuclear M-M dimer
[LMPCy <sub>2</sub> ]	$\beta$ -diketiminato-metal(II) dicyclohexylphosphanide	Metal dicyclohexylphosphanide
[LMPPPh <sub>2</sub> ]	$\beta$ -diketiminato-metal(II) diphenylphosphanide	Metal diphenylphosphanide
[LM(S) <sub>2</sub> PCy <sub>2</sub> ]	$\beta$ -diketiminato-metal(II) dicyclohexylphosphinodithioate	Metal dicyclohexylphosphinodithioate
[LM(Se) <sub>2</sub> PCy <sub>2</sub> ]	$\beta$ -diketiminato-metal(II) dicyclohexylphosphinodiselenoate	Metal dicyclohexylphosphinodiselenoate
[LM(Se)PCy <sub>2</sub> ]	$\beta$ -diketiminato-metal(II) dicyclohexylphosphinoselenoite	Metal dicyclohexylphosphinoselenoite

Structure	Nomenclature	Abbreviated name
[LM(Te) <sub>2</sub> PCy <sub>2</sub> ]	β-diketiminato-metal(II) dicyclohexylphosphinoditellunoate	Metal dicyclohexylphosphinoditellunoate
[LM(Te)PCy <sub>2</sub> ]	β-diketiminato-metal(II) dicyclohexylphosphinotellunoite	Metal dicyclohexylphosphinotellunoite
[LM(Se) <sub>2</sub> PPh <sub>2</sub> ]	β-diketiminato-metal(II) diphenylphosphinodiselenoate	Metal diphenylphosphinodiselenoate
[LM(Se)PPh <sub>2</sub> ]	β-diketiminato-metal(II) diphenylphosphinoselenoite	Metal diphenylphosphinoselenoite
[LM(Te) <sub>2</sub> PPh <sub>2</sub> ]	β-diketiminato-metal(II) diphenylphosphinoditellunoate	Metal diphenylphosphinoditellunoate
[LM(Te)PPh <sub>2</sub> ]	β-diketiminato-metal(II) diphenylphosphinotellunoite	Metal diphenylphosphinotellunoite
[LM] <sub>2</sub> Te	β-diketiminato-metal(II) tellunoite bridged dimer	Metal tellunoite bridged dimer
Cy-N $\begin{array}{c} \diagup \\ \text{H} \end{array}$ -N-Cy	dicyclohexyl formamidine	DC-Fo
<sup>i</sup> Pr-N $\begin{array}{c} \diagup \\ \text{H} \end{array}$ -N- <sup>i</sup> Pr	diisopropyl formamidine	DI-Fo
Cy-N $\begin{array}{c} \diagup \\ \text{M} \end{array}$ -N-Cy	dicyclohexyl amidinate metal(II)	DC-Am metal (M = Li or Cd)
<sup>i</sup> Pr-N $\begin{array}{c} \diagup \\ \text{M} \end{array}$ -N- <sup>i</sup> Pr	diisopropyl amidinate metal(II)	DI-Am metal (M = Li or Cd)
Cy-N=C=N-Cy	dicyclohexylcarbodiimide	DCC
<sup>i</sup> Pr-N=C=N- <sup>i</sup> Pr	diisopropylcarbodiimide	DIC

## List of Figures

- Figure 1: BDI Substitution sites. Left, bare ligand with delocalized electron. Right, metallocycle formed with metal centre with  $\alpha$ ,  $\beta$  and  $\gamma$  positions. 2
- Figure 2: Left, planar conformation of BDI. Right, puckered boat conformation of BDI. Substitution sites have been removed for clarity. 3
- Figure 3:  $\beta$ -Diketiminato ligands used in this project. 4
- Figure 4: A typical salt metathesis reaction followed by an example. 5
- Figure 5: Common insertion geometries, 1,2 (top) and 1,1 (below). 5
- Figure 6: From left to right: Classical (A), non-classical (B), asymmetric bridging (C), symmetric bridging (D) and interstitial (E,F). Other substituents are omitted for clarity. 6
- Figure 7: Examples of compounds involving a Zn-P interaction. Top left, phosphorus integrated into the ligand with dative bonding.<sup>92</sup> Top right, dimeric compound with dative bonding.<sup>89</sup> Bottom left, anionic phosphorus ligand.<sup>98</sup> Bottom middle, multiple phosphorus binding including a phosphanide.<sup>94</sup> Bottom right, a niche phosphano example.<sup>97</sup> 22
- Figure 8: Examples of zinc chalcogenides. Left, an oligomeric example.<sup>108</sup> Middle and right, terminal examples.<sup>114, 116</sup> 23
- Figure 9: ORTEP diagram of XXX showing thermal ellipsoids at 30% probability. Only bonds for P2 are shown. One set of cyclohexyl peaks are shown (a). 27
- Figure 10: ORTEP diagram of XXXII showing thermal ellipsoids at 30% probability. 29
- Figure 11: ORTEP diagram of XXXIII showing thermal ellipsoids at 30% probability. 32
- Figure 12: ORTEP diagram of XXXIV showing thermal ellipsoids at 30% probability. 34
- Figure 13: ORTEP diagram of 1 showing thermal ellipsoids at 30% probability. Hydrogens omitted for clarity. 39
- Figure 14: ORTEP diagram of 3 showing thermal ellipsoids at 30% probability. Selected hydrogens omitted for clarity. 43
- Figure 15: ORTEP diagram of 5 showing thermal ellipsoids at 30% probability. Isopropyl groups and hydrogens omitted for clarity. 46
- Figure 16: Possible salt metathesis product showing Cd<sup>111</sup> and Cd<sup>113</sup> satellites. 50

Figure 17: ORTEP diagram of 10 bridged dimer showing thermal ellipsoids at 30% probability. Isopropyl groups and hydrogens omitted for clarity.	53
Figure 18: ORTEP diagram of one molecule of 11 showing thermal ellipsoids at 30% probability. Hydrogens omitted for clarity.	56
Figure 19: ORTEP diagram of 13 showing thermal ellipsoids at 30% probability. Hydrogens omitted for clarity.	59
Figure 20: ORTEP diagram of 14 showing thermal ellipsoids at 30% probability. Hydrogens omitted for clarity.	61
Figure 21: From left to right. 16 with $^{77}\text{Se}$ satellites, the dicyclohexylphosphinoselenoite product with smaller $^{77}\text{Se}$ satellites, unreacted lithium dicyclohexylphosphanide and unreacted 13.	64
Figure 22: ORTEP diagram of 16 showing thermal ellipsoids at 30% probability. Hydrogens and solvent molecule omitted for clarity.	65
Figure 23: ORTEP diagram of 17 showing thermal ellipsoids at 30% probability. Hydrogens and solvent molecule omitted for clarity.	67
Figure 24: ORTEP diagram of 19 showing thermal ellipsoids at 30% probability. Isopropyl groups, the solvent molecule and hydrogens omitted for clarity.	70
Figure 25: Examples of crystals collected under a microscope. Left, Cubic crystals of dicyclohexylphosphanide 13. Right, Plate-like crystals of tellunoite bridged dimer 19.	72
Figure 26: UV/vis absorption spectra of complexes 10-18 between 220 and 520 nm.	75
Figure 27: Fluorescence excitation and emission spectra of compounds 10-18.	75
Figure 28: Summary showing absorption $\lambda_{\text{max}}$ , extinction coefficient ( $\epsilon$ ) of $\lambda_{\text{max}}$ peaks, excitation and emission wavelengths and quantum yield of compounds 10-18.	75
Figure 29: Left, samples in ambient light. Right samples under a broad range of UV light. Samples from left to right: Addition of tellurium, selenium and sulfur into the Zn-P bond of complex 13.	77

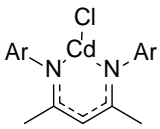
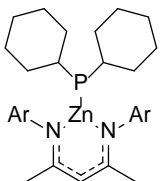
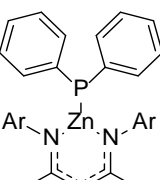
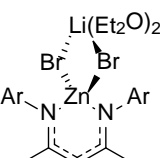
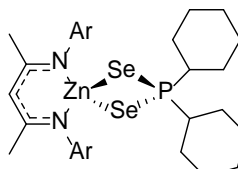
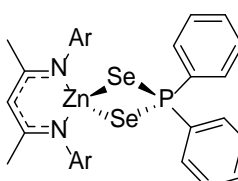
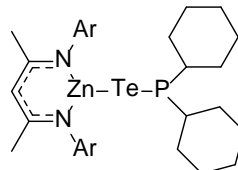
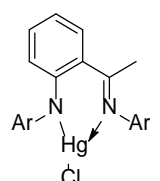
## List of Schemes

Scheme 1: Reaction and equilibrium of II.	10
Scheme 2: Reported thermolysis and trapping of an organo-mercury radical from VI.	12
Scheme 3: Synthesis of IX.	13
Scheme 4: Synthesis of X, XI and XII.	15
Scheme 5: Synthesis of XVI via XV.	16
Scheme 6: Synthesis of XVII and XVIII.	17
Scheme 7: Synthesis of XIX and XX.	18
Scheme 8: Synthesis of XXIII.	19
Scheme 9: Synthesis of XXIV. Synthesis and reactivity of XXV with O <sub>2</sub> .	24
Scheme 10: Synthesis of XXVI, XXVII and XXVII.	24
Scheme 11: Synthesis of [Ar-BDl <sub>Dipp</sub> -H].	37
Scheme 12: Synthesis of [Ar-BDl <sub>Dipp</sub> -Li] followed by the synthesis of 1.	38
Scheme 13: Alternative synthesis of XVI.	41
Scheme 14: Proposed catalytic production of homonuclear Cd-Cd dimer 5 through amidinate 4 from hydride 3.	48
Scheme 15: Methods A and B to generate complexes 6 and 7.	48
Scheme 16: Proposed routes to complex 4.	49
Scheme 17: Syntheses of zinc amides 11 and 12 from 10.	55
Scheme 18: Synthesis of complexes 15, 16 and 17 from phosphanide 13.	62
Scheme 19: Selenium insertion reaction with 13 to generate 16.	64
Scheme 20: Synthesis of 18 and 19 from 14.	69

## List of Tables

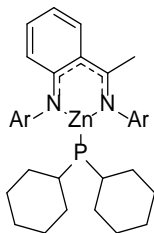
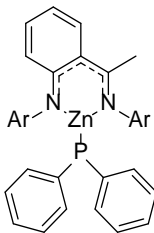
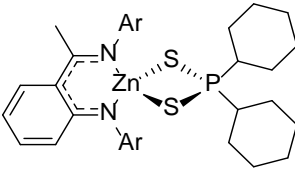
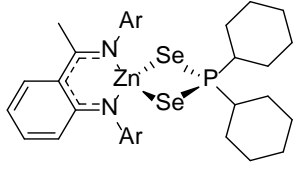
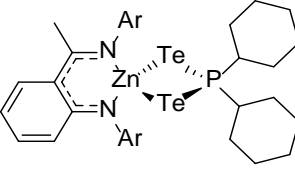
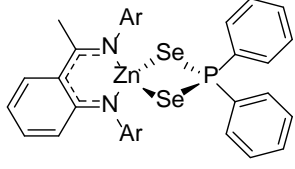
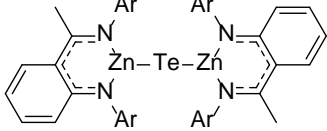
Table 1: Selected bond lengths (Å) and angles (°) for XXX.	28
Table 2: Selected bond lengths (Å) and angles (°) for XXXII.	30
Table 3: Selected bond lengths (Å) and angles (°) for XXXIII.	33
Table 4: Selected bond lengths (Å) and angles (°) for XXXIV.	35
Table 5: Selected bond lengths (Å) and angles (°) for 1.	40
Table 6: Selected bond lengths (Å) and angles (°) for 3.	44
Table 7: Selected bond lengths (Å) and angles (°) for 5.	47
Table 8: Selected bond lengths (Å) and angles (°) for 10.	55
Table 9: Selected bond lengths (Å) and angles (°) for 11.	57
Table 10: Selected bond lengths (Å) and angles (°) for 13.	60
Table 11: Selected bond lengths (Å) and angles (°) for 14.	62
Table 12: Selected bond lengths (Å) and angles (°) for 16.	66
Table 13: Selected bond lengths (Å) and angles (°) for 17.	68
Table 14: Selected bond lengths (Å) and angles (°) for 19.	72

## Structural List of Newly Synthesized Compounds

Abbreviated name	Complex	Structure
Cadmium chloride	XVI	
Zinc dicyclohexylphosphanide	XXX	
Zinc diphenylphosphanide	XXXI	
Zinc dibromide lithium salt	XXXII	
Zinc dicyclohexylphosphinodiselenoate	XXXIII	
Zinc diphenylphosphinodiselenoate	XXXIV	
Zinc dicyclohexylphosphinotellunoite	XXXV	
Mercury chloride	1	

Abbreviated name	Complex	Structure
Cadmium dicyclohexylphosphanide	2	
Cadmium hydride	3	
Homonuclear cadmium-cadmium dimer	5	
Bis-DC-Am,Fo-Am cadmium	8	
Zinc dibromide lithium salt	9	
Zinc bromide	10	
Zinc HMDS	11	
Zinc anilido	12	



Abbreviated name	Complex	Structure
Zinc dicyclohexylphosphanide	13	
Zinc diphenylphosphanide	14	
Zinc dicyclohexylphosphinodithioate	15	
Zinc dicyclohexylphosphinodiselenoate	16	
Zinc dicyclohexylphosphinitellunoate	17	
Zinc diphenylphosphinodiselenoate	18	
Zinc tellunoite bridged dimer	19	

# Chapter 1

---

## Background and Literature

### 1.1 Introduction

#### 1.1.1 Group 12 Elements

Group 12 elements include the three naturally occurring elements zinc (Zn), cadmium (Cd) and mercury (Hg) and the recently synthesized element copernicium (Cn).<sup>1</sup> Despite sharing qualities based on their appearance in the periodic table, each of the three natural group 12 elements differ to each other in chemical reactivity and coordination chemistry.

The natural abundance of zinc is 65 ppm, the low abundance of cadmium and mercury, 0.1 ppm 0.08 ppm respectively, limits their use in higher biological organisms.<sup>2</sup> Zinc is the only group 12 element that is an essential trace element and after iron is the second most abundant transition metal in the human body. Zinc has been shown to be present in approximately 10% of human proteins and is heavily regulated within the body.<sup>3</sup> This makes zinc the only biologically relevant group 12 element.

The low melting and boiling points of the group 12 elements indicates a weak metallic bond with little valence band and conduction band overlap. This pushes their metallic properties close to the boundary of a metalloid element like the main-group elements gallium (Ga) and germanium (Ge).<sup>4</sup> The predominant oxidation state for group 12 elements in complexes is +2, giving them a  $d^{10}$  electronic configuration with other oxidation states being rare. Coordination to substituents only occurs through the s-orbitals, the d-orbitals remain core-like. In these ways the group 12 elements share similarities with main-group elements.

IUPAC (The International Union of Pure and Applied Chemistry) defines a transition metal element “... as an element whose atom has an incomplete d sub-shell” of which mercury is the only culprit with an oxidation state higher than +2 in the rare non-equilibrium conditions

creating mercury (IV) fluoride.<sup>5</sup> Group 12 elements zinc and cadmium share qualities to group 2 elements beryllium (Be) and magnesium (Mg) in atomic radii, ionic radii, electronegativities, binary compound structure and their ability to form complex ions with natural nitrogen and oxygen ligands.<sup>6</sup> The similarity with group 2 elements goes as far as the old IUPAC system naming them as 2-B.<sup>7</sup> The group 12 elements have been given the name *outer transition metals* in earlier scientific texts due to their differences to transition metals but similarities to group 2 elements.<sup>8</sup>

The ambiguity of the classification and inconsistent qualities for all three naturally occurring group 12 elements calls for an in depth investigation into their synthetic and coordination chemistry. Zinc has been heavily investigated due to its non-toxic qualities and biological relevance. In contrast cadmium and mercury have received less attention. There is therefore a gap in the understanding of zinc, cadmium and mercury's coordination chemistry.

### 1.1.2 The $\beta$ -Diketimate Ligand

The  $\beta$ -diketimate ligand, abbreviated as either NacNac or more commonly BDI, can be utilized as an ancillary ligand, supplying both steric and electronic stabilization to a metal centre.  $\beta$ -Diketimate ligands have been coordinated to almost every available element with exceptions including some heavier transition and main-group metals or rare elements.<sup>9</sup>  $\beta$ -Diketimate ligands have been used to understand the behaviour of metals and metal coordination in biological environments.<sup>10-12</sup> The  $\beta$ -diketimate system represents a perfect chemical environment for an investigation into the coordination of group 12 elements to compare their complexes.

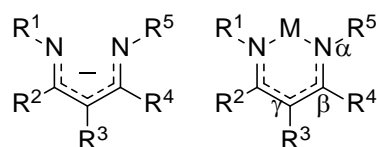


**Figure 1: BDI Substitution sites. Left, bare ligand with delocalized electron. Right, metallocycle formed with metal centre with  $\alpha$ ,  $\beta$  and  $\gamma$  positions.**

The substituents on the backbone of  $\beta$ -diketimate ligands can be varied to allow fine tuning of the ligand's electronic and steric properties (Figure 1).<sup>9</sup> At the  $\gamma$ -position, the  $R^3$

substituent is typically a hydrogen atom and is referred to as the  $\gamma$ -proton. The  $\pi$ -electrons are delocalized across the backbone when the ligand is coordinated to a metal centre. The coordination of  $\beta$ -diketiminate ligands is commonly through the two nitrogen atoms, forming a metallocycle with the metal centre.

The coordination of BDI to a metal centre results in planar geometry of the ligand due to delocalized  $\pi$ -electrons. The BDI ligand is typically a 4-electron donor, formally through amide and imine donor nitrogens of the ligand. Amsterdam Density Functional Theory Calculations were used to explain the metal's bonding orbitals which were in plane with the  $\sigma$ -bonds that formed with the ligands nitrogen atoms.<sup>13</sup> With sufficient steric crowding of the BDI substituents, the ligand can adopt a highly puckered boat configuration which has varying amount of non-planarity (Figure 2). The highly puckered boat system allows occupied out of phase  $\pi$ -orbitals from the nitrogen atoms to bond to the metal centre making the BDI ligand a 6-electron donor in a  $2\sigma + \pi$  process.



**Figure 2: Left, planar conformation of BDI. Right, puckered boat conformation of BDI. Substitution sites have been removed for clarity.**

## 1.2 Project Aims

The aim of this project was to investigate two  $\beta$ -diketiminate ligands as appropriate ancillary ligands for each group 12 element for the synthesis of novel complexes. The two  $\beta$ -diketiminate ligands contain sufficient steric bulk to prevent oligomerisation of the resulting group 12 complexes (Figure 3).

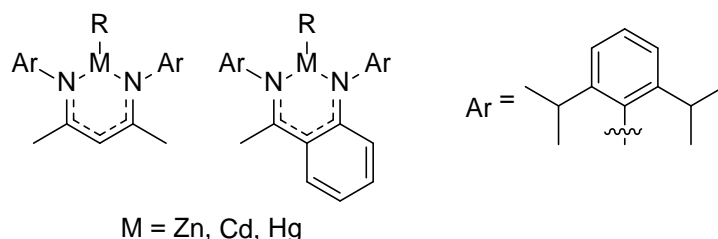


**Figure 3:  $\beta$ -Diketiminato ligands used in this project.**

To date, only a handful of cadmium and mercury complexes bearing the  $\beta$ -diketiminate ligand have been synthesised, generally from toxic reagents. As the reactivity of the resulting cadmium and mercury complexes have not been completely investigated, this provided an opportunity to explore unseen novel functionality including the synthesis of hydrides and homonuclear metal-metal (M-M) bonded dimers. Many zinc complexes bearing the  $\beta$ -diketiminate ligand have been synthesized but certain functionalities remain absent in the literature.

## 1.3 Important Chemical Reactions

Throughout this thesis specific reactions are conducted and discussed. The following are important reaction archetypes and chemical processes that involve the metal complexes and the novel functionalities in this project.

### Salt Metathesis Reaction

A salt metathesis reaction is defined as the exchange of bonds between two chemical species or reactants where one of the reactants and one of the products is a salt ( $\text{AgNO}_3$  and  $\text{AgCl}$ , Figure 4). The resulting products share similar bonding associations but contain new substituents.<sup>14</sup> Usually one of the products is a precipitate in solution, often the

salt, leaving the other product dissolved in a solvent. The two products can therefore be separated by a filtration. When a coordinating solvent is used, such as diethyl ether (Et<sub>2</sub>O) or tetrahydrofuran (THF), the salt metathesis reaction doesn't always go to completion resulting in a solvated salt coordinated to one of the reactants.

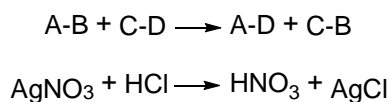


**Figure 4: A typical salt metathesis reaction followed by an example.**

### Insertion Reaction

An insertion, or addition reaction, involves the interposition of a molecule or an atom into an existing bond of another molecule (Figure 5). In inorganic chemistry, this type of reaction is used to describe a circumstance where the metal centre (M) remains mostly unchanged with no alterations to the coordination number or the oxidation state.<sup>15</sup> The ligand (R), or pre-existing substituent, can change oxidation state or coordination when a substrate (X-Y) is inserted between the M-R bond. The reaction can be reversible as is often the case when an insertion reaction is a step in a catalytic cycle. The reverse reaction is referred to as an elimination or an extrusion reaction.

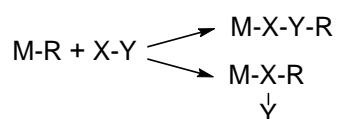


**Figure 5: Common insertion geometries, 1,2 (top) and 1,1 (below).**

### Hydride Ligand and Reactivity

A hydride is formally the anionic form of hydrogen, referred to as H<sup>-</sup>. A metal hydride complex or *hydride* may refer to a compound containing one or more of these hydride ligands. Hydride containing complexes represent catalytic intermediates in various homo- and hetero-geneous catalytic cycles. This includes hydrogenation, hydroformylation, hydrosilylation and hydrodesulfurization.<sup>16</sup>

Spectroscopic characterization of metal hydrides involves multinuclear NMR and IR spectroscopies. Structural characterization is possible with X-ray diffraction by finding residual electron densities in the difference density map and using distortions from neighbouring atoms to indirectly determine the hydrides position. Since hydride ligands lack substantial electron density, only neutron diffraction can accurately measure the metal-hydride bond distance and associated angles.

A variety of different types of coordination environments have been observed for metal hydride complexes including classical (A), non-classical (B), bridging (C,D) and interstitial (E,F) hydrides (Figure 6). Classical refers to a hydride ligand acting as an  $H^-$  ligand, non-classical refers to dihydrogen coordinating to a metal via a  $\sigma$ -bond, bridging refers to a hydride ligand shared between metal centres and an interstitial hydride refers to an internal hydride typically within a metal cluster.<sup>17-18</sup>

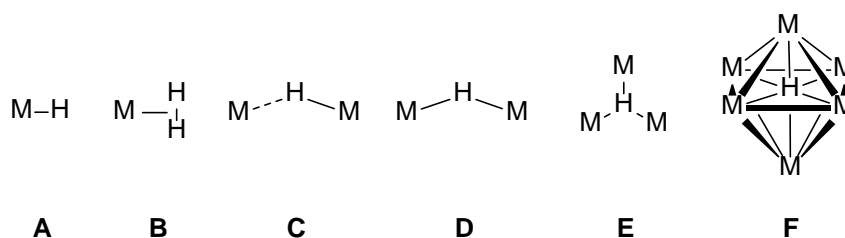
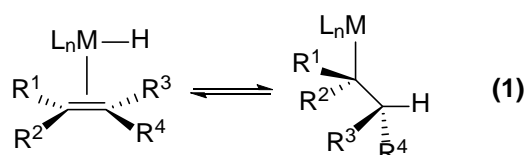


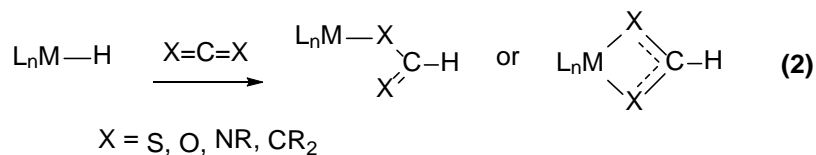
**Figure 6: From left to right: Classical (A), non-classical (B), asymmetric bridging (C), symmetric bridging (D) and interstitial (E,F). Other substituents are omitted for clarity.**

The reactivity of a classical or *terminal* metal hydride includes migratory insertion, classical insertion and protonolysis, all of which require the metal complex to lose the hydride ligand. Migratory insertion involves the reversible insertion of a hydride across an already coordinated  $\pi$ -complex, such as an alkene (eq 1).

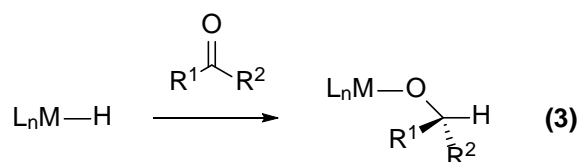


In classical insertion reactions the hydride acts as a nucleophile. An insertion reaction may involve a heteroallene containing a central carbon (eq 2). The product has the reacting

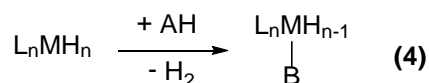
heteroallene incorporated between the metal-hydride bond (M-H). With the hydride now situated on the central carbon of the reacting heteroallene. The exact reactivity can vary depending on the heteroallene used.



Organic compounds containing carbonyl functional groups often react in a similar fashion as heteroallenes but the metal binds to the oxygen preferentially in a mono-dentate manner (eq 3).



Protonolysis of the metal hydride involves a reaction with an acid (AH). This reaction releases dihydrogen, resulting in the conjugate base (B) coordinated to the metal centre (eq 4).





## 1.4 Mercury Compounds

### 1.4.1 Background

In the elemental form, mercury has been used in various devices including thermometers, float valves and fluorescent lamps.<sup>6</sup> However, the use of elemental mercury has dropped due to the concern over its toxicity. Metallic mercury's electronic configuration strongly resists the removal of an electron and so behaves similarly to a noble gas forming weak intermolecular bonds and thus is a liquid at room temperature (RT).

Mercury(I) is a stable oxidation state and found as the diamagnetic, dimeric cation  $\text{Hg}_2^{2+}$ . Calomel or mercury(I) chloride is a common example and is used as a standard in electrochemistry. Due to mercury's tendency to bond to itself, mercury(I) will form mercury polycations consisting of linear chains capped with a positive charge.<sup>19</sup> Mercury(II) is the more common oxidation state. Naturally occurring halides, oxides and heavier chalcogens sulfur, selenium and tellurium form stable compounds with mercury(II). Hard-acid-soft-base (HSAB) theory dictates a large soft cation like mercury(II) will have high affinity for a soft anion such as the heavier chalcogens.<sup>20</sup> The mercury chalcogenides and derivatives are semiconductors and have found use as infrared detectors for numerous devices.<sup>21</sup> Mercury has a strong affinity for organic substituents, resulting in stable organo-mercury compounds. These include compounds like methylmercury, which are a dangerous family of compounds that undergo biomethylation and accumulate in waterways, interfering with vital cellular processes of higher organisms upon exposure.<sup>22</sup>

Mercury(II) almost exclusively adopts a linear geometry.<sup>23-24</sup> The valence electrons are in the 6s orbital. The poorly screened 4f orbitals increase the effective nuclear charge on the valence electrons which in turn increases the Coulombic interaction of the 6s shell to the nucleus. This interaction is absent in zinc and cadmium due to the absence of electrons in the f-orbitals. Relativistic effects and the poorly shielded 6s orbitals provides poor hybridization in the mercury coordination sphere.<sup>25</sup> This results in coordination based on the repulsion of the substituents, thus creating linear coordination.

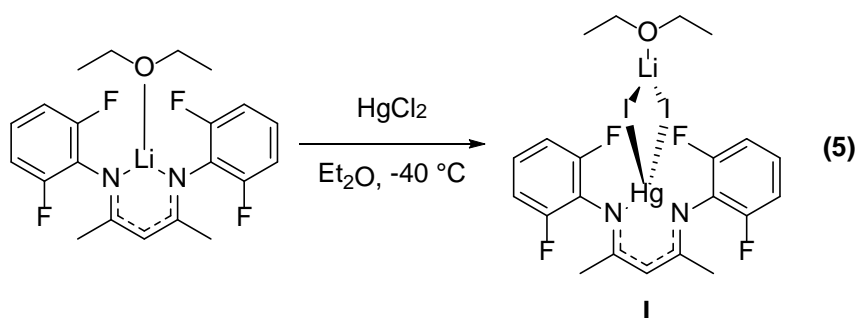
Mercury has two NMR active nuclei,  $^{199}\text{Hg}$  with a 16.87% natural abundance and  $^{201}\text{Hg}$  with a 13.18% natural abundance. The  $^{199}\text{Hg}$  nuclei are spin 1/2 and produce sharp signals and thus are used for the study of mercury compounds, their structure, dynamics and conformation.  $^{199}\text{Hg}$  coupling to other NMR active nuclei, such as  $^1\text{H}$ , can be observed in an NMR spectrum. The  $^{201}\text{Hg}$  nuclei is quadrupolar and produces broad signals so is not used for characterization and coupling to other NMR active nuclei is not observed.

## 1.4.2 Coordination Chemistry

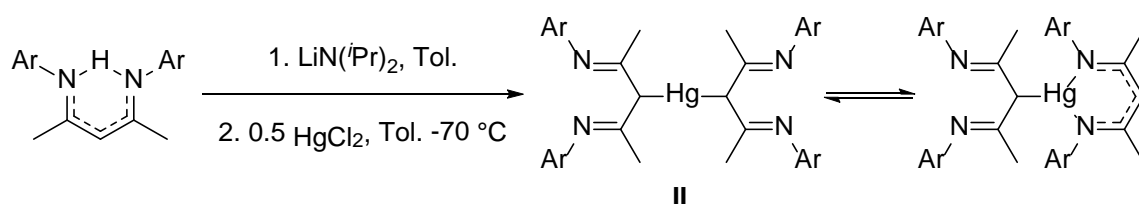
### $\beta$ -Diketiminato Mercury Complexes

There have been a limited number of investigations into the coordination chemistry of mercury due to its inherent toxicity. Use of a  $\beta$ -diketiminato ligand as an appropriate ancillary ligand for mercury has been restricted due to the traditional methods of synthesizing group 12 BDI complexes. The general synthesis involves short chained organometallics such as diethyl and dimethyl zinc and cadmium, all of which are toxic and hazardous. Translating this to mercury, organo-mercury complexes would be used where dimethyl mercury is notoriously deadly and much less reactive.<sup>26</sup>

Routes via a more viable reagent such as a metal halide salt have been successful for zinc<sup>27</sup> and have only been partially successful for cadmium and mercury. An incomplete salt metathesis complex with mercury diiodide and a fluorinated BDI derivative showed that in ethereal solvents, solvent coordination to lithium prevented complete conversion to a  $\beta$ -diketiminato-mercury iodide (**I**, eq 5).<sup>28</sup> These complexes are highly soluble, which restricts growth of crystals for structural characterization, and are also very stable, resisting further reactivity.

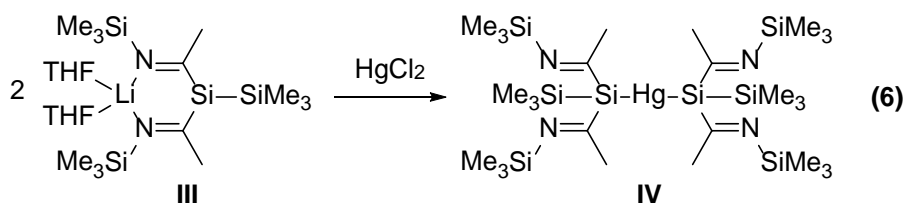


Earlier attempts at generating a  $\beta$ -diketiminato-mercury complex resulted in a homolytic bound complex (**II**).<sup>29</sup> Two BDI ligands were bound to the mercury centre through the  $\gamma$ -carbon, which was in equilibrium in solution where one of the ligands switched to the N,N'-binding mode (Scheme 1). Crystallographic data was only obtained for **II** and showed linear mercury coordination where the equilibrium companion was only observed via  $^1\text{H}$  NMR spectroscopy. This study showed that it was possible for mercury to bind in the N,N'-binding mode of BDI and crystallographic data could be obtained.



**Scheme 1: Reaction and equilibrium of II.**

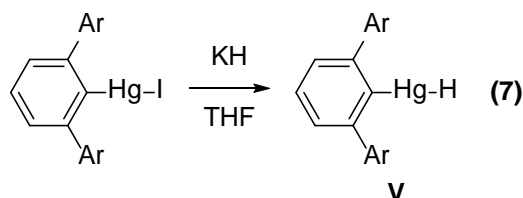
Other related syntheses involved a sila- $\beta$ -diketiminato derivative where the  $\gamma$ -carbon was replaced by a silicon atom (**III**, eq 6).<sup>30</sup> Treatment of mercury dichloride in THF with **III** resulted in a complex with the mercury metal centre bound in a homolytic complex through the silicon of each ligand (**IV**). This showed that the homolytic complex was favoured when the  $\gamma$ -position was not sterically encumbered. Considering the  $\gamma$ -position is susceptible to electrophilic attack<sup>31-32</sup> and the high affinity molecular mercury has for carbon atoms, homolytic binding was not unexpected with the silicon derivative **III**. For a  $\beta$ -diketiminato-mercury that has a terminal substituent for further reactivity, the  $\gamma$ -position of BDI must be blocked to restrict homolytic bonding.



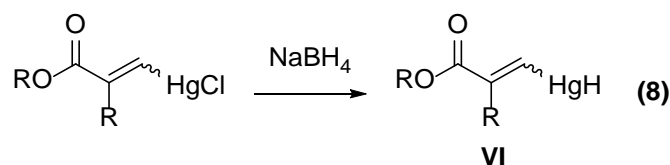
## Mercury Hydrides

Simple mercury hydrides have mostly been computationally studied<sup>33</sup> with the only mercury hydride on the Cambridge Crystallographic Data Centre (CCDC) being a cluster complex,  $(\text{CO})_{42}\text{Os}_{18}\text{HgH}$ .<sup>34</sup> This complex consisted of a mercury bridged  $\text{Os}_9$  cluster where the hydride ligand was assigned based on indirect methods to be on the mercury centre. This provided little indication on the nature of the mercury hydride or its reactivity.

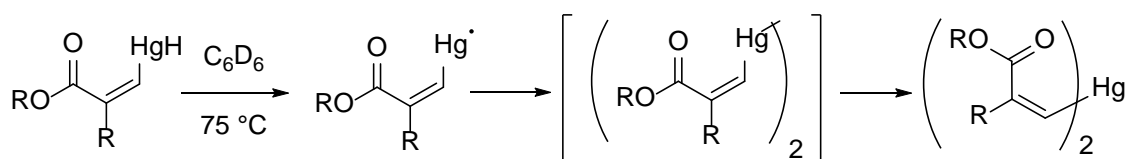
The terphenyl ligand (terp) has provided enough steric bulk and electronic stabilization to produce group 12 hydride examples.<sup>35</sup> The mercury hydride derivative (**V**, eq 7) has been synthesized via a salt metathesis reaction and characterized by  $^1\text{H}$  and  $^{199}\text{Hg}$  NMR spectroscopy, but the solid state structure was not reported. The  $^{199}\text{Hg}$  NMR spectrum showed Hg-H coupling with a coupling constant of 2,910 Hz. A resonance, corresponding to the mercury hydride was found at 14.59 ppm in the  $^1\text{H}$  NMR spectrum, but coupling to  $^{199}\text{Hg}$  was not observed. Computational analysis indicated that a bridged hydride would not be stable in contrast to the iso-structural cadmium and zinc analogues which both form bridged dimers in the solid state. Complex **V** was only studied in solution, crystallographic comparisons and investigations with other hydrides therefore have not been conducted.



Organo-mercury hydride compounds are highly unstable and often oligomerize, however this has only been detected with mass spectrometry (MS).<sup>36</sup> A stable mercury hydride complex (**VI**) was synthesized by addition of sodium borohydride to a chloride precursor (eq 8). A resonance was found at 13.14 ppm in the  $^1\text{H}$  NMR spectrum of **VI**, but coupling to  $^{199}\text{Hg}$  was not observed. The stability of **VI** was due to the electron-withdrawing effects of the acrylic acid moiety which shortened and stabilized the Hg-H bond.



Thermolysis of mercury hydride **VI** generated a divinyl-mercury complex, which was postulated to form via a relatively long lived mercury radical intermediate, observed by  $^1\text{H}$  NMR spectroscopy (Scheme 2). This species formed from the net loss of dihydrogen from **VI**.<sup>36</sup>

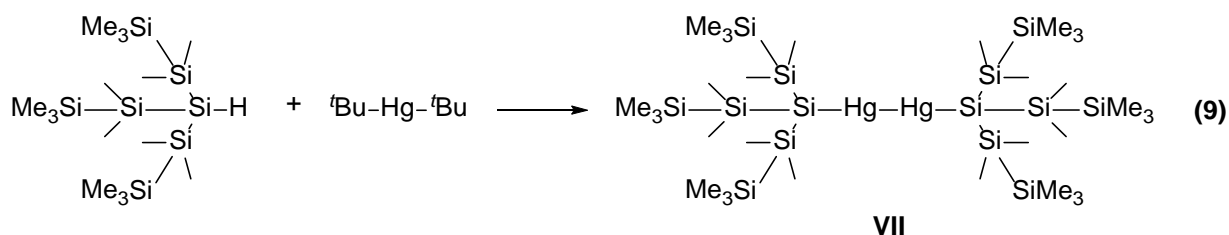


**Scheme 2: Reported thermolysis and trapping of an organo-mercury radical from VI.**

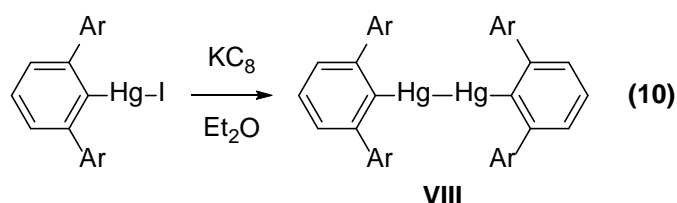
### Homonuclear Mercury-Mercury Dimers

In contrast to zinc and cadmium which adopt primarily divalent oxidation states, monovalent mercury as the  $[\text{Hg}_2]^{2+}$  cation, are reasonably common in the literature. Mercury's affinity to bond to itself provides examples of complexes with oligomeric structures which are often salt-like ionic species.<sup>37</sup>

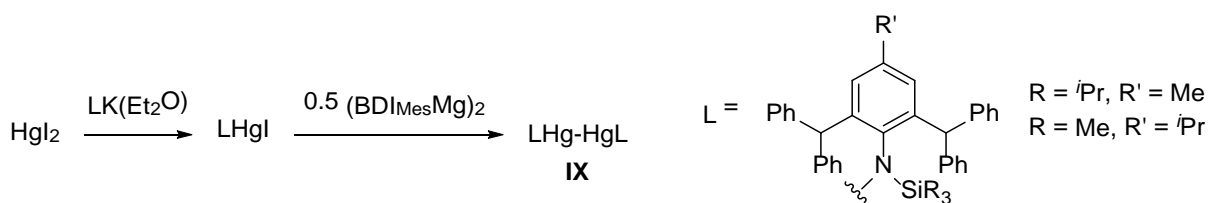
The first molecular Hg-Hg complexes with alkyl groups were short lived intermediates that were only characterized by NMR spectroscopy and MS. The first dimeric Hg-Hg complex that was structurally characterized was **VII** (eq 9) revealing a linear molecular R-Hg-Hg-R core with a Hg-Hg bond length of 2.656 Å.<sup>38</sup> This bond length was longer than the cationic  $[\text{Hg}_2]^{2+}$  and other mercury halide salts with the Hg-Hg distance ranging between 2.49-2.59 Å.



The precursor used to generate mercury hydride **V** (eq 7) yielded the homonuclear Hg-Hg dimer (**VIII**) under reducing conditions (eq 10).<sup>35</sup> The Hg-Hg bond distance in **VIII** of 2.574 Å was shorter than the sum of Pauling's single-bond metallic radii for mercury of 2.88 Å, indicating a bonding interaction was present.<sup>39</sup>



A molecular mercury-mercury complex bearing a bulky amide ligand on both metal centres was recently synthesized (**IX** in Scheme 3).<sup>40</sup> The Hg-Hg bond length in **IX** was 2.359 Å. Other structurally characterized relevant complexes bearing Hg-Hg bonds include the collinear tetranuclear R-Co-Hg-Hg-Co-R species, although the Hg-Hg bond length of 2.651 Å was elongated compared to other [Hg<sub>2</sub>]<sup>2+</sup> cations.<sup>41</sup> Mercury(I) trifluoroacetate exhibited such small crystal dimensions (0.02 x 0.02 x 0.01 nm) that it was only crystallographically characterized explored on a synchrotron. The Hg-Hg bond length in mercury(I) trifluoroacetate was 2.520 Å.<sup>42</sup>



**Scheme 3: Synthesis of IX.**

## 1.5 Cadmium Compounds

### 1.5.1 Background

Like mercury, elemental cadmium has a low melting point but similar to zinc, cadmium will almost exclusively adopt a +2 oxidation state in complexes. However, differing to zinc, cadmium is not biologically relevant but its compounds have found use as coloured pigments, corrosive resistant platings, batteries and semiconductors. Due to its toxicity, cadmium's use has decreased in battery technologies in the push for more reliable and recyclable elements, and cadmium based pigments and coatings have also been replaced by less toxic materials. Recently, cadmium has been used for semiconductor and solar cell research.<sup>43</sup> Cadmium chalcogenide nanoparticles exhibit band gaps dictated by tuneable properties like size and shape, making them desirable for devices requiring specific wavelengths and energies. This is readily observed with quantum dots like CdSe, whose fluorescence energy depends on the size of the CdSe quantum dot.<sup>44-45</sup>

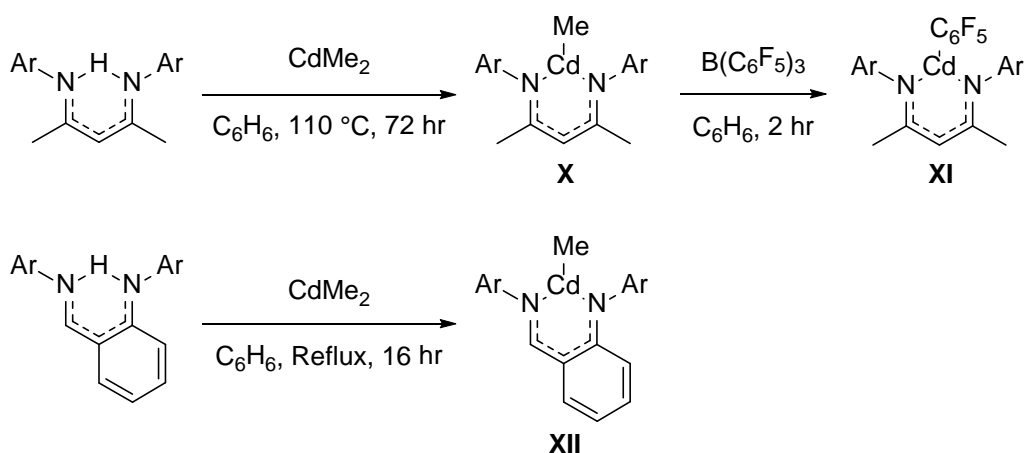
Similar to mercury, cadmium(I) can be produced as the  $[\text{Cd}_2]^{2+}$  cation as seen with  $[\text{Cd}_2\text{Cl}_6]^{4-}$ , but these compounds are highly reactive. Most other complexes involve cadmium(II), with a variety of natural oxides, halides and nitrates known. Structures with nucleobases, amino acids and vitamins have also been determined.<sup>46</sup> Cadmium complexes share similar coordination geometries with zinc complexes, adopting a tetrahedral coordination when possible. Although not shown to be biologically important, known coordination chemistry indicates a biological affinity and similarity to zinc.

Cadmium has two NMR active nuclei,  $^{111}\text{Cd}$  with a 12.80% natural abundance, and  $^{113}\text{Cd}$ , with a 12.22% natural abundance. Both  $^{111}\text{Cd}$  and  $^{113}\text{Cd}$  are spin 1/2 and can be used to study cadmium containing compounds, although  $^{113}\text{Cd}$  is slightly more sensitive and is the preferred nucleus for cadmium NMR spectroscopy.  $^{111}\text{Cd}$  and  $^{113}\text{Cd}$  coupling to other NMR active nuclei, such as  $^1\text{H}$ , can both be observed in an NMR spectrum.

## 1.5.2 Coordination Chemistry

### $\beta$ -Diketiminato Cadmium Complexes

The synthesis of  $\beta$ -diketiminato-zinc compounds use the readily available reagent diethyl zinc,<sup>10</sup> the cadmium alternative is dimethyl cadmium which is less available and significantly more toxic. Two  $\beta$ -diketiminato-cadmium methyl complexes were synthesized by treatment of a protonated  $\beta$ -diketiminato ligand with dimethyl cadmium (**X** and **XII**, Scheme 4).<sup>47</sup> Complex **X** was used to synthesize another organo-cadmium complex, **XI**, by treatment with tris-tetrafluorobenzene borane in benzene. X-ray diffraction data showed the cadmium centre was in the plane of the  $\beta$ -diketiminato ligand with an overall distorted trigonal planar geometry for all 3 complexes. When crystals of **XI** were grown in dimethyl formamide (DMF), a four coordinate geometry at the cadmium centre with a coordinated DMF was found.

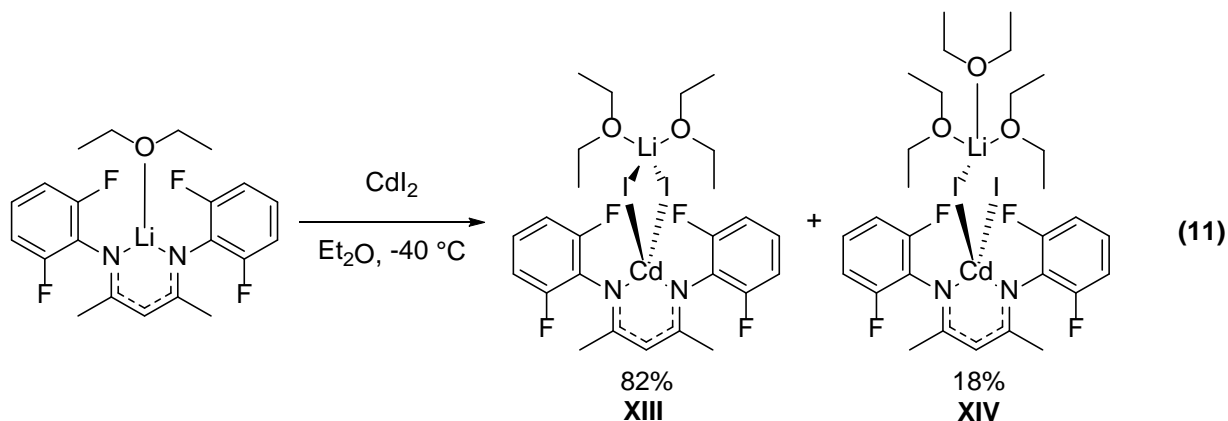


**Scheme 4: Synthesis of X, XI and XII.**

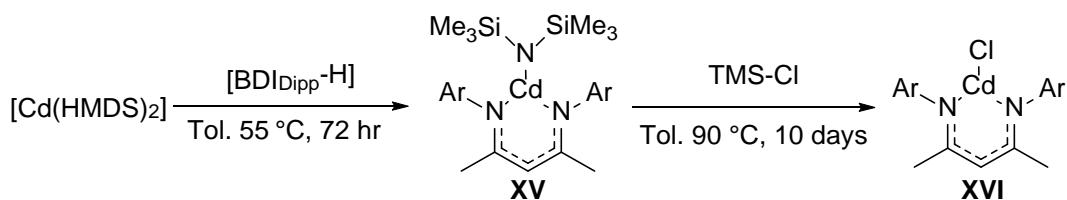
As an alternative, cadmium halide salts can also be used to synthesize  $\beta$ -diketiminato-cadmium complexes. Cadmium halide salts are only sparingly soluble in ethereal solvents such as THF and  $\text{Et}_2\text{O}$ . This results in an incomplete salt metathesis complex when a salt metathesis is attempted with a cadmium halide salt. For instance, treatment of cadmium diiodide with a lithium salt of a BDI ligand in  $\text{Et}_2\text{O}$  resulted in the formation of bimetallic complexes **XIII** and **XIV** (eq 11).<sup>28</sup> The crystal structure of **XIII** showed the cadmium centre in a distorted tetrahedral geometry lying in a 6 membered



metallocycle with the BDI ligand. A second metallocycle with the cadmium centre was with the two bridging iodide atoms and the solvated lithium atom. Attempts to remove one of the iodide substituents with either elemental sodium or potassium were unsuccessful.



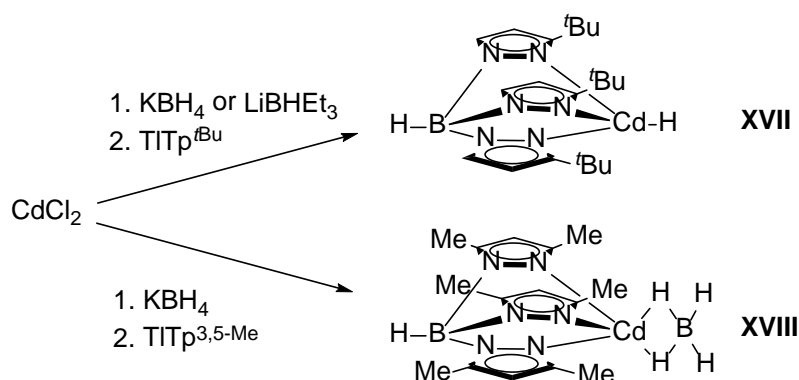
A  $\beta$ -diketiminato-cadmium complex with a terminal chloride (**XVI**) had been recently isolated (Scheme 5).<sup>48-50</sup> The problems with both the use of toxic dimethyl cadmium and the incomplete salt metathesis issue was circumvented by the use of the bis-hexamethyldisilazane cadmium precursor,  $[\text{Cd}(\text{HMDS})_2]$ . Addition of the  $\beta$ -diketiminato ligand,  $[\text{BDI}_{\text{Dipp}}\text{-H}]$ , to  $[\text{Cd}(\text{HMDS})_2]$  resulted in the formation of a  $\beta$ -diketiminato-cadmium amido complex (**XV**). This was converted to  $\beta$ -diketiminato-cadmium chloride (**XVI**) by treatment with trimethylsilyl chloride at 90 °C in toluene for 10 days. Complex **XVI** existed as a dimer in the solid state. Each cadmium centre had a distorted tetrahedral geometry forming a four membered metallocycle through the two bridging chlorides and a six membered metallocycle with the BDI ligand.



**Scheme 5: Synthesis of XVI via XV.**

## Cadmium Hydrides

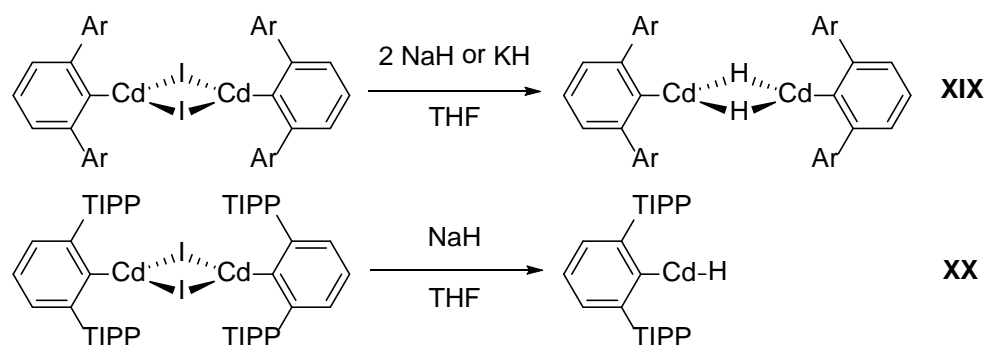
The bulky trispyrazol borate ligand  $[\text{HB}(3\text{-Bu}^t\text{pz})_3]$ , or  $\text{Tp}^{t\text{Bu}}$ , was utilized in the synthesis of the first homonuclear molecular cadmium hydride complex.<sup>51</sup>  $[\text{Tp}^{t\text{Bu}}\text{CdH}]$  (**XVII**) was synthesized by treatment of cadmium dichloride with a hydride source followed by addition of  $[\text{TiTp}^{t\text{Bu}}]$  (Scheme 6). The  $^1\text{H}$  NMR resonance for the hydride on complex **XVII** was at 6.30 ppm,  $^{113}\text{Cd}$  and  $^{111}\text{Cd}$  ( $J_{\text{CdH}}$ ) coupling was observed to confirm the presence of a Cd-H bond. A different product was synthesized using a less sterically encumbered trispyrazol borate ligand which contained methyl substituents at the 3 and 5 positions of the pyrazole ring ( $\text{Tp}^{3,5\text{-Me}}$ ). A bridging borohydride complex with  $\eta_2$ -coordination to cadmium through two hydrogen atoms (**XVIII**) generated when  $\text{KBH}_4$  was used as the  $\text{H}^-$  source.



**Scheme 6: Synthesis of XVII and XVIII.**

Similar to the mercury hydride **V**, the terphenyl cadmium hydride (**XIX**) was generated by addition of  $\text{KH}$  or  $\text{NaH}$  to terphenyl cadmium iodide (Scheme 7). Complex **XIX** was structurally determined as a loosely associated bridged dimer with Cd-H bond distances of 1.786 Å and 2.276 Å. A broad  $^1\text{H}$  NMR resonance at 6.84 ppm was observed with no apparent  $^{113}\text{Cd}$  and  $^{111}\text{Cd}$  coupling. The crystal structure showed distorted trigonal planar conformation at the cadmium centre due to a weak interaction of a neighbouring bridging complex in the unit cell.<sup>35</sup> A monomeric variation (**XX**) was synthesized using 2,4,6-triisopropylphenyl (TIPP) as the flanking aryl group instead of 2,6-diisopropylphenyl (Dipp) (Scheme 7). Structural characterization determined a Cd-H bond distance of 1.794 Å and a similar  $^1\text{H}$  NMR resonance of 6.79 ppm to **XIX**. For the terminal hydride complex **XX** the crystal structure showed linear coordination at the cadmium centre.<sup>52</sup> Degradation was

not readily observed at room temperature, showing that the increased ancillary ligand bulk was important in the stability of the terminal cadmium hydride.

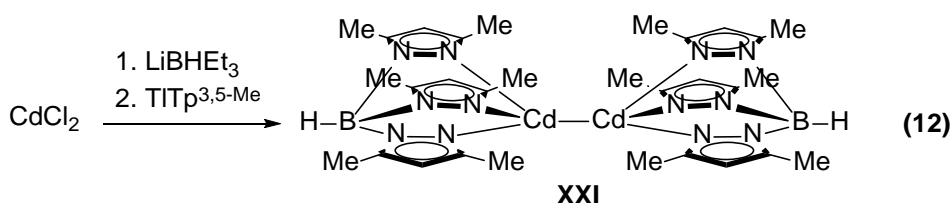


**Scheme 7: Synthesis of XIX and XX.**

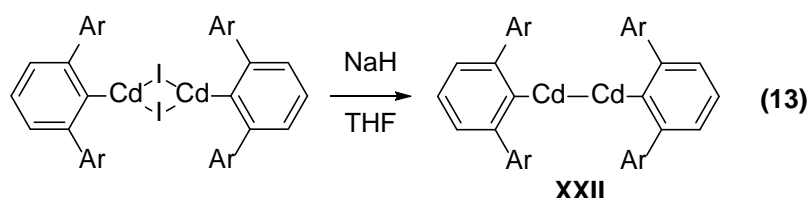
Complexes **XVII** and **XX** have been described as the only organo-cadmium examples where the hydride is at a terminal position making it available for further reactivity. The only known reactivity of the cadmium hydride functionality is the reduction to a homonuclear cadmium-cadmium dimer.<sup>35</sup>

### Homonuclear Cadmium-Cadmium Dimers

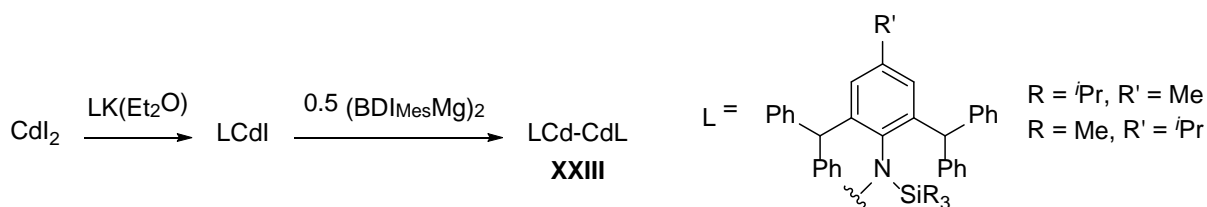
The first homonuclear cadmium-cadmium (Cd-Cd) dimer complex (**XXI**) was synthesized alongside the previously discussed first cadmium hydride (**XVII**).<sup>51</sup> The large bulky Tp ligand with methyl substituents at the 3 and 5 positions was used to generate the homonuclear Cd-Cd dimer in a similar fashion as the cadmium hydride (eq 12). By altering the sterics of the ancillary ligand a different cadmium complex was generated. Complex **XXI** was not structurally determined but was confirmed via  $^{113}\text{Cd}$  NMR spectroscopy with a  $^{111}\text{Cd}$ - $^{113}\text{Cd}$  coupling constant of 20,646 Hz which indicated a strong bond between the cadmium atoms. Mercury equivalents of these compounds are also known but are less stable than their cadmium counterparts.<sup>53</sup>



The terphenyl ligand has also been used to generate a homonuclear Cd-Cd dimer derivative (**XXII**).<sup>35</sup> Under similar conditions for the synthesis of hydride complexes **XX** and **XXI**, but using half the equivalence of sodium hydride, complex **XXII** was generated (eq 13). The Cd-Cd bond had a bond length of 2.574 Å. In the <sup>113</sup>Cd NMR spectrum, the <sup>111</sup>Cd-<sup>113</sup>Cd coupling constant of 8,650 Hz was smaller than **XXI**.



A recent molecular Cd-Cd complex bearing a bulky amide ligand on both metal centres was recently synthesized, similar to the mercury analogue **IX** (**XXIII**, Scheme 8).<sup>40</sup> The steric bulk in **XXIII** prevents further reduction to elemental cadmium. In the <sup>113</sup>Cd NMR spectrum, the <sup>111</sup>Cd-<sup>113</sup>Cd coupling constant was 18,900 Hz, more than double that of **XXII**, suggesting a stronger and higher s-character Cd-Cd bond than complex **XXII**. The bond length of **XXIII** was similar to complex **XXII** at 2.579 Å.



**Scheme 8: Synthesis of XXIII.**

The rare examples of homonuclear Cd-Cd examples show that their syntheses requires reducing reagents that can often be too harsh for the ancillary ligand or not harsh enough to reduce the cadmium centre.

## 1.6 Zinc Compounds

### 1.6.1 Background

Zinc is the most abundant and available group 12 element.<sup>3, 16</sup> Several human enzymes and biochemical processes require a zinc metal centre which is obtained through a standard diet.<sup>54</sup> Zinc is not a typical transition metal since its d-orbitals are full and core-like which results in zinc compounds lacking colour.<sup>55</sup> Zinc is considered a chalcophile due to its affinity for heavier group 11-16 elements and is usually found naturally as ZnS.<sup>56</sup> As a strongly corrosive resistant metal, the industrial applications of zinc metal include galvanization and alloys, such as brass. Zinc metal is a strong reducing agent and burns in air with a bright blue-green flame.

The +2 oxidation state dominates the chemistry of zinc; however, there are a few examples of zinc in the +1 oxidation state, often containing the highly reactive  $[\text{Zn}_2]^{+2}$  core similar to cadmium and mercury.<sup>57</sup> Zinc complexes are commonly 4 or 6 coordinate, and unlike standard transition metals, zinc bonds have great covalency and stability with nitrogen and sulfur containing substituents.<sup>56</sup> The zinc chalcogenides are used in various electronic and optic applications.<sup>58-60</sup> Zinc containing compounds are used as reagents in synthetic chemistry and are heavily researched as catalysts for various organic syntheses.<sup>61-65</sup>

Zinc has one NMR active nuclei,  $^{67}\text{Zn}$  with a 4.10% natural abundance which has low sensitivity and produces broad signals with its spin of 5/2. The broad nature of the signal increases with larger compounds, therefore  $^{67}\text{Zn}$  NMR spectroscopy is not a standard technique and is only used for studying very small complexes of zinc such as zinc dichloride, zinc dibromide and zinc diiodide.

## 1.6.2 Coordination Chemistry

### $\beta$ -Diketiminato Zinc Complexes

There are many reported  $\beta$ -diketiminato-zinc complexes with varying substituents along the BDI backbone ( $R^1$ - $R^5$ , Figure 1).<sup>27, 47, 66-87</sup> The most commonly used BDI backbones involve  $R^2$  and  $R^4$  being methyl groups and  $R^3$  or the  $\gamma$ -position as a hydrogen atom.<sup>82</sup> The  $R^1$  and  $R^5$  positions of the  $\beta$ -diketiminato ligand often differ when used for catalysis. Variations across the backbone include integrated aromatic ring systems providing differing electronic effects.<sup>67-68, 81</sup>

Several different zinc precursors can be used to generate heteroleptic  $\beta$ -diketiminato-zinc complexes. For instance, organo-zinc precursors, such as dimethyl zinc and diethyl zinc, can react directly with a protonated BDI ligand to form zinc complexes bearing a methyl or ethyl substituent<sup>27, 47, 66-68, 74, 76-77, 79-80</sup> although tert-butyl, phenyl<sup>80</sup> and penta-fluorophenyl complexes have also been reported.<sup>47</sup> Zinc bis-amido complexes can also react directly with the protonated BDI ligand to form complexes bearing amide functionality such as hexamethyldisilazane<sup>27, 66, 74, 78, 82</sup> (HMDS). Other common  $\beta$ -diketiminato-zinc amide complexes include a dimethyl amide<sup>75</sup> and diisopropylamide.<sup>69</sup> Zinc halides can also be used, these react with the lithium salt of the BDI ligand to form bridging<sup>27</sup> and terminal  $\beta$ -diketiminato-zinc complexes.<sup>71, 73, 79-80</sup> Other functionalities include various alkoxides,<sup>27, 47, 66-67, 69, 73-74, 78, 82</sup> hydrides,<sup>73, 83</sup> homonuclear Zn-Zn bonds,<sup>70, 72</sup> bis- $\beta$ -diketiminato complexes<sup>27, 47, 67, 74, 76-77, 81</sup> and bimetallic species.<sup>71, 84-87</sup>

Although  $\beta$ -diketiminato-zinc has a vast library of variations, there are still gaps that could further expand their capabilities as reagents or catalysts. Functionalities that are not heavily explored are phosphorus containing substituents, amide derivatives, aryl groups and chalcogenides. Amides and chalcogenides are of particular interest considering zinc's affinity for these atoms compared to other transition metals and their use in biochemistry.<sup>3, 56</sup>

## Zinc Phosphanide Complexes

Most zinc complexes with a phosphorus bond are either involved in clusters,<sup>88-89</sup> oligomers,<sup>89-91</sup> are internally bound<sup>92-93</sup> or have multiple and varying phosphorus atoms within the structure.<sup>94-95</sup> Although several zinc phosphine complexes are known where the phosphine plays the role of a dative ancillary ligand, relatively few examples of zinc phosphanide complexes are known.<sup>96-98</sup>

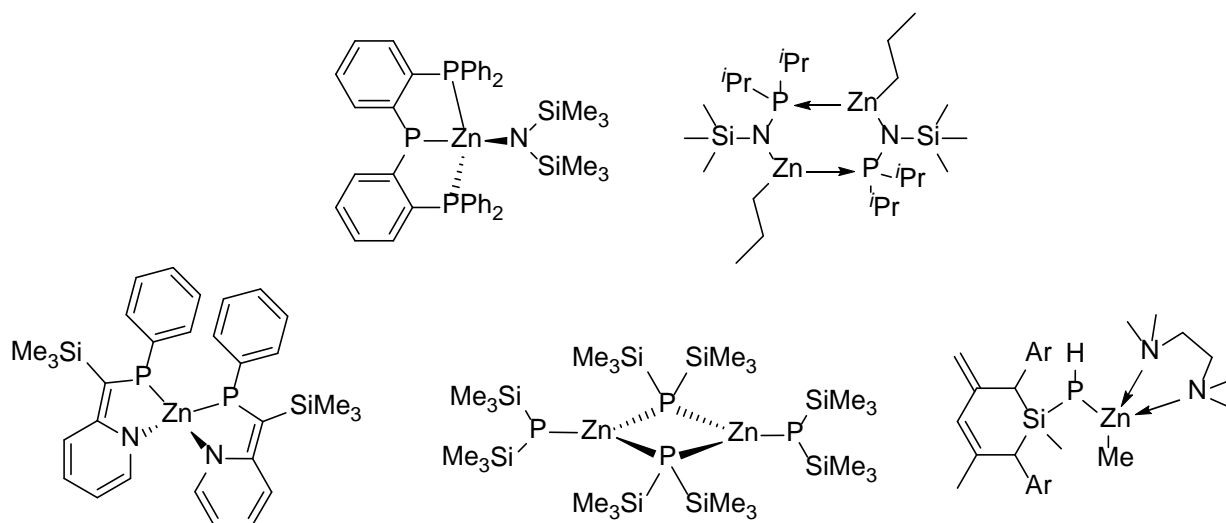


**Figure 7: Examples of compounds involving a Zn-P interaction. Top left, phosphorus integrated into the ligand with dative bonding.<sup>92</sup> Top right, dimeric compound with dative bonding.<sup>89</sup> Bottom left, anionic phosphorus ligand.<sup>98</sup> Bottom middle, multiple phosphorus binding including a phosphanide.<sup>94</sup> Bottom right, a niche phosphano example.<sup>97</sup>**

A phosphane, or phosphine, is a derivative of  $\text{PH}_3$  with organic substituents where a phosphanide ligand is typically an anionic  $\text{PR}_2^-$  ligand in which R can be hydrogen, alkyl, aryl or another heteroatom. A phosphide refers to  $\text{P}^{3-}$ . Basic zinc phosphide ( $\text{Zn}_3\text{P}_2$ ) is a semiconductor with a band gap of 1.5 eV and may have applications in photovoltaic cells.<sup>99-</sup>

<sup>100</sup> Terminal and accessible zinc phosphanide bonds are rare with only a few examples.<sup>94-95,</sup>

<sup>97</sup> The advantage to having a phosphanide ligand is that they are highly sensitive to chemical environments and are easily detectable with  $^{31}\text{P}$  NMR spectroscopy which has a high spectral range from 430 to -250 Hz and a 1/2 spin.<sup>101</sup> Functionally accessible zinc phosphanides could be used as scaffolding for further reactivity with the option of oxidation at the phosphorus centre. To date there is only one  $\beta$ -diketiminato-zinc phosphanide

complex reported, which was synthesized by treatment of 5 equivalents of phenylphosphine to a  $\beta$ -diketiminato-zinc diethyl complex. This compound was not successfully purified or structurally characterized and was only observed in the  $^{31}\text{P}$  NMR spectrum as a peak at  $\delta$  -152 ppm with a corresponding doublet in the  $^1\text{H}$  NMR spectrum at  $\delta$  4.92 ppm.<sup>77</sup>

## Zinc Chalcogenides

There are several zinc complexes, as  $[\text{L}_n\text{ZnE-R}]$  ( $\text{E} = \text{S}, \text{Se}, \text{Te}$ ), where thiolates, selenates and tellurates have been bond directly to the metal. Examples mostly involve clusters,<sup>102-105</sup> oligomers,<sup>106-110</sup> ligand integrated atoms<sup>111-117</sup> and mixtures of these. There are few examples involving chalcogenides, referring to the anionic forms, sulfide, selenide and telluride ( $\text{E}^{2-}$ ) which maintain a single bond to the metal centre, as terminal substituents.<sup>114, 116</sup> Synthetic routes to these compounds involve many precursors, making their synthetic strategies low on step and atom economy.<sup>118-119</sup> Zinc sulfide, selenide and telluride nano particles are semiconductors with large and controllable band gaps allowing them to be used in various optical and electronic applications including solar cells.<sup>120</sup> Considering the semiconductor nature of zinc chalcogenides it is important to research potential single source precursors.

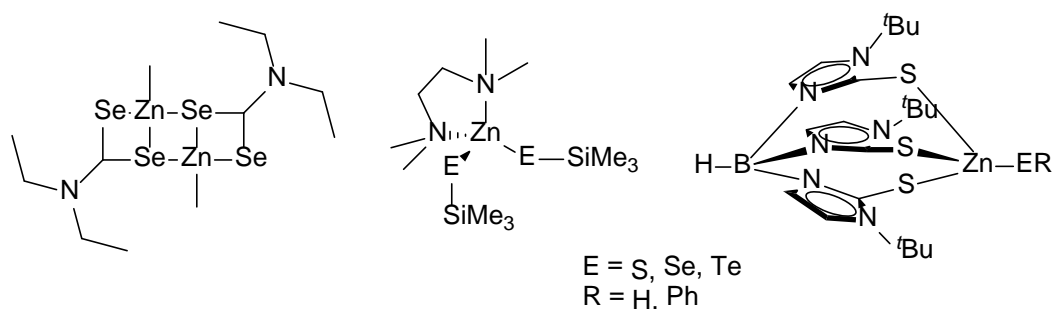
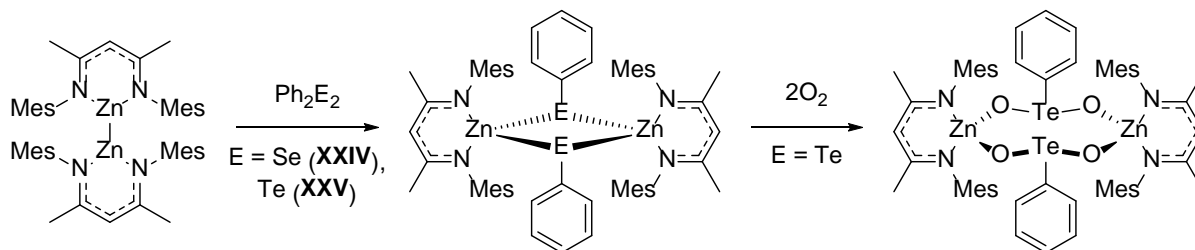


**Figure 8: Examples of zinc chalcogenides. Left, an oligomeric example.<sup>108</sup> Middle and right, terminal examples.<sup>114, 116</sup>**

Only a few examples of  $\beta$ -diketiminato-zinc complexes with chalcogen containing ligands exist.<sup>121-122</sup>  $\beta$ -Diketiminato-zinc selenide and telluride containing complexes (**XXIV** and **XXV**) were synthesized by treating a homonuclear Zn-Zn dimer complex with diphenyl diselenide and ditelluride ( $\text{Ph}_2\text{E}_2$ ) to produce bridging complexes (Scheme 9).<sup>122</sup> Only the selenide **XXIV** was structurally characterized and showed a Zn-Se bond distances of 2.429 and 2.595 Å with

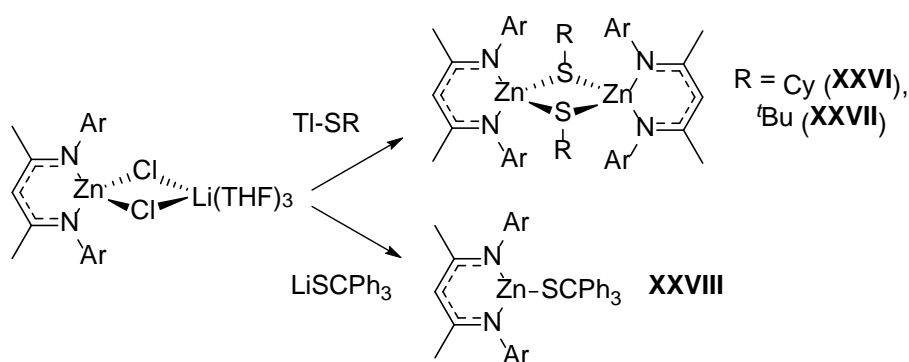


E-Zn-E angles close to 90° at 90.99°. Insertion of oxygen into the Te-Zn bond of the telluride **XXV** was achieved upon addition of O<sub>2</sub>, the product was structurally characterized and showed the insertion of 2 oxygen molecules.



**Scheme 9: Synthesis of XXIV. Synthesis and reactivity of XXV with O<sub>2</sub>.**

Reacting a  $\beta$ -diketiminato-zinc chloride with thallium thiol reagents (TI-SR) produced bridged dimers **XXVI** and **XXVII** (Scheme 10). The Zn-S bond distances of **XXVI** and **XXVII** ranged from 2.31-2.42 Å with S-Zn-S bond angles of 90.22° for **XXVI** and 109.19° for **XXVII**, the latter contained a bulkier R group. When LiSCPh<sub>3</sub> was added, a monomer complex **XXVIII** was isolated with a Zn-S bond distance of 2.21(4) Å.<sup>121</sup>



**Scheme 10: Synthesis of XXVI, XXVII and XXVIII.**

## NMR Active Nuclei of Chalcogens

The NMR spectroscopy of the NMR active nuclei of the chalcogens can be useful characterization tools when investigating complexes containing varying amounts of the chalcogen. The least useful, in terms of NMR characterization, is sulfur due to the low abundance (0.76%) of its only NMR active nuclei, <sup>33</sup>S, which has a 3/2 spin producing broad

signals. The signals are broader with larger and more asymmetric compounds leading to  $^{33}\text{S}$  NMR spectroscopy only being used for the characterization of small sulfur containing compounds such as dimethyl sulfoxide (DMSO). Coupling to other NMR active nuclei is not observed in other NMR spectra due to the low abundance of the  $^{33}\text{S}$  nuclei.

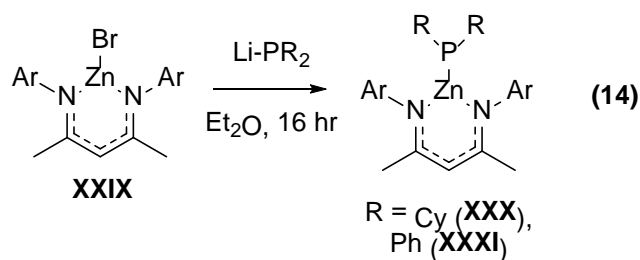
Selenium has one NMR active nuclei,  $^{77}\text{Se}$  with a 7.63% natural abundance and a spin of 1/2, producing narrow signals. The  $^{77}\text{Se}$  nuclei can couple to other NMR active nuclei, such as  $^{31}\text{P}$ , which can be observed and used to characterize the selenium nuclei environment. Tellurium has two NMR active nuclei,  $^{125}\text{Te}$  with a 7.07% natural abundance and  $^{123}\text{Te}$  with a 0.89% natural abundance. Both nuclei are 1/2 spin and produce narrow signals but  $^{125}\text{Te}$  is used for tellurium NMR since  $^{125}\text{Te}$  is more abundant, has higher sensitivity and yields sharper signals. The  $^{125}\text{Te}$  nuclei can couple to other NMR active nuclei, such as  $^{31}\text{P}$ , which can be observed and used to characterize the tellurium nuclei environment.

### 1.6.1 Research from 2014

Research with novel zinc coordination was conducted as part of a Summer Research Project in 2014. This work is related to zinc phosphanides, zinc chalcogenides and later work in Chapter 2 of this thesis and so has been included as part of this introduction.

The use of zinc halide salts is problematic since they are hygroscopic. The presence of water can produce undesired protonation products when these halide salts are used for the synthesis of water sensitive compounds. The standard purification method for zinc dichloride is to recrystallize zinc dichloride from hot dioxane.<sup>123</sup> This method proved unsuccessful in producing water free zinc dichloride and so zinc dibromide was considered. The standard purification method for zinc dibromide is sublimation. With the correct sublimation gear and heating apparatus it was possible to sublime zinc dibromide under vacuum at temperatures above 350 °C. The purified zinc dibromide was used in a known synthesis to generate the starting material  $[\text{BDI}_{\text{Dipp}}\text{ZnBr}]$  (**XXIX**).<sup>27</sup> The common BDI ligand,  $\text{BDI}_{\text{Dipp}}$ , was used which contains two Dipp groups at  $\text{R}^1$  and  $\text{R}^5$ , methyl groups at  $\text{R}^2$  and  $\text{R}^4$  and a hydrogen atom known as the  $\gamma$ -proton at  $\text{R}^3$  (Figure 1).

## Synthesis of Zinc Phosphanide Complexes



Attempts to generate zinc-phosphanide complexes from lithium phosphanide salts were attempted via a salt metathesis reaction with **XXIX**. The lithium phosphanide salts, lithium dicyclohexylphosphanide (Li-PCy<sub>2</sub>) and lithium diphenylphosphanide (Li-PPh<sub>2</sub>), were generated by the treatment of the corresponding phosphine with *n*-butyllithium (*n*BuLi). β-Diketiminato-zinc dicyclohexylphosphanide was synthesized by treatment of **XXIX** with Li-PCy<sub>2</sub>. To minimize the possibility of incomplete salt metathesis, non-ethereal solvents were initially used. However, no reaction was observed in those solvents. When the reaction was performed in diethyl ether the zinc dicyclohexylphosphanide (**XXX**) was produced with no evidence of an incomplete salt metathesis (eq 14).

The <sup>1</sup>H NMR spectrum of **XXX** shows one septet at δ 3.22 ppm (formally a quartet of quartets), indicating a single environment for the methine proton on the isopropyl groups and a singlet at 5.00 ppm for the γ-proton, downfield to the γ-proton of the precursor **XXIX**. There is an inclusion of cyclohexyl signals at 1.56 and 1.28 ppm. The <sup>31</sup>P NMR spectrum shows a single peak at δ -22.2 ppm, slightly downfield to Li-PCy<sub>2</sub> (δ -21.9 ppm).

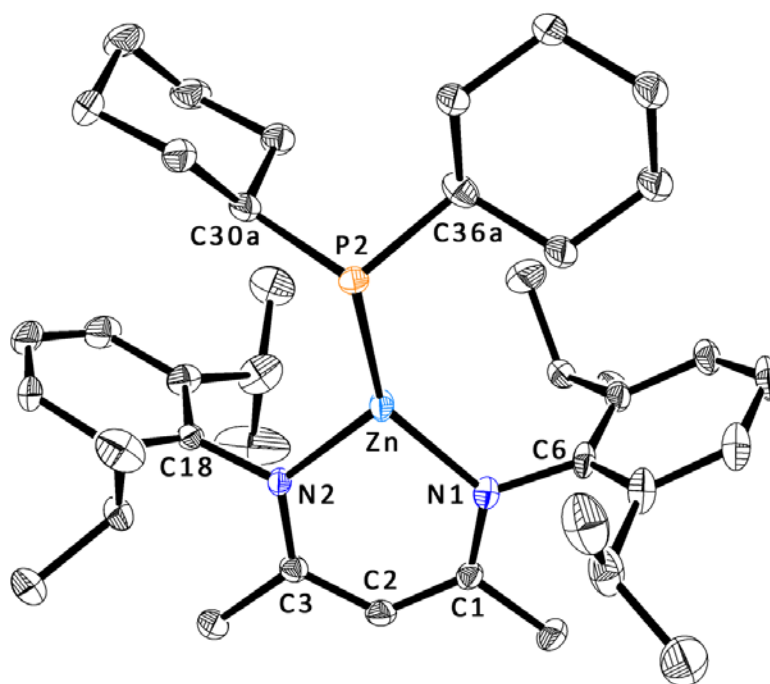


**Figure 9: ORTEP diagram of XXX showing thermal ellipsoids at 30% probability. Only bonds for P2 are shown. One set of cyclohexyl peaks are shown (a). Hydrogens omitted for clarity.**

Yellow cube shaped crystals suitable for an X-ray diffraction study were grown from diethyl ether at  $-30\text{ }^{\circ}\text{C}$ . Complex **XXX** is monomeric in the solid state and showed disorder at the phosphorus nucleus and the two cyclohexyl groups. Both positions were modelled and what are shown in Figure 9 are the nuclei with the highest occupancy (81%).

The nitrogens of the BDI ligand do not show any amide or imine character and are statistically indistinguishable from each other, indicative of a delocalized  $\pi$ -system in the BDI backbone. Complex **XXX** has a BDI bite angle of  $95.5(1)^{\circ}$ .

The Zn-P2 bond length of  $2.285(1)\text{ \AA}$  is shorter than a dative phosphanide bond with bond lengths ranging  $2.393\text{--}2.401\text{ \AA}$ <sup>93</sup> and a P-metallated phosphasilene with a Zn-P bond length of  $2.367\text{ \AA}$ .<sup>97</sup> The Zn-P2 bond length in complex **XXX** is closer to that of an internally bound zinc phosphanide in a cluster with bond lengths ranging from  $2.302$  to  $2.334\text{ \AA}$ .<sup>95</sup> The phosphanide ligand is asymmetric to the zinc metal centre, skewed towards N2 as represented with a shorter N2-Zn-P2 bond angle of  $123.8(1)^{\circ}$  compared to the N1-Zn-P2 bond angle of  $137.7(1)^{\circ}$ .

**Table 1:** Selected bond lengths (Å) and angles (°) for **XXX**.

Zn-P2	2.285(1)	Zn-N1	1.971(4)	Zn-N2	1.981(3)
N1-C1	1.318(6)	C1-C2	1.398(6)	C2-C3	1.395(6)
C3-N2	1.329(6)	N1-C6	1.441(6)	N2-C18	1.432(5)
P2-C30a	1.942(5)	P2-C36a	1.856(5)		
N1-Zn-N2	95.5(1)	Zn-N1-C1	122.4(3)	N1-C1-C2	125.6(4)
C1-C2-C3	127.9(4)	C2-C3-N2	124.2(4)	C3-N2-Zn	122.8(3)
N1-Zn-P2	137.7(1)	N2-Zn-P2	123.8(1)	Zn-P2-C30a	104.9(1)
Zn-P2-C36a	110.1(2)	C30a-P2-C36a	103.8(2)		

Addition of Li-PPh<sub>2</sub> to a diethyl ether solution of zinc bromide **XXIX** resulted in the formation of multiple products. The <sup>1</sup>H NMR spectrum of the reaction mixture revealed [BDI<sub>Dipp</sub>-Li] and potentially two new BDI containing compounds as indicated by the presence of two signals (δ 5.02 and 5.00 ppm) which typically correspond to the γ-proton of the BDI backbone. The <sup>31</sup>P NMR spectrum shows a single peak at δ -45.8 ppm, up-field of Li-PPh<sub>2</sub> (δ -43.9 ppm).

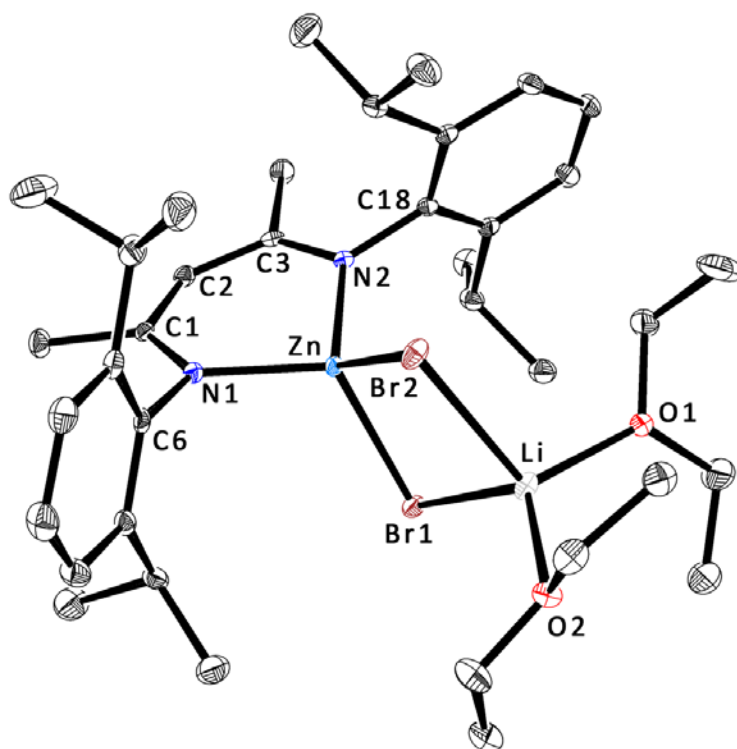


**Figure 10: ORTEP diagram of XXXII showing thermal ellipsoids at 30% probability. Hydrogens omitted for clarity.**

Yellow cube shaped crystals suitable for an X-ray diffraction study were grown from diethyl ether at  $-30\text{ }^{\circ}\text{C}$  over a week. The product was not the expected zinc phosphanide complex **XXXI** and was instead an incomplete salt metathesis complex with two diethyl ether molecules coordinated to the lithium centre (**XXXII**) in a similar manner to other group 12 salt metathesis complexes **I** and **XIII**.

Complex **XXXII** is monomeric in the solid state. The zinc centre lies  $0.412\text{ }\text{\AA}$  out of the plane consisting of N1-C1-C2-C3-N2 (referred to herein as BDI plane). The plane consisting of O1-Li-O2 is  $8.74^{\circ}$  from the BDI plane. The bromide atoms are not equivalent based on their bond lengths to zinc,  $2.4581(4)$  and  $2.4172(4)\text{ }\text{\AA}$ , but their bond lengths only differ slightly to the lithium,  $2.549(4)$  and  $2.553(5)\text{ }\text{\AA}$ . The BDI backbone has delocalization as observed by the statistically indistinguishable C-C bond lengths  $1.390(3)$  and  $1.407(4)\text{ }\text{\AA}$  and N-C bond lengths  $1.329(3)$  and  $1.325(3)\text{ }\text{\AA}$ . Complex **XXXII** has a smaller bite angle for the BDI ligand compared to the zinc phosphanide **XXX** due to the accommodation of large bromide atoms. The bite is in range of existing bridged  $\beta$ -diketiminato-zinc bromide complexes which exhibit a BDI bite angle range of  $96.67\text{--}98.33^{\circ}$ .<sup>28</sup>

The BDI plane is 84.38° from the plane consisting of Zn-Br1-Li-Br2. The metallocycle with lithium is square shaped, the Zn-Br1-Li and Zn-Br2-Li bond angles (82.3(1)° and 83.0(1)°) are shorter than the Br1-Zn-Br2 and Br1-Li-Br2 bond angles (99.33(2)° and 93.5(2)°). The Li-O bond lengths of 1.940(5) and 1.995(5) Å, and the variable bond angles about the lithium centre indicates asymmetry at the lithium metal centre with the Et<sub>2</sub>O molecules.

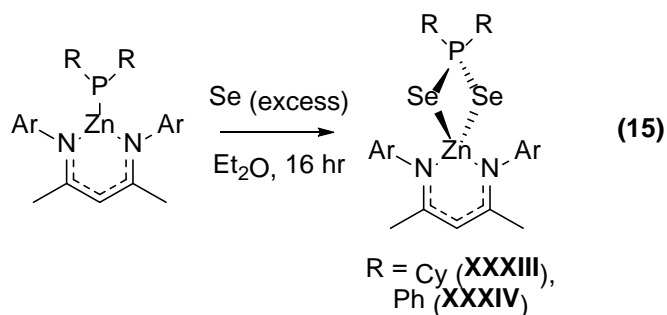
The zinc-bromide bond lengths are longer than standard zinc dibromide at 2.21 Å<sup>124</sup> potentially due to the bridging geometry. The Zn-Br bond lengths follow the same trend as a bridged β-diketiminato-zinc bromides which have shorter bond lengths ranging 2.402-2.408 Å for one bromide and longer bond lengths ranging 2.418-2.435 Å for the other bromide.<sup>28</sup> Both bromide atoms are formally Br<sup>2-</sup> contributing 0.5- to zinc and 1.5- to lithium. The Br1-Li-Br2 functionality is a bidentate ligand, formally contributing a single charge to Zn(II).

**Table 2:** Selected bond lengths (Å) and angles (°) for **XXXII**.

Zn-N1	1.975(2)	Zn-N2	1.978(2)	N1-C1	1.329(3)
C1-C2	1.390(3)	C2-C3	1.407(4)	C3-N2	1.325(3)
N1-C6	1.444(3)	N2-C18	1.445(3)	Zn-Br1	2.4581(4)
Zn-Br2	2.4172(4)	Br1-Li	2.549(4)	Br2-Li	2.553(5)
Li-O1	1.940(5)	Li-O2	1.995(5)		
N1-Zn-N2	97.69(8)	Zn-N1-C1	120.3(2)	N1-C1-C2	123.6(2)
C1-C2-C3	130.5(2)	C2-C3-N2	124.1(2)	C3-N2-Zn	119.6(2)
Br1-Zn-Br2	99.33(2)	Br1-Li-Br2	93.5(2)	Zn-Br1-Li	82.3(1)
Zn-Br2-Li	83.0(1)	O1-Li-O2	116.9(2)	N1-Zn-Br1	115.93(6)
N1-Zn-Br2	113.61(6)	N2-Zn-Br1	112.66(6)	N2-Zn-Br2	118.67(6)
O1-Li-Br1	106.6(2)	O1-Li-Br2	110.0(2)	O2-Li-Br1	122.3(2)
O2-Li-Br2	104.6(2)				

Unfortunately repeated attempts at obtaining pure diphenylphosphanide **XXXI** were unsuccessful with only contaminated  $^1\text{H}$  NMR and  $^{31}\text{P}$  NMR spectra indicating diphenylphosphanide **XXXI** as a possible product. Complex **XXXII** is potentially the product of a degradation pathway.

### Addition of Chalcogens into Zinc Phosphanide Bonds



Addition of selenium powder to a  $\text{Et}_2\text{O}$  solution of the dicyclohexylphosphanide **XXX** resulted in the formation of the dicyclohexylphosphinodiselenoate complex **XXXIII** (eq 15). The  $^1\text{H}$  NMR spectrum of **XXXIII** shows one septet at  $\delta$  3.49 ppm, indicating a single environment for the methine proton on the isopropyl groups and a singlet at  $\delta$  4.85 ppm for the  $\gamma$ -proton, up-field from dicyclohexylphosphanide **XXX**. The  $^{31}\text{P}$  NMR spectrum shows a single peak at  $\delta$  51.2 ppm, downfield from **XXX**, with  $^{77}\text{Se}$  satellites. The  $^{77}\text{Se}$ - $^{31}\text{P}$  coupling constant of 451.5 Hz is consistent with the addition of two selenium atoms to a phosphorus atom seen in  $\beta$ -diketiminato-tin and germanium phosphanide complexes.<sup>125</sup> Throughout the reaction no other signals were observed in the  $^{31}\text{P}$  NMR spectrum that would indicate a complex with only one selenium atom added, a dicyclohexylphosphinoselenoite complex.



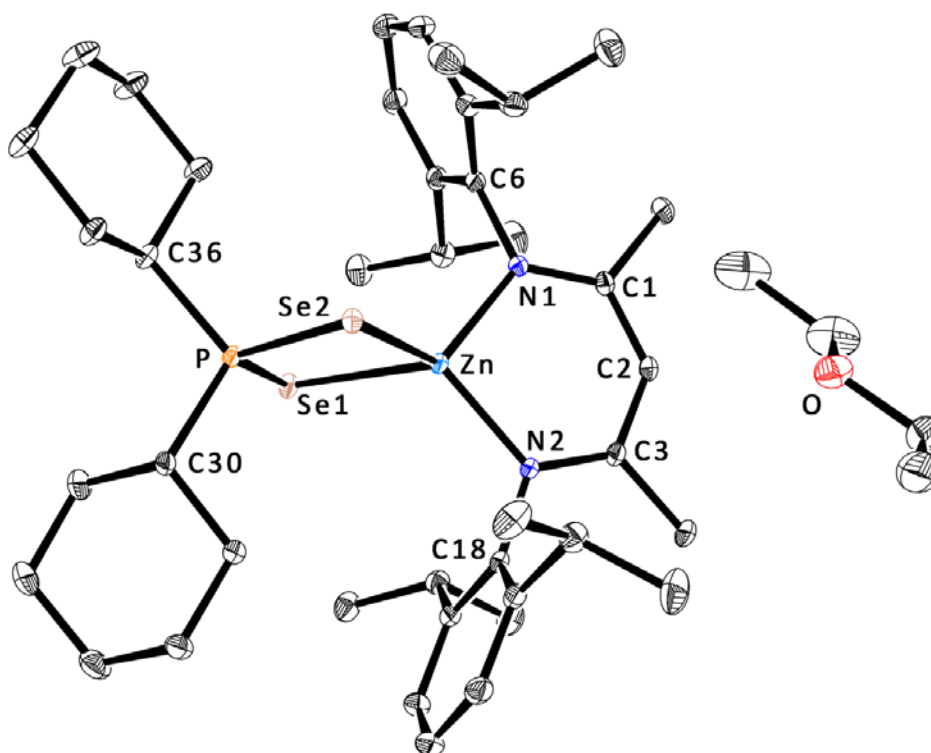


**Figure 11: ORTEP diagram of XXXIII showing thermal ellipsoids at 30% probability. There was one diethyl ether molecule per complex XXXIII in the crystal packing. Hydrogens omitted for clarity.**

Orange rectangular crystals suitable for an X-ray diffraction study were grown from diethyl ether at  $-30\text{ }^{\circ}\text{C}$ . Complex **XXXIII** is monomeric in the solid state with a molecule of diethyl ether in the unit cell. The phosphorus atom is formally  $\text{P}^{5+}$  and the selenium atoms are both  $\text{Se}^{2-}$ . The Zn-Se bond lengths of 2.5002(4) and 2.5010(5) Å are very similar where the Se-P bond lengths of 2.1708(4) and 2.1737(5) Å only differ slightly. In contrast to  $\beta$ -diketiminato-germanium dicyclohexylphosphinodiselenoate complexes, which are three coordinate, the dicyclohexylphosphinodiselenoate ligand in complex **XXXIII** is bidentate resulting in a tetrahedral zinc centre.<sup>125</sup> The Zn-Se bonds are in range of the Zn-Se bonds in the selenium bridged BDI complex **XXIV** which range from 2.429-2.595 Å.<sup>122</sup> Other Zn-Se bonds from various compounds range from 2.320-2.609 Å.<sup>102-117</sup> Attempts to produce a mono-insertion product proved unsuccessful even with treatment of a single equivalent or less of selenium powder.

The nitrogens of the BDI ligand do not show any amide or imine character and are statistically indistinguishable from each other, indicative of a delocalized  $\pi$ -system in the BDI

backbone. Complex **XXXIII** has a slightly larger BDI bite angle of 99.07(5)° to the starting material dicyclohexylphosphanide **XXX**.

The plane consisting of N1-C1-C2-C3-N2 is 89.61° from the plane of the phosphinodiselenoate ligand. The phosphinodiselenoate ligand is square shaped, the Zn-Se1-P and Zn-Se2-P bond angles (80.25(2) and 80.29(2)°) are shorter than the Se1-Zn-Se2 and Se1-P-Se2 bond angles (90.11(2) and 109.13(2)°).

**Table 3:** Selected bond lengths (Å) and angles (°) for **XXXIII**.

Zn-N1	1.971(1)	Zn-N2	1.974(1)	N1-C1	1.327(2)
C1-C2	1.405(2)	C2-C3	1.401(2)	C3-N2	1.328(2)
N1-C6	1.437(2)	N2-C18	1.437(2)	Zn-Se1	2.5010(5)
Zn-Se2	2.5002(4)	Se1-P	2.1708(4)	Se2-P	2.1737(5)
P-C30	1.828(1)	P-C36	1.832(1)		
N1-Zn-N2	99.07(5)	Zn-N1-C1	120.86(9)	N1-C1-C2	124.1(1)
C1-C2-C3	130.9(1)	C2-C3-N2	124.5(1)	C3-N2-Zn	120.46(9)
Zn-Se1-P	80.29(2)	Zn-Se2-P	80.25(2)	Se1-Zn-Se2	90.11(2)
Se1-P-Se2	109.13(2)	C30-P-C36	108.26(6)	N1-Zn-Se1	115.44(4)
N1-Zn-Se2	116.19(4)	N2-Zn-Se1	117.89(4)	N2-Zn-Se2	119.54(4)
C30-P-Se1	110.17(5)	C30-P-Se2	109.14(5)	C36-P-Se1	109.31(5)
C36-P-Se2	110.81(5)				

Addition of selenium powder to a Et<sub>2</sub>O solution of zinc diphenylphosphanide complex **XXXI** resulted in the formation of a diphenylphosphinodiselenoate, complex **XXVI** (eq 15). Although impure diphenylphosphanide **XXXI** was used, **XXXIV** was isolated as a single compound. The <sup>1</sup>H NMR spectrum of **XXXIV** shows one septet at δ 3.53 ppm, indicating a single environment for the methine proton on the isopropyl groups and a singlet at 4.84 ppm, up-field to the suspected phosphanide **XXXI** γ-proton signal. The <sup>31</sup>P NMR spectrum shows a single peak at δ 6.3 ppm with a <sup>77</sup>Se-<sup>31</sup>P coupling constant of 472.7 Hz, similar to the dicyclohexylphosphinodiselenoate **XXXIII**, indicating two selenium atoms had been added into the zinc-phosphanide bond. Throughout the reaction no other signals were observed in

the  $^{31}\text{P}$  NMR spectrum that would indicate a complex with only one selenium atom added, a diphenylphosphinoselenoite complex.

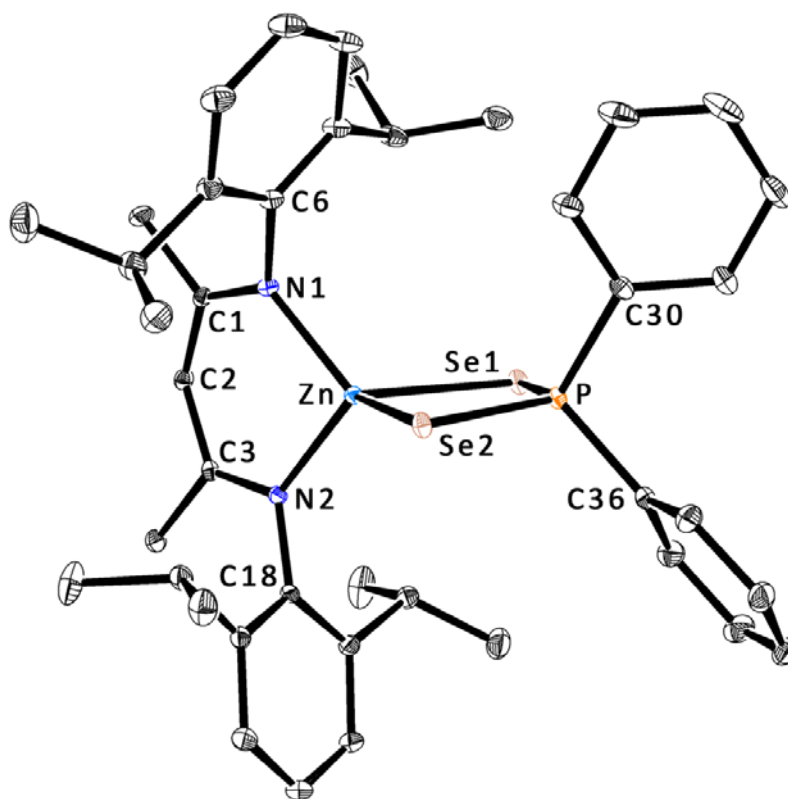


**Figure 12: ORTEP diagram of XXXIV showing thermal ellipsoids at 30% probability. Hydrogens omitted for clarity.**

Orange rectangular crystals suitable for an X-ray diffraction study were grown from diethyl ether at  $-30\text{ }^{\circ}\text{C}$ . Complex **XXXIV** is monomeric in the solid state. The phosphorus atom is formally  $\text{P}^{5+}$  and the selenium atoms are both  $\text{Se}^{2-}$ . The Zn-Se bond lengths, Zn-Se1 of  $2.4749(5)$  and Zn-Se2 of  $2.5235(3)$  Å, differ where the Se-P bond lengths of  $2.1588(6)$  and  $2.1671(5)$  Å are similar. In contrast to  $\beta$ -diketiminato-germanium diphenylphosphinodiselenoate complexes, which are three coordinate, the diphenylphosphinodiselenoate ligand in complex **XXXVI** is bidentate resulting in a tetrahedral zinc centre.<sup>125</sup> The Zn-Se bonds are in range of the Zn-Se bonds in the selenium bridged BDI complex **XXIV** which range from  $2.429$ - $2.595$  Å.<sup>122</sup> Other Zn-Se bonds from various compounds range from  $2.320$ - $2.609$  Å.<sup>102-117</sup> Attempts to produce a mono-insertion product proved unsuccessful even with treatment of a single equivalent or less of selenium powder.

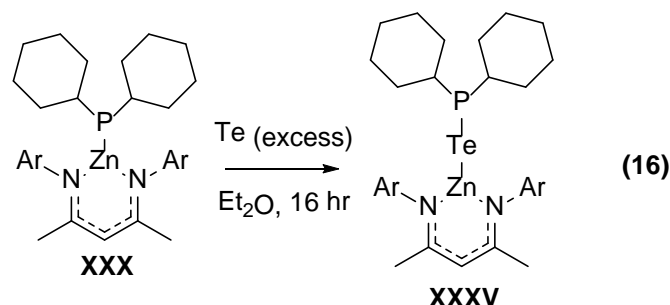
The nitrogens of the BDI ligand do not show any amide or imine character and are statistically indistinguishable from each other, indicative of a delocalized  $\pi$ -system in the BDI backbone. Complex **XXXVI** has a similar BDI bite angle of  $99.23(5)^\circ$  to dicyclohexylphosphinodiselenoate **XXXIII**.

The plane consisting of N1-C1-C2-C3-N2 is  $89.70^\circ$  from the plane of the phosphinodiselenoate ligand. The phosphinodiselenoate ligand is square shaped, the Zn-Se1-P and Zn-Se2-P bond angles ( $80.22(2)$  and  $81.18(2)^\circ$ ) are shorter than the Se1-Zn-Se2 and Se1-P-Se2 bond angles ( $89.47(3)$  and  $108.84(2)^\circ$ ). The phosphinodiselenoate ligand shares similar bond angles to the phosphinodiselenoate ligand of dicyclohexylphosphinodiselenoate **XXXIII**.

**Table 4:** Selected bond lengths (Å) and angles ( $^\circ$ ) for **XXXIV**.

Zn-N1	1.967(1)	Zn-N2	1.969(1)	N1-C1	1.329(2)
C1-C2	1.399(2)	C2-C3	1.404(2)	C3-N2	1.328(2)
N1-C6	1.438(2)	N2-C18	1.435(2)	Zn-Se1	2.5235(3)
Zn-Se2	2.4749(5)	Se1-P	2.1588(6)	Se2-P	2.1671(5)
P-C30	1.807(1)	P-C36	1.809(1)		
N1-Zn-N2	99.23(5)	Zn-N1-C1	118.6(1)	N1-C1-C2	124.7(1)
C1-C2-C3	129.9(1)	C2-C3-N2	124.0(1)	C3-N2-Zn	119.2(1)
Se1-Zn-Se2	89.47(2)	Se1-P-Se2	108.84(2)	Zn-Se1-P	80.22(2)
Zn-Se2-P	81.18(2)	C30-P-C36	104.77(7)	N1-Zn-Se1	117.68(4)
N1-Zn-Se2	118.79(4)	N2-Zn-Se1	114.97(4)	N2-Zn-Se2	118.10(4)
Se1-P-C30	110.05(5)	Se1-P-C36	111.84(5)	Se2-P-C30	110.80(5)
Se2-P-C36	110.51(5)				

Addition of tellurium powder to the dicyclohexylphosphanide **XXX** did not give the double addition product. Instead, a mono-insertion product was suspected, a dicyclohexylphosphinotellunoite, complex **XXXV** (eq 16).



The  $^1\text{H}$  NMR spectrum of the reaction mixture has both  $[\text{BDI}_{\text{Dipp}}\text{-H}]$  and a potentially new BDI containing complex as indicated by the presence of a signal ( $\delta$  5.06 ppm) in the  $^1\text{H}$  NMR spectrum which typically corresponds to the  $\gamma$ -proton of the BDI backbone. The  $^{31}\text{P}$  NMR spectrum shows a peak at  $\delta$  7.2 ppm with a pair of satellites. Only the satellites from  $^{125}\text{Te}$  were observed with a  $^{125}\text{Te}$ - $^{31}\text{P}$  coupling constant of 285.0 Hz. This is a smaller coupling constant compared to the phosphinodiselenoate complexes **XXXIII** and **XXXIV**. This coupling is similar to  $\beta$ -diketiminato-germanium dicyclohexylphosphinotellunoite complexes, thus we suspect the new BDI containing complex to be the mono-inserted product (**XXXV**).<sup>125</sup> Two types of crystals appeared to grow out of an orange reaction mixture at  $-30^\circ\text{C}$ , yellow needles and yellow cubes of which could not be separated. Both crystals were not suitable for an X-ray diffraction study.

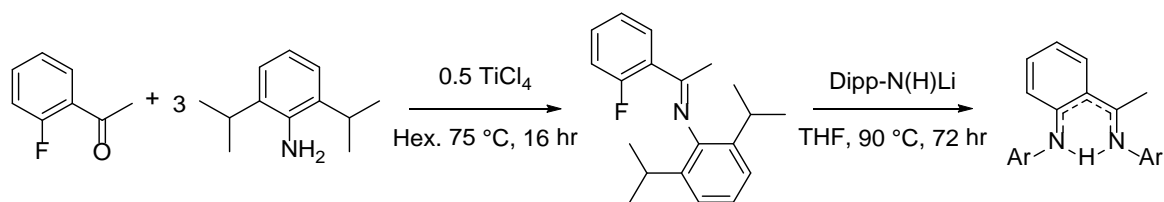
Attempts to insert sulfur into the zinc-phosphanide bond of the dicyclohexylphosphanide complex **XXX** to synthesize a dicyclohexylphosphinodithioate proved unsuccessful. Additions of elemental sulfur resulted in multiple products, detected by  $^1\text{H}$  and  $^{31}\text{P}$  NMR spectroscopy, which were suspected to be both the single and double addition products. Isolation and determination of the products in the reaction mixture was inconclusive.

## 1.7 Pre-Thesis Research Motive

The recent synthesis of the cadmium chloride (**XVI**) was the basis for some of the following research outlined in Chapter 2. Further investigation into complex **XVI** as a viable synthon to other novel cadmium complexes was influenced by pre-thesis research (December 2015) on the reduction of the cadmium centre to a cadmium hydride (**3**). Optimized synthetic details were further investigated for complexes **XVI** and **3** during this project and have been included in Chapter 2. This created interest in developing a suitable mercury synthon for similar reductions which required the development of a compatible BDI ancillary ligand. The resulting BDI ancillary ligand used for mercury was also used with zinc to act as a comparison and was the basis of further research into novel zinc functionalities.

### 1.7.1 Synthesis of $[Ar-BDI_{Dipp}-H]$

Due to reported unsuccessful attempts with BDI and mercury, an alternative BDI ligand was used. The alternative BDI had success with copper(II) complexes that were found to form similar homolytic complexes.<sup>126</sup> Due to the incorporation of an aryl group across the BDI backbone, the ligand is denoted as  $Ar-BDI_{Dipp}$  where Dipp refers to the flanking 2,6-diisopropylphenyl groups at positions  $R^1$  and  $R^5$  (Figure 3). Ligand synthesis is according to a previously published procedure (Scheme 11).<sup>126</sup> Addition of 2'-fluoroacetophenone to titanium tetrachloride ( $TiCl_4$ ) and 2,6-diisopropylaniline in hexane produced a dense brown precipitate. The imine intermediate was isolated by filtration and dissolved in THF, lithium 2,6-diisopropylanilide was added, after which the reaction mixture changed from a dark orange to a dark yellow solution. Following three days under reflux and workup, the ligand,  $[Ar-BDI_{Dipp}-H]$ , was crystallized as pale yellow-orange crystals from a 1:1 methanol: dichloromethane (DCM) solution.



**Scheme 11: Synthesis of  $[Ar-BDI_{Dipp}-H]$ .**

# Chapter 2

---

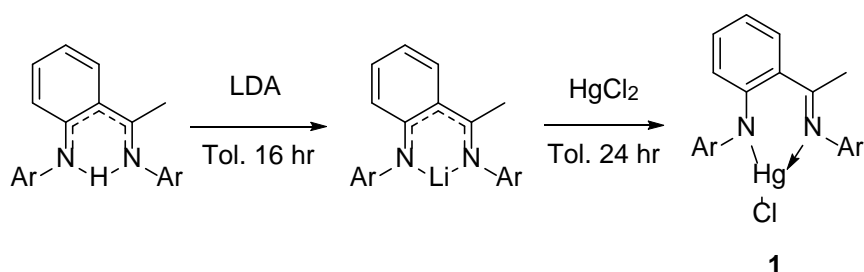
## Results and Discussion

### 2.1 Mercury

#### 2.1.1 Synthesis of $\beta$ -Diketiminato-mercury Chloride

The standard procedure to create the lithium salt of a BDI ligand is to use  $n\text{BuLi}$  as a strong base. To prevent residual  $n\text{BuLi}$  reacting with the mercury halide salt, lithium diisopropylamide (LDA) was used as an alternative strong base as demonstrated in the synthesis of bis- $\beta$ -diketiminato-mercury **II**. To a toluene solution of  $[\text{Ar-BDI}_{\text{Dipp-H}}]$ , a toluene slurry of LDA was added. The light yellow solution was left stirring overnight, after which a dark yellow precipitate had formed. After removing the volatiles *in vacuo*, the lithium salt,  $[\text{Ar-BDI}_{\text{Dipp-Li}}]$ , was isolated as a dark yellow powder. Impurities were further removed by triturations in hexane.

Complex **1** was synthesized by treatment of a toluene slurry of mercury dichloride with a toluene solution of fresh  $[\text{Ar-BDI}_{\text{Dipp-Li}}]$  (Scheme 12). After 24 hours at room temperature the reaction mixture was filtered through celite and the volatiles removed *in vacuo*, yielding a light yellow solid (**1**).



**Scheme 12:** Synthesis of  $[\text{Ar-BDI}_{\text{Dipp-Li}}]$  followed by the synthesis of **1**.

The  $^1\text{H}$  NMR spectrum of **1** shows two septets at  $\delta$  3.48 and 3.11 ppm corresponding to two different environments for the methine proton on the isopropyl groups. Four doublets for the isopropyl methyl groups are found at  $\delta$  1.33, 1.24, 1.14 and 1.04 ppm, producing evidence of an asymmetrical ligand environment. The  $^1\text{H}$  NMR resonances differ from that of  $[\text{Ar-BDl}_{\text{Dipp}}\text{-Li}]$ .

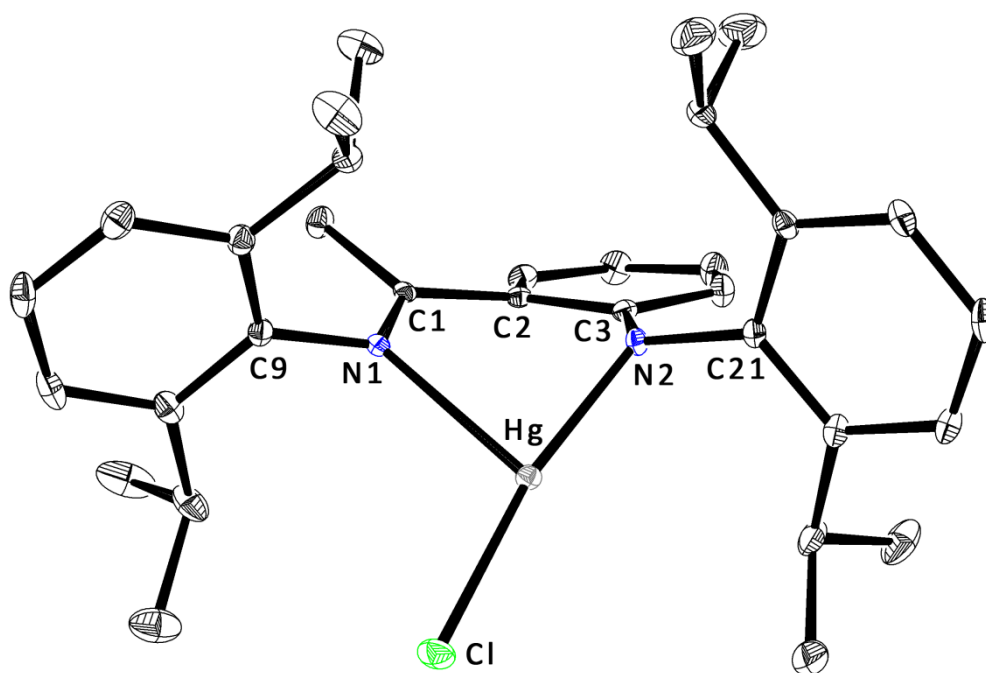


**Figure 13: ORTEP diagram of **1** showing thermal ellipsoids at 30% probability. Hydrogens omitted for clarity.**

Yellow floret-shaped crystals suitable for an X-ray diffraction study were grown from hexane at  $-30\text{ }^{\circ}\text{C}$ . Complex **1** is monomeric in the solid state. The mercury centre has a large angle between N2 and Cl with a N2-Hg-Cl angle of  $169.18^{\circ}$ . The N2-Hg bond length of  $2.044(2)\text{ \AA}$  is significantly shorter than the N1-Hg bond length of  $2.444(2)\text{ \AA}$ , consistent with a more anionic N2-Hg bond and a dative N1-Hg, with the N1-Hg-N2 bond angle approaching  $90^{\circ}$  ( $81.33(7)^{\circ}$ ). The N1-C1 bond length of  $1.441(3)\text{ \AA}$  is shorter than the N2-C3 bond length of  $1.282(3)\text{ \AA}$ , indicating N1 retains its imine character whereas N2 has more amido-imine character. Nitrogens with the amido-imine character are henceforth referred to as an amide. This type of bonding is commonly observed for three coordinate mercury complexes



where the mercury centre remains relatively linear with an added stabilizing dative bond influencing the linear character of the mercury centre.<sup>127-129</sup>

The plane consisting of N1-C1-C2-C3-N2 (referred to herein as BDI plane) exhibits little distortion. The mercury atom is displaced by 1.172 Å from the BDI plane due to the unusual distorted trigonal planar geometry of the mercury metal centre. The angle between the BDI plane and the plane consisting of N1-N2-Hg-Cl is 44.21°.

**Table 5:** Selected bond lengths (Å) and angles (°) for **1**.

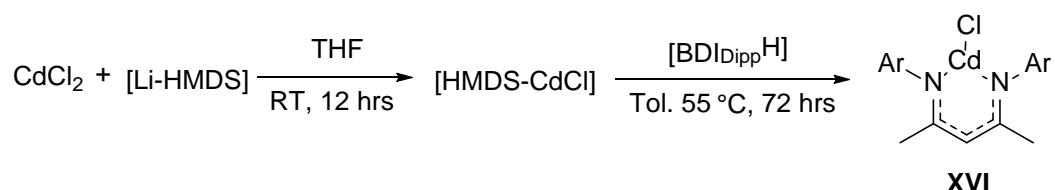
Hg-N1	2.444(2)	Hg-N2	2.044(2)	Hg-Cl	2.2813(7)
N1-C9	1.441(3)	N2-C21	1.442(3)	N2-C3	1.385(3)
C3-C2	1.429(3)	C2-C1	1.480(3)	C1-N1	1.282(3)
N1-Hg-N2	81.33(7)	N1-Hg-Cl	109.48(5)	N2-Hg-Cl	169.18(6)
Hg-N1-C1	119.0(2)	N1-C1-C2	122.1(2)	C1-C2-C3	125.4(2)
C2-C3-N2	123.5(2)	C3-N2-Hg	117.9(2)		

This is the first structurally characterized 3-coordinate  $\beta$ -diketiminato-mercury complex; unfortunately further derivatization of **1** was unsuccessful. Reactions with lithium salts including Li-PCy<sub>2</sub>, Li-PPh<sub>2</sub> and lithium hexamethyldisilazane ([Li-HMDS]) yielded [Ar-BDI<sub>Dipp</sub>-Li] and small amounts of [Ar-BDI<sub>Dipp</sub>-H]. Attempts to synthesize a hydride using lithium tetraethyl borohydride and potassium hydride proved unsuccessful, yielding similar results. The unique structure, geometry and strong Hg-Cl bond in complex **1** possibly hindered salt metathesis with lithium salts and hydride sources. A more pliable substituent, such as HMDS, may yield better reactivity.

## 2.2 Cadmium

### 2.2.1 Alternative Synthesis of $\beta$ -Diketiminato-cadmium Chloride

A new route to  $\beta$ -diketiminato-cadmium chloride (**XVI**) was used in this project. This new route involves two steps instead of three and allows the synthesis of the chloride **XVI** in three days instead of ten (Scheme 13).<sup>49</sup> The intermediate, [HMDS-CdCl], was synthesized *in situ* by addition of one equivalent of [Li-HMDS] to a THF slurry of cadmium chloride. After 24 hours at room temperature, the volatiles were removed *in vacuo* to yield a thick grey oil that contained a single peak in the <sup>1</sup>H NMR spectrum at  $\delta$  0.289 ppm, downfield to both [Li-HMDS] ( $\delta$  0.135 ppm) and [CdHMDS<sub>2</sub>] ( $\delta$  0.210 ppm). Cadmium chloride **XVI** was synthesized by filtering a toluene solution of [HMDS-CdCl], adding a toluene solution of [BDI<sub>Dipp</sub>-H] and stirring for 72 hours at 55 °C. Volatiles were removed *in vacuo*, triturations with hexane further removed impurities. Pure cadmium chloride **XVI** was obtained by crystallization from toluene.



**Scheme 13: Alternative synthesis of XVI.**

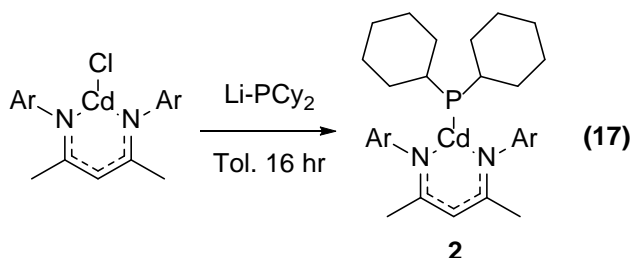
### 2.2.2 Derivatization of $\beta$ -Diketiminato-cadmium Chloride

#### Phosphanide Synthesis

Attempts to generate cadmium-phosphanide complexes from lithium phosphanide salts were attempted via a salt metathesis reaction with **XVI**. The lithium phosphanide salts, Li-PCy<sub>2</sub> and Li-PPh<sub>2</sub>, were used. To remove the possibility of an incomplete salt metathesis in the reaction with chloride **XVI**, a non-coordinating solvent, toluene, was used.

Cadmium dicyclohexylphosphanide (**2**) was synthesized by addition of cadmium chloride **XVI** to a toluene slurry of Li-PCy<sub>2</sub>. After 16 hours the resulting reaction mixture was filtered

through celite and the volatiles were removed *in vacuo* yielding the sticky yellow residue of complex **2** (eq 17). Treatment of cadmium chloride **XVI** with Li-PPh<sub>2</sub> led to multiple products.



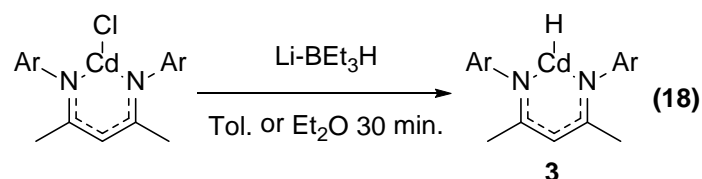
The <sup>1</sup>H NMR spectrum of the reaction mixture is not consistent with a single compound and shows [BDI<sub>Dipp</sub>-Li] and [BDI<sub>Dipp</sub>-H] alongside the suspected new product (phosphanide **2**) indicated by a new singlet from the γ-proton at δ 4.92 ppm, downfield to the γ-proton of chloride **XVI** (δ 4.64 ppm). The <sup>31</sup>P NMR spectrum shows a single peak at δ 5.4 ppm with <sup>113</sup>Cd and <sup>111</sup>Cd satellites which have coupling constants of 570.8 Hz and 545.8 Hz respectively.

The coupling between cadmium and phosphorus can be related to existing compounds. The coupling <sup>1</sup>J<sub>PCd</sub>, seen in <sup>31</sup>P NMR spectroscopy, is around 1500 Hz for a phosphine<sup>130-131</sup> and around 700 Hz for a phosphanide.<sup>132</sup> Although complex **2** has a more up field shift to existing cadmium phosphanides, it was determined that the phosphanide had been successfully bound to the cadmium centre in complex **2** from a salt metathesis reaction. Attempts to produce a crystalline product suitable for an X-ray diffraction study proved unsuccessful. The reaction always produced multiple degradation products which would increase in abundance over time, as such; we were unable to grow crystals of complex **2**.

## Hydride Synthesis

Several hydride sources were screened in order to produce a cadmium hydride from chloride **XVI**. This included potassium hydride, sodium hydride and calcium hydride of which only lithium triethylborohydride, or Super Hydride, resulted in the clean formation of the desired cadmium hydride (**3**). Complex **3** was synthesized by the slow addition of Super Hydride to a toluene or diethyl ether solution of chloride **XVI** (eq 18). The resulting residue

was re-dissolved in a minimum amount of hexane or diethyl ether and kept at -30 °C to produce **3** as a crystalline solid.



The  $^1\text{H}$  NMR spectrum of **3** shows one septet at  $\delta$  3.29 ppm, indicating a single environment for the central proton on the isopropyl groups, and a singlet from the  $\gamma$ -proton at  $\delta$  4.91 ppm, downfield to that of chloride **XVI**. The hydride resonance was found as a very broad signal at  $\delta$  5.63 ppm which was up field to reported cadmium hydride complexes.<sup>35</sup> Due to the broad nature of the hydride peak, cadmium satellites were not observed. The broad signal could be due to coupling to the quadrupolar  $^{14}\text{N}$  nuclei.

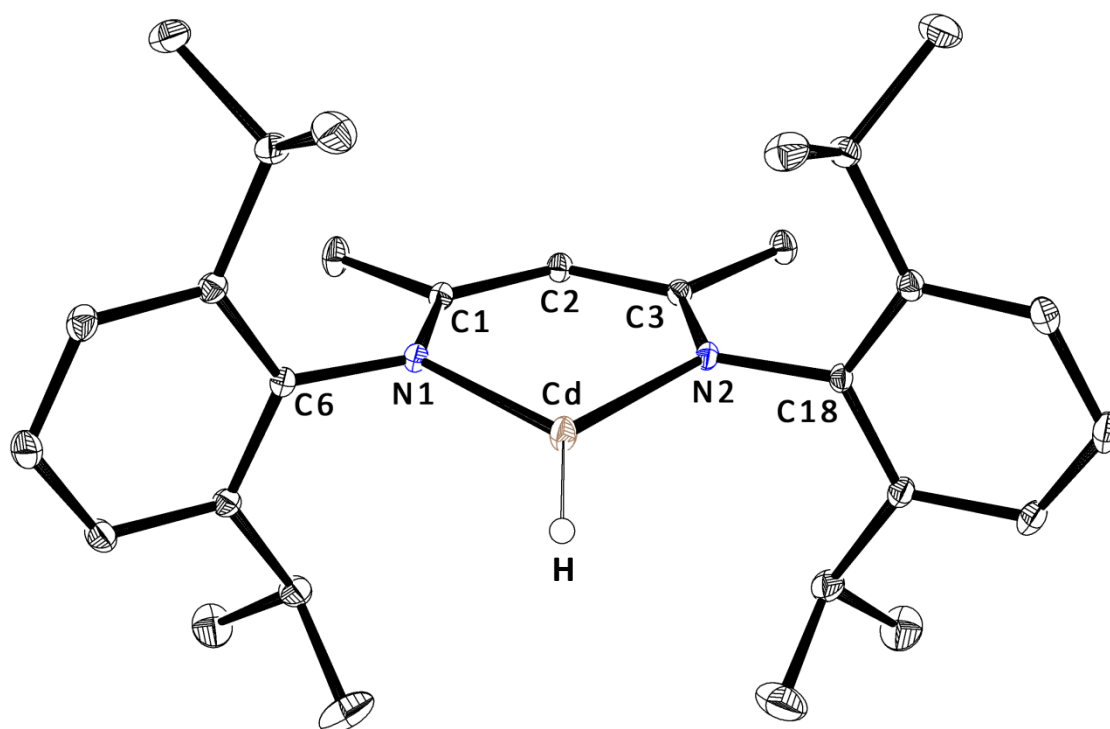


**Figure 14: ORTEP diagram of **3** showing thermal ellipsoids at 30% probability. Selected hydrogens omitted for clarity.**

Small white cubic crystals suitable for an X-ray diffraction study were grown from hexane at -30 °C. Complex **3** is monomeric in the solid state. The 3-coordinate cadmium centre is

co-planar with the BDI backbone. The location of the hydride was calculated from residual densities in the difference density map.

The N1-Cd and N2-Cd bond lengths 2.160(1) and 2.163(1) Å are statistically indistinguishable from each other and show symmetrical bonding to both nitrogens of the ligand. The bite angle, N1-Cd-N2, of 88.45(5)° is similar to other three coordinate  $\beta$ -diketiminato-cadmium complexes involving Dipp groups at the R<sup>1</sup> and R<sup>5</sup> positions, BDI organo-cadmium complexes **X** and **XI**, with bite angles of 88.45° and 90.54°, respectively. The bite angle is larger than *Ar*-BDI organo-cadmium **XII** which used a variation of the ligand with a smaller bite angle range of 86.79-87.35°. <sup>47</sup> The N1-C1 and N2-C3 bond lengths of 1.332(2) and 1.328(2) Å and N1-C6 and N2-C18 bond lengths of 1.432(2) and 1.430(2) Å are statistically indistinguishable from each other, indicative of a delocalized  $\pi$ -system in the BDI backbone.

**Table 6:** Selected bond lengths (Å) and angles (°) for **3**.

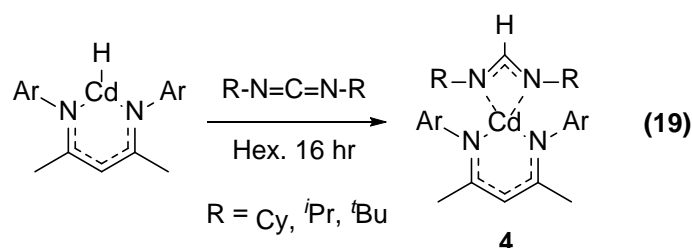
Cd-N1	2.160(1)	Cd-N2	2.163(1)	N1-C6	1.435(2)
N2-C18	1.430(2)	N1-C1	1.322(2)	C1-C2	1.408(2)
C2-C3	1.403(2)	C3-N2	1.328(2)		
N1-Cd-N2	88.44(5)	Cd-N1-C1	125.6(1)	N1-C1-C2	125.2(1)
C1-C2-C3	130.4(1)	C2-C3-N2	124.6(1)	C3-N2-Cd	125.8(1)

The hydride in complex **3** is comparable to the terphenyl hydride complex **XX**'s as they are both terminal cadmium hydride complexes. Similar Cd-H stretches are found, 1734 cm<sup>-1</sup> for **3** and 1735 cm<sup>-1</sup> for monomeric terphenyl cadmium hydride **XX**.<sup>52</sup> Density functional theory (DFT) calculations with THF and **3** showed the cadmium centre does not possess the geometry or available orbitals required to expand its coordination, seen with bridging terphenyl cadmium hydride **XIX**. This was confirmed experimentally as addition of THF does not alter the chemical shifts in the <sup>1</sup>H NMR spectrum at room temperature or with increased temperatures. A melting point of hydride **3** was not obtained as it degrades to a black material upon heating. Slow degradation of hydride **3** was observed in the <sup>1</sup>H NMR spectrum with [BDI<sub>Dipp</sub>-H], small amounts of a homonuclear Cd-Cd dimer (**5**) and a black precipitate, accumulating after two weeks.

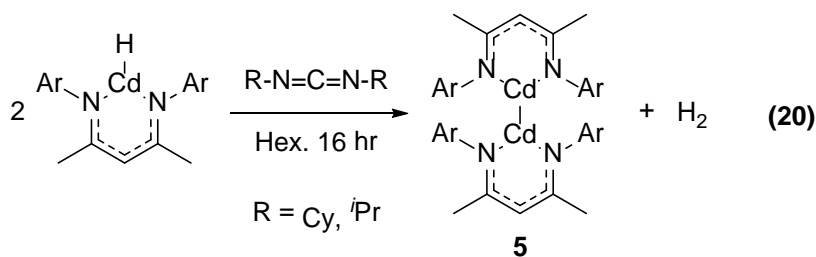
### 2.2.3 Reactivity of $\beta$ -Diketiminato-cadmium Hydride

#### Reactivity with Carbodiimides

The nucleophilicity of the cadmium hydride was examined by the reaction of complex **3** with dicyclohexylcarbodiimide (DCC), diisopropylcarbodiimide (DIC) and di-tert-butylcarbodiimide (DBC). Similar reactivity studies have been conducted with  $\beta$ -diketiminato-tin and  $\beta$ -diketiminato-zinc hydrides<sup>133-134</sup> to give a net insertion of the carbodiimide into the metal hydride bond. As such, with this cadmium hydride an insertion of the carbodiimide was expected to produce the cadmium amidinate, complex **4** (eq 19).



However when DIC or DCC was added to hydride **3**, the product was not the expected insertion amidinate product **4** but was instead the homonuclear Cd-Cd dimer (**5**).



The  $^1H$  NMR spectrum of **5** shows one septet at  $\delta$  3.12 ppm, indicating a single environment for the central proton on the isopropyl groups and a singlet at  $\delta$  4.78 ppm, up-field to hydride **3**. When the reaction was monitored by  $^1H$  NMR spectroscopy,  $H_2$  was observed in the reaction mixture.

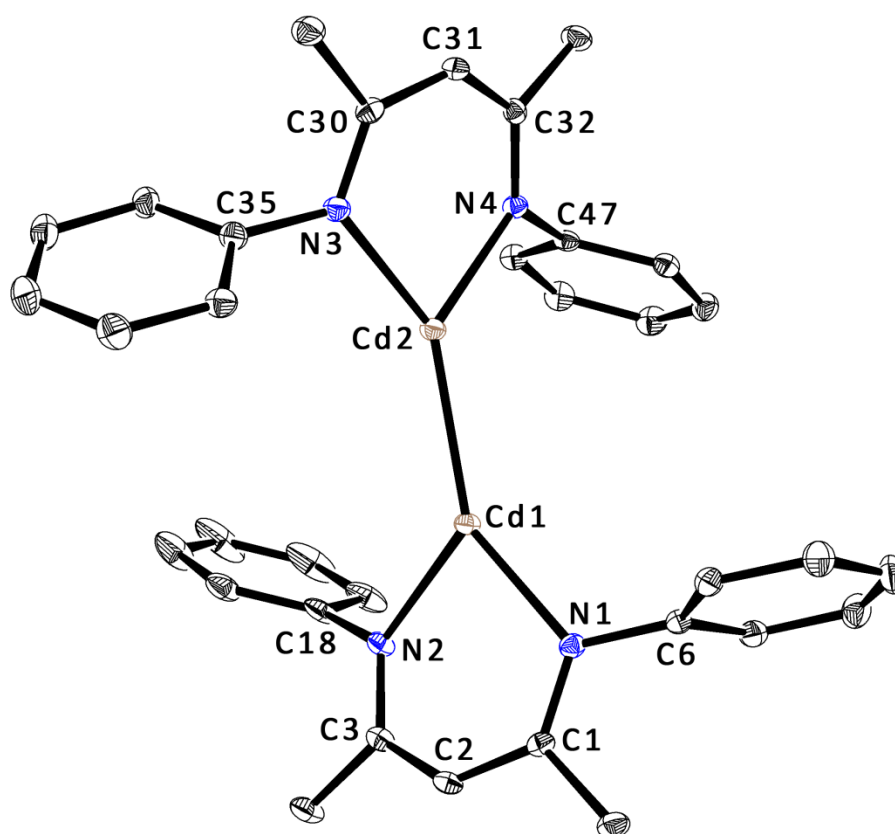


**Figure 15: ORTEP diagram of **5** showing thermal ellipsoids at 30% probability. Isopropyl groups and hydrogens omitted for clarity.**

Small transparent cubic crystals suitable for an X-ray diffraction study were grown from hexane at  $-30\text{ }^{\circ}\text{C}$ . Complex **5** is monomeric in the solid state. The two cadmium centres are not planar with the ligand, displaced by  $0.657\text{ }\text{\AA}$  for Cd1 and  $0.526\text{ }\text{\AA}$  for Cd2 out of the BDI ligand planes, N1-C1-C2-C3-N2 and N3-C30-C31-C32-N4, respectively. Both cadmium centres are three coordinate in a pseudo-trigonal planar conformation. The N-Cd bond lengths are quite similar and range from  $2.197$  to  $2.212\text{ }\text{\AA}$ . The N-Cd bonds are larger than those observed in hydride **3** which can be evidence of a change in the oxidation state of the cadmium centres. In **3** the formal oxidation state of the cadmium was Cd(II), in **5** the cadmium centres changed and approach Cd(I) or a  $[\text{Cd}_2]^{+2}$  core, the increase of the ionic radii resulted in the increased bond lengths to the nitrogens of the BDI ligand.

The nitrogen-carbon bonds of the backbone have a small range from  $1.310$  to  $1.330\text{ }\text{\AA}$ , indicative of a delocalized  $\pi$ -system in the BDI backbones. The two bite angles, N1-Cd1-N2 and N3-Cd2-N4, of  $87.14(8)^{\circ}$  and  $87.46(8)^{\circ}$  are similar to hydride **3** and the other three

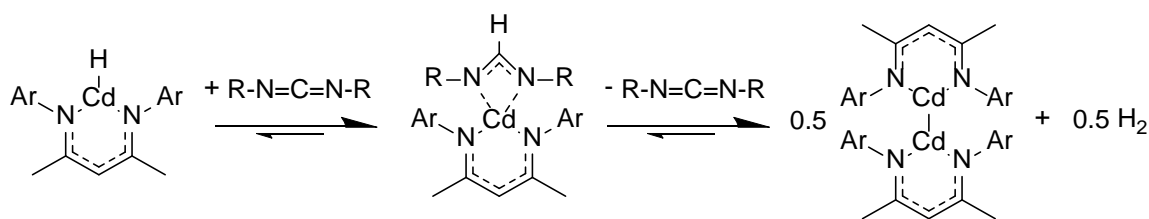
coordinate  $\beta$ -diketiminato-cadmium complexes.<sup>28, 47-49</sup> The cadmium atoms in **5** have a Cd1-Cd2 bond length of 2.5952(4) Å which is longer than the two coordinate cadmium centres in homonuclear dimer complexes **XXI** and **XXII**, which have Cd-Cd bond lengths of 2.574 and 2.579 Å, respectively.<sup>35, 40</sup> The BDI-cadmium centres are not planar to each other and are rotated 74.57° from the other, potentially due to the sterics of the isopropyl groups in the solid state. The <sup>1</sup>H and <sup>13</sup>C NMR spectra indicate that the ligands at Cd1 and Cd2 are symmetrical in solution as only one set of signals for the BDI ligand is observed.

**Table 7:** Selected bond lengths (Å) and angles (°) for **5**.

Cd1-Cd2	2.5952(4)	Cd1-N1	2.200(2)	Cd1-N2	2.212(2)
N1-C1	1.330(3)	C1-C2	1.399(4)	C2-C3	1.405(4)
C3-N2	1.316(3)	N1-C6	1.432(4)	N2-C18	1.429(4)
Cd2-N3	2.197(2)	Cd2-N4	2.205(2)	N3-C30	1.328(3)
C30-C31	1.408(4)	C31-C32	1.403(4)	C32-N4	1.310(3)
N3-C35	1.436(3)	N4-C47	1.438(3)		
N1-Cd1-N2	87.14(8)	Cd1-N1-C1	121.7(2)	N1-C1-C2	125.3(2)
C1-C2-C3	130.8(2)	C2-C3-N2	124.2(2)	C3-N2-Cd1	122.8(2)
N3-Cd2-N4	87.46(8)	Cd2-N3-C30	122.1(2)	N3-C30-C31	125.4(2)
C30-C31-C32	130.9(2)	C31-C32-N4	123.9(2)	C32-N4-Cd2	124.7(2)
N1-Cd1-Cd2	141.65(6)	N2-Cd1-Cd2	130.96(6)	N3-Cd2-Cd1	142.14(6)
N4-Cd2-Cd1	130.00(6)				

The synthesis of complex **5** was only possible upon addition of DCC and DIC to hydride **3**, addition of DBC to **3** resulted in a slow degradation of the cadmium hydride to multiple products. The reaction of complex **3** and DDC or DIC (eq 20) did not occur cleanly with minor products being detected throughout the reaction but repeated isolation attempts only yielded complex **5**. With smaller equivalents (0.5 and 0.1) of DCC and DIC a cleaner and complete conversion of **3** to **5** was observed. Although small amounts of **5** were observed when **3** degrades over time, other degradation products are not observed during the reaction converting complex **3** to **5**. This provides evidence that the reduction of the cadmium hydride is catalytic with DCC or DIC.



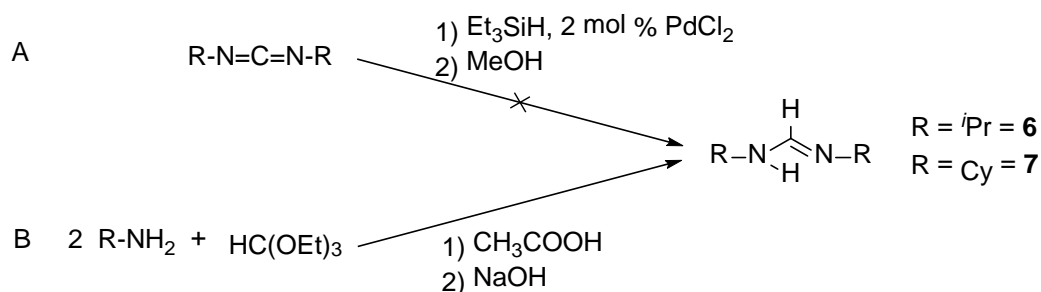


**Scheme 14: Proposed catalytic production of homonuclear Cd-Cd dimer **5** through amidinate **4** from hydride **3**.**

This type of reactivity has never been reported with other metal hydride species or carbodiimides. The mechanism for this transformation is unclear, GC-MS (Gas chromatography MS) analysis of the reaction mixture found primarily DCC or DIC in solution, other volatiles were not observed. The initial step could be the insertion of the carbodiimide into the Cd-H bond to give the amidinate **4**, this could then decompose to give the homonuclear Cd-Cd dimer (Scheme 14). To do this, we attempted to independently synthesize amidinate **4** via multiple methods.

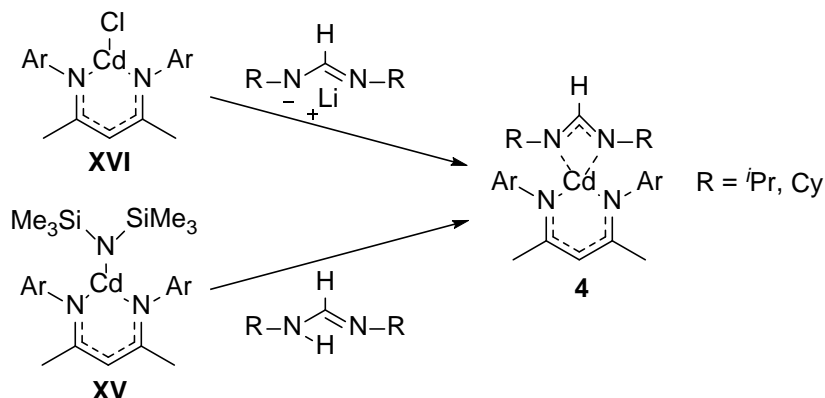
### Cadmium Amidinate Synthesis

Two synthetic methods (A and B) were attempted to synthesize the formamidine starting material (Scheme 15). Method A involved adding a catalytic amount of palladium dichloride and triethylsilane to neat DIC, although this route was reported, we were unable to obtain the desired formamidine.<sup>135</sup> Method B is a known method that involves addition of acetic acid to triethylorthoformate and two equivalents of either neat diisopropylamine or neat cyclohexylamine to form formamidines **6** and **7** respectively.<sup>136-137</sup> Method B proved successful.



**Scheme 15: Methods A and B to generate complexes **6** and **7**.**

Two methods were attempted to synthesize the cadmium amidinate **4**, either via salt metathesis between cadmium chloride complex **XVI** and lithium amidinate or by treatment of cadmium HMDS complex **XV** with the formamidine (Scheme 16).



**Scheme 16: Proposed routes to complex 4.**

The method using the lithium amidinate was attempted by addition of  $n$ BuLi to diisopropyl formamidine **6** in hexane generating the lithium amidinate, which was then added to a toluene solution of chloride **XVI**. Small white cubic crystals suitable for an X-ray diffraction study from a filtered reaction mixture at  $-30\text{ }^{\circ}\text{C}$ . These crystals were not the expected amidinate product (**4**) but were instead a lithium atom coordinating many amidinate molecules in a “caged” structure. The  $^1\text{H}$  NMR spectrum shows a singlet at  $\delta$  8.46 ppm for the proton on the amidinate backbones and a septet at  $\delta$  3.38 ppm which indicates a single environment for the central proton on the isopropyl groups of the amidinates.

When cadmium dichloride was used instead of cadmium chloride **XVI**, a different signal was observed in the  $^1\text{H}$  NMR spectrum. The  $^1\text{H}$  NMR spectrum showed multiple products, with a singlet at  $\delta$  7.94 ppm with satellites proposed to be  $^{111}\text{Cd}$  and  $^{113}\text{Cd}$  satellites coupling to the proton of the amidinate backbone. The proposed  $^{113}\text{Cd}$ - $^1\text{H}$  coupling constant,  $^3J_{\text{HCd}}$ , is 80.5 Hz and  $^{111}\text{Cd}$ - $^1\text{H}$  with 58.5 Hz (Figure 16). The compound was not isolated from the reaction as the lithium “caged” product would preferentially form over time and would crystallize out of the reaction mixture.

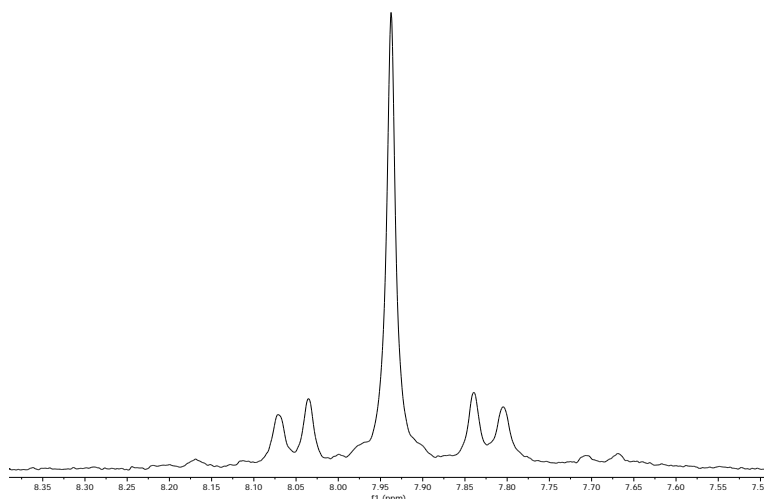
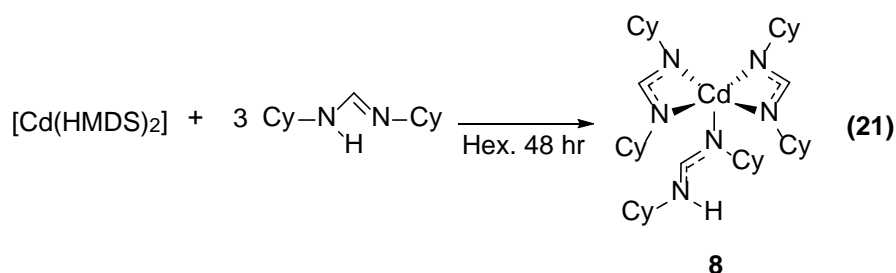


**Figure 16: Possible salt metathesis product showing  $\text{Cd}^{111}$  and  $\text{Cd}^{113}$  satellites.**

The route using cadmium HMDS complex **XV** was first attempted using  $[\text{Cd}(\text{HMDS})_2]$ . A hexane solution of dicyclohexyl formamidine (**7**) was added to a solution of  $[\text{Cd}(\text{HMDS})_2]$  synthesized *in situ*. The reaction mixture yielded a white residue (**8**).



The  $^1\text{H}$  NMR spectrum of **8** shows a singlet at  $\delta$  7.90 ppm, indicating a single environment for the central proton on the amidinate backbone with satellites to cadmium with a coupling constant of 52.4 Hz. The backbone signal is downfield to formamidine **7** ( $\delta$  7.14 ppm). Cyclohexyl peaks are observed as a range of multiplets from  $\delta$  2.04 to 1.28 ppm. Added  $\text{D}_2\text{O}$  would not cause degradation and shifted a broad amine hydrogen peak at  $\delta$  3.15 ppm leaving behind a multiplet determined to be the cyclohexyl ipso-carbon's hydrogen peaks. Transparent rectangular crystals suitable for an X-ray diffraction study were grown from diethyl ether at  $-30^\circ\text{C}$ . Although a crystal structure could not fully solved, the connectivity between the cadmium centre and the formamidine ligands were confirmed.

The success with  $[\text{Cd}(\text{HMDS})_2]$  gave evidence that the method from cadmium amide complex **XV** would be successful. Attempts to use this method to generate the amidinate complex **4** are ongoing.

### Other Reactivity

Addition of phenyl acetylene to hydride **3** resulted in the formation of a black precipitate,  $[\text{BDI}_{\text{Dipp}}\text{-H}]$  and  $\text{H}_2$ . Addition of isocyanate to hydride **3** resulted in a mixture of products, none of which were isolable. Addition of Super Hydride, potassium hydride or sodium hydride to reduce the cadmium in hydride **3** to generate the homonuclear dimer **5** only formed  $[\text{BDI}_{\text{Dipp}}\text{-Li}]$  or  $[\text{BDI}_{\text{Dipp}}\text{-K}]$ .

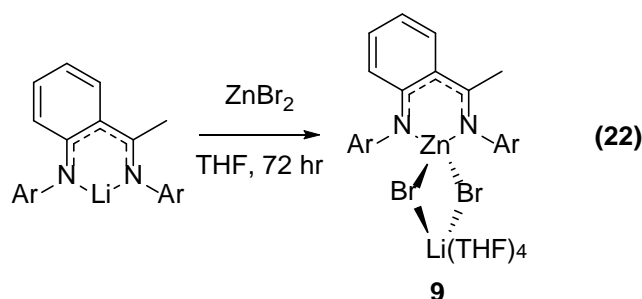
Attempts to synthesize  $[\text{Ar-BDI}_{\text{Dipp}}\text{-CdCl}]$ , a cadmium analogue of mercury chloride **1**, were unsuccessful. The salt metathesis route used in the synthesis of complex **1** produced many products with cadmium dichloride, none of which were solid or cleanly isolable. Cadmium halide salts tend to react in ethereal solvents so the route used to synthesize chloride **XVI** was attempted but addition of  $[\text{Ar-BDI}_{\text{Dipp}}\text{-H}]$  to  $[\text{HMDS-CdCl}]$  did not result in the formation of any isolable products.

## 2.3 Zinc

### 2.3.1 Synthesis of a Novel $\beta$ -Diketiminato-zinc Bromide

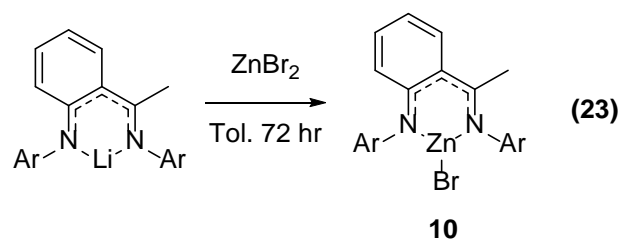
As the ligand  $[Ar-BDI_{Dipp-H}]$  was able to coordinate to mercury(II), a zinc analogue was synthesized as a comparison.  $[Ar-BDI_{Dipp-Li}]$  was generated by adding a solution of  $^nBuLi$  to a toluene solution of  $[Ar-BDI_{Dipp-H}]$ .<sup>126</sup> The intensely yellow precipitate was collected by removing the volatiles *in vacuo*; impurities were further removed via triturations in hexane.

The first attempt at generating a  $\beta$ -diketiminato-zinc bromide using the novel BDI involved addition of  $[Ar-BDI_{Dipp-Li}]$  to a zinc dibromide slurry in THF. Unfortunately, only a bright yellow oil was isolated, complex **9** (eq 22).



The  $^1H$  NMR spectrum of **9** shows two septets at  $\delta$  3.50 and 3.03 ppm indicating two environments for the methine proton on the isopropyl groups. The proton resonances differ to  $[Ar-BDI_{Dipp-Li}]$ . Resonances associated with THF are situated at  $\delta$  3.57 and 1.24 ppm, consistent with coordinated THF molecules integrating for 16 hydrogens, indicating four THF molecules are incorporated. Although this complex could never be isolated in the solid state, it is suspected that it is similar to the salt metathesis zinc complex **XXXII** but with more coordinating solvent molecules. This type of reactivity is common with group 12  $\beta$ -diketiminato complexes.<sup>28, 85</sup>

To avoid coordinating solvents, toluene was then used as an alternative. A toluene solution of  $[Ar-BDI_{Dipp-Li}]$  was added to a toluene solution of zinc dibromide (eq 23). The reaction retained a strong yellow colour. After 72 hours the reaction mixture was filtered and the volatiles removed *in vacuo* to give a bright yellow solid (**10**).



The  $^1\text{H}$  NMR spectrum shows two septets at  $\delta$  3.34 and 2.83 ppm corresponding to two different environments for the methine proton on the isopropyl groups and four doublets for the isopropyl methyl groups at  $\delta$  1.37, 1.31, 1.25 and 0.99, evidence of an asymmetrical ligand environment. The  $^1\text{H}$  NMR resonances differ to  $[\text{Ar-BDl}_{\text{Dipp}}\text{-Li}]$ .

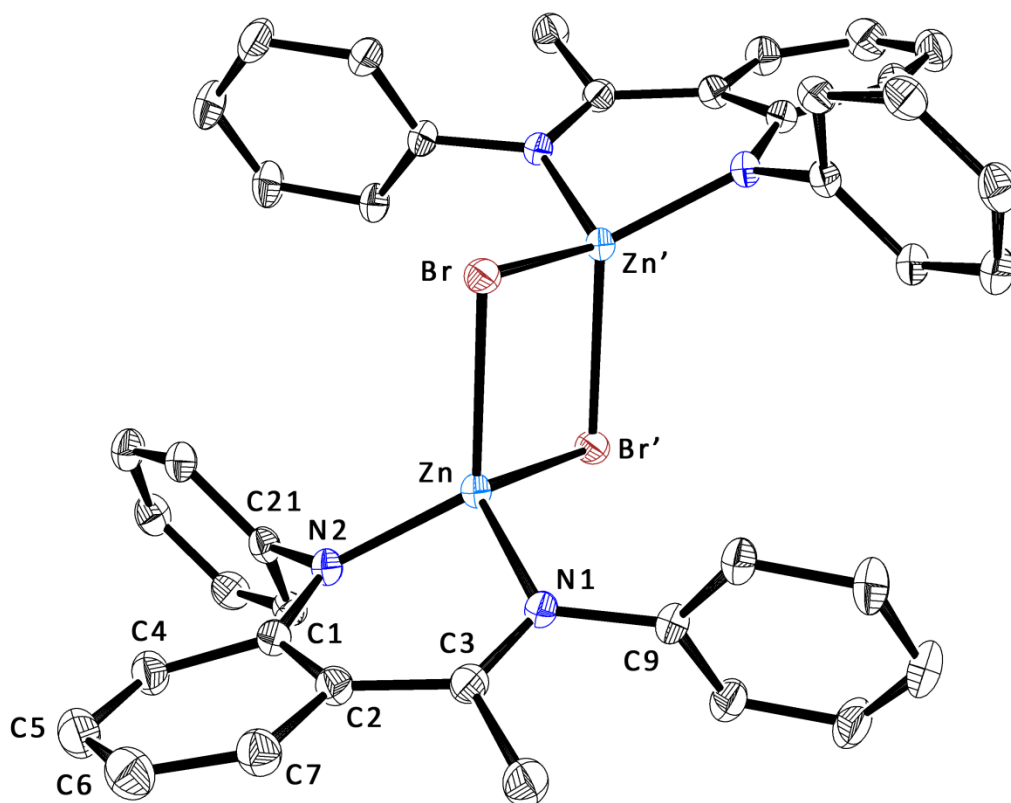


**Figure 17: ORTEP diagram of 10 bridged dimer showing thermal ellipsoids at 30% probability. Isopropyl groups and hydrogens omitted for clarity.**

Small bright yellow cubic crystals suitable for an X-ray diffraction study were grown from hexane at -30 °C. Complex **10** is a bridged dimer in the solid state in which the bromide atoms bridge the zinc centres. The zinc lies out of the BDI backbone plane (N1-C3-C2-C1-N2) by 0.546 Å. The N1-Zn-N2 plane is bent 23.68° from the BDI plane. The backbone aryl group plane consisting of C1-C2-C4-C5-C6-C7 is also bent to a small degree (8.13°) from the BDI plane.

The bridging metallocycle (Zn-Br-Zn'-Br') is planar, with the Br-Zn-Br' angle being 89.30(2)° and the Zn-Br-Zn' angle being 90.70(2)°. The geometry of the zinc metal centre is a distorted tetrahedral with the BDI ligand bite angle of 95.8(1)°. The BDI bite angle is similar to the zinc phosphanide **XXX** but smaller than reported bridged β-diketiminato-zinc bromide complexes which exhibit a BDI bite angle range of 96.67-98.33° and a bridging bromide bite angle range of 101.26-103.29°. <sup>28</sup>

The Zn-N1 bond length of 1.998(3) Å is longer than the Zn-N2 bond length of 1.940(2) Å. This is consistent with different types of nitrogen ligands; N1 can be considered an imine, a neutral ligand, whereas N2 can be considered an amide, an anionic ligand. N1 has more imine or double bond character, as observed by the shorter N1-C3 bond length of 1.308(5) Å compared to N2 with a longer N2-C1 bond length of 1.356(5) Å. This asymmetry has been observed with copper complexes bearing this ligand.<sup>126</sup> For existing β-diketiminato-zinc complexes bearing asymmetric BDI ligands the amide nitrogens Zn-N bond distance range from 1.907 to 1.949 Å and to the backbone carbon range from 1.340 to 1.374 Å. For the imine nitrogens, the Zn-N bond distance range from 1.978 to 2.044 Å and to the backbone carbon range from 1.289 to 1.318 Å.<sup>67-68, 81</sup>

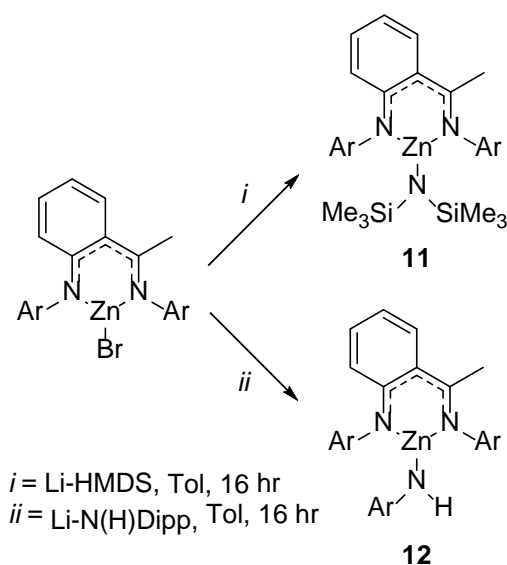
The Zn-Br bond is 2.5177(5) Å and the Zn-Br' bond is 2.4503(5) Å. The zinc-bromide bond lengths are longer than standard zinc dibromide at 2.21 Å<sup>124</sup> due to the bridging and electron sharing between two zinc atoms. The Zn-Br bond lengths are similar to reported bridged β-diketiminato-zinc bromides, one bromide bears a shorter bond length ranging 2.402-2.408 Å and one bromide bears longer bond length ranging 2.418-2.435 Å.<sup>28</sup>

**Table 8:** Selected bond lengths (Å) and angles (°) for **10**.

Zn-N1	1.998(3)	Zn-N2	1.940(2)	N1-C3	1.308(5)
C3-C2	1.455(4)	C2-C1	1.437(5)	C1-N2	1.356(5)
N1-C9	1.449(4)	N2-C21	1.442(4)	Zn-Br	2.5177(5)
Zn-Br'	2.4503(5)	Zn'-Br	2.4503(5)	Zn'-Br'	2.5177(5)
N1-Zn-N2	95.8(1)	Zn-N1-C3	122.0(2)	N1-C3-C2	123.8(3)
C2-C1-N2	124.0(3)	C1-N2-Zn	121.1(2)	Br-Zn-Br'	90.70(2)
Zn-Br-Zn'	89.30(2)	N1-Zn-Br	114.56(8)	N2-Zn-Br	119.45(8)
N1-Zn-Br'	117.54(8)	N2-Zn-Br'	120.69(8)		

### 2.3.2 Derivatization of a Novel $\beta$ -Diketiminato-zinc Bromide

#### Synthesis of Amides



**Scheme 17:** Syntheses of zinc amides **11** and **12** from **10**.

Addition of [Li-HMDS] to zinc bromide **10** resulted in the formation of a zinc HMDS complex (**11**). This complex has a similar intense yellow colour to that of **10** (Scheme 17). The  $^1\text{H}$  NMR spectrum of **11** shows two septets at  $\delta$  3.47 and 3.00 ppm corresponding to two different environments for the methine proton on the isopropyl groups and four doublets for the



isopropyl methyl groups at  $\delta$  1.45, 1.29, 1.17 and 0.97 ppm. These peaks are evidence of an asymmetrical ligand environment. The  $^1\text{H}$  NMR resonances differ to zinc bromide **10**. There is a large singlet at -0.03 ppm integrating for 18 protons for the HMDS substituent, up-field from protonated HMDS and [Li-HMDS].

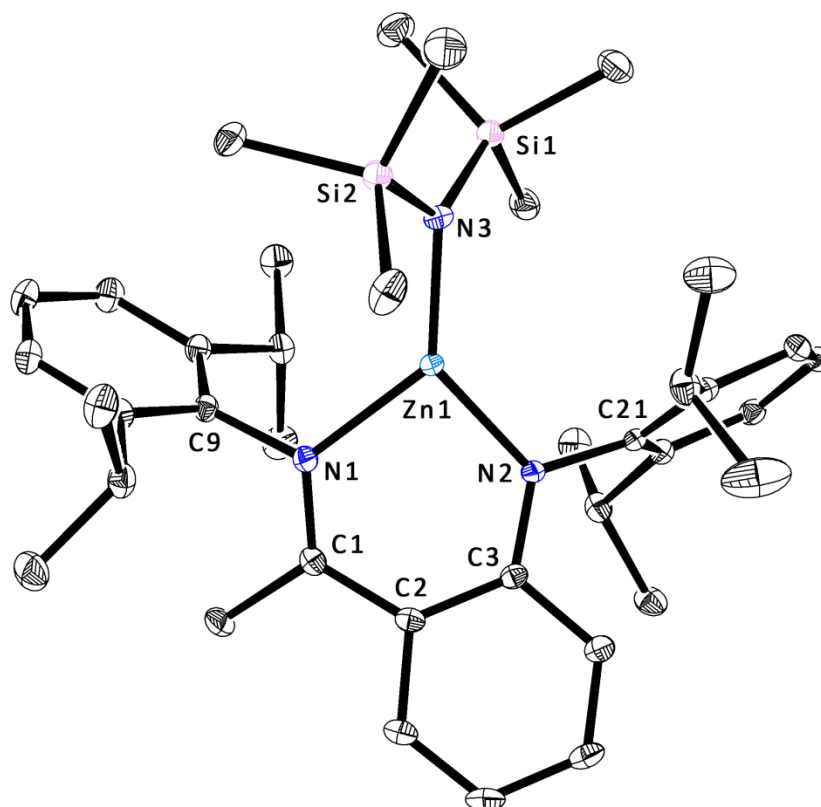


**Figure 18: ORTEP diagram of one molecule of **11** showing thermal ellipsoids at 30% probability. Hydrogens omitted for clarity.**

Bright yellow rectangular plate-like crystals suitable for an X-ray diffraction study were grown from hexane at -30 °C. Complex **11** is a monomer in the solid state and shows two crystallographically identical independent molecules not related by symmetry in the asymmetric unit. The plane consisting of Si1-N6-Si2 is 62.24° to the N1-Zn1-N2 plane potentially due to the crystal packing. Other  $\beta$ -diketiminato-zinc HMDS compounds are all rotated differently to accommodate differing packing and ligand sterics.<sup>27, 66, 74, 78, 82</sup>

Similar to zinc bromide **10**, the two Zn-N bond lengths differ to each other. The Zn-N1 bond length of 2.017(1) Å is longer than the Zn-N2 bond length of 1.906(1) Å, consistent with different types of nitrogen ligands. N1 can be considered an imine, a neutral ligand, whereas

N2 can be considered an amide, an anionic ligand. N1 has more imine or double bond character due to the shorter N1-C1 bond length of 1.312(2) Å compared to N1 with a longer N2-C3 bond length of 1.362(2) Å.

The Zn-N3 bond length is 1.887(2) Å and the N3-Si bonds are 1.711(2) and 1.715(2) Å. These bond distances are similar to existing  $\beta$ -diketiminato-zinc HMDS compounds which have Zn-N bonds ranging from 1.880 to 1.897 Å and N-Si bond distances ranging from 1.702 to 1.723 Å.<sup>27, 47, 66, 74, 78, 82, 138</sup>

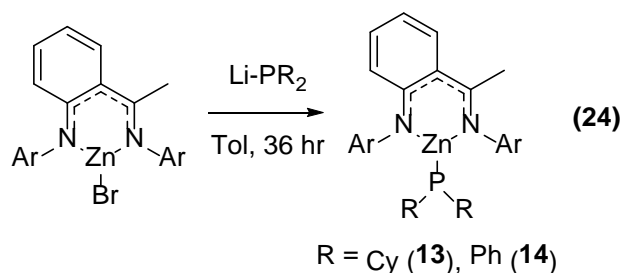
**Table 9:** Selected bond lengths (Å) and angles (°) for **11**.

Si2-N3	1.715(2)	Si1-N3	1.711(2)	Zn1-N3	1.887(2)
Zn1-N2	1.906(1)	Zn1-N1	2.017(1)	N2-C21	1.434(2)
N1-C9	1.447(2)	N2-C3	1.362(2)	C3-C2	1.442(2)
C2-C1	1.462(2)	C1-N1	1.312(2)		
N1-Zn1-N2	95.65(6)	Zn1-N1-C1	123.6(1)	N1-C1-C2	123.5(2)
C1-C2-C3	125.7(2)	C2-C3-N2	123.4(2)	C3-N2-Zn1	124.3(1)
Zn1-N3-Si1	113.79(9)	Zn1-N3-Si2	112.01(9)	Si2-N6-Si1	123.8(1)
N3-Zn1-N1	130.25(6)	N3-Zn1-N2	134.04(7)		

Addition of lithium 2,6-diisopropylphenyl amide (Li-N(H)Dipp) to zinc bromide **10** gives an anilido complex **12**. The <sup>1</sup>H NMR spectrum of **12** shows three septets at  $\delta$  3.33, 2.93 and 2.54 ppm corresponding to two different environments for the methine proton on the isopropyl groups and one for the NH(Dipp) group, all integrating for two protons. The <sup>1</sup>H NMR spectrum shows four doublets for isopropyl methyl groups at  $\delta$  1.26, 1.10, 1.08 and 0.99 ppm which integrate for 6 protons each, denoted as the BDI ligand isopropyl groups, and a doublet at 1.02 ppm integrating for 12 protons, denoted as the NH(Dipp) isopropyl groups. A singlet for the proton off the amide is at 2.96 ppm, integrating for a single proton. This confirms the incorporation of the NH(Dipp) group via a salt metathesis reaction.

Intensely yellow floret-shaped crystals were grown in hexane at room temperature within 12 hours. Despite repeated attempts, the crystals were not suitable for an X-ray diffraction study. This was the first BDI zinc complex to include an aryl amine, other nitrogen containing substituent are either HMDS<sup>27, 66, 74, 78, 82</sup> or a small amine.<sup>69, 75</sup>

### Synthesis of Phosphanides



Zinc-phosphanide complexes from lithium phosphanide salts were attempted via a salt metathesis reaction with **11**. The lithium phosphanide salts Li-PCy<sub>2</sub> and Li-PPh<sub>2</sub> were used.  $\beta$ -Diketiminato-zinc dicyclohexylphosphanide (**13**) was synthesized by treatment of zinc bromide **11** with Li-PCy<sub>2</sub> (eq 24). To minimize the possibility of incomplete salt metathesis, a non-etheral solvent, toluene, was used.

The <sup>1</sup>H NMR spectrum of **13** shows two septets at  $\delta$  3.42 and 2.98 ppm corresponding to two different environments for the methine proton on the isopropyl groups and four doublets for the isopropyl methyl groups at  $\delta$  1.41, 1.38, 1.14 and 0.98 ppm, evidence of an asymmetrical ligand environment. Cyclohexyl peaks are observed in the <sup>1</sup>H NMR spectrum at  $\delta$  1.58 ppm and between  $\delta$  1.32 and 0.98 ppm. The <sup>31</sup>P NMR spectrum shows a single peak at  $\delta$  -22.3 ppm, downfield to Li-PCy<sub>2</sub> with a shift strikingly similar to zinc dicyclohexylphosphanide **XXX**.

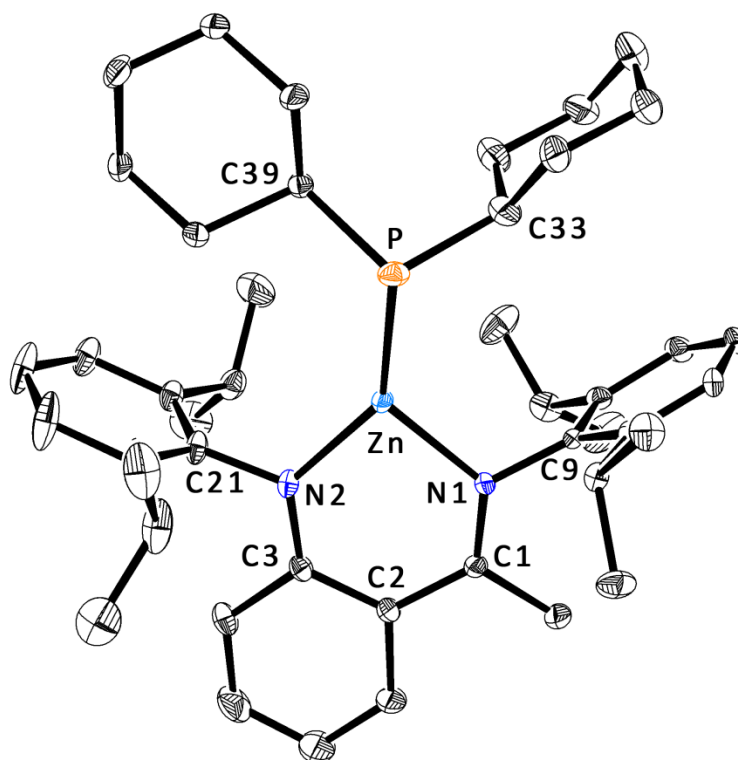


**Figure 19: ORTEP diagram of **13** showing thermal ellipsoids at 30% probability. Hydrogens omitted for clarity.**

Yellow cube shaped crystals suitable for an X-ray diffraction study were grown from hexane at -30 °C. Complex **13** is monomeric in the solid state and shows disorder at one of the cyclohexyl groups and one of the isopropyl peaks. Both positions were modelled and what are shown in Figure 19 are the nuclear positions with the highest occupancy.

Like the previous compounds bearing the same ligand, there are amide and imine nitrogens of the BDI ligand. The shorter N1-C1 bond (1.312(3) Å) and longer N1-Zn bond (2.018(2) Å) indicates N1 is the imine nitrogen. The longer N2-C3 bond (1.351(4) Å) and shorter N2-Zn bond (1.935(2) Å) indicates N2 is the amide nitrogen. The bite angle (N1-Zn-N2) of 93.13(9)° is similar to the other complexes synthesized bearing the same ligand.

The Zn-P bond length, 2.2822(8) Å, is shorter than a dative phosphanide bond with bond lengths ranging 2.393-2.401 Å<sup>93</sup> and a P-metallated phosphasilene with a bond length of 2.367 Å.<sup>97</sup> The Zn1-P1 bond length in complex **13** is closer to that of an internally bound zinc phosphanide in a cluster with bond lengths ranging from 2.302 to 2.334 Å<sup>95</sup>, like zinc dicyclohexylphosphanide **XXX**. The phosphanide ligand is asymmetric to the zinc metal

centre, skewed towards N1 as represented with a shorter N1-Zn-P angle of 127.18(7)° compared to the N2-Zn-P angle of 137.54(7)°. This is observed with zinc dicyclohexylphosphanide **XXX** to a lesser extent. This is evidence the asymmetric BDI ligand has more of an influence on the terminal phosphanide coordination than a symmetrical BDI ligand.<sup>126</sup>

**Table 10:** Selected bond lengths (Å) and angles (°) for **13**.

Zn-P	2.2822(8)	Zn-N1	2.018(2)	Zn-N2	1.935(2)
N1-C1	1.312(3)	C1-C2	1.454(4)	C2-C3	1.442(4)
C3-N2	1.351(4)	N1-C9	1.442(3)	N2-C21	1.435(4)
P-C33	1.896(4)	P-C39	1.94(1)		
N1-Zn-N2	93.13(9)	Zn-N1-C1	126.5(2)	N1-C1-C2	123.1(2)
C1-C2-C3	125.4(3)	C2-C3-N2	123.9(3)	C3-N2-Zn	126.7(2)
N1-Zn-P	127.18(7)	N2-Zn-P	137.54(7)	Zn-P-C33	104.8(1)
Zn-P-C39	105.2(3)	C33-P-C39	107.2(3)		

Addition of Li-PPh<sub>2</sub> to a toluene solution of zinc bromide **10** produced the zinc diphenylphosphanide complex **14** (eq 24). The <sup>1</sup>H NMR spectrum of **14** shows two septets at δ 3.37 and 2.91 ppm corresponding to two different environments for the methine proton on the isopropyl groups and four doublets for the isopropyl methyl groups at δ 1.13, 1.10, 1.07 and 0.95 ppm, evidence of an asymmetrical ligand environment. Phenyl peaks are observed in the <sup>1</sup>H NMR spectrum as multiple peaks around δ 6.88 ppm. The <sup>31</sup>P NMR spectrum shows a single peak at δ -47.7 ppm, downfield to Li-PPh<sub>2</sub> and similar to zinc diphenylphosphanide **XXXI**.

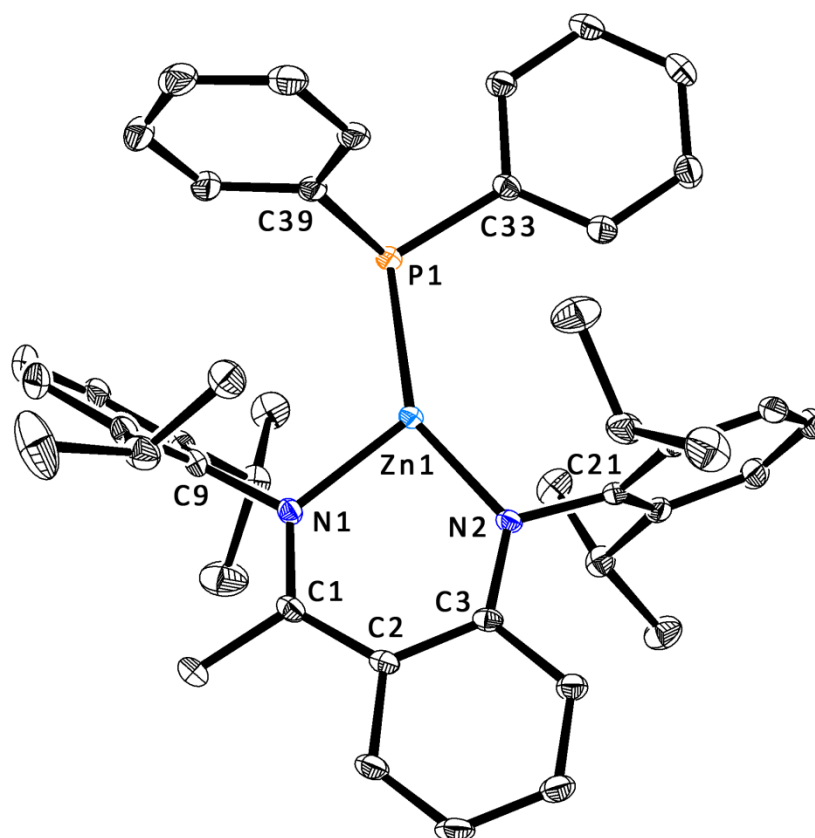


**Figure 20: ORTEP diagram of **14** showing thermal ellipsoids at 30% probability. Hydrogens omitted for clarity.**

Yellow cube shaped crystals suitable for an X-ray diffraction study were grown from hexane at -30 °C. Complex **14** is a monomer in the solid state and shows two crystallographically identical independent molecules not related by symmetry in the asymmetric unit. Like the previous compounds bearing the same ligand, there are amide and imine nitrogens of the BDI ligand. The shorter N1-C1 bond (1.311(6) Å) and longer N1-Zn1 bond (2.019(4) Å) indicates N1 is the imine nitrogen. The longer N2-C3 bond (1.395(6) Å) and shorter N2-Zn1 bond (1.909(4) Å) indicates N2 is the amide nitrogen. The bite angle (N1-Zn-N2) of 93.6(2)° is similar to dicyclohexylphosphanide **13**.

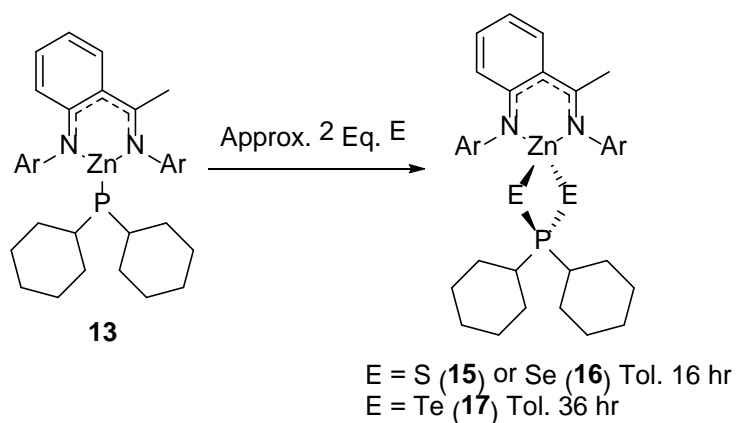
The Zn1-P1 bond length, 2.303(1) Å, is shorter than a dative phosphanide bond with bond lengths ranging 2.393-2.401 Å<sup>93</sup> and a P-metallated phosphasilene with a bond length of 2.367 Å.<sup>97</sup> The Zn1-P1 bond length in complex **14** is closer to that of an internally bound zinc phosphanide in a cluster with bond lengths ranging from 2.302 to 2.334 Å<sup>95</sup>, like the zinc dicyclohexylphosphanide complexes **XXX** and **13**. The phosphanide ligand is asymmetric to

the zinc metal centre, skewed towards N1 as represented with a shorter N1-Zn1-P1 angle of 119.4(1)° compared to the N2-Zn1-P1 angle of 146.1(1)°. This is observed with zinc dicyclohexylphosphanide complexes **XXX** and **13** to a lesser extent. This is further evidence the asymmetric BDI ligand influence on terminal phosphanide coordination.<sup>126</sup>

**Table 11:** Selected bond lengths (Å) and angles (°) for **14**.

Zn1-P1	2.303(1)	Zn1-N1	2.019(4)	Zn1-N2	1.909(4)
N1-C1	1.311(6)	C1-C2	1.494(8)	C2-C3	1.352(7)
C3-N2	1.395(6)	N1-C9	1.478(7)	N2-C21	1.426(7)
P1-C33	1.860(6)	P1-C39	1.831(6)		
N1-Zn1-N2	93.6(2)	Zn1-N1-C1	128.0(3)	N1-C1-C2	119.2(5)
C1-C2-C3	127.8(5)	C2-C3-N2	125.1(4)	C3-N2-Zn1	124.8(3)
N1-Zn1-P1	119.4(1)	N2-Zn1-P1	146.1(1)	Zn1-P1-C33	102.9(2)
Zn1-P1-C39	110.2(2)	C33-P1-C39	101.7(2)		

### Addition of Chalcogens into Zinc Phosphanide Bonds



**Scheme 18:** Synthesis of complexes **15**, **16** and **17** from phosphanide **13**.

Addition of elemental sulfur to a toluene solution of dicyclohexylphosphanide **13** resulted in the formation of a dicyclohexylphosphinodithioate, complex **15** (Scheme 18). The <sup>1</sup>H NMR spectrum of **15** shows two septets at δ 3.65 and 3.15 ppm which correspond to two different environments for the methine proton on the isopropyl groups and four doublets

for the isopropyl methyl groups at  $\delta$  1.63, 1.59, 1.21 and 0.96 ppm, evidence of an asymmetrical ligand environment. Cyclohexyl peaks are observed in the  $^1\text{H}$  NMR spectrum as a range of multiplets from  $\delta$  1.55 to 1.13 ppm. The  $^{31}\text{P}$  NMR spectrum shows a single peak at  $\delta$  93.4 ppm, downfield to complex **13**. Since the NMR active nuclei of sulfur,  $^{33}\text{S}$ , has a low abundance and sensitivity, satellites in the  $^{31}\text{P}$  NMR spectrum are not observed. Intensely yellow crystals were grown in hexane at  $-30\text{ }^\circ\text{C}$ .

Despite repeated attempts, the crystals of **15** were not suitable for an X-ray diffraction study. The downfield phosphorus peak in the  $^{31}\text{P}$  NMR is similar for the other addition complexes **XXXIII** and **XXXIV**. The double addition product, a dicyclohexylphosphinodithioate, is the likely product based on the equivalence of elemental sulfur used.

Addition of selenium powder to a toluene solution of dicyclohexylphosphanide **13** resulted in the formation of the dicyclohexylphosphinodiselenoate, complex **16** (Scheme 18). The  $^1\text{H}$  NMR spectrum of **16** shows two septets at  $\delta$  3.67 and 3.17 ppm corresponding to two different environments for the methine proton on the isopropyl groups and four doublets for the isopropyl methyl groups at  $\delta$  1.64, 1.61, 1.23 and 0.98 ppm, evidence of an asymmetrical ligand environment. Cyclohexyl peaks are observed in the  $^1\text{H}$  NMR spectrum as a range of multiplets from  $\delta$  1.57 to 0.88 ppm. The  $^{31}\text{P}$  NMR spectrum shows a single peak at  $\delta$  51.2 ppm, downfield from dicyclohexylphosphanide **13**, with  $^{77}\text{Se}$  satellites. The  $^{77}\text{Se}$ - $^{31}\text{P}$  coupling constant of 447.9 Hz is consistent with the addition of two selenium atoms to a phosphorus atom seen in  $\beta$ -diketiminato-tin and germanium phosphanide complexes.<sup>125</sup>

When the reaction to synthesize complex **16** is monitored by  $^{31}\text{P}$  NMR spectroscopy, another peak can be observed at  $\delta$  25.6 ppm with  $^{77}\text{Se}$  satellites and a  $^{77}\text{Se}$ - $^{31}\text{P}$  coupling constant of 145.8 Hz. The coupling is consistent with the addition of one selenium atom to a phosphorus atom seen in reactions with  $\beta$ -diketiminato-tin and germanium phosphanide complexes.<sup>125</sup> The signal at  $\delta$  25.6 ppm is slowly replaced by the signal of the dicyclohexylphosphinodiselenoate at  $\delta$  51.2 ppm over time.



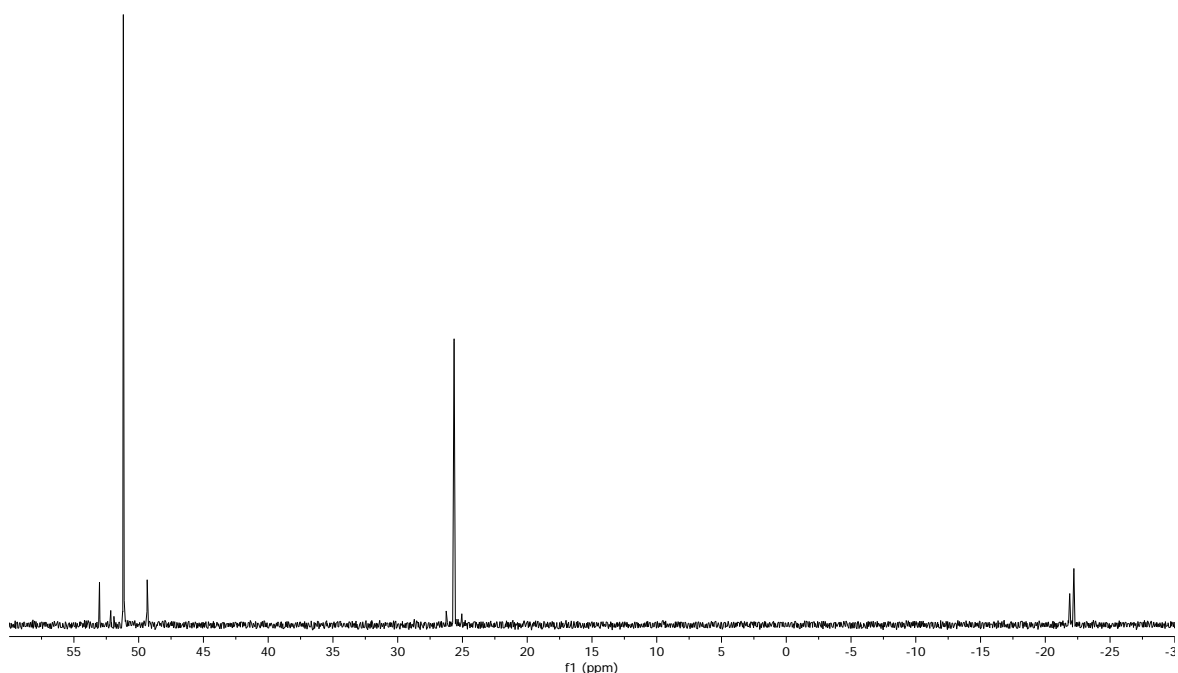
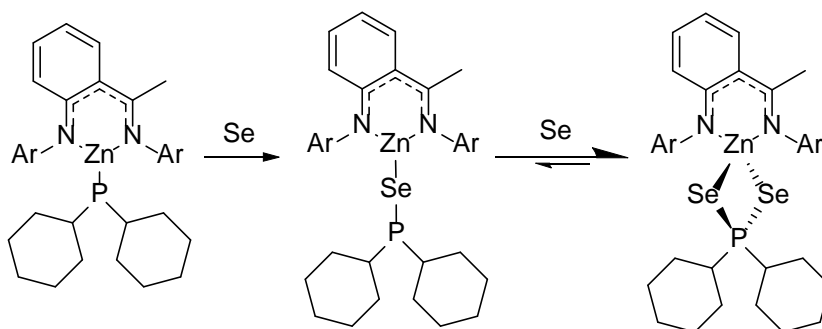


**Figure 21: From left to right. **16** with  $^{77}\text{Se}$  satellites, the dicyclohexylphosphinoselenoite product with smaller  $^{77}\text{Se}$  satellites, unreacted lithium dicyclohexylphosphanide and unreacted **13**.**

It was suspected that the mono-insertion product occurred prior to the addition of a second selenium atom, the equilibrium of which is driven towards the double addition product, dicyclohexylphosphinodiselenoate **16** (Scheme 19). Attempts to isolate the suspected mono-insertion product proved unsuccessful with complex **16** forming preferentially even when treated with a single equivalent or less of selenium powder.



**Scheme 19: Selenium insertion reaction with **13** to generate **16**.**

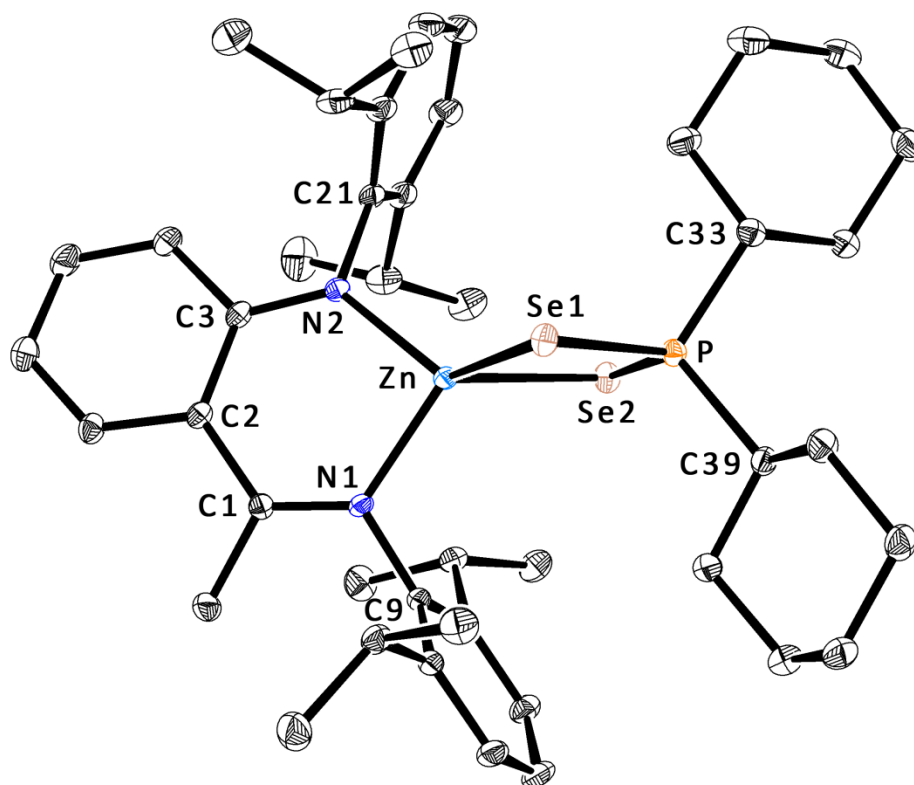


**Figure 22: ORTEP diagram of 16 showing thermal ellipsoids at 30% probability. Hydrogens and solvent molecule omitted for clarity.**

Orange rectangular crystals suitable for an X-ray diffraction study were grown from hexane at  $-30\text{ }^{\circ}\text{C}$ . Complex **16** is monomeric in the solid state with a half a molecule of hexane in the unit cell. The phosphorus atom is formally  $\text{P}^{5+}$  and the selenium atoms are both  $\text{Se}^{2-}$ . The Zn-Se bond lengths of 2.4995(8) and 2.4969(9) Å are very similar where the Se-P bond lengths of 2.166(2) and 2.180(1) Å differ slightly. In contrast to  $\beta$ -diketiminato-germanium dicyclohexylphosphinodiselenoate complexes, which are three coordinate, the dicyclohexylphosphinodiselenoate ligand in complex **16** is bidentate resulting in a tetrahedral zinc centre.<sup>125</sup> The Zn-Se bonds are in range of the Zn-Se bonds in the selenium bridged BDI complex **XXIV** which range from 2.429–2.595 Å.<sup>122</sup> Other Zn-Se bonds from various compounds range from 2.320–2.609 Å.<sup>102–117</sup>

Like the previous compounds bearing the same ligand, there are amide and imine nitrogens of the BDI ligand. The shorter N1–C1 bond (1.317(6) Å) and longer N1–Zn bond (2.004(4) Å) indicates N1 is the imine nitrogen. The longer N2–C3 bond (1.350(7) Å) and shorter N2–Zn1 bond (1.947(3) Å) indicates N2 is the amide nitrogen. The bite angle (N1–Zn–N2) of  $94.2(2)^{\circ}$  is

similar to the other complexes synthesized bearing the same ligand including dicyclohexylphosphanide **13**. The plane consisting of N1-C1-C2-C3-N2 is 87.60° from the plane of the phosphinodiselenoate. The phosphinodiselenoate ligand is square shaped, the Zn-Se1-P and Zn-Se2-P bond angles (80.95(4) and 80.74(4)°) are shorter than the Se1-Zn-Se2 and Se1-P-Se2 bond angles (99.77(3) and 108.42(6)°). The bond lengths and angles of the phosphinodiselenoate ligand are similar to zinc phosphinodiselenoate complexes **XXXIII** and **XXXIV**.

**Table 12:** Selected bond lengths (Å) and angles (°) for **16**.

Zn-N1	2.004(4)	Zn-N2	1.947(3)	N1-C1	1.317(6)
C1-C2	1.458(6)	C2-C3	1.442(7)	C3-N2	1.350(7)
Zn-Se1	2.4995(8)	Zn-Se2	2.4969(9)	Se1-P	2.166(2)
Se2-P	2.180(1)	P-C39	1.835(4)	P1-C33	1.825(5)
N1-C9	1.448(5)	N2-C21	1.432(6)		
N1-Zn-N2	94.2(2)	Zn-N1-C1	124.6(3)	N1-C1-C2	123.6(5)
C1-C2-C3	125.6(5)	C2-C3-N2	123.6(5)	C3-N2-Zn	125.2(3)
Se1-Zn-Se2	89.77(3)	Zn-Se1-P	80.95(4)	Zn-Se2-P	80.74(4)
Se1-P-Se2	108.42(6)	C33-P-C39	107.3(2)	Se1-P-C39	110.0(2)
Se1-P-C33	110.3(2)	Se2-P-C39	111.0(2)	Se2-P-C33	110.3(2)
N1-Zn-Se1	116.4(1)	N1-Zn-Se2	119.2(1)	N2-Zn-Se1	118.6(1)
N2-Zn-Se2	121.1(1)				

Addition of tellurium powder to a toluene solution of dicyclohexylphosphanide **13** resulted in the formation of a dicyclohexylphosphinoditellunoate, complex **17** (Scheme 18). The <sup>1</sup>H NMR spectrum of **17** shows two septets at δ 3.74 and 3.27 ppm corresponding to two different environments for the methine proton on the isopropyl groups and three doublets for the isopropyl methyl groups. The isopropyl signal δ 1.64 ppm integrates for 12 protons and 1.29 and 1.05 ppm integrate for 6 protons each, evidence of an asymmetrical ligand environment. Cyclohexyl peaks are observed in the <sup>1</sup>H NMR as a range of multiplets from δ 1.55 to 0.87 ppm. The <sup>31</sup>P NMR spectrum shows a single peak at δ 160.3 ppm, downfield to dicyclohexylphosphanide **13**. The <sup>125</sup>Te-<sup>31</sup>P coupling is not observed for this complex and

so the double addition product, a zinc dicyclohexylphosphinoditellunoate, is not confirmed by  $^{31}\text{P}$  NMR spectroscopy.

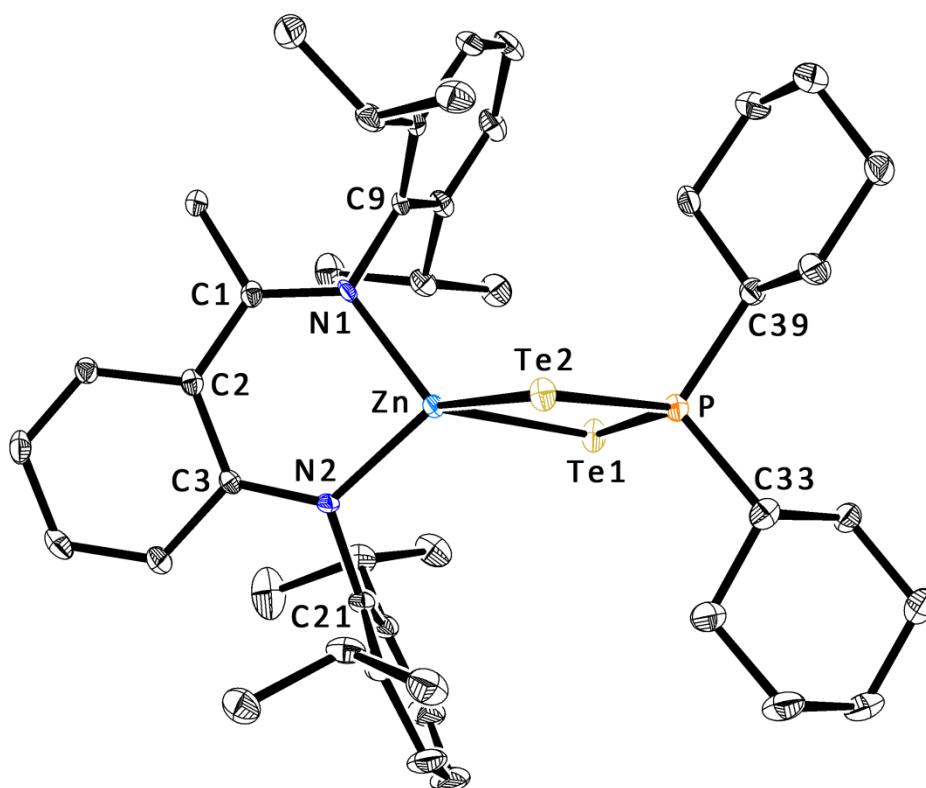


**Figure 23: ORTEP diagram of **17** showing thermal ellipsoids at 30% probability. Hydrogens and solvent molecule omitted for clarity.**

Orange rectangular crystals suitable for an X-ray diffraction study were grown from hexane at  $-30\text{ }^{\circ}\text{C}$ . Complex **17** is monomeric in the solid state with a half a molecule of hexane in the unit cell. The phosphorus atom is formally  $\text{P}^{5+}$  and the selenium atoms are both  $\text{Se}^{2-}$ .

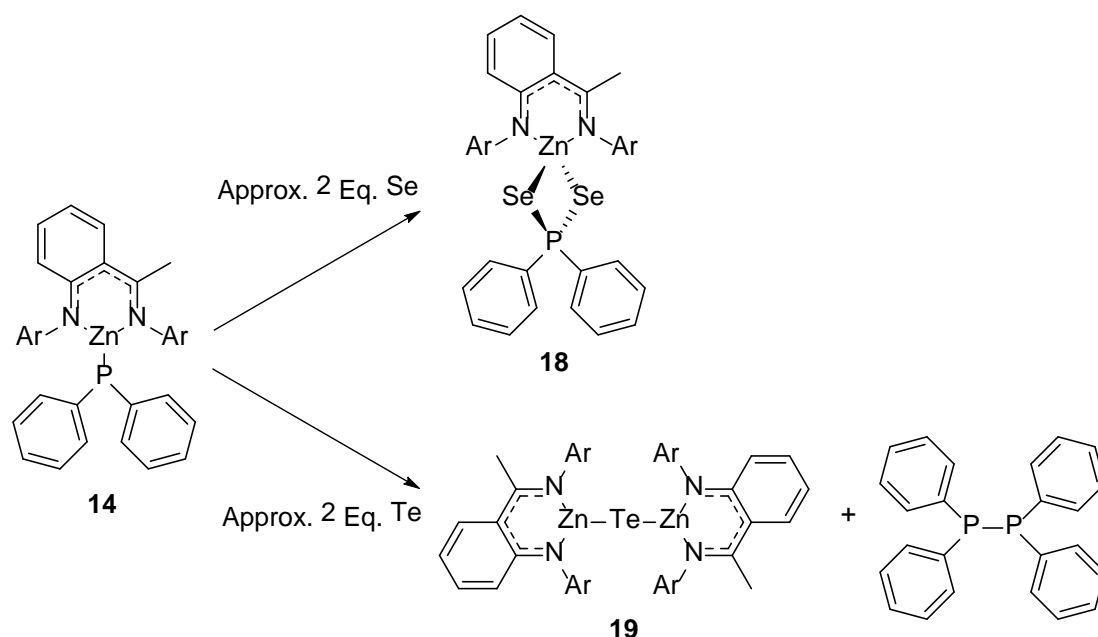
The Zn-Te bond lengths of  $2.6793(6)$  and  $2.6885(8)$  Å and the Te-P bond lengths of  $2.400(1)$  and  $2.412(1)$  Å are similar to each other. In complex **17** the Zn-Te bond lengths are shorter than complexes of zinc bearing a telluride which range from  $2.573$  to  $2.581$  Å.<sup>112, 116, 139</sup> The angles between the zinc and the phosphorus (Zn-Te-P) of  $80.56(3)^{\circ}$  and  $80.16(3)^{\circ}$  are shorter than reported telluride angles bound to zinc ( $97.45$ - $103.84^{\circ}$ )<sup>112, 116, 139</sup> but are similar to dicyclohexylphosphinodiselenoate **16**. In contrast to  $\beta$ -diketiminato-germanium dicyclohexylphosphinoditellunoate complexes, which are three coordinate, the

dicyclohexylphosphinitellunoate ligand in complex **17** is bidentate resulting in a tetrahedral zinc centre.<sup>125</sup>

The BDI ligand has an imine and an amide nitrogen like the previous compounds bearing the same BDI ligand. The shorter N1-C1 bond (1.305(5) Å) and longer N1-Zn bond (2.014(3) Å) indicates N1 is the imine nitrogen. The longer N2-C3 bond (1.353(5) Å) and shorter N2-Zn bond (1.951(3) Å) indicates N2 is the amide nitrogen. The bite angle (N1-Zn-N2) of 93.9(2)° is very similar to dicyclohexylphosphiniteselenoate **16**. The plane consisting of N1-C1-C2-C3-N2 is 87.44° from the plane of the phosphinitellunoate ligand. The phosphiniteselenoate ligand is square shaped, the Zn-Te1-P and Zn-Te2-P bond angles (80.56(3) and 80.16(3)°) are shorter than the Te1-Zn-Te2 and Te1-P-Te2 bond angles (92.01(2) and 106.74(5)°).

**Table 13:** Selected bond lengths (Å) and angles (°) for **17**.

Zn-N1	2.014(3)	Zn-N2	1.951(3)	N1-C1	1.305(5)
C1-C2	1.457(5)	C2-C3	1.440(6)	C3-N2	1.353(5)
Zn-Te1	2.6793(6)	Zn-Te2	2.6885(8)	Te1-P	2.400(1)
Te2-P	2.412(1)	P1-C33	1.837(5)	P1-C39	1.840(4)
N1-C9	1.453(5)	N2-C21	1.434(5)		
N1-Zn-N2	93.9(1)	Zn-N1-C1	124.3(3)	N1-C1-C2	124.4(4)
C1-C2-C3	125.0(4)	C2-C3-N2	123.6(4)	C3-N2-Zn	125.1(3)
Te1-Zn-Te2	92.01(2)	Zn-Te1-P	80.56(3)	Zn-Te2-P	80.16(3)
Te1-P-Te2	106.74(5)	C33-P-C39	107.4(2)	Te1-P-C33	110.2(1)
Te1-P-C39	110.2(1)	Te2-P-C33	110.9(1)	Te2-P-C39	111.5(1)
N1-Zn-Te1	117.9(1)	N1-Zn-Te2	118.0(1)	N2-Zn-Te1	116.1(1)
N2-Zn-Te2	121.2(1)				



**Scheme 20: Synthesis of **18** and **19** from **14**.**

Addition of selenium powder to a toluene solution of diphenylphosphanide **14** resulted in the formation of a diphenylphosphinodiselenoate, complex **18** (Scheme 20). The  $^1\text{H}$  NMR spectrum of **18** shows two septets at  $\delta$  3.78 and 3.27 ppm corresponding to two different environments for the methine proton on the isopropyl groups and four doublets for the isopropyl methyl groups at  $\delta$  1.41, 1.40, 1.26 and 1.03 ppm, evidence of an asymmetrical ligand environment. The  $^{31}\text{P}$  NMR spectrum shows a single peak at  $\delta$  6.1 ppm, downfield from phosphanide **14** with  $^{77}\text{Se}$  satellites.

A  $^{77}\text{Se}$ - $^{31}\text{P}$  coupling constant of 466.5 Hz is consistent with the addition of two selenium atoms to a phosphorus atom seen in  $\beta$ -diketiminato-tin and germanium phosphanide complexes.<sup>125</sup> The downfield phosphorus peak and the  $^{77}\text{Se}$ - $^{31}\text{P}$  coupling in the  $^{31}\text{P}$  NMR are similar to the other phosphinodiselenoate complexes **XXXIII**, **XXXIV** and **16**. This evidence confirms the diphenylphosphinodiselenoate as the product. Dark yellow crystals were grown in hexane at  $-30\text{ }^\circ\text{C}$ . Despite repeated attempts, the crystals of **18** were not suitable for an X-ray diffraction study.

Addition of tellurium powder to a toluene solution of complex **14** resulted in the formation of multiple products. The  $^1\text{H}$  NMR spectrum of the reaction mixture revealed two septets at  $\delta$  3.40 and 2.85 ppm and four doublets at  $\delta$  1.16, 1.14, 1.07 and 1.03 ppm, evidence of an asymmetrical ligand environment. The  $^{31}\text{P}$  NMR spectrum of the reaction mixture shows a single peak at  $\delta$  -15.0 ppm, downfield to  $\text{Li-PPh}_2$  ( $\delta$  -43.9 ppm) and diphenylphosphanide **14**. The  $^{125}\text{Te}$ - $^{31}\text{P}$  coupling is not observed. The crystallized product is a zinc tellunoite bridged dimer (**19**), which does not contain a phosphorus atom so the signal in the  $^{31}\text{P}$  NMR spectrum is from a by-product.

Phenyl resonances in the  $^1\text{H}$  NMR spectrum are at  $\delta$  7.54-7.48 and 6.94-6.89 ppm as multiplets integrating for 10 protons each. In the  $^{13}\text{C}$  NMR spectrum the peaks not associated with isolated **19** are at  $\delta$  136.61, 134.83, 128.90 and 128.59 ppm. The by-product was proposed to be diphenyldiphosphane,  $[(\text{Ph}_2\text{P})_2]$ , due to the reported  $^{31}\text{P}$  NMR shift at -15.2 ppm and  $^{13}\text{C}$  NMR shifts of  $\delta$  136.40, 134.86, 128.76 and 129.27.<sup>140</sup>

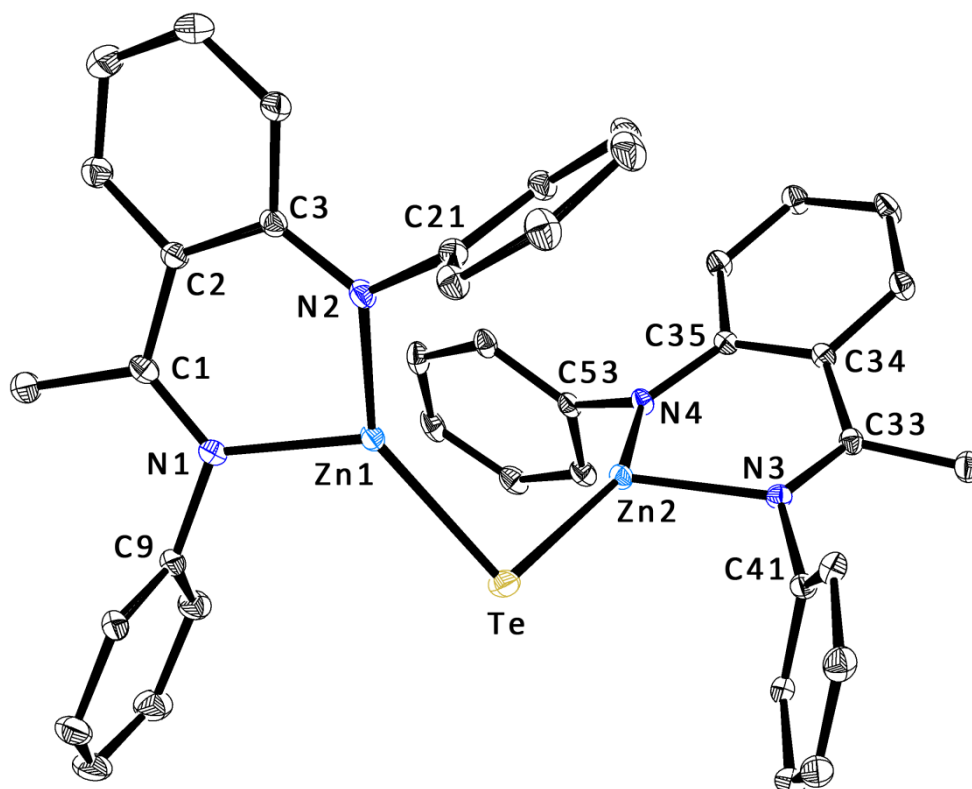


Figure 24: ORTEP diagram of **19** showing thermal ellipsoids at 30% probability. Isopropyl groups, the solvent molecule and hydrogens omitted for clarity.

Golden rectangular plate-like crystals suitable for an X-ray diffraction study were grown from hexane at -30 °C. Complex **19** is monomeric in the solid state with half a molecule of hexane in the unit cell. The tellurium atom is formally  $\text{Te}^{2-}$  with a bent geometry. The Zn1-Te-Zn2 bond angle is  $99.09(2)^\circ$  and has bond lengths to Zn1 and Zn2 of 2.4549(7) and 2.4768(6) Å respectively. In complex **19** the Zn-Te bond lengths are shorter than complexes of zinc bearing a telluride which range from 2.573 to 2.581 Å but the bent angle is within the range of telluride angles involving zinc ( $97.45\text{--}103.84^\circ$ ).<sup>112, 116, 139</sup>

N1 and N3 have longer bonds to their respective zinc centres (1.992(6) and 2.029(4) Å) and shorter bonds to their backbone carbons C1 and C33 (1.307(6) and 1.303(5) Å) making them the imine nitrogens. N2 and N4 have shorter bonds to their respective zinc centres (1.914(4) and 1.910(3) Å) and longer bonds to the backbone carbons C3 and C35 (1.362(6) and 1.374(4) Å) making them the amide nitrogens.

The two BDI ligands are not equivalent and have different bond lengths and angles. The zinc metal centres are displaced from their respective BDI ligand planes (N1-C1-C2-C3-N2 and N3-C33-C34-C35-N4) with Zn1 displaced by 0.426 Å and Zn2 by 0.528 Å. The Zn-Te bonds are skewed, similar to the Zn-P bonds in phosphanide complexes **13**, **14** and **XXX**. For Zn1, Te is skewed towards N1 as represented with a shorter N1-Zn1-Te angle of  $121.5(1)^\circ$  compared to the N2-Zn1-Te angle of  $141.2(1)^\circ$ . For Zn2, Te is skewed towards N3 as represented with a shorter N3-Zn2-Te angle of  $112.6(1)^\circ$  compared to the N4-Zn2-Te angle of  $152.0(1)^\circ$ . For both centres the Te substituent is skewed towards the imine nitrogen of the BDI ligand, similar to phosphanide complexes **13**, **14** which bare the same ligand. The bite angles differ to each other where the N1-Zn1-N2 angle of  $97.1(1)^\circ$  is larger than previous complexes and the N3-Zn2-N4 angle of  $94.2(1)^\circ$  is similar to the complexes synthesized bearing the same ligand.



**Table 14:** Selected bond lengths (Å) and angles (°) for **19**.

Zn1-Te	2.4549(7)	Zn2-Te	2.4768(6)	Zn1-N1	1.992(6)
Zn1-N2	1.914(4)	Zn2-N3	2.029(4)	Zn2-N4	1.910(3)
N1-C1	1.307(6)	C1-C2	1.469(5)	C2-C3	1.447(5)
C3-N2	1.362(6)	N1-C9	1.451(5)	N2-C21	1.438(5)
N3-C33	1.303(5)	C33-C34	1.465(5)	C34-C35	1.437(5)
C35-N4	1.374(4)	N3-C41	1.440(5)	N4-C53	1.442(4)
Zn1-Te-Zn2	99.09(2)	N1-Zn1-N2	97.1(1)	N1-Zn1-Te	121.5(1)
N2-Zn1-Te	141.2(1)	Zn1-N1-C1	122.9(3)	N1-C1-C2	123.3(3)
C1-C2-C3	125.5(3)	C2-C3-N2	124.0(3)	C3-N2-Zn1	122.2(3)
N3-Zn2-N4	94.2(1)	N3-Zn2-Te	112.6(1)	N4-Zn2-Te	152.0(1)
Zn2-N3-C33	124.5(3)	N3-C33-C34	121.7(3)	C33-C34-C35	125.3(3)
C34-C35-N4	124.0(3)	C35-N4-Zn2	121.2(3)		

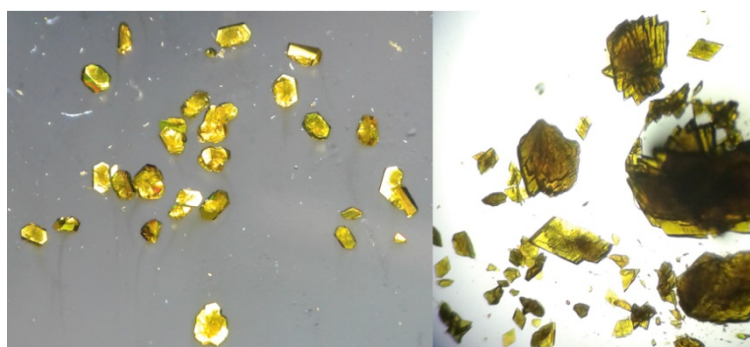


**Figure 25:** Examples of crystals collected under a microscope. Left, Cubic crystals of dicyclohexylphosphanide **13**. Right, Plate-like crystals of tellunoite bridged dimer **19**.

### 2.3.3 Photoluminescence of $\beta$ -Diketiminato-zinc Complexes

Absorption occurs when an incoming photon causes an electron to be excited from a lower electronic energy level to a higher electronic energy level. The excited electron then releases energy to return to the original energy level. This energy release can occur through non-radiative processes such as vibrations or through radiative processes which expels a photon, a process called fluorescence. The expelled photon is lower in energy to the photon that caused the absorption, a phenomenon known as the Stokes Shift. Fluorescent molecules often absorb high energy UV light and emit lower energy visible light. An absorption spectrum reveals the wavelengths of photons absorbed over a broad range of light from the UV range through to the visible range.

The photoluminescent properties of molecules can be probed using a spectrofluorophotometer. Two spectra can be obtained from a spectrofluorophotometer, one to determine the wavelengths and intensities of the photons released during fluorescence (an emission spectrum, using a fixed excitation wavelength) and the wavelengths and intensities of the photons being absorbed or causing the excitation of an observed emission (an excitation spectrum, using a fixed emission wavelength). Quantum yield, or fluorescence quantum yield, ( $\phi_f$ ) is a unitless ratio of photons absorbed to photons emitted, providing information on the efficiency of a molecules fluorescent properties. Emission and excitation intensities and quantum yields have been reported to be influenced by an electron transfer from neighbouring lone pairs on heteroatoms to fluorescing  $\pi$ -systems.<sup>141-145</sup>

During the characterization of zinc bromide **10**, which is intensely yellow in solution, it was found to be fluorescent under a broad range of UV light giving a lime green glow. The amides **11** and **12**, the phosphanides **13** and **14**, and the addition complexes **15**, **16**, **17** and **18** were also found to be fluorescent. The  $\beta$ -diketiminato-zinc complexes **XXX**, **XXXI**, **XXXIII**, and **XXXIV** bear the BDI<sub>Dipp</sub> ligand and are not fluorescent; the  $\pi$ -system of the *Ar*-BDI<sub>Dipp</sub> ligand must be the contributing factor.

The fluorescence was occurring due to binding of the BDI ligand to the d<sup>10</sup> metal ion, zinc,<sup>146</sup> resulting in an increase in the rigidity of the overall structure compared to the protonated

ligand,  $[Ar-BDl_{Dipp}-H]$ , which is not fluorescent. This gives an extended  $\pi$ -system involving the BDI ligand backbone and the metal centre.<sup>147</sup> The mercury chloride **1** does not exhibit fluorescent properties potentially due to an insufficient  $\pi$ -system with the mercury metal centre. The orbitals of the metal centre are not directly involved, either from metal-metal transitions or charge transfers from metal to ligand or ligand to metal. This is because it is difficult to oxidize or reduce a highly stabilized full  $d^{10}$  configuration, as such found in zinc(II).<sup>148</sup> The lithium salt,  $[Ar-BDl_{Dipp}-Li]$ , was not fluorescent and did not readily dissolved in solvents used.

Measurements for absorption and photoluminescence were conducted by dissolving a known amount of a sample in hexane, followed by serial dilutions in order to achieve an absorption of approximately 0.1 Abs for the peak around 440 nm. Hexane was chosen as a solvent to avoid solvating processes. The absorption spectra are presented as the extinction coefficient ( $\epsilon$ ) calculated by Beer-Lambert's Law ( $A = c \cdot \epsilon \cdot l$ ).<sup>149</sup>

An absorption spectrum was collected (Figure 26) followed by an emission spectrum with the fixed excitation wavelength matching the peak found around 440 nm. The emission spectra gave a single broad peak for each compound around 510 nm. The excitation spectra were then collected using the peak around 510 nm for the fixed emission wavelength. The excitation and emission spectra are presented as the intensity normalized by the concentration to allow approximate comparisons (Figure 27).

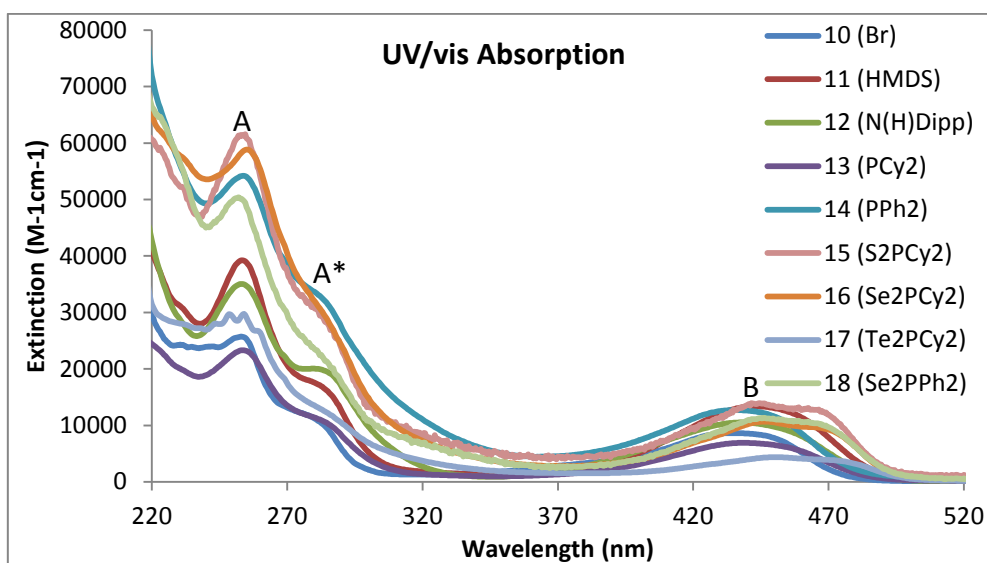


Figure 26: UV/vis absorption spectra of complexes 10-18 between 220 and 520 nm.

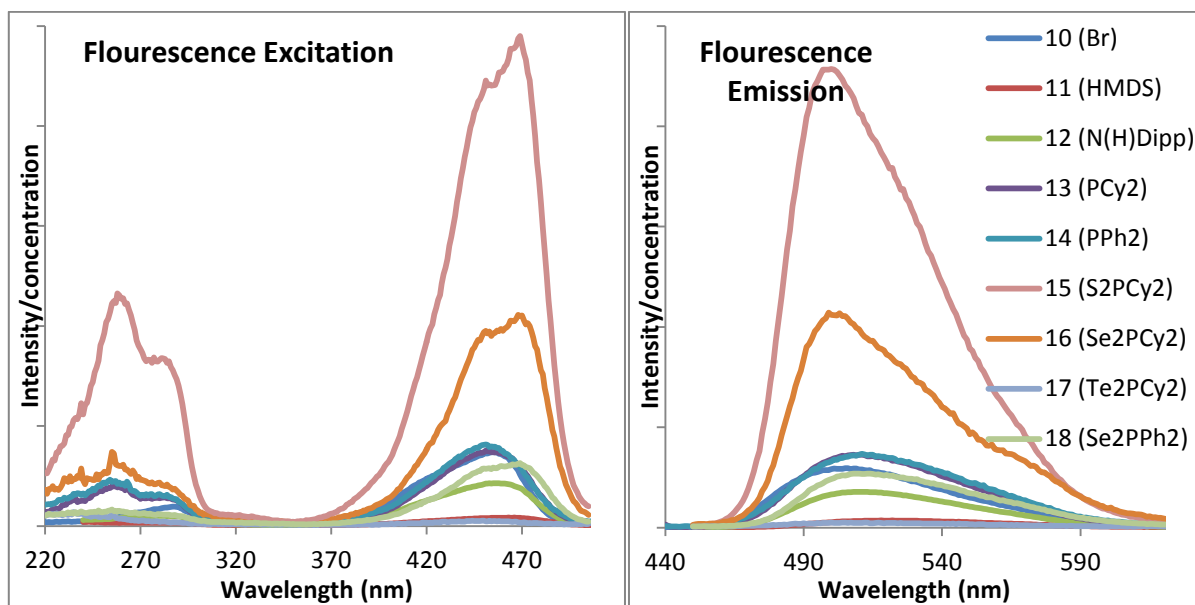


Figure 27: Fluorescence excitation and emission spectra of compounds 10-18.

Quantum yield ( $\phi_f$ ) was calculated for the fluorescent compounds using fluorescein ( $\phi_f = 0.18$ ) in a 2.9 pH citrate-phosphate buffer as a reference, which gives a maximum emission at 510 nm and excitation at 450 nm.<sup>150</sup> The calculation used to determine  $\phi_f$  is shown in equation 25.<sup>151</sup> R is the reference compound, fluorescein, A is absorbance at a specified wavelength and  $\eta$  is the solvent refractive index.

$$\phi_f = \phi_{f(R)} \times \frac{\eta^2}{\eta_{(R)}^2} \times \frac{I}{I_{(R)}} \times \frac{1 - 10^{-A_{(R)}}}{1 - 10^{-A}} \quad (25)$$

Compound	$\lambda_{\max} A$ (nm)	$\epsilon A$ (M <sup>-1</sup> cm <sup>-1</sup> )	$\lambda_{\max} B$ (nm)	$\epsilon B$ (M <sup>-1</sup> cm <sup>-1</sup> )	Excitation (nm)	Emission (nm)	Quantum Yield
10 (Br)	435	8646	253	25722	434	505	0.01
11 (HMDS)	443	13389	253	39222	443	520	0.001
12 (N(H)Dipp)	437	10521	253	35014	437	510	0.007
13 (PCy <sub>2</sub> )	439	6911	253	23278	439	525	0.011
14 (PPh <sub>2</sub> )	436	12703	254	54208	436	525	0.006
15 (S <sub>2</sub> PCy <sub>2</sub> )	446	13901	253	61451	445	510	0.026
16 (Se <sub>2</sub> PCy <sub>2</sub> )	446	10687	255	58868	445	510	0.016
17 (Te <sub>2</sub> PCy <sub>2</sub> )	451	4374	254	29748	442	510	0.001
18 (Se <sub>2</sub> PPh <sub>2</sub> )	446	11315	252	50407	445	510	0.005

Figure 28: Summary showing absorption  $\lambda_{\max}$ , extinction coefficient ( $\epsilon$ ) of  $\lambda_{\max}$  peaks, excitation and emission wavelengths and quantum yield of compounds 10-18.

These spectra show that the excitation and emissions are not blue or red shifted significantly between each compound, as such, the electronic transitions must be same for each compound. The absorption spectra of the zinc complexes shows two peaks at approximately 440 nm (B) and a higher energy peak at 253 nm (A) (Figure 26) note that the higher energy peak has a shoulder at approximately 290 nm (A\*). The literature using this ligand describes similar absorption properties, however the metal centre in the literature, Cu(II), has empty d-orbitals so the transitions were denoted as a  $\pi$ - $\pi^*$  and a d-d transition.<sup>126</sup> This latter transition cannot occur in the zinc complexes.

The transition around 440 nm in the zinc complexes is proposed to be an n- $\pi^*$  transition from an available lone pair (n) on the substituent off the zinc metal centre (a bromide, amide, phosphanide or chalcogenide) based on reported fluorescent zinc complexes.<sup>152-154</sup> The n- $\pi^*$  transition occurs via an electron transfer into the  $\pi^*$  molecular orbitals of the  $\pi$ -system created when the BDI ligand is coordinated to the zinc centre. The n- $\pi^*$  transition is at a lower energy (B) and the  $\pi$ - $\pi^*$  transition is at a higher energy (A) based on the relative energy between those molecular energy levels.

It is difficult to determine the exact orbitals contributing to fluorescence without a similar system to compare to. This type of system is novel and denotations of the transitions are based on fluorescent zinc molecules that do not contain similar substituents and have different ancillary ligands. The transitions proposed could be confirmed with computational analysis. Density functional theory (DFT) is a computational quantum modelling method used to investigate the electronic structure of systems, including atoms and molecules. Time-dependent density functional theory (TD-DFT) is an extension of DFT. TD-DFT is used to investigate the properties of dynamic systems in the presence of time-dependent processes to extract features including excitation energies and photoluminescence spectra. TD-DFT calculations on the fluorescent zinc complexes could accurately model the transitions involved, the calculations of which are currently ongoing.

The  $\phi_f$  are comparable to some zinc complexes involving Schiff bases<sup>148, 155</sup> but less than zinc salen complexes. This is potentially due to the different coordination and intermolecular aggregations occurring with salen complexes.<sup>153, 156</sup> Interestingly the ligands used in

reported fluorescent zinc species often exhibit some fluorescence and are enhanced with zinc coordination<sup>157</sup> In contrast, *Ar*-BDI<sub>Dipp</sub> is only fluorescent when coordinated to a zinc centre.

One of the least fluorescent compounds is zinc HMDS complex **11**. In this complex, the nitrogen lone pair has significant back-bonding into the silicon atoms, thus less overlap with the zinc-ligand  $\pi$ -system would be expected. Although the zinc anilido complex **12** is only mildly fluorescent, anilide ligands typically have less back-bonding of the nitrogen lone pair into the aromatic ring. Quenching of electron transfer has been reported to decrease fluorescence output.<sup>141-144</sup>

Both of the phosphanide complexes are fluorescent; dicyclohexylphosphanide **13** produces a larger fluorescence intensity compared to diphenylphosphanide **14**. The lone pair on the phosphorus in **14** is involved in back-donation into the phenyl substituents, which decreases its  $n\text{-}\pi^*$  transition contribution. The chalcogen addition products, complexes **15** (S), **16** (Se) and **17** (Te), show increasing fluorescence with a decrease in the size of the chalcogen. The two sulfur and selenium atoms have effective orbital overlap to contribute highly in the  $n\text{-}\pi^*$  transition where tellurium has less donation capabilities due to insufficient orbital overlap, resulting in a dramatic loss of fluorescence.

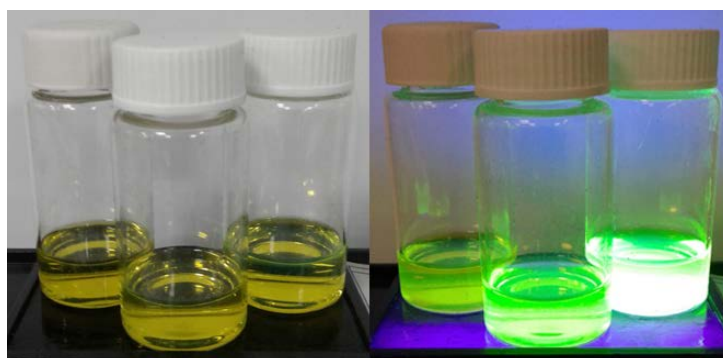


**Figure 29: Left, samples in ambient light. Right samples under a broad range of UV light. Samples from left to right: Addition of tellurium, selenium and sulfur into the Zn-P bond of complex 13.**

## 2.4 Summary of Results

Pre-thesis research was conducted using zinc bromide **XXIX** to synthesize two phosphanides, dicyclohexyl **XXX** and diphenyl **XXXI**. The salt metathesis degradation product (**XXXII**) was isolated from the reaction mixture of **XXXI**. The selenium addition product, dicyclohexylphosphinodiselenoate **XXXIII**, was synthesized from dicyclohexylphosphanide **XXX**. The selenium addition product, diphenylphosphinodiselenoate **XXXIV**, was synthesized from diphenylphosphanide **XXXI**. The tellurium addition product, dicyclohexylphosphinotellunoite **XXXV**, was synthesized from dicyclohexylphosphanide **XXX** and confirmed by  $^{125}\text{Te}$  satellites in the  $^{31}\text{P}$  NMR spectrum.

The novel  $\beta$ -diketiminato-mercury chloride (**1**) was synthesized by addition of  $[\text{Ar-BDl}_{\text{Dipp}}\text{-Li}]$ , generated by addition of LDA to  $[\text{Ar-BDl}_{\text{Dipp}}\text{-H}]$ , to mercury dichloride. Attempts to derivatise **1** using salt metathesis reactions proved unsuccessful with only ligand degradation products being observed.

The recently synthesized  $\beta$ -diketiminato-cadmium chloride (**XVI**) was derivatized to a  $\beta$ -diketiminato-cadmium phosphanide (**2**) via a lithium phosphanide, confirmed by  $\text{Cd}^{111}$  and  $\text{Cd}^{113}$  satellites in the  $^{31}\text{P}$  NMR spectrum, and a novel  $\beta$ -diketiminato-cadmium hydride (**3**) using Super Hydride. Initial reactivity studies of **3** with various carbodiimides to isolate an insertion product, an amidinate (**4**), yielded a  $\beta$ -diketiminato with a homonuclear Cd-Cd dimer (**5**). Complex **5** was formed by catalytic reduction of cadmium hydride **3**. Further study is required to confirm the catalytic activity of the carbodiimides and the mechanism with the hydride **3** to produce the homonuclear dimer **5**. Attempts to synthesize **4** via a salt metathesis reaction or a ligand exchange reaction from formamidines **6** and **7** proved unsuccessful. A novel cadmium amidinate (**8**) was synthesized from addition of the formamidine **7** to  $[\text{Cd}(\text{HMDS})_2]$ .

The same  $\beta$ -diketiminato ligand used to produce mercury chloride **1**,  $[\text{Ar-BDl}_{\text{Dipp}}\text{-H}]$ , was used to synthesize complexes with zinc. An incomplete salt metathesis reaction product (**9**) was found when  $[\text{Ar-BDl}_{\text{Dipp}}\text{-Li}]$  was added to zinc dibromide in THF and a novel  $\beta$ -diketiminato-zinc bromide (**10**) when the reaction was conducted in toluene. Zinc bromide

**10** was derivatized to a variety of complexes (including amides **11** and **12** and phosphanides **13** and **14**) by a salt metathesis reaction. Chalcogen addition reactions from dicyclohexylphosphanide **13** gave a zinc dicyclohexylphosphinodithioate (**15**), dicyclohexylphosphinodiselenoate (**16**) and a dicyclohexylphosphinitellunoate (**17**). Mono-addition products were not isolated. Chalcogen addition reactions from diphenylphosphanide **14** gave a zinc diphenylphosphinodiselenoate (**18**) and a zinc tellunoite bridged dimer (**19**). A total of 14 compounds were characterized via X-ray diffraction.

Photoluminescence studies of fluorescent compounds **10-18** were conducted. It was proposed that an electron transfer from the lone pair on the hetero-atom influenced the quantum yield and fluorescence intensities. Further study is required to determine the mechanism of the fluorescence.



# Chapter 3

---

## Experimental

All manipulations, unless specified otherwise, were carried out under dry nitrogen using standard Schlenk-line and cannula techniques, or in an inert atmosphere glovebox. Solvents used were dried using a PureSolv. system (Innovative Technologies) and stored over 4 Å sieves unless otherwise stated.  $^1\text{H}$ ,  $^{13}\text{C}$  and  $^{31}\text{P}$  NMR spectra were recorded in deuterated benzene ( $\text{C}_6\text{D}_6$ ) at 298 K using a Varian INOVA system at 300 and 600 MHz: ( $^1\text{H}$ ), 151 MHz ( $^{13}\text{C}$  { $^1\text{H}$ }) or 121 MHz ( $^{31}\text{P}$  { $^1\text{H}$ }).  $^1\text{H}$  and  $^{13}\text{C}$  chemical shifts were referenced internally to residual solvent resonances. Elemental analyses were performed by Campell Micro-analytical Laboratory, Otago. Infrared spectra were recorded on a Bruker Tensor 27 FTIR spectrometer using Nujol mineral oil. Melting points were determined using a Gallenkamp Melting Point Apparatus. Absorption spectra were obtained on a Shimadzu UV-2600 Spectrophotometer. Photoluminescence spectra were obtained on a Shimadzu RF-5301PC Spectrofluorophotometer. Diatomaceous earth used for filtration was Celite<sup>TM</sup> and is referred to as celite throughout.

Samples suitable for X-ray diffraction were grown in a saturated solution of the sample using at  $-30\text{ }^\circ\text{C}$  unless stated otherwise. Crystals were covered in inert oil and suitable crystals were selected under a microscope and mounted on an Agilent SuperNova X-ray Diffraction system fitted with an Atlas detector. Data were collected at the temperature indicated using focused Mo  $\text{K}\alpha$  radiation at  $0.71073\text{ \AA}$  or Cu  $\text{K}\alpha$  radiation at  $1.54128\text{ \AA}$ . Intensities were collected for Lorentz and polarization effects and for absorption using multi-scan methods. Space groups were determined from systematic absences and checked for higher symmetry. All structures were solved using direct methods with SHELXS, refined on F2 using all data by full matrix least-squares procedures with SHELXL-97, within OLEX-2.3. Non-hydrogen atoms were refined with anisotropic displacement parameters. Hydrogen atoms were placed in calculated positions or manually assigned from residual electron density where appropriate unless otherwise stated. The functions minimized were  $\Sigma w(F2o-$

$F2c$ ), with  $w = [\sigma^2(F2o) + aP^2 + bP]^{-1}$ , where  $P = [\max(Fo)^2 + 2F2c]/3$ . The isotropic displacement parameters are 1.2 or 1.5 times the isotropic equivalent of their carrier atoms.

The lithium salts of the following: dicyclohexylphosphine, diphenylphosphine, hexamethyldisilazane and 2,6-diisopropylphenylamine were synthesized by slow addition of 1.6 M  $n\text{BuLi}$  in hexane (1.02 mL, 5.04 mmol) to a solution of one of the compounds (5.04 mmol) in hexane (10 mL) for 6 hours. The volatiles were removed in *vacuo* to yield the product. For lithium dicyclohexylphosphanide, diphenylphosphanide and 2,6-diisopropylphenylamine, triturations in hexane (3 x 5 mL) were conducted to remove impurities. Remaining volatiles were removed in *vacuo* to reveal the clean lithium salt used throughout.

**[CH{(CH<sub>3</sub>)CN-2,6-*i*Pr<sub>2</sub>C<sub>6</sub>H<sub>3</sub>}<sub>2</sub>], [BDI<sub>Dipp</sub>-H]** This known compound was synthesized by the following literature procedure.<sup>125</sup> 12 M HCl (8 mL) was added dropwise to a mixture of acetylacetone (4.7 mL, 45.8 mmol) and freshly distilled 2,6-diisopropylaniline (19.5 mL, 103.4 mmol) in ethanol (200 mL) while stirring. The light pink reaction solution was left to reflux for 72 hours where a milky white precipitate was observed. The precipitate was filtered off and washed with cold petroleum ether (30 mL). Dichloromethane (50 mL) and saturated sodium carbonate solution (100 mL) was added to the solid phase. The aqueous phase was washed further with dichloromethane (50 mL). The organic layers were collected and dried over magnesium sulfate and the volatiles were removed in *vacuo*. The residue was re-dissolved in methanol (50 mL) and dichloromethane (20 mL) and left to slowly evaporate in a fume cupboard. After 72 hours crystalline product was observed. The product was collected using a Buchner filtration. For use in the inert atmosphere glovebox the crystalline product was crushed and dried at 50 °C under vacuum overnight (14.0 g, 73%). [lit. 73%].<sup>125</sup> <sup>1</sup>H NMR data is in agreement with the literature values. <sup>1</sup>H NMR (299.74 MHz, C<sub>6</sub>D<sub>6</sub>, 298 K):  $\delta$  12.49 (s, 1H, NH), 7.18 (s, 6H, ArH), 4.89 (s, 1H,  $\gamma$ -CH), 3.32 (septet,  $J$  = 6.9 Hz, 4H CHMe<sub>2</sub>), 1.67 (s, 6H, NCMe), 1.23 (d,  $J$  = 7.0 Hz, 12H, CHMe<sub>2</sub>), 1.16 (d,  $J$  = 7.0 Hz, 12H, CHMe<sub>2</sub>).

**[CH{(CH<sub>3</sub>)CN-2,6-<sup>i</sup>Pr<sub>2</sub>C<sub>6</sub>H<sub>3</sub>}<sub>2</sub>ZnBr], [BDI<sub>Dipp</sub>ZnBr]** An adapted synthesis was used for this known compound from the following literature procedure.<sup>27</sup> [BDI<sub>Dipp</sub>-H] (1.20 g, 2.86 mmol) was dissolved in THF (5 mL) and 1.6 M <sup>n</sup>BuLi (2.14 mL, 3.43 mmol) was added dropwise to the stirring solution. The reaction was left to react for 30 minutes. Freshly sublimed ZnBr<sub>2</sub> (0.77 g, 3.43 mmol) was dissolved in THF (5 mL) and added to the now yellow solution of [BDI<sub>Dipp</sub>-Li] and left to react for 48 hours. The volatiles were removed in *vacuo* followed by triturations in hexane (3 x 5 mL) to remove impurities. The product was extracted into toluene (12 mL). Toluene and remaining volatiles were removed in *vacuo* to reveal the product as a white powder. The resulting solid was clean via <sup>1</sup>H NMR and used without further purification (1.04 g, 65%). [lit. 96% as chloride derivative].<sup>27</sup> <sup>1</sup>H NMR (299.74 MHz, C<sub>6</sub>D<sub>6</sub>, 298 K): δ 7.14 (s, 6H, *ArH*), 4.89 (s, 1H, γ-CH), 3.69 (m, 4H, CHMe<sub>2</sub>), 1.76 (s, 6H, NCMe), 1.54 (d, J = 3.8 Hz, 12H, CHMe<sub>2</sub>), 1.22 (d, J = 4.7 Hz, 12H, CHMe<sub>2</sub>).

**[CH{(CH<sub>3</sub>)CN-2,6-<sup>i</sup>Pr<sub>2</sub>C<sub>6</sub>H<sub>3</sub>}<sub>2</sub>ZnP(C<sub>6</sub>H<sub>11</sub>)<sub>2</sub>], [BDI<sub>Dipp</sub>ZnPCy<sub>2</sub>] (XXX)** To a stirring solution of [BDI<sub>Dipp</sub>ZnBr] (0.200 g, 0.355 mmol) in diethyl ether (5 mL) a lithium dicyclohexylphosphanide (0.073 g, 0.355 mmol) slurry in diethyl ether (10 mL) was added. The reaction was left stirring for 16 hours where a white solid was suspended in a yellow solution. The reaction was filtered through celite and the volatiles were removed in *vacuo*. The resulting sticky yellow solid was clean via <sup>1</sup>H NMR and used without further purification (0.128 g, 52.9 %). Crystals were grown in a minimum amount of diethyl ether. <sup>1</sup>H NMR (299.74 MHz, C<sub>6</sub>D<sub>6</sub>, 298 K): δ 7.09 (s, 6H, *ArH*), 5.00 (s, 1H, γ-CH), 3.22 (m, 4H, CHMe<sub>2</sub>), 1.68 (s, 6H, NCMe), 1.56 (m, 18, PCy<sub>2</sub>), 1.38 (d, J = 6.8 Hz, 12H, CHMe<sub>2</sub>), 1.28 (m, 6H, PCy<sub>2</sub>), 1.13 (d, J = 7.1 Hz, 12H, CHMe<sub>2</sub>). <sup>13</sup>C NMR (150.76 MHz, C<sub>6</sub>D<sub>6</sub>, 298 K): δ 167.78 (NCMe), 145.79 (*ipso-ArC*), 141.84 (*o-ArC*), 126.25 (*m-ArC*), 124.11 (*p-ArC*), 95.77 (γ-C), 36.63 (d, J<sub>CP</sub> = 11.6 Hz, *o*-PCy), 31.14 (d, J<sub>CP</sub> = 16.8 Hz, *ipso*-PCy), 28.70 (CHMe<sub>2</sub>), 28.45 (d, J<sub>CP</sub> = 10.4 Hz, *m*-PCy), 26.41 (CHMe<sub>2</sub>), 24.36 (d, J<sub>CP</sub> = 4.6 Hz, *p*-PCy), 23.93 (CHMe<sub>2</sub>), 23.78 (NCMe). <sup>31</sup>P {<sup>1</sup>H} NMR (121.32 MHz, C<sub>6</sub>D<sub>6</sub>, 298 K): δ -22.2.

**[CH{(CH<sub>3</sub>)CN-2,6-<sup>i</sup>Pr<sub>2</sub>C<sub>6</sub>H<sub>3</sub>}<sub>2</sub>ZnP(C<sub>6</sub>H<sub>5</sub>)<sub>2</sub>], [BDI<sub>Dipp</sub>ZnPPh<sub>2</sub>] (XXXI)** To a stirring solution of [BDI<sub>Dipp</sub>ZnBr] (0.260 g, 0.462 mmol) in diethyl ether (5 mL) a lithium diphenylphosphanide (0.089 g, 0.462 mmol) slurry in diethyl ether (10 mL) was added. The reaction was left stirring for 16 hours where a white solid was suspended in a yellow solution. The reaction was filtered through celite and the volatiles were removed in *vacuo*. The resulting residue was not clean but contained suspected product via <sup>31</sup>P NMR. For use in further reactions the product was made *in situ*. <sup>31</sup>P {<sup>1</sup>H} NMR (121.32 MHz, C<sub>6</sub>D<sub>6</sub>, 298 K): δ -45.8.

**[CH{(CH<sub>3</sub>)CN-2,6-<sup>i</sup>Pr<sub>2</sub>C<sub>6</sub>H<sub>3</sub>}<sub>2</sub>ZnSe<sub>2</sub>P(C<sub>6</sub>H<sub>11</sub>)<sub>2</sub>], [BDI<sub>Dipp</sub>Zn(Se)<sub>2</sub>PCy<sub>2</sub>] (XXXIII)** To a stirring slurry of [BDI<sub>Dipp</sub>ZnPCy<sub>2</sub>] (0.120 g, 0.176 mmol) in diethyl ether (5 mL) dried selenium powder was added (0.070 g, 0.882 mmol). The reaction was left to react for 16 hours. The resulting orange solution with dark precipitate was filtered through celite and the volatiles were removed in *vacuo*. Diethyl ether was added to the residue (2 mL) and kept at -30 °C. Orange rectangular crystals suitable for characterization and X-ray diffraction grew after 72 hours (0.062 g, 42%). <sup>1</sup>H NMR (299.74 MHz, C<sub>6</sub>D<sub>6</sub>, 298 K): δ 7.22 (s, 6H, *ArH*), 4.85 (s, 1H, γ-CH), 3.49 (m, 4H, CHMe<sub>2</sub>), 1.80 (s, 6H, NCMe), 1.64 (d, J = 7.0 Hz, 12H, CHMe<sub>2</sub>), 1.50 (m, 16H, PCy<sub>2</sub>), 1.17 (d, J = 6.7 Hz, 12H, CHMe<sub>2</sub>), 0.95 (m, 12H, PCy<sub>2</sub>). <sup>13</sup>C NMR (150.76 MHz, C<sub>6</sub>D<sub>6</sub>, 298 K): δ 167.84 (NCMe), 145.00 (*ipso-ArC*), 143.34 (*o-ArC*), 125.62 (*m-ArC*), 123.91 (*p-ArC*), 93.44 (γ-C), 40.05 (d, J<sub>CP</sub> = 28.3 Hz, *ipso-PCy*), 28.93 (CHMe<sub>2</sub>), 26.54 (d, J<sub>CP</sub> = 2.5 Hz, *m-PCy*), 26.37 (d, J<sub>CP</sub> = 14.5 Hz, *o-PCy*), 26.10 (d, J<sub>CP</sub> = 2.0 Hz, *p-PCy*), 25.50 (CHMe<sub>2</sub>), 25.08 (CHMe<sub>2</sub>), 24.48 (NCMe). <sup>31</sup>P {<sup>1</sup>H} NMR (121.32 MHz, C<sub>6</sub>D<sub>6</sub>, 298 K): δ 51.2 (J<sub>PSe</sub> = 451.5 Hz).

**[CH{(CH<sub>3</sub>)CN-2,6-<sup>i</sup>Pr<sub>2</sub>C<sub>6</sub>H<sub>3</sub>}<sub>2</sub>ZnSe<sub>2</sub>P(C<sub>6</sub>H<sub>5</sub>)<sub>2</sub>], [BDI<sub>Dipp</sub>Zn(Se)<sub>2</sub>PPh<sub>2</sub>] (XXXIV)** To a stirring slurry of [BDI<sub>Dipp</sub>ZnPPh<sub>2</sub>] (0.100 g, 0.150 mmol) in diethyl ether (6 mL) dried selenium powder was added (0.059 g, 0.748 mmol). The reaction was left to react for 16 hours. The resulting orange solution with dark precipitate was filtered through celite and the volatiles were removed in *vacuo*. Diethyl ether was added to the residue (2 mL) and kept at -30 °C. Orange rectangular crystals suitable for characterization and X-ray diffraction grew after 72 hours (0.059 g, 48%). <sup>1</sup>H NMR (299.74 MHz, C<sub>6</sub>D<sub>6</sub>, 298 K): δ 7.41 (ddd, J<sub>HH</sub> = 15.3, 6.9 Hz, J<sub>HP</sub> = 1.9 Hz, 4H, Ph-*m-H*), 7.14 (s, 6H, *ArH*), 6.80 (m, 6H, Ph-*o,p-H*), 4.84 (s, 1H, γ-CH), 3.53 (m, 4H, CHMe<sub>2</sub>), 1.73 (s, 6H, NCMe), 1.41 (d, J = 6.7 Hz, 12H, CHMe<sub>2</sub>), 1.20 (d, J = 6.7 Hz, 12H, CHMe<sub>2</sub>). <sup>13</sup>C NMR (150.76 MHz, C<sub>6</sub>D<sub>6</sub>, 298 K): δ 168.30 (NCMe), 144.73 (*ipso-ArC*), 143.34

(*o*-ArC), 136.04 (d,  $J_{CP}$  = 62.6 Hz, *ipso*-PPh), 131.06 (d,  $J_{CP}$  = 12.4 Hz, *o*-PPh), 130.73 (d,  $J_{CP}$  = 3.4 Hz, *m*-PPh), 128.35 (*p*-PhC), 125.93 (*m*-ArC), 124.22 (*p*-ArC), 94.53 ( $\gamma$ -C), 28.74 (CHMe<sub>2</sub>), 25.49 (CHMe<sub>2</sub>), 25.18 (CHMe<sub>2</sub>), 24.35 (NCMe). <sup>31</sup>P {<sup>1</sup>H} NMR (121.32 MHz, C<sub>6</sub>D<sub>6</sub>, 298 K):  $\delta$  6.3 ( $J_{PSe}$  = 472.7 Hz).

**[CH{(CH<sub>3</sub>)CN-2,6-<sup>i</sup>Pr<sub>2</sub>C<sub>6</sub>H<sub>3</sub>}<sub>2</sub>ZnTeP(C<sub>6</sub>H<sub>11</sub>)<sub>2</sub>], [BDI<sub>Dipp</sub>Zn(Te)PCy<sub>2</sub>] (XXXV)** To a stirring slurry of [BDI<sub>Dipp</sub>ZnPCy<sub>2</sub>] (0.050 g, 0.074 mmol) in diethyl ether (5 mL) dried tellurium powder was added (0.047 g, 0.037 mmol). The reaction was left to react for 48 hours. The resulting dark orange solution with dark precipitate was filtered through celite and the volatiles were removed in *vacuo*. The resulting residue was not clean but contained suspected product via <sup>31</sup>P NMR. <sup>31</sup>P {<sup>1</sup>H} NMR (121.32 MHz, C<sub>6</sub>D<sub>6</sub>, 298 K):  $\delta$  7.2 ( $J_{PTe}$  = 285.0 Hz).

**[*o*-C<sub>6</sub>H<sub>4</sub>{C(CH<sub>3</sub>)=N-2,6-<sup>i</sup>Pr<sub>2</sub>C<sub>6</sub>H<sub>3</sub>}{F}]** An adapted synthesis was used for this known compound from the following literature procedure.<sup>126</sup> An ampule fitted with a Young's tap was charged with TiCl<sub>4</sub> (2.05 g, 0.011 mol) in hexane (15 mL) and 2,6-diisopropylaniline (11.5 g, 0.065 mol) in hexane (15 mL) to form a dense brown precipitate. 2'-fluoroacetophenone (2.6 mL, 0.022 mol) was added via syringe which lightened the brown precipitate and allowed to react for 16 hours at 75 °C under N<sub>2</sub>. The resulting thick green-yellow solution was opened to air and allowed to cool to room temperature. The contents of the reaction vessel were removed, diethyl ether (3 x 30 mL) was used to remove as much of the solid and liquid from the reaction vessel as possible. The resulting mixture was filtered through celite and a silica plug, the solid fraction was discarded and the orange organic fraction was collected. The orange solution was dried over magnesium sulfate and volatiles were removed in *vacuo* to yield an orange oil. The oil was clean by <sup>1</sup>H NMR and used without further purification. This compound was made *in situ* for the complete synthesis of [Ar-BDI<sub>DIPP</sub>-H] (2.53 g, 79%). [lit. 57%.]<sup>126</sup> <sup>1</sup>H NMR (299.74 MHz, C<sub>6</sub>D<sub>6</sub>, 298 K):  $\delta$  7.94 (td,  $J$  = 7.7, 1.9 Hz, 1H, ArH), 7.49 (ddd,  $J$  = 8.1, 7.3, 5.3 Hz, 1H, ArH), 7.31-7.08 (m, 5H, ArH), 2.86 (septet,  $J$  = 6.9 Hz, 2H, CHMe<sub>2</sub>), 2.17 (d,  $J_{HF}$  = 3.5 Hz, 3H, NCMe), 1.32 (d,  $J$  = 6.9 Hz, 6H, CHMe<sub>2</sub>), 1.22 (d,  $J$  = 6.8 Hz, 6H, CHMe<sub>2</sub>).

**[*o*-C<sub>6</sub>H<sub>4</sub>{C(CH<sub>3</sub>)=N-2,6-*i*Pr<sub>2</sub>C<sub>6</sub>H<sub>3</sub>}{NH(2,6-*i*Pr<sub>2</sub>C<sub>6</sub>H<sub>3</sub>)}], [Ar-BDI<sub>Dipp</sub>-H]** An adapted synthesis was used for this known compound from the following literature procedure.<sup>126</sup> 1.6 M <sup>n</sup>BuLi (7.4 mL, 0.012 mol) in hexane was added to 2,6-diisopropylaniline (2.30 g, 0.013 mmol) in THF (12 mL). The reaction was allowed to react for 3 hours. [*o*-C<sub>6</sub>H<sub>4</sub>{C(CH<sub>3</sub>)=N-2,6-*i*Pr<sub>2</sub>C<sub>6</sub>H<sub>3</sub>}{F}] was made *in situ* (above), was dissolved in THF (12 mL) and added to the lithium 2,6-diisopropylanilide reaction. The total reaction was allowed to react at 90 °C for 72 hours under N<sub>2</sub>. The dark and yellow solution was allowed to cool to room temperature and quenched with H<sub>2</sub>O (30 mL) and extracted into hexanes (50 mL). The aqueous fraction was further washed with hexanes (2 x 20 mL). The organic fractions were combined and dried over magnesium sulfate. Volatiles were removed in *vacuo* to yield an oily orange solid. The residue was re-dissolved in methanol (30 mL) and dichloromethane (10 mL) and left to slowly crystallize in a fume hood. Yellow crystalline product was observed within 72 hours (3.66 g, 67%). [lit. 46%].<sup>126</sup> <sup>1</sup>H NMR (299.74 MHz, C<sub>6</sub>D<sub>6</sub>, 298 K): δ 11.58 (s, 1H, NH), 7.48 (d, J = 8.2 Hz, 1H, C<sub>6</sub>H<sub>4</sub>), 7.28-7.18 (m, 6H, ArH), 7.00 (t, J = 7.6 Hz, 1H, C<sub>6</sub>H<sub>4</sub>), 6.58 (t, J = 7.5 Hz, 1H, C<sub>6</sub>H<sub>4</sub>), 6.48 (d, J = 8.5 Hz, 1H, C<sub>6</sub>H<sub>4</sub>), 3.44 (septet, J = 7.3 Hz, 2H, CHMe<sub>2</sub>), 3.05 (septet, J = 7.0 Hz, 2H, CHMe<sub>2</sub>), 1.96 (s, 6H, NCM<sub>e</sub>), 1.17 (d, J = 2.1 Hz, 6H, CHMe<sub>2</sub>), 1.13 (d, J = 7.0 Hz, 6H, CHMe<sub>2</sub>).

**[*o*-C<sub>6</sub>H<sub>4</sub>{C(CH<sub>3</sub>)=N-2,6-*i*Pr<sub>2</sub>C<sub>6</sub>H<sub>3</sub>}{NLi(2,6-*i*Pr<sub>2</sub>C<sub>6</sub>H<sub>3</sub>)}], [Ar-BDI<sub>Dipp</sub>-Li]** An adapted synthesis was used for this known compound from the following literature procedure.<sup>126</sup> 1.6 M <sup>n</sup>BuLi in hexanes (0.62 mL, 0.992 mmol) was added slowly to a stirring solution of [Ar-BDI<sub>Dipp</sub>-H] (0.410 g, 0.902 mmol) in toluene (10 mL). The solution immediately turned orange from yellow. A bright yellow precipitate was observed within 4 hours. The reaction was left to react for 16 hours. The volatiles were removed in *vacuo* followed by triturations in hexane (2 x 10 mL) to further remove impurities. The bright yellow solid was clean by <sup>1</sup>H NMR and was used without further purification (0.35 g, 84%). [lit. 86%].<sup>126</sup> <sup>1</sup>H NMR (299.74 MHz, C<sub>6</sub>D<sub>6</sub>, 298 K): δ 7.63 (d, J = 8.8 Hz, 1H, C<sub>6</sub>H<sub>4</sub>), 7.32-7.10 (m, 6H, ArH), 7.03 (t, J = 7.3 Hz, 1H, C<sub>6</sub>H<sub>4</sub>), 6.55 (d, 1H, J = 9.0 Hz, C<sub>6</sub>H<sub>4</sub>), 6.35 (t, 1H, J = 7.1 Hz, C<sub>6</sub>H<sub>4</sub>), 3.31 (m, 2H, CHMe<sub>2</sub>), 2.78 (m, 2H, CHMe<sub>2</sub>), 2.06 (s, 6H, NCM<sub>e</sub>), 1.21 (d, J = 6.7 Hz, 3H, CHMe<sub>2</sub>), 1.17 (d, J = 6.7 Hz, 3H, CHMe<sub>2</sub>), 1.06 (d, J = 6.7 Hz, 3H, CHMe<sub>2</sub>), 1.03 (d, J = 6.7 Hz, 3H, CHMe<sub>2</sub>). The reaction was repeated using lithium diisopropylamide (0.106 g, 0.992 mmol) dried from a slurry in hexane to yield a

slightly darker yellow solid. This sample had shifted peaks and was used for use with HgCl<sub>2</sub>. (0.34 g, 83%). <sup>1</sup>H NMR (299.74 MHz, C<sub>6</sub>D<sub>6</sub>, 298 K): δ 7.58 (d, J = 7.0 Hz, 1H, C<sub>6</sub>H<sub>4</sub>), 7.32-7.04 (m, 6H, ArH), 7.01 (t, J = 6.4 Hz, 1H, C<sub>6</sub>H<sub>4</sub>), 6.58 (d, J = 6.9 Hz, 1H, C<sub>6</sub>H<sub>4</sub>), 6.35 (t, J = 7.0 Hz, 1H, C<sub>6</sub>H<sub>4</sub>), 3.54 (septet, J = 6.8 Hz, 2H, CHMe<sub>2</sub>), 3.10 (septet, J = 7.1 Hz, 2H, CHMe<sub>2</sub>), 2.01 (s, 6H, NCMe), 1.32 (d, J = 7.0 Hz, 3H, CHMe<sub>2</sub>), 1.16 (d, J = 7.1 Hz, 3H, CHMe<sub>2</sub>), 1.14 (d, J = 7.0 Hz, 3H, CHMe<sub>2</sub>), 1.11 (d, J = 7.0 Hz, 3H, CHMe<sub>2</sub>).

**[*o*-C<sub>6</sub>H<sub>4</sub>{C(CH<sub>3</sub>)=N-2,6-*i*Pr<sub>2</sub>C<sub>6</sub>H<sub>3</sub>}{NH(2,6-*i*Pr<sub>2</sub>C<sub>6</sub>H<sub>3</sub>)}HgCl], [Ar-BDl<sub>Dipp</sub>HgCl] (1)** To a stirring solution of [Ar-BDl<sub>Dipp</sub>-Li] (0.140 g, 0.304 mmol) in toluene (10 mL) at -30 °C, HgCl<sub>2</sub> (0.083 g, 0.304 mmol) was added dry. The reaction was left to react for 24 hours where a white solid was suspended in a light yellow solution. The reaction was filtered through celite and the volatiles were removed in *vacuo*. The resulting light yellow solid was clean via <sup>1</sup>H NMR (0.040 g, 69%). Light yellow flower shaped crystals was grown in hexane. <sup>1</sup>H NMR (299.74 MHz, C<sub>6</sub>D<sub>6</sub>, 298 K): δ 7.29 (d, 1H, J = 8.0 Hz, C<sub>6</sub>H<sub>4</sub>), 7.21-7.14 (m, 6H, ArH), 6.84 (td, 1H, J = 7.8, 1.6 Hz, C<sub>6</sub>H<sub>4</sub>), 6.54 (d, 1H, J = 8.7 Hz, C<sub>6</sub>H<sub>4</sub>), 6.51 (td, 1H, J = 7.5, 1.1 Hz, C<sub>6</sub>H<sub>4</sub>), 3.48 (septet, 2H, J = 6.9 Hz, CHMe<sub>2</sub>), 3.11 (septet, 2H, J = 6.9 Hz, CHMe<sub>2</sub>), 1.89 (s, 6H, NCMe), 1.33 (d, 6H, J = 6.9 Hz, CHMe<sub>2</sub>), 1.24 (d, 6H, J = 7.0 Hz, CHMe<sub>2</sub>), 1.14 (d, 6H, J = 6.9 Hz, CHMe<sub>2</sub>), 1.04 (d, 6H, J = 6.8 Hz, CHMe<sub>2</sub>). <sup>13</sup>C NMR (150.76 MHz, C<sub>6</sub>D<sub>6</sub>, 298 K): δ 175.04 (NCMe), 155.86 (ArC), 145.93 (ArC), 145.10 (ArC), 143.67 (ArC), 137.94 (ArC), 132.69 (ArC), 131.80 (ArC), 126.83 (ArC), 126.19 (ArC), 125.19 (ArC), 124.18 (ArC), 122.18 (ArC), 120.48 (ArC), 116.56 (ArC), 28.86 (CHMe<sub>2</sub>), 27.83 (CHMe<sub>2</sub>), 24.78 (CHMe<sub>2</sub>), 24.72 (CHMe<sub>2</sub>), 24.52 (CHMe<sub>2</sub>), 24.00 (CHMe<sub>2</sub>), 23.34 (NCMe).

**[CH{(CH<sub>3</sub>)CN-2,6-*i*Pr<sub>2</sub>C<sub>6</sub>H<sub>3</sub>}<sub>2</sub>CdCl], [BDl<sub>Dipp</sub>CdCl] (XVI)** An adapted synthesis was used for this known compound from the following literature procedure.<sup>48</sup> Lithium hexamethyldisilazane (0.830 g, 4.96 mmol) was dissolved in 5 mL of THF and added drop-wise to a slurry of CdCl<sub>2</sub> (0.910 g, 4.96 mmol) in THF (5 mL). The reaction mixture was left to stir 16 hours where a grey solution had appeared. The volatiles were removed in *vacuo* to yield a thick grey oil. The oil was re-dissolved in toluene and filtered through celite. This solution contained (HMDS)CdCl. A solution of BDl<sub>Dipp</sub>H (1.20 g, 2.86 mmol) in toluene was added to the (HMDS)CdCl solution and left to react for 72 hours at 55 °C. The volatiles were removed in *vacuo* followed by triturations in hexane (3 x 10 mL) to remove impurities. Hexane was

evaporated under reduced pressure followed by [BDI<sub>Dipp</sub>CdCl] extraction into toluene (3 x 10 mL). Removing volatiles in *vacuo* gave the product as a white powder (0.283 g, 18%). [lit. 57%].<sup>48</sup> <sup>1</sup>H NMR (299.74 MHz, C<sub>6</sub>D<sub>6</sub>, 298 K): δ 7.13 (s, 6H, *ArH*), 4.64 (s, 1H, γ-CH), 3.23 (septet, J = 6.9 Hz, 4H, CHMe<sub>2</sub>), 1.56 (s, 6H, NCMe), 1.14 (d, J = 7.0 Hz, 12H, CHMe<sub>2</sub>), 1.01 (d, J = 6.7 Hz, 12H, CHMe<sub>2</sub>).

**[CH{(CH<sub>3</sub>)CN-2,6-<sup>i</sup>Pr<sub>2</sub>C<sub>6</sub>H<sub>3</sub>}<sub>2</sub>CdP(C<sub>6</sub>H<sub>11</sub>)<sub>2</sub>], [BDI<sub>Dipp</sub>CdPCy<sub>2</sub>] (2)** To a stirring solution of [BDI<sub>Dipp</sub>CdCl] (0.200 g, 0.350 mmol) in toluene (5 mL) a lithium dicyclohexylphosphanide (0.072 g, 0.350 mmol) slurry in toluene (10 mL) was added. The reaction was left stirring for 16 hours where a white solid was suspended in a yellow solution. The reaction was filtered through celite and the volatiles were removed in *vacuo*. The resulting yellow solid was washed with hexane. A product was not cleanly isolated but suspected product peaks were observed via <sup>1</sup>H and <sup>31</sup>P NMR. <sup>1</sup>H NMR (299.74 MHz, C<sub>6</sub>D<sub>6</sub>, 298 K): δ 7.06 (s, 6H, *ArH*), 4.92 (s, 1H, γ-CH), 3.31 (m, 4H, CHMe<sub>2</sub>), 1.72 (s, 6H, NCMe), 1.35 (d, J = 6.8 Hz, 12H, CHMe<sub>2</sub>), 1.16 (d, J = 6.7 Hz, 12H, CHMe<sub>2</sub>), cyclohexyl peaks were a range of multiplets from 1.86-0.78 ppm. <sup>31</sup>P {<sup>1</sup>H} NMR (121.32 MHz, C<sub>6</sub>D<sub>6</sub>, 298 K): δ 5.4 (J<sub>P<sup>m</sup>Cd</sub> = 545.8 Hz, J<sub>P<sup>m</sup>Cd</sub> = 570.8 Hz)

**[CH{(CH<sub>3</sub>)CN-2,6-<sup>i</sup>Pr<sub>2</sub>C<sub>6</sub>H<sub>3</sub>}<sub>2</sub>CdH], [BDI<sub>Dipp</sub>CdH] (3)** 238 μL of LiHBEt<sub>3</sub> in THF (0.0252 g, 0.238 mmol) was added drop-wise to a slurry of [BDI<sub>Dipp</sub>CdCl] (0.150 g, 0.265 mmol) in 4 mL of toluene at -30 °C. The mixture was allowed to stir for 1 minute where it was filtered through celite to remove black precipitate and the volatiles were removed in *vacuo*. Solid was re-dissolved and crystalized from hexane or diethyl ether to give [BDI<sub>Dipp</sub>CdH] as small colourless cubic crystals (0.0944 g, 74.6%). The product was stable at room temperature but decomposed above 126 °C. <sup>1</sup>H NMR (299.74 MHz, C<sub>6</sub>D<sub>6</sub>, 298 K): δ 7.11 (s, 6H, *ArH*), 5.63 (br, 1H, CdH), 4.91 (s, 1H, γ-CH), 3.29 (septet, J = 6.7 Hz, 4H, CHMe<sub>2</sub>), 1.70 (s, 6H, NCMe), 1.23 (d, J = 6.8 Hz, 12H, CHMe<sub>2</sub>), 1.16 (d, J = 6.7 Hz, 12H, CHMe<sub>2</sub>). <sup>31</sup>C {<sup>1</sup>H} NMR (150.76 MHz, C<sub>6</sub>D<sub>6</sub>, 298 K): δ 168.14 (NCMe), 146.42 (*ipso*-C), 141.10 (*o*-C), 125.76 (*p*-C), 124.00 (*m*-C), 94.71 (γ-C), 28.21 (CHMe<sub>2</sub>), 24.79 (CHMe<sub>2</sub>), 24.10 (CHMe<sub>2</sub>), 23.30 (NCMe). IR (Nujol): ν(Cd-H) 1734 cm<sup>-1</sup>



**[CH{(CH<sub>3</sub>)CN-2,6-<sup>i</sup>Pr<sub>2</sub>C<sub>6</sub>H<sub>3</sub>}<sub>2</sub>Cd]<sub>2</sub>, [BDI<sub>Dipp</sub>Cd]<sub>2</sub> (5)** To a solution of [BDI<sub>Dipp</sub>CdH] (0.050 g, 0.094 mmol) in hexane (5 mL) a solution of dicyclohexylcarbodiimide (0.019 g, 0.094 mmol) in hexane (5 mL) was added. The colourless reaction was left to react for 16 hours. Volatiles were removed in *vacuo* from the colourless and transparent solution. The resulting residue was re-dissolved into hexane (2 mL) and kept at -30 °C. Transparent colourless cubic crystals suitable for X-ray diffraction were grown within 24 hours (0.078 g, 78%). The same procedure was used with diisopropylcarbodiimide and smaller equivalents of either yielded the same results. <sup>1</sup>H NMR (299.74 MHz, C<sub>6</sub>D<sub>6</sub>, 298 K): δ 7.04 (s, 6H, ArH), 4.78 (s, 1H, γ-CH), 3.12 (septet, J = 6.9 Hz, 4H, CHMe<sub>2</sub>), 1.57 (s, 6H, NCMe), 1.16 (d, J = 6.7 Hz, 12H, CHMe<sub>2</sub>), 0.92 (d, J = 7.0 Hz, 12H, CHMe<sub>2</sub>). <sup>13</sup>C NMR (150.76 MHz, C<sub>6</sub>D<sub>6</sub>, 298 K): δ 166.74 (NCMe), 147.79 (*ipso*-C), 141.06 (*o*-C), 125.02 (*p*-C), 123.88 (*m*-C), 95.04 (γ-C), 28.24 (CHMe<sub>2</sub>), 24.94 (CHMe<sub>2</sub>), 24.63 (CHMe<sub>2</sub>), 23.06 (NCMe).

**[{CH(N-C<sub>6</sub>H<sub>11</sub>)<sub>2</sub>}<sub>2</sub>{CH(N-C<sub>6</sub>H<sub>11</sub>)(N(H)-C<sub>6</sub>H<sub>11</sub>)}Cd], [(DC-Am)<sub>2</sub>(DC-Fo)Cd] (8)** Lithium hexamethyldisilazane (0.420 g, 2.51 mmol) was dissolved in 5 mL of THF and added drop-wise to a slurry of CdCl<sub>2</sub> (0.230 g, 1.23 mmol) in THF (5 mL). The reaction mixture was left to stir 16 hours where an orange solution had appeared. The volatiles were removed in *vacuo* to yield a thick orange-grey oil. The oil was re-dissolved in toluene (5 mL) and filtered through celite. This solution contained Cd(HMDS)<sub>2</sub> determined by <sup>1</sup>H NMR. A solution of DC-Fo (0.52 g, 2.51 mmol) in hexane was added to the Cd(HMDS)<sub>2</sub> solution and left to react for 48 hours. The volatiles were removed in *vacuo* yielding a thick yellow oil. Diethyl ether was added to the residue (2 mL) and kept at -30 °C. Transparent rectangular crystals suitable for characterization and X-ray diffraction grew after 24 hours (0.47 g, 52%) <sup>1</sup>H NMR (299.74 MHz, C<sub>6</sub>D<sub>6</sub>, 298 K): δ 7.90 (s, <sup>3</sup>J<sub>HCd</sub> = 52.4 Hz, 3H, NC(H)N), 3.15 (br, NC(H)N-H), 2.01 (m, NCy), 1.85 (m, NCy), 1.59 (m, NCy), 1.31 (m, NCy).

**[*o*-C<sub>6</sub>H<sub>4</sub>{C(CH<sub>3</sub>)=N-2,6-<sup>i</sup>Pr<sub>2</sub>C<sub>6</sub>H<sub>3</sub>}{NH(2,6-<sup>i</sup>Pr<sub>2</sub>C<sub>6</sub>H<sub>3</sub>)}ZnBr<sub>2</sub>Li(THF)<sub>4</sub>], [Ar-BDI<sub>Dipp</sub>ZnBr<sub>2</sub>Li(THF)<sub>4</sub>] (9)** To a stirring solution of ZnBr<sub>2</sub> (0.034 g, 0.152 mmol) in THF (5 mL), [Ar-BDI<sub>Dipp</sub>-Li] (0.070 g, 0.152 mmol) in THF (5 mL) was added dropwise. The reaction was left to stir for 72 hours where a yellow precipitate was suspended in a yellow solution. The reaction was filtered through celite and the volatiles were removed in *vacuo*. The bright yellow sticky oil was clean via <sup>1</sup>H NMR (0.132 g, 89%). Further removal of solvent proved impossible. <sup>1</sup>H NMR

(299.74 MHz, C<sub>6</sub>D<sub>6</sub>, 298 K):  $\delta$  7.30 (dd, 1H,  $J$  = 8.5, 1.5 Hz, C<sub>6</sub>H<sub>4</sub>), 7.21-6.99 (s, 6H, ArH), 6.78 (td,  $J$  = 6.9, 1.8 Hz, 1H, C<sub>6</sub>H<sub>4</sub>), 6.53 (dd,  $J$  = 8.7, 1.2 Hz, 1H, C<sub>6</sub>H<sub>4</sub>), 6.30 (td,  $J$  = 6.5, 1.5 Hz, 1H, C<sub>6</sub>H<sub>4</sub>), 3.57 (m, 16H,  $J$  = 6.9 Hz, THF), 3.50 (septet,  $J$  = 6.7 Hz, 2H, CHMe<sub>2</sub>), 3.03 (septet,  $J$  = 6.7 Hz, 2H, CHMe<sub>2</sub>), 1.94 (s, 6H, NCMe), 1.39 (d,  $J$  = 6.8 Hz, 3H, CHMe<sub>2</sub>), 1.37 (d,  $J$  = 6.7 Hz, 3H, CHMe<sub>2</sub>), 1.24 (m, 16H, THF), 1.13 (d,  $J$  = 6.7 Hz, 6H, CHMe<sub>2</sub>), 0.95 (d,  $J$  = 6.8 Hz, 6H, CHMe<sub>2</sub>).

**[*o*-C<sub>6</sub>H<sub>4</sub>{C(CH<sub>3</sub>)=N-2,6-*i*Pr<sub>2</sub>C<sub>6</sub>H<sub>3</sub>}{NH(2,6-*i*Pr<sub>2</sub>C<sub>6</sub>H<sub>3</sub>)}ZnBr], [Ar-BDl<sub>Dipp</sub>ZnBr] (10)** To a stirring slurry of sublimed ZnBr<sub>2</sub> (0.068 g, 0.304 mmol) in toluene (10 mL), [Ar-BDl<sub>Dipp</sub>-Li] (0.140 g, 0.304 mmol) in toluene (5 mL) was added dropwise. The reaction was left to stir for 72 hours where a yellow precipitate was suspended in a yellow solution. The reaction was filtered through celite and the volatiles were removed in *vacuo*. The bright yellow product was clean via <sup>1</sup>H NMR (0.150 g, 82%). Bright yellow cubic crystals were grown in minimum hexane. <sup>1</sup>H NMR (299.74 MHz, C<sub>6</sub>D<sub>6</sub>, 298 K):  $\delta$  7.44 (d,  $J$  = 6.6 Hz, 1H, C<sub>6</sub>H<sub>4</sub>), 7.24 (s, 3H, ArH), 7.08 (m, 3H, ArH), 6.88 (t,  $J$  = 7.3 Hz, 1H, C<sub>6</sub>H<sub>4</sub>), 6.69 (d,  $J$  = 9.1 Hz, 1H, C<sub>6</sub>H<sub>4</sub>), 6.40 (t,  $J$  = 7.8 Hz, 1H, C<sub>6</sub>H<sub>4</sub>), 3.34 (septet,  $J$  = 6.8 Hz, 2H, CHMe<sub>2</sub>), 2.83 (septet,  $J$  = 6.9 Hz, 2H, CHMe<sub>2</sub>), 1.99 (s, 6H, NCMe), 1.37 (d,  $J$  = 6.8 Hz, 3H, CHMe<sub>2</sub>), 1.31 (d,  $J$  = 6.7 Hz, 3H, CHMe<sub>2</sub>), 1.25 (d,  $J$  = 7.0 Hz, 3H, CHMe<sub>2</sub>), 0.99 (d,  $J$  = 6.8 Hz, 3H, CHMe<sub>2</sub>). <sup>13</sup>C NMR (150.76 MHz, C<sub>6</sub>D<sub>6</sub>, 298 K):  $\delta$  177.86 (NCMe), 159.15 (ArC), 144.00 (ArC), 143.07 (ArC), 142.38 (ArC), 139.95 (ArC), 134.36 (ArC), 133.89 (ArC), 127.62 (ArC), 126.57 (ArC), 124.74 (ArC), 124.53 (ArC), 118.66 (ArC), 114.82 (ArC), 114.44 (ArC), 29.18 (CHMe<sub>2</sub>), 28.59 (CHMe<sub>2</sub>), 24.92 (CHMe<sub>2</sub>), 24.28 (CHMe<sub>2</sub>), 24.18 (CHMe<sub>2</sub>), 23.64 (CHMe<sub>2</sub>), 21.51 (NCMe). UV-vis (Hexane, 25 °C) [ $\lambda_{\max}$ , nm ( $\epsilon$ , mol<sup>-1</sup> L cm<sup>-1</sup>): 253 (25,700), 435 (8,600).

**[*o*-C<sub>6</sub>H<sub>4</sub>{C(CH<sub>3</sub>)=N-2,6-*i*Pr<sub>2</sub>C<sub>6</sub>H<sub>3</sub>}{NH(2,6-*i*Pr<sub>2</sub>C<sub>6</sub>H<sub>3</sub>)}ZnN(SiMe<sub>3</sub>)<sub>2</sub>], [Ar-BDl<sub>Dipp</sub>ZnHMDS] (11)** To a stirring solution of [Ar-BDl<sub>Dipp</sub>ZnBr] (0.050 g, 0.084 mmol) in hexane (5 mL) a lithium Hexamethyldisilazane (0.014 g, 0.084 mmol) solution in hexane (5 mL) was added. The reaction was left stirring for 16 hours where a white solid was suspended in a yellow solution. The reaction was filtered through celite and the volatiles were removed in *vacuo*. The resulting yellow solid was clean via <sup>1</sup>H NMR (0.040 g, 70%). Rectangular plate-like crystals were grown in hexane. <sup>1</sup>H NMR (299.74 MHz, C<sub>6</sub>D<sub>6</sub>, 298 K):  $\delta$  7.33 – 7.25 (m, 4H), 7.11 (t,  $J$  = 1.9 Hz, 3H), 6.83 (ddd,  $J$  = 8.6, 6.6, 1.6 Hz, 1H, C<sub>6</sub>H<sub>4</sub>), 6.60 (dd,  $J$  = 8.8, 1.2 Hz, 1H,

C<sub>6</sub>H<sub>4</sub>), 6.35 (ddd, J = 8.2, 6.7, 1.2 Hz, 1H, C<sub>6</sub>H<sub>4</sub>), 3.47 (septet, J = 6.8 Hz, 2H, CHMe<sub>2</sub>), 3.00 (septet, J = 6.7 Hz, 2H, CHMe<sub>2</sub>), 1.93 (s, 3H, NCMe), 1.45 (d, J = 6.9 Hz, 6H, CHMe<sub>2</sub>), 1.29 (d, J = 6.7 Hz, 6H, CHMe<sub>2</sub>), 1.17 (d, J = 6.8 Hz, 6H, CHMe<sub>2</sub>), 0.97 (d, J = 6.7 Hz, 6H, CHMe<sub>2</sub>), -0.03 (s, 18H, N(SiMe<sub>3</sub>)<sub>2</sub>). <sup>13</sup>C NMR (150.76 MHz, C<sub>6</sub>D<sub>6</sub>, 298 K): δ 178.88 (NCMe), 158.42 (ArC), 145.54 (ArC), 144.62 (ArC), 144.54 (ArC), 140.18 (ArC), 133.23 (ArC), 132.90 (ArC), 127.34 (ArC), 125.97 (ArC), 124.95 (ArC), 124.92 (ArC), 120.73 (ArC), 116.91 (ArC), 113.78 (ArC), 29.51 (CHMe<sub>2</sub>), 28.72 (CHMe<sub>2</sub>), 25.95 (CHMe<sub>2</sub>), 24.99 (CHMe<sub>2</sub>), 24.66 (CHMe<sub>2</sub>), 24.40 (CHMe<sub>2</sub>), 24.26 (NCMe), 5.64 (N(SiMe<sub>3</sub>)<sub>2</sub>). UV-vis (Hexane, 25 °C) [λ<sub>max</sub>, nm (ε, mol<sup>-1</sup> L cm<sup>-1</sup>)]: 253 (39,200), 443 (13,400).

**[*o*-C<sub>6</sub>H<sub>4</sub>{C(CH<sub>3</sub>)=N-2,6-*i*Pr<sub>2</sub>C<sub>6</sub>H<sub>3</sub>}{NH(2,6-*i*Pr<sub>2</sub>C<sub>6</sub>H<sub>3</sub>)ZnNH(2,6-*i*Pr<sub>2</sub>C<sub>6</sub>H<sub>3</sub>)},**

**[Ar-BDl<sub>Dipp</sub>ZnNH(Dipp)] (12)** To a stirring solution of [Ar-BDl<sub>Dipp</sub>ZnBr] (0.050 g, 0.084 mmol) in hexane (5 mL) a lithium 2,6-diisopropylaniline (0.015 g, 0.084 mmol) solution in hexane (5 mL) was added. The reaction was left stirring for 16 hours where a white solid was suspended in a yellow solution. The reaction was filtered through celite and the volatiles were removed in *vacuo*. The resulting yellow solid was clean via <sup>1</sup>H NMR (0.046 g, 82%). A bright yellow flower shaped crystals were grown in hexane but proved inappropriate for X-ray diffraction. <sup>1</sup>H NMR (299.74 MHz, C<sub>6</sub>D<sub>6</sub>, 298 K): δ 7.41 (dd, J = 8.5, 1.6 Hz, 1H, C<sub>6</sub>H<sub>4</sub>), 7.21 (s, 3H, ArH), 7.09 (m, 3H, ArH), 7.04 (d, J = 7.6 Hz, 2H, DippArH), 6.83 (dd, J = 8.4, 7.0 Hz, 2H, C<sub>6</sub>H<sub>4</sub>), 6.80 (d, J = 7.4 Hz, 1H, DippArH), 6.55 (dd, J = 9.0, 1.2 Hz, 1H, C<sub>6</sub>H<sub>4</sub>), 6.39 (ddd, J = 8.1, 6.6, 1.2 Hz, 1H, C<sub>6</sub>H<sub>4</sub>), 3.33 (septet, J = 6.9 Hz, 2H, CHMe<sub>2</sub>), 2.96 (s, 1H, DippNH), 2.93 (septet, J = 6.9 Hz, 2H, CHMe<sub>2</sub>), 2.54 (septet, J = 6.7 Hz, 2H, CHMe<sub>2</sub>), 1.93 (s, 3H, NCMe), 1.26 (d, J = 6.9 Hz, 6H, CHMe<sub>2</sub>), 1.10 (d, J = 7.0 Hz, 6H, CHMe<sub>2</sub>), 1.08 (d, J = 6.9 Hz, 6H, CHMe<sub>2</sub>), 1.02 (d, J = 6.7 Hz, 12H, DippCHMe<sub>2</sub>), 0.99 (d, J = 6.8 Hz, 6H, CHMe<sub>2</sub>). <sup>13</sup>C NMR (150.76 MHz, C<sub>6</sub>D<sub>6</sub>, 298 K): δ 177.03 (NCMe), 158.70 (ArC), 148.85 (ArC), 145.08 (ArC), 144.09 (ArC), 143.38 (ArC), 140.04 (ArC), 134.91 (ArC), 133.72 (ArC), 133.37 (ArC), 127.40 (ArC), 126.45 (ArC), 125.24 (ArC), 124.71 (ArC), 122.54 (ArC), 119.24 (ArC), 116.57 (ArC), 115.71 (ArC), 114.15 (ArC), 29.28 (CHMe<sub>2</sub>), 28.76 (CHMe<sub>2</sub>), 28.51 (CHMe<sub>2</sub>), 24.61 (CHMe<sub>2</sub>), 23.89 (CHMe<sub>2</sub>), 23.77 (CHMe<sub>2</sub>), 23.71 (CHMe<sub>2</sub>), 23.46 (CHMe<sub>2</sub>), 22.06 (NCMe). UV-vis (Hexane, 25 °C) [λ<sub>max</sub>, nm (ε, mol<sup>-1</sup> L cm<sup>-1</sup>)]: 253 (35,000), 437 (10,500).

**[*o*-C<sub>6</sub>H<sub>4</sub>{C(CH<sub>3</sub>)=N-2,6-*i*Pr<sub>2</sub>C<sub>6</sub>H<sub>3</sub>}{NH(2,6-*i*Pr<sub>2</sub>C<sub>6</sub>H<sub>3</sub>)}ZnP(C<sub>6</sub>H<sub>11</sub>)<sub>2</sub>], [Ar-BDl<sub>Dipp</sub>ZnPCy<sub>2</sub>] (13)** To a stirring solution of [Ar-BDl<sub>Dipp</sub>ZnBr] (0.80 g, 0.134 mmol) in hexane (5 mL) a lithium dicyclohexylphosphanide (0.027 g, 0.134 mmol) slurry in hexane (5 mL) was added. The reaction was left stirring for 36 hours where a white solid was suspended in a yellow solution. The reaction was filtered through celite and the volatiles were removed in *vacuo*. The resulting yellow solid was clean via <sup>1</sup>H NMR and used without further purification (0.059 g, 61%). Yellow cubic crystals were grown from hexane. <sup>1</sup>H NMR (299.74 MHz, C<sub>6</sub>D<sub>6</sub>, 298 K): δ 7.49 (d, J = 8.5 Hz, 1H, C<sub>6</sub>H<sub>4</sub>), 7.29-7.02 (m, 6H, ArH), 6.89 (t, J = 7.8 Hz, 1H, C<sub>6</sub>H<sub>4</sub>), 6.64 (d, J = 8.9 Hz, 1H, C<sub>6</sub>H<sub>4</sub>), 6.40 (t, J = 7.7 Hz, 1H, C<sub>6</sub>H<sub>4</sub>), 3.42 (septet, J = 6.8 Hz, 2H, CHMe<sub>2</sub>), 2.98 (septet, J = 6.8 Hz, 2H, CHMe<sub>2</sub>), 2.00 (s, 6H, NCMe), 1.58 (m, 8H, PCy<sub>2</sub>), 1.41 (d, J = 6.9 Hz, 6H, CHMe<sub>2</sub>), 1.38 (d, J = 6.8 Hz, 6H, CHMe<sub>2</sub>), 1.14 (d, J = 6.9 Hz, 6H, CHMe<sub>2</sub>), 0.98 (d, J = 6.8 Hz, 6H, CHMe<sub>2</sub>), other cyclohexyl peaks were a range of multiplets from 1.32-0.98 ppm. <sup>13</sup>C NMR (150.76 MHz, C<sub>6</sub>D<sub>6</sub>, 298 K): δ 175.15 (NCMe), 158.03 (ArC), 146.13 (ArC), 145.48 (ArC), 144.24 (ArC), 140.03 (ArC), 133.45 (ArC), 133.40 (ArC), 127.09 (ArC), 126.01 (ArC), 124.76 (ArC), 124.62 (ArC), 119.03 (ArC), 115.25 (ArC), 113.49 (ArC), 36.86 (d, J<sub>CP</sub> = 11.6 Hz, *o*-PCy), 31.35 (d, J<sub>CP</sub> = 17.4 Hz, *ipso*-PCy), 29.24 (NCMe<sub>2</sub>), 28.67 (NCMe<sub>2</sub>), 28.52 (d, J<sub>CP</sub> = 10.0 Hz, *m*-PCy), 26.40 (*p*-PCy), 25.05 (CHMe<sub>2</sub>), 24.57 (d, J<sub>CP</sub> = 3.5 Hz, CHMe<sub>2</sub>), 24.05 (d, J<sub>CP</sub> = 5.3 Hz, CHMe<sub>2</sub>), 23.98 (CHMe<sub>2</sub>), 21.84 (NCMe). <sup>31</sup>P {<sup>1</sup>H} NMR (121.32 MHz, C<sub>6</sub>D<sub>6</sub>, 298 K): δ -22.3. UV-vis (Hexane, 25 °C) [λ<sub>max</sub>, nm (ε, mol<sup>-1</sup> L cm<sup>-1</sup>): 253 (23,300), 439 (6,900). Anal. Calcd for C<sub>44</sub>H<sub>63</sub>N<sub>2</sub>PZn: C, 73.77; H, 8.86; N, 3.91. Found: C, 73.65; H, 9.01; N, 3.87

**[*o*-C<sub>6</sub>H<sub>4</sub>{C(CH<sub>3</sub>)=N-2,6-*i*Pr<sub>2</sub>C<sub>6</sub>H<sub>3</sub>}{NH(2,6-*i*Pr<sub>2</sub>C<sub>6</sub>H<sub>3</sub>)}ZnP(C<sub>6</sub>H<sub>5</sub>)<sub>2</sub>], [Ar-BDl<sub>Dipp</sub>ZnPPh<sub>2</sub>] (14)** To a stirring solution of [Ar-BDl<sub>Dipp</sub>ZnBr] (0.080 g, 0.134 mmol) in hexane (5 mL) a lithium diphenylphosphanide (0.026 g, 0.134 mmol) slurry in hexane (5 mL) was added. The reaction was left stirring for 36 hours where a white solid was suspended in a yellow solution. The reaction was filtered through celite and the volatiles were removed in *vacuo*. The resulting yellow solid was clean via <sup>1</sup>H NMR (0.046 g, 49%). Crystals were grown from minimum hexane. <sup>1</sup>H NMR (299.74 MHz, C<sub>6</sub>D<sub>6</sub>, 298 K) δ 7.46 (d, J = 8.5 Hz, 1H, C<sub>6</sub>H<sub>4</sub>), 7.29-7.03 (m, 7H, ArH), 6.88 (m, 10H, PPh<sub>2</sub>), 6.67 (d, J = 8.9 Hz, 1H, C<sub>6</sub>H<sub>4</sub>), 6.40 (t, J = 7.6 Hz, 1H, C<sub>6</sub>H<sub>4</sub>), 3.37 (septet, J = 6.8 Hz, 2H, CHMe<sub>2</sub>), 2.91 (septet, J = 6.8 Hz, 2H, CHMe<sub>2</sub>), 1.96 (s, 3H, NCMe), 1.13 (d, J = 7.3 Hz, 6H, CHMe<sub>2</sub>), 1.10 (d, J = 7.3 Hz, 6H, CHMe<sub>2</sub>), 1.07 (d, J = 7.0 Hz, 6H, CHMe<sub>2</sub>),

0.95 (d,  $J = 6.8$  Hz, 6H, CHMe<sub>2</sub>). <sup>13</sup>C NMR (150.76 MHz, C<sub>6</sub>D<sub>6</sub>, 298 K):  $\delta$  176.04 (NCMe), 158.15 (ArC), 145.26 (d,  $J_{CP} = 105.4$  Hz, *ipso*-PPh), 144.30 (ArC), 139.92 (ArC), 139.67 (ArC), 139.55 (ArC), 135.21 (d,  $J_{CP} = 18.1$  Hz, *m*-PPh), 133.63 (d,  $J_{CP} = 37.9$  Hz, *o*-PPh), 127.17 (ArC), 126.32 (ArC), 125.56 (ArC), 125.07 (ArC), 124.95 (ArC), 118.78 (ArC), 115.27 (ArC), 113.95 (ArC), 29.30 (CHMe<sub>2</sub>), 28.64 (CHMe<sub>2</sub>), 24.62 (CHMe<sub>2</sub>), 24.32 (d,  $J_{CP} = 3.4$  Hz, CHMe<sub>2</sub>), 23.83 (CHMe<sub>2</sub>), 23.46 (d,  $J_{CP} = 5.3$  Hz, CHMe<sub>2</sub>), 21.51 (NCMe). <sup>31</sup>P {<sup>1</sup>H} NMR (121.32 MHz, C<sub>6</sub>D<sub>6</sub>, 298 K):  $\delta$  -47.7. UV-vis (Hexane, 25 °C) [ $\lambda_{max}$ , nm ( $\epsilon$ , mol<sup>-1</sup> L cm<sup>-1</sup>): 254 (54,200), 436 (12,700).

**[*o*-C<sub>6</sub>H<sub>4</sub>{C(CH<sub>3</sub>)=N-2,6-*i*Pr<sub>2</sub>C<sub>6</sub>H<sub>3</sub>}{NH(2,6-*i*Pr<sub>2</sub>C<sub>6</sub>H<sub>3</sub>)Zn(S)<sub>2</sub>P(C<sub>6</sub>H<sub>11</sub>)<sub>2</sub>], [Ar-BDI<sub>Dipp</sub>Zn(S)<sub>2</sub>PCy<sub>2</sub>]**

**(15)** To a stirring slurry of [Ar-BDI<sub>Dipp</sub>ZnPCy<sub>2</sub>] (0.120 g, 0.176 mmol) in toluene (5 mL) dried sulfur powder was added (0.028 g, 0.882 mmol). The reaction was left to react for 16 hours. The resulting bright yellow solution with light precipitate was filtered through celite and the volatiles were removed in *vacuo*. Hexane was added to the residue (2 mL) and filtered again. The resulting solution was kept at -30 °C. Bright yellow/green highly fluorescent rectangular crystals grew after 24 hours (0.087 g, 63%). <sup>1</sup>H NMR (299.74 MHz, C<sub>6</sub>D<sub>6</sub>, 298 K):  $\delta$  7.49 (dd,  $J = 8.6, 1.7$  Hz, 1H, C<sub>6</sub>H<sub>4</sub>), 7.40 – 7.25 (m, 6H, ArH), 6.86 (ddd,  $J = 8.5, 6.5, 1.7$  Hz, 1H, C<sub>6</sub>H<sub>4</sub>), 6.65 (dd,  $J = 8.9, 1.3$  Hz, 1H, C<sub>6</sub>H<sub>4</sub>), 6.35 (ddd,  $J = 8.4, 6.7, 1.8$  Hz, 1H, C<sub>6</sub>H<sub>4</sub>), 3.65 (septet,  $J = 6.8$  Hz, 2H, CHMe<sub>2</sub>), 3.15 (p,  $J = 6.7$  Hz, 2H, CHMe<sub>2</sub>), 2.09 (s, 3H, NCMe), 1.63 (d,  $J = 6.8$  Hz, 6H, CHMe<sub>2</sub>), 1.59 (d,  $J = 6.8$  Hz, 6H, CHMe<sub>2</sub>), 1.21 (d,  $J = 6.8$  Hz, 6H, CHMe<sub>2</sub>), 0.96 (d,  $J = 6.7$  Hz, 6H, CHMe<sub>2</sub>), cyclohexyl peaks were a range of multiplets from 1.55-1.13 ppm. <sup>13</sup>C NMR (150 MHz, C<sub>6</sub>D<sub>6</sub>, 298 K):  $\delta$  175.96 (NCMe), 159.38 (ArC), 145.25 (ArC), 145.18 (ArC), 144.42 (ArC), 141.31 (ArC), 133.81 (ArC), 132.86 (ArC), 126.45 (ArC), 125.32 (ArC), 124.38 (ArC), 124.29 (ArC), 120.30 (ArC), 114.19 (ArC), 112.24 (ArC), 29.19 (CHMe<sub>2</sub>), 28.88 (CHMe<sub>2</sub>), 26.33 (CHMe<sub>2</sub>), 25.48 (br, PCy<sub>2</sub>), 25.21 (CHMe<sub>2</sub>), 24.41 (CHMe<sub>2</sub>), 24.30 (CHMe<sub>2</sub>), 23.70 (NCMe). <sup>31</sup>P {<sup>1</sup>H} NMR (121.32 MHz, C<sub>6</sub>D<sub>6</sub>, 298 K):  $\delta$  93.4. UV-vis (Hexane, 25 °C) [ $\lambda_{max}$ , nm ( $\epsilon$ , mol<sup>-1</sup> L cm<sup>-1</sup>): 253 (61,000), 446 (13,900).

**[*o*-C<sub>6</sub>H<sub>4</sub>{C(CH<sub>3</sub>)=N-2,6-*i*Pr<sub>2</sub>C<sub>6</sub>H<sub>3</sub>}{NH(2,6-*i*Pr<sub>2</sub>C<sub>6</sub>H<sub>3</sub>)Zn(Se)<sub>2</sub>P(C<sub>6</sub>H<sub>11</sub>)<sub>2</sub>], [Ar-BDI<sub>Dipp</sub>Zn(Se)<sub>2</sub>PCy<sub>2</sub>]**

**(16)** To a stirring slurry of [Ar-BDI<sub>Dipp</sub>ZnPCy<sub>2</sub>] (0.120 g, 0.176 mmol) in toluene (5 mL) dried selenium powder was added (0.070 g, 0.882 mmol). The reaction was left to react for 16 hours. The resulting orange solution with dark precipitate was filtered through celite and the volatiles were removed in *vacuo*. Hexane was added to the residue (2 mL) and kept at

-30 °C. Bright yellow rectangular crystals suitable for characterization and X-ray diffraction grew after 24 hours (0.062 g, 42%). <sup>1</sup>H NMR (299.74 MHz, C<sub>6</sub>D<sub>6</sub>, 298 K): δ 7.46 (d, J = 8.7 Hz, 1H, C<sub>6</sub>H<sub>4</sub>), 7.39-7.19 (m, 6H, ArH), 6.86 (t, J = 8.1 Hz, 1H, C<sub>6</sub>H<sub>4</sub>), 6.66 (d, J = 9.5 Hz, 1H, C<sub>6</sub>H<sub>4</sub>), 6.34 (t, J = 7.5 Hz, 1H, C<sub>6</sub>H<sub>4</sub>), 3.67 (septet, J = 6.6 Hz, 2H, CHMe<sub>2</sub>), 3.17 (septet, J = 6.7 Hz, 2H, CHMe<sub>2</sub>), 2.09 (s, 6H, NCMe), 1.64 (d, J = 6.8 Hz, 6H, CHMe<sub>2</sub>), 1.61 (d, J = 6.9 Hz, 6H, CHMe<sub>2</sub>), 1.23 (d, J = 6.4 Hz, 6H, CHMe<sub>2</sub>), 0.98 (d, J = 6.7 Hz, 6H, CHMe<sub>2</sub>), cyclohexyl peaks were a range of multiplets from 1.57-0.88 ppm. <sup>13</sup>C NMR (150.76 MHz, C<sub>6</sub>D<sub>6</sub>, 298 K): δ 175.61 (NCMe), 159.15 (ArC), 145.48 (ArC), 145.17 (ArC), 144.69 (ArC), 141.25 (ArC), 133.75 (ArC), 132.63 (ArC), 126.39 (ArC), 125.25 (ArC), 124.40 (ArC), 124.32 (ArC), 120.64 (ArC), 114.39 (ArC), 112.18 (ArC), 29.31 (CHMe<sub>2</sub>), 29.03 (CHMe<sub>2</sub>), 26.61 (PCy), 26.38 (PCy), 26.36 (d, J<sub>CP</sub> = 15.3 Hz, *ipso*-PCy), 26.09 (PCy), 25.28 (CHMe<sub>2</sub>), 24.76 (CHMe<sub>2</sub>), 24.66 (CHMe<sub>2</sub>), 24.23 (NCMe). <sup>31</sup>P {<sup>1</sup>H} NMR (121.32 MHz, C<sub>6</sub>D<sub>6</sub>, 298 K): δ 51.2 (J<sub>PSe</sub> = 447.9 Hz). UV-vis (Hexane, 25 °C) [λ<sub>max</sub>, nm (ε, mol<sup>-1</sup> L cm<sup>-1</sup>): 255 (58,900), 446 (10,600).

**[*o*-C<sub>6</sub>H<sub>4</sub>{C(CH<sub>3</sub>)=N-2,6-*i*Pr<sub>2</sub>C<sub>6</sub>H<sub>3</sub>}{NH(2,6-*i*Pr<sub>2</sub>C<sub>6</sub>H<sub>3</sub>)Zn(Se)<sub>2</sub>P(C<sub>6</sub>H<sub>11</sub>)<sub>2</sub>], [Ar-BDl<sub>Dipp</sub>Zn(Te)<sub>2</sub>PCy<sub>2</sub>]**  
**(17)** To a stirring slurry of [Ar-BDl<sub>Dipp</sub>ZnPCy<sub>2</sub>] (0.030 g, 0.042 mmol) in toluene (5 mL) dried tellurium powder was added (0.011 g, 0.084 mmol). The reaction was left to react for 72 hours. The resulting orange solution with dark precipitate was filtered through celite and the volatiles were removed in *vacuo*. Hexane was added to the residue (2 mL) and kept at -30 °C. Orange rectangular crystals suitable for characterization and X-ray diffraction grew after 24 hours (0.017 g, 41%). δ 7.48 – 7.21 (m, 6H, ArH), 6.93 – 6.79 (m, 2H, C<sub>4</sub>H<sub>4</sub>), 6.62 (d, J = 8.8 Hz, 1H, C<sub>6</sub>H<sub>4</sub>), 6.31 (t, J = 7.4 Hz, 1H, C<sub>6</sub>H<sub>4</sub>), 3.74 (septet, J = 6.8 Hz, 2H, CHMe<sub>2</sub>), 3.27 (septet, J = 6.7 Hz, 2H, CHMe<sub>2</sub>), 2.05 (s, 3H, NCMe), 1.64 (d, J = 6.8 Hz, 12H, CHMe<sub>2</sub>), 1.29 (d, J = 6.7 Hz, 6H, CHMe<sub>2</sub>), 1.05 (d, J = 6.7 Hz, 6H, CHMe<sub>2</sub>). cyclohexyl peaks were a range of multiplets from 1.55-0.87 ppm. <sup>13</sup>C NMR (150.76 MHz, C<sub>6</sub>D<sub>6</sub>, 298 K): δ 175.29 (NCMe), 158.82 (ArC), 145.97 (ArC), 145.41 (ArC), 141.30 (ArC), 133.60 (ArC), 132.27 (ArC), 128.37 (ArC), 126.63 (ArC), 125.45 (ArC), 124.57 (ArC), 124.55 (ArC), 121.12 (ArC), 115.22 (ArC), 112.23 (ArC), 37.32 (d, J = 14.4 Hz, *o*-PCy), 29.30 (CHMe<sub>2</sub>), 29.09 (*m*-PCy), 28.97 (CHMe<sub>2</sub>), 26.22 (CHMe<sub>2</sub>), 26.17 (CHMe<sub>2</sub>), 26.12 (NCMe<sub>2</sub>), 26.00 (PCy), 25.86 (d, J = 17.4 Hz, *ipso*-PCy), 25.25 (NCMe<sub>2</sub>), 25.00 (NCMe). <sup>31</sup>P {<sup>1</sup>H} NMR (121.32 MHz, C<sub>6</sub>D<sub>6</sub>, 298 K): δ 160.3. UV-vis (Hexane, 25 °C) [λ<sub>max</sub>, nm (ε, mol<sup>-1</sup> L cm<sup>-1</sup>): 254 (29,700), 451 (4,400).

**[*o*-C<sub>6</sub>H<sub>4</sub>{C(CH<sub>3</sub>)=N-2,6-*i*Pr<sub>2</sub>C<sub>6</sub>H<sub>3</sub>}{NH(2,6-*i*Pr<sub>2</sub>C<sub>6</sub>H<sub>3</sub>)Zn(Se)<sub>2</sub>P(C<sub>6</sub>H<sub>5</sub>)<sub>2</sub>], [Ar-BDI<sub>Dipp</sub>ZnSe<sub>2</sub>PPh<sub>2</sub>]**

**(18)** To a stirring slurry of [Ar-BDI<sub>Dipp</sub>ZnPPh<sub>2</sub>] (0.090 g, 0.128 mmol) in toluene (5 mL) dried selenium powder was added (0.060 g, 0.760 mmol). The reaction was left to react for 16 hours. The resulting orange solution with dark precipitate was filtered through celite and the volatiles were removed in *vacuo*. Hexane was added to the residue (2 mL) and kept at -30 °C. Orange rectangular crystals grew after 24 hours but were not suitable for X-ray diffraction (0.057 g, 52%). <sup>1</sup>H NMR (299.74 MHz, C<sub>6</sub>D<sub>6</sub>, 298 K): δ 7.37 (d, J = 8.7 Hz, 1H, C<sub>4</sub>H<sub>4</sub>), 7.34 – 7.26 (m, 5H, ArH), 6.83 (m, 12H, ArH), 6.63 (d, J = 8.9 Hz, 1H, C<sub>4</sub>H<sub>4</sub>), 6.33 (t, J = 7.5 Hz, 1H, C<sub>4</sub>H<sub>4</sub>), 3.78 (septet, J = 6.8 Hz, 2H, CHMe<sub>2</sub>), 3.27 (septet, J = 6.9 Hz, 2H, CHMe<sub>2</sub>), 2.03 (s, 3H, NCMe), 1.41 (d, J = 3.6 Hz, 6H, CHMe<sub>2</sub>), 1.40 (d, J = 3.5 Hz, 6H, CHMe<sub>2</sub>), 1.26 (d, J = 6.8 Hz, 6H, CHMe<sub>2</sub>), 1.03 (d, J = 6.7 Hz, 6H, CHMe<sub>2</sub>). <sup>13</sup>C NMR (150.76 MHz, C<sub>6</sub>D<sub>6</sub>, 298 K): δ 176.02 (NCMe), 159.47 (ArC), 145.32 (ArC), 145.29 (ArC), 144.39 (ArC), 141.25 (ArC), 133.72 (ArC), 132.73 (ArC), 131.14 (ArC), 131.06 (ArC), 130.85 (ArC), 128.36 (ArC), 126.70 (ArC), 125.50 (ArC), 124.66 (ArC), 120.49 (ArC), 115.55 (ArC), 112.51 (ArC), 29.16 (CHMe<sub>2</sub>), 28.71 (CHMe<sub>2</sub>), 25.91 (CHMe<sub>2</sub>), 25.31 (CHMe<sub>2</sub>), 25.09 (CHMe<sub>2</sub>), 24.90 (CHMe<sub>2</sub>), 24.09 (NCMe). <sup>31</sup>P {<sup>1</sup>H} NMR (121.32 MHz, C<sub>6</sub>D<sub>6</sub>, 298 K): δ 6.14 (J<sub>PSe</sub> = 466.5 Hz). UV-vis (Hexane, 25 °C) [λ<sub>max</sub>, nm (ε, mol<sup>-1</sup> L cm<sup>-1</sup>): 252 (50,400), 446 (11,300).

**[*o*-C<sub>6</sub>H<sub>4</sub>{C(CH<sub>3</sub>)=N-2,6-*i*Pr<sub>2</sub>C<sub>6</sub>H<sub>3</sub>}{NH(2,6-*i*Pr<sub>2</sub>C<sub>6</sub>H<sub>3</sub>)Zn]Te, [Ar-BDI<sub>Dipp</sub>Zn]<sub>2</sub>Te (19)**

To a stirring slurry of [Ar-BDI<sub>Dipp</sub>ZnPPh<sub>2</sub>] (0.030 g, 0.043 mmol) in toluene (5 mL) dried tellurium powder was added (0.060 g, 0.470 mmol). The reaction was left to react for 48 hours. The resulting orange solution with dark precipitate was filtered through celite and the volatiles were removed in *vacuo*. Hexane was added to the residue (2 mL) and kept at -30 °C. Golden yellow rectangular crystals suitable for characterization and X-ray diffraction grew after 72 hours (0.037 g, 73%). <sup>1</sup>H NMR (599.48 MHz, C<sub>6</sub>D<sub>6</sub>, 298 K): δ 7.34 (dd, J = 8.5, 1.6 Hz, 2H, C<sub>4</sub>H<sub>4</sub>), 7.28 – 7.19 (m, 18H, ArH), 7.10 – 7.00 (m, 18H, ArH), 6.81 (ddd, J = 8.6, 6.6, 1.6 Hz, 2H, C<sub>4</sub>H<sub>4</sub>), 6.47 (dd, J = 8.9, 1.8 Hz, 2H, C<sub>4</sub>H<sub>4</sub>), 6.36 (ddd, J = 8.4, 6.6, 1.5 Hz, 2H, C<sub>4</sub>H<sub>4</sub>), 3.40 (septet, J = 6.9 Hz, 4H, CHMe<sub>2</sub>), 2.85 (septet, J = 6.8 Hz, 4H, CHMe<sub>2</sub>), 1.94 (s, 6H, NCMe), 1.16 (d, J = 6.9 Hz, 12H, CHMe<sub>2</sub>), 1.12 (d, J = 6.8 Hz, 12H, CHMe<sub>2</sub>), 1.07 (d, J = 6.8 Hz, 12H, CHMe<sub>2</sub>), 1.03 (d, J = 6.8 Hz, 12H, CHMe<sub>2</sub>). <sup>13</sup>C NMR (150.76 MHz, C<sub>6</sub>D<sub>6</sub>, 298 K): δ 175.16 (NCMe), 157.94 (ArC), 145.34 (ArC), 144.91 (ArC), 143.58 (ArC), 140.36 (ArC), 133.17 (ArC),

132.76 (*ArC*), 126.86 (*ArC*), 125.85 (*ArC*), 124.83 (*ArC*), 124.25 (*ArC*), 119.33 (*ArC*), 117.10 (*ArC*), 113.79 (*ArC*), 29.15 (**CHMe<sub>2</sub>**), 28.37 (**CHMe<sub>2</sub>**), 25.65 (**CHMe<sub>2</sub>**), 25.22 (**CHMe<sub>2</sub>**), 24.74 (**CHMe<sub>2</sub>**), 24.18 (**NCMe**). Note the impurity [(Ph<sub>2</sub>P)<sub>2</sub>]: <sup>1</sup>H NMR (599.48 MHz, C<sub>6</sub>D<sub>6</sub>, 298 K): δ 7.54 – 7.48 (m, 10H, **PPh**), 6.94 – 6.89 (m, 10H, **PPh**). <sup>13</sup>C NMR (150.76 MHz, C<sub>6</sub>D<sub>6</sub>, 298 K): δ 136.61 (t, J<sub>CP</sub> = 11.1 Hz, **PPh**), 134.83 (t, J<sub>CP</sub> = 12.9 Hz, **PPh**), 128.90 (s, **PPh**), 128.59 (t, J<sub>CP</sub> = 7.7 Hz, **PPh**).



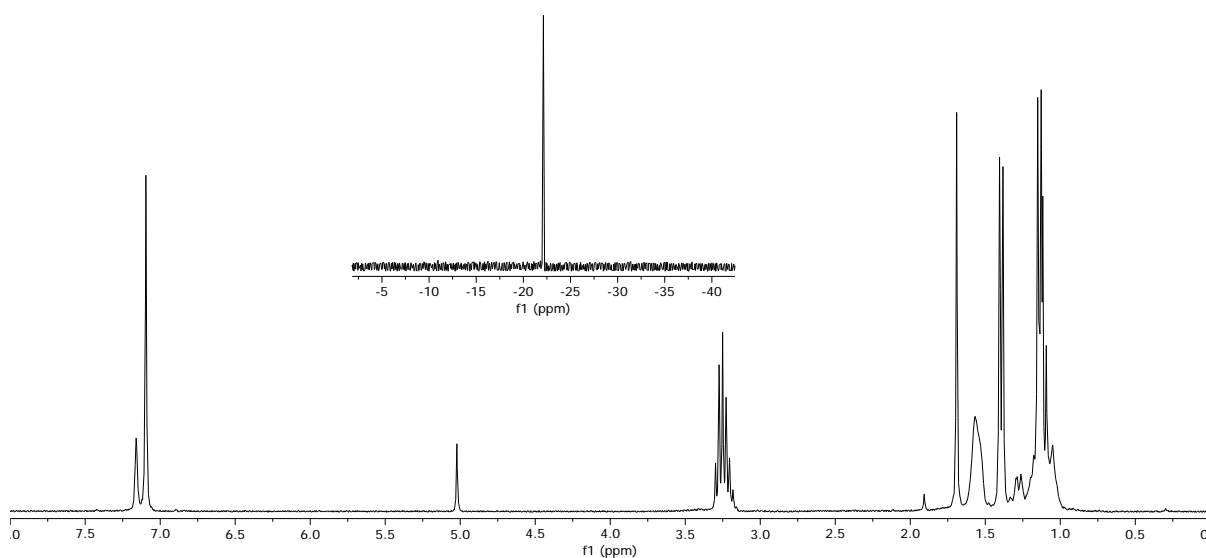
# Chapter 4

---

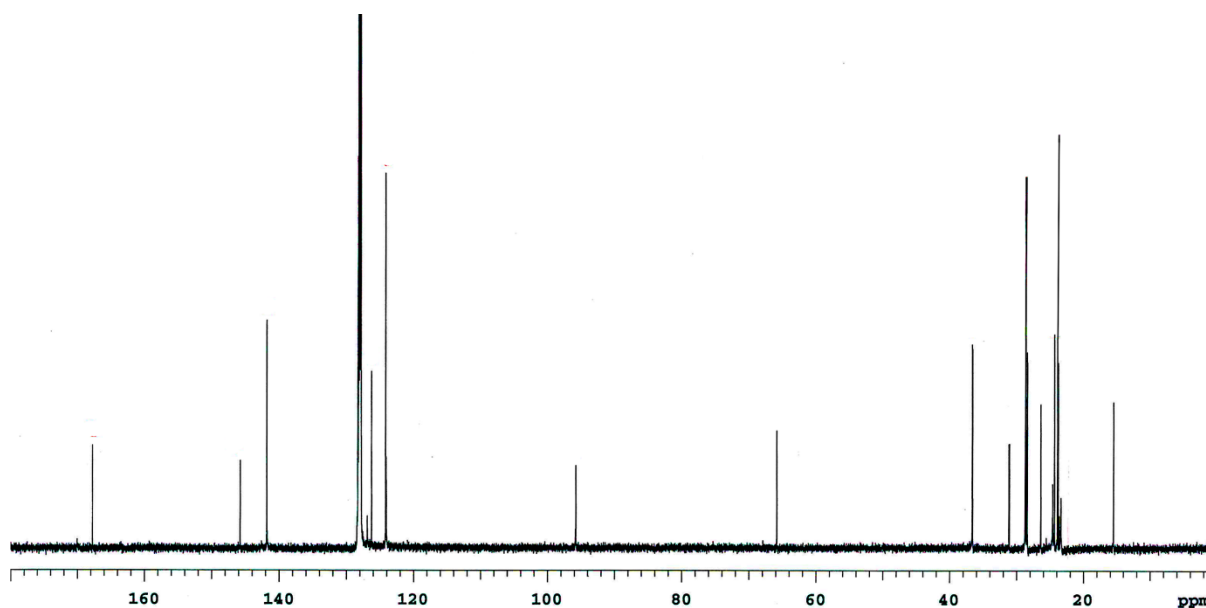
## Appendices

### 4.1 Appendix A: NMR Spectra of Novel Compounds

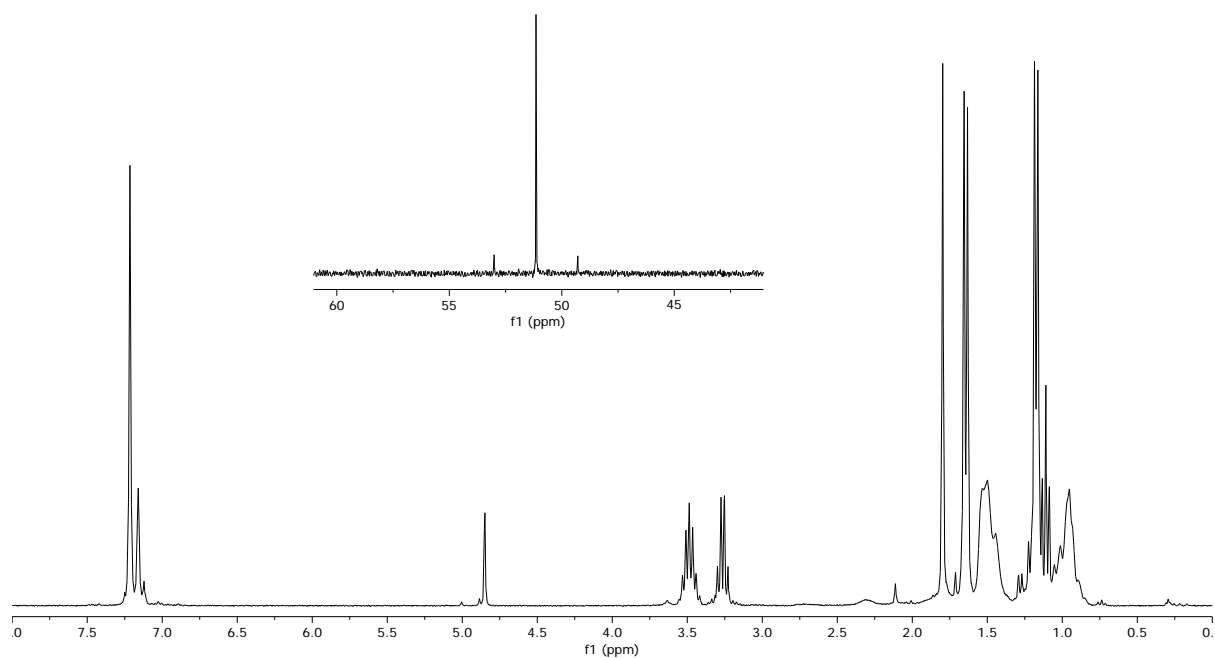
$^1\text{H}$  NMR (299.74 MHz,  $\text{C}_6\text{D}_6$ , 298 K) and  $^{31}\text{P}$  NMR (121.32 MHz  $\text{C}_6\text{D}_6$ , 298 K) spectra of  $[\text{BDI}_{\text{Dipp}}\text{ZnPCy}_2]$  **XXX** with diethyl ether



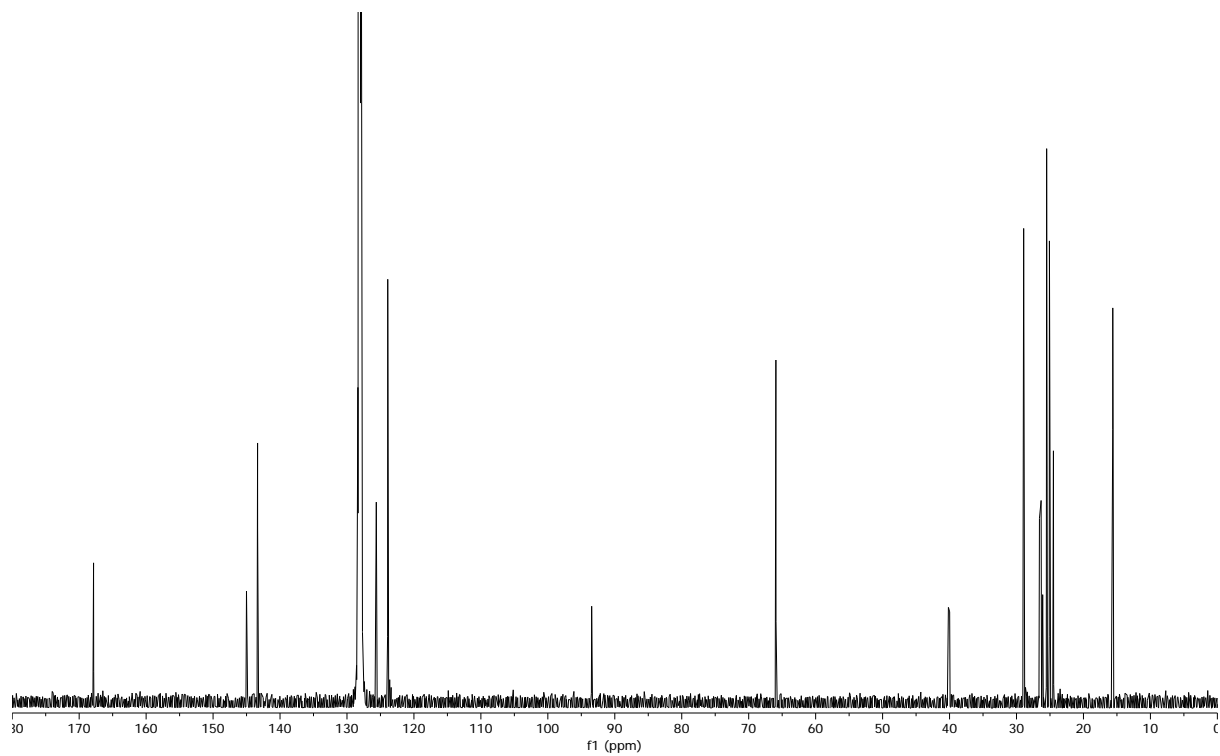
$^{13}\text{C}$  NMR spectrum of  $[\text{BDI}_{\text{Dipp}}\text{ZnPCy}_2]$  **XXX** (150.76 MHz,  $\text{C}_6\text{D}_6$ , 298 K) with diethyl ether



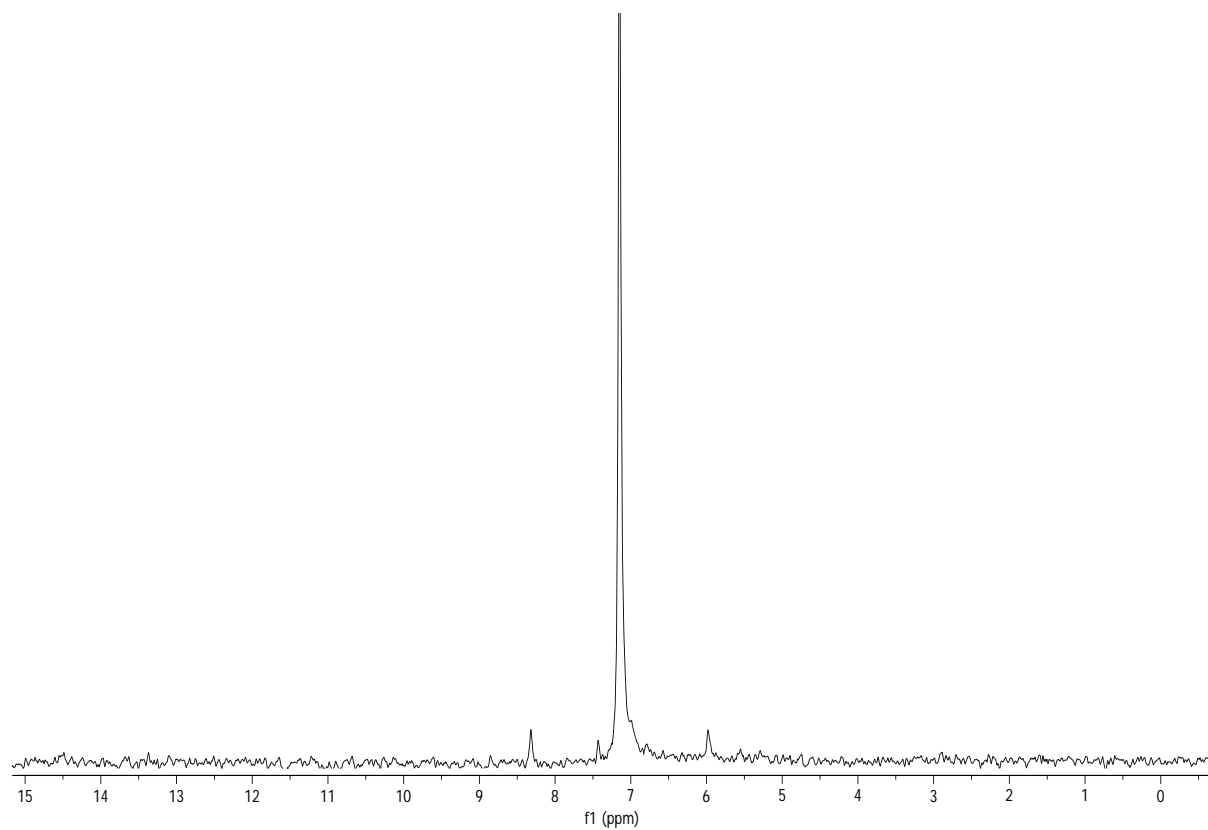
$^1\text{H}$  NMR (299.74 MHz  $\text{C}_6\text{D}_6$ , 298 K) and  $^{31}\text{P}$  NMR (121.32 MHz  $\text{C}_6\text{D}_6$ , 298 K) spectra of  $[\text{BDI}_{\text{Dipp}}\text{Zn}(\text{Se})_2\text{PCy}_2]$  **XXXIII** with diethyl ether



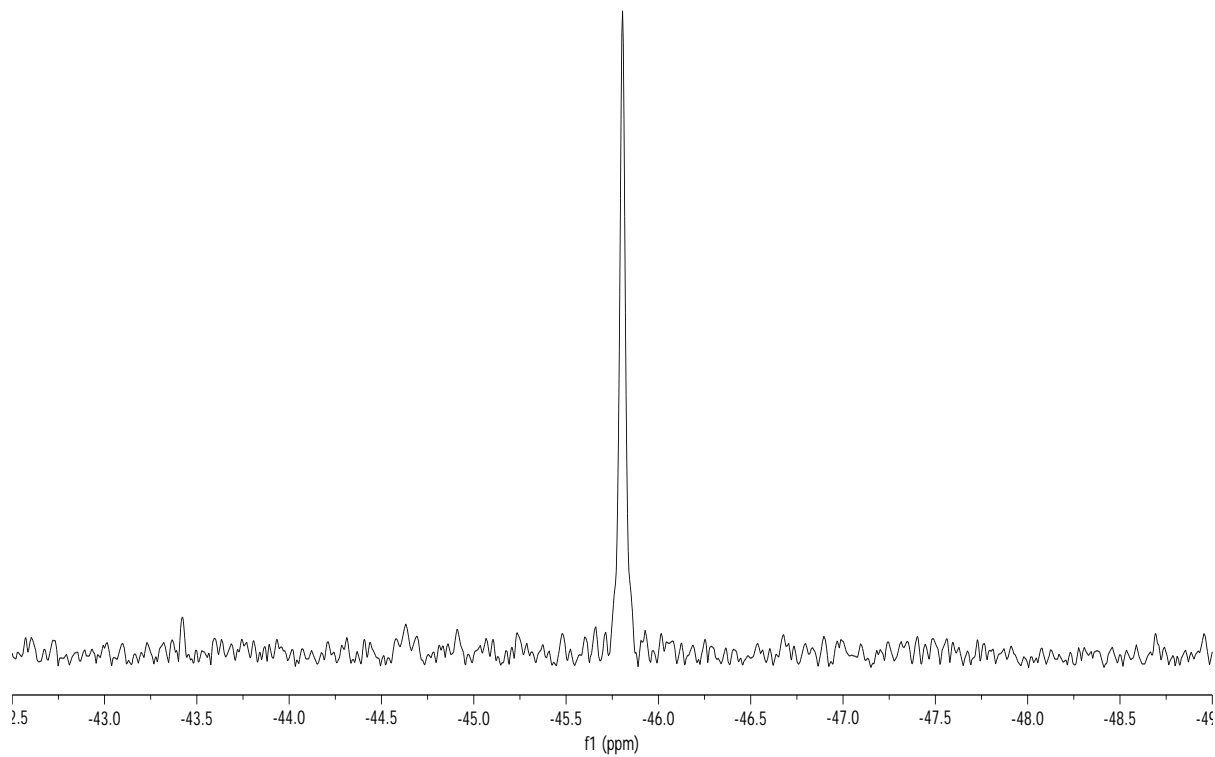
$^{13}\text{C}$  NMR spectrum of  $[\text{BDI}_{\text{Dipp}}\text{Zn}(\text{Se})_2\text{PCy}_2]$  **XXXIII** (150.76 MHz,  $\text{C}_6\text{D}_6$ , 298 K) with diethyl ether



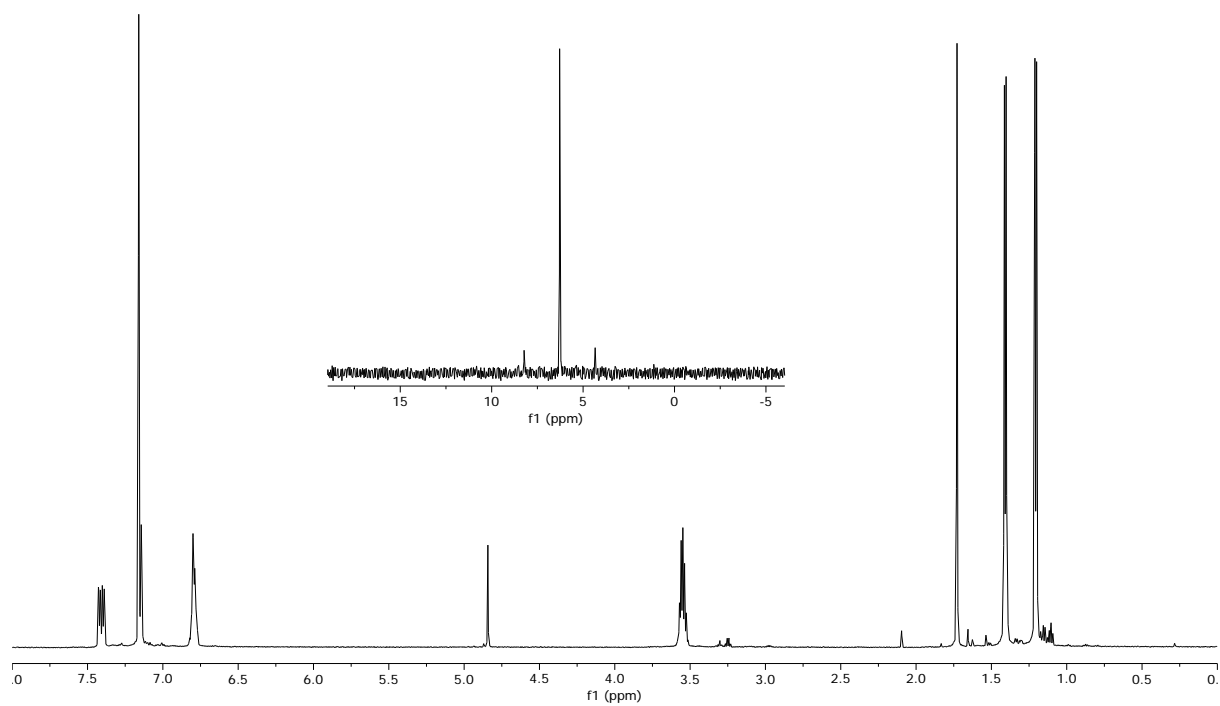
$^{31}\text{P}$  NMR (121.32 MHz,  $\text{C}_6\text{D}_6$ , 298 K) spectrum of  $[\text{BDI}_{\text{Dipp}}\text{Zn}(\text{Te})\text{PCy}_2]$  **XXXV**



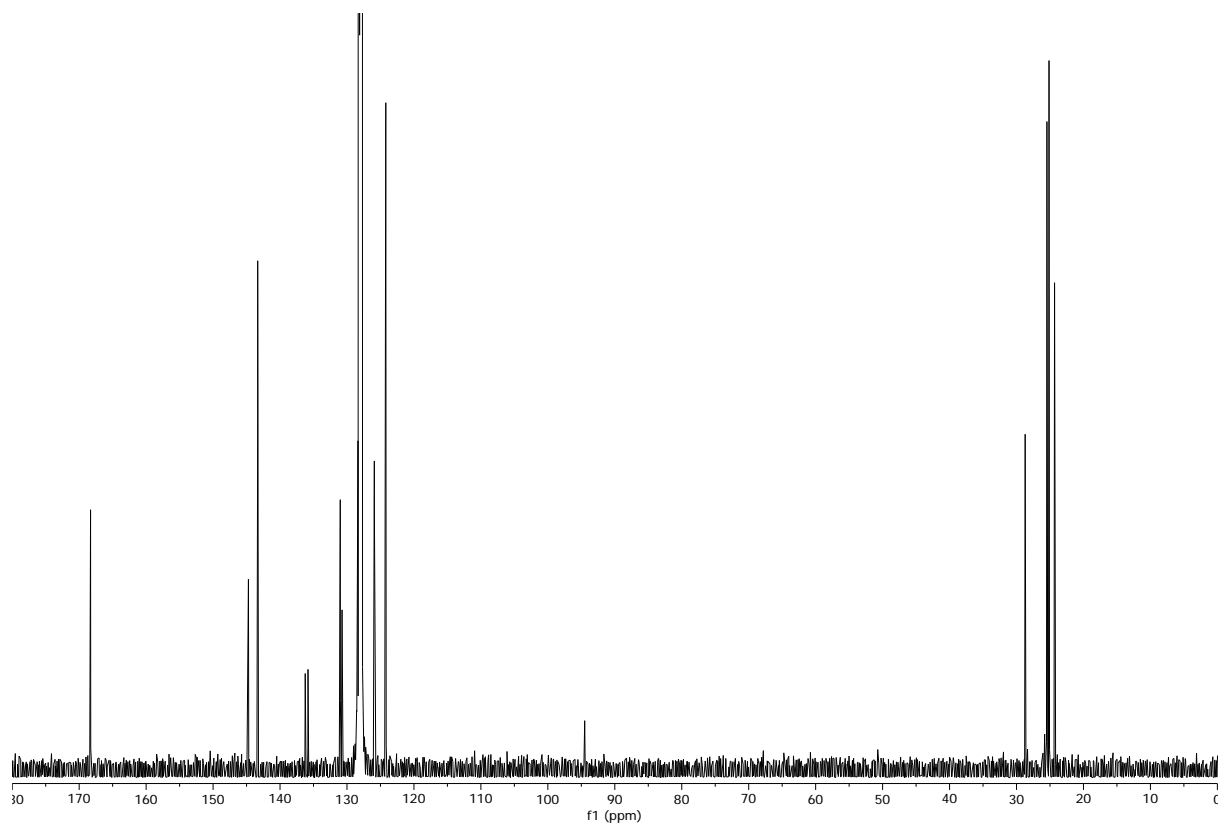
$^{31}\text{P}$  NMR (121.32 MHz,  $\text{C}_6\text{D}_6$ , 298 K) spectrum of  $[\text{BDI}_{\text{Dipp}}\text{ZnPPh}_2]$  **XXXI**



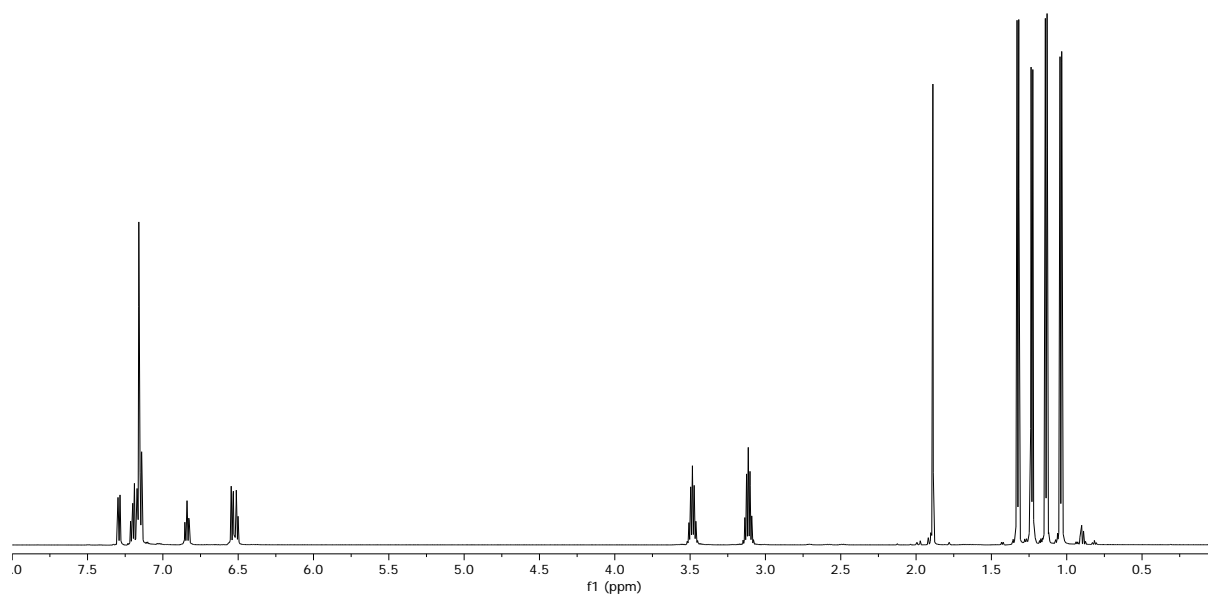
$^1\text{H}$  NMR (599.48 MHz  $\text{C}_6\text{D}_6$ , 298 K) and  $^{31}\text{P}$  NMR (121.32 MHz  $\text{C}_6\text{D}_6$ , 298 K) spectra of  $[\text{BDI}_{\text{Dipp}}\text{Zn}(\text{Se})_2\text{PPh}_2]$  **XXXIV**



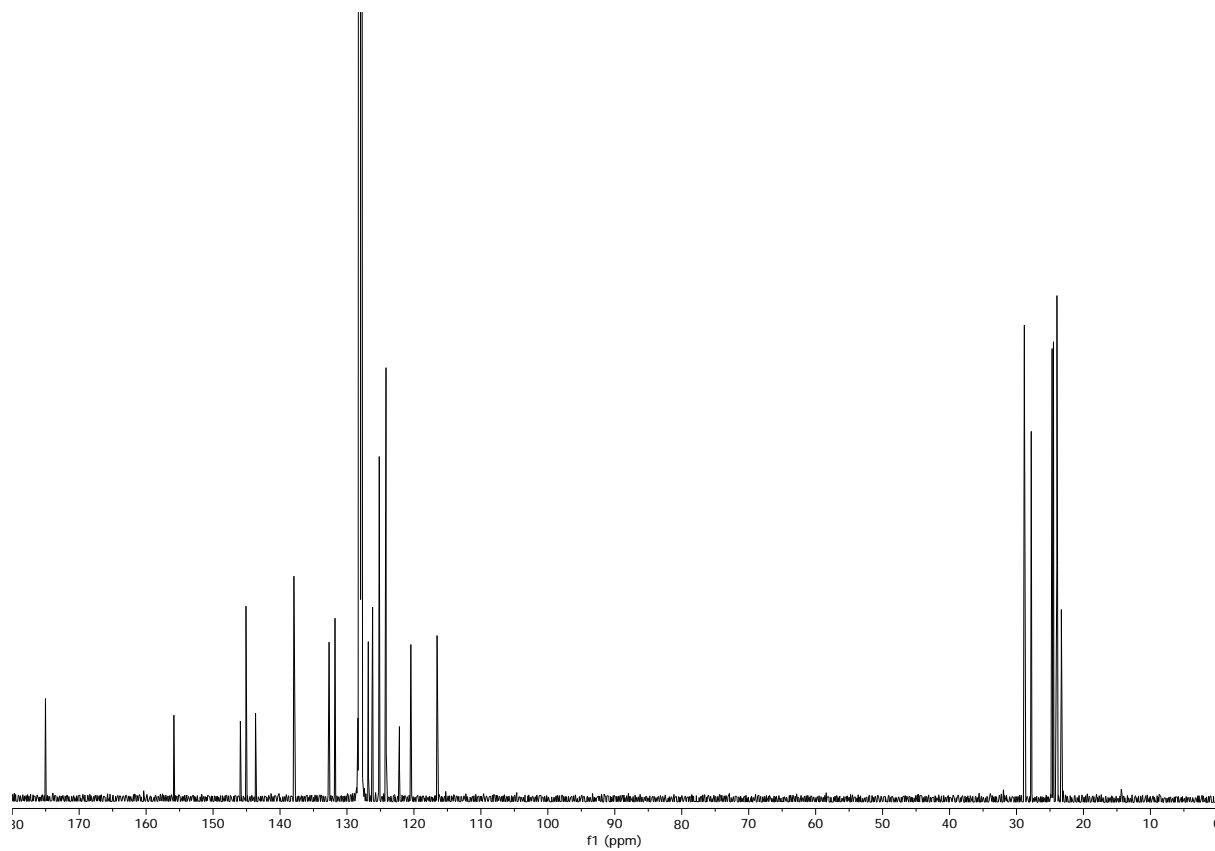
$^{13}\text{C}$  NMR spectrum of  $[\text{BDI}_{\text{Dipp}}\text{Zn}(\text{Se})_2\text{PPh}_2]$  **XXXIV** (150.76 MHz,  $\text{C}_6\text{D}_6$ , 298 K)



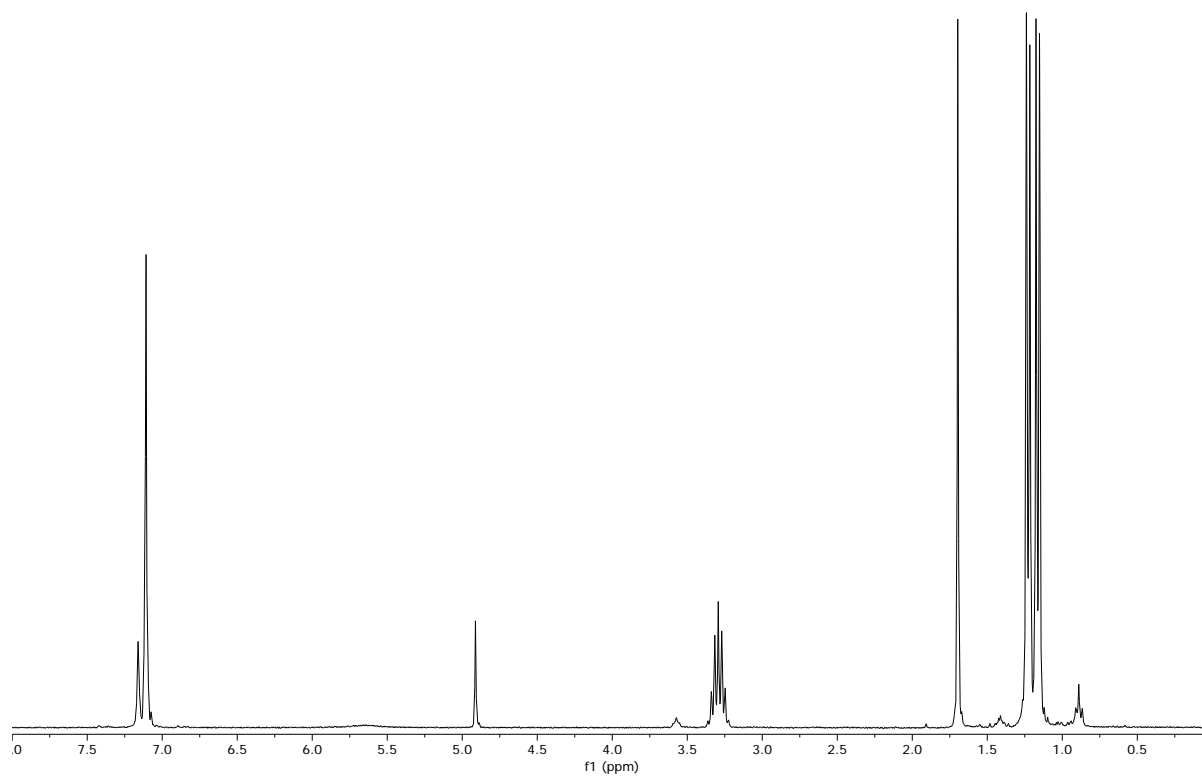
$^1\text{H}$  NMR spectrum of  $[\text{Ar-BDl}_{\text{Dipp}}\text{HgCl}]$  **1** (599.48 MHz,  $\text{C}_6\text{D}_6$ , 298 K)



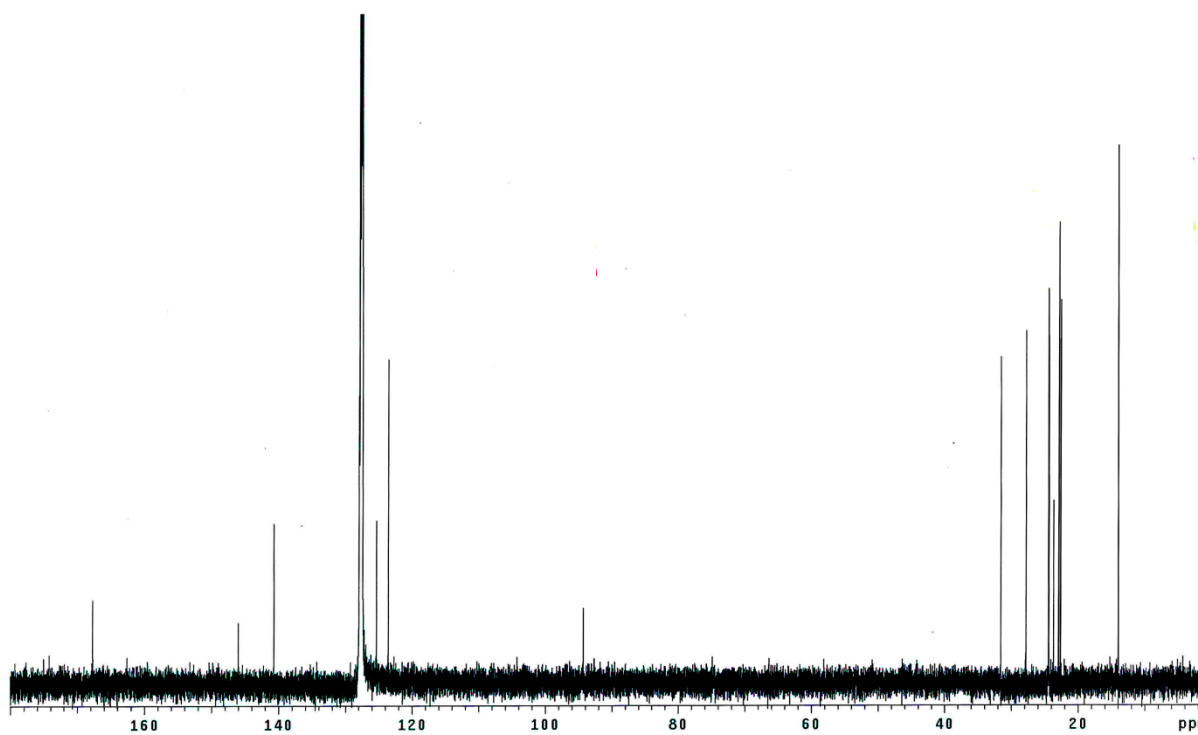
$^{13}\text{C}$  NMR spectrum of  $[\text{Ar-BDl}_{\text{Dipp}}\text{HgCl}]$  **1** (150.76 MHz,  $\text{C}_6\text{D}_6$ , 298 K)



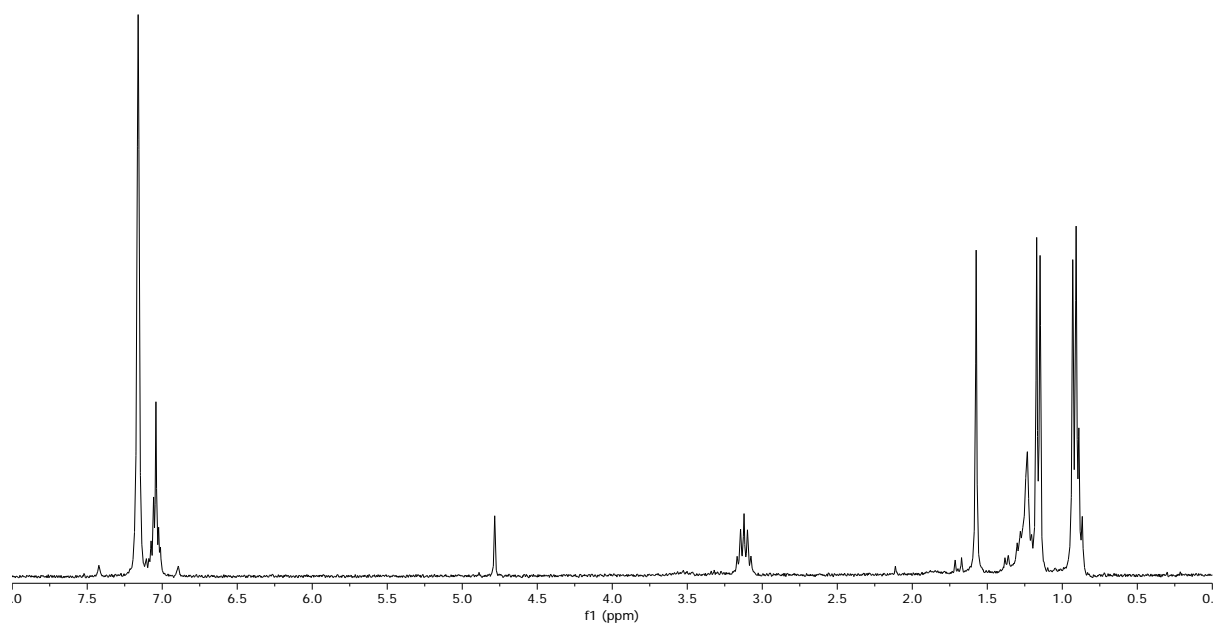
$^1\text{H}$  NMR spectrum of  $[\text{BDI}_{\text{Dipp}}\text{CdH}]$  **3** (299.74 MHz,  $\text{C}_6\text{D}_6$ , 298 K)



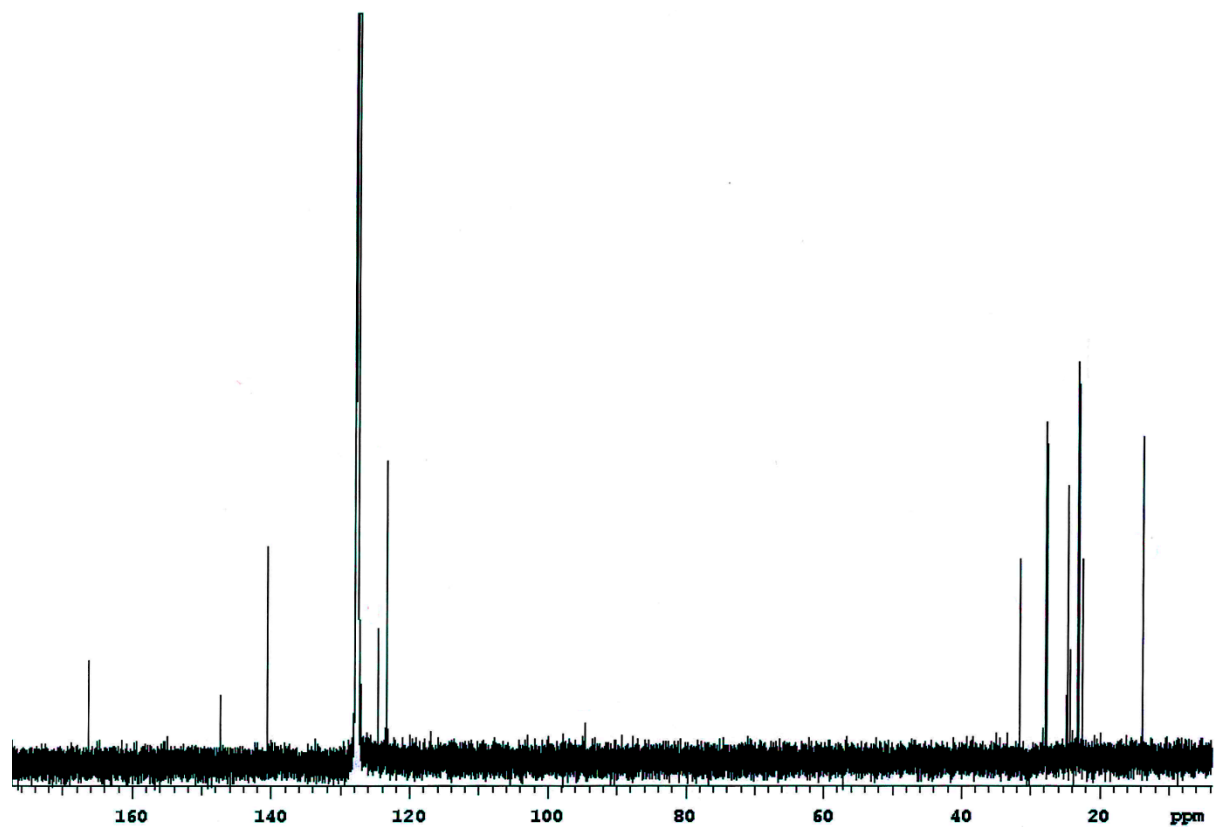
$^{13}\text{C}$  NMR spectrum of  $[\text{BDI}_{\text{Dipp}}\text{CdH}]$  **3** (150.76 MHz,  $\text{C}_6\text{D}_6$ , 298 K)



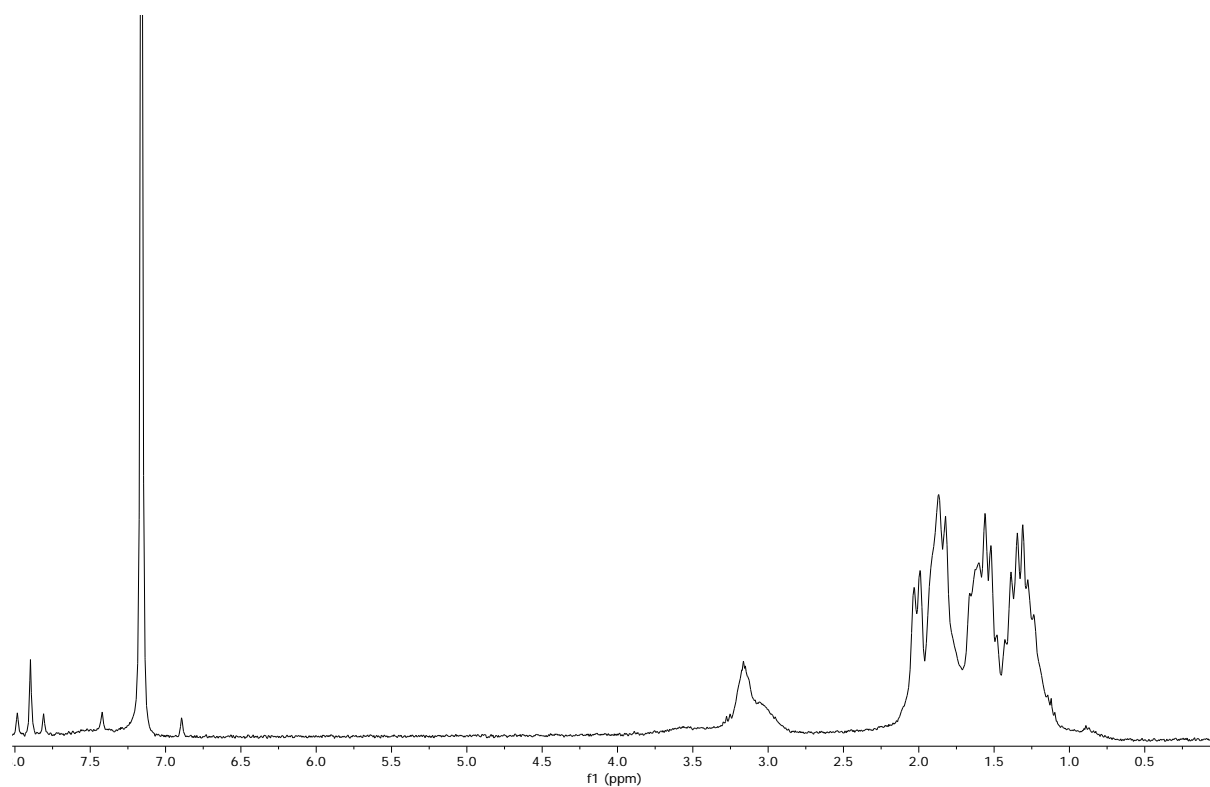
$^1\text{H}$  NMR spectrum of  $[\text{BDI}_{\text{Dipp}}\text{Cd}]_2$  **5** (299.74 MHz,  $\text{C}_6\text{D}_6$ , 298 K) with hexane



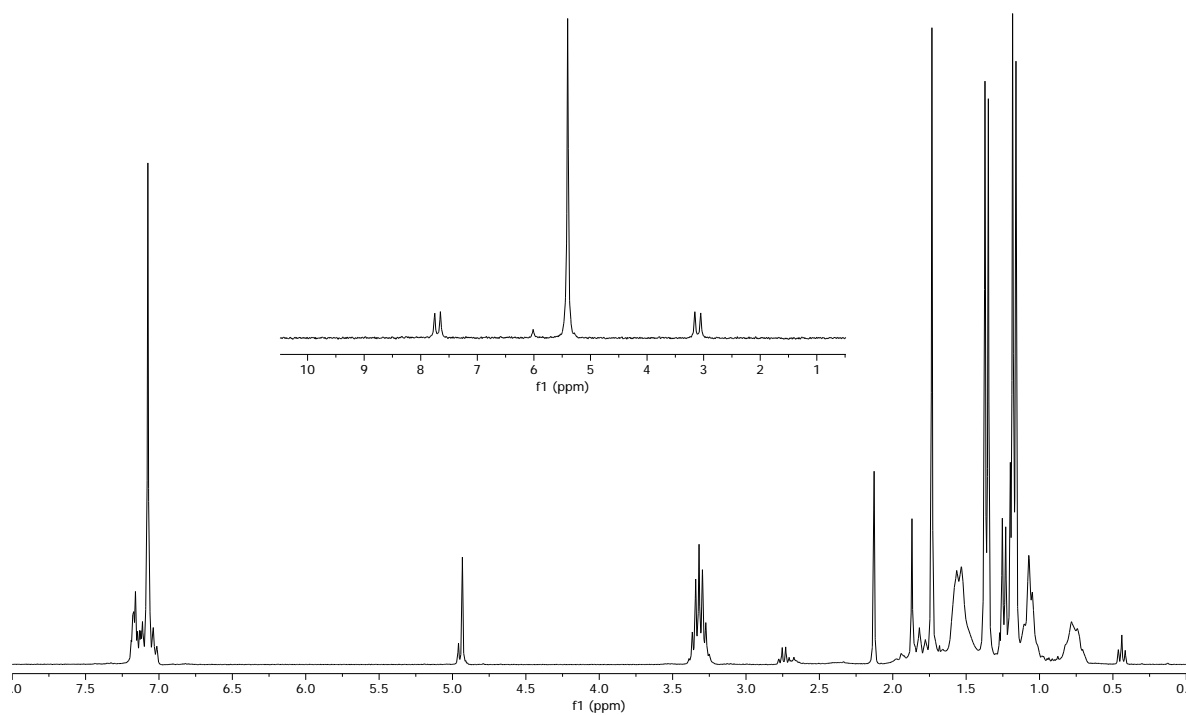
$^{13}\text{C}$  NMR spectrum of  $[\text{BDI}_{\text{Dipp}}\text{Cd}]_2$  **5** (150.76 MHz,  $\text{C}_6\text{D}_6$ , 298 K)



$^1\text{H}$  NMR spectrum of  $[(\text{DC-Am})_2(\text{DC-Fo})\text{Cd}]$  **8** (299.74 MHz,  $\text{C}_6\text{D}_6$ , 298 K)

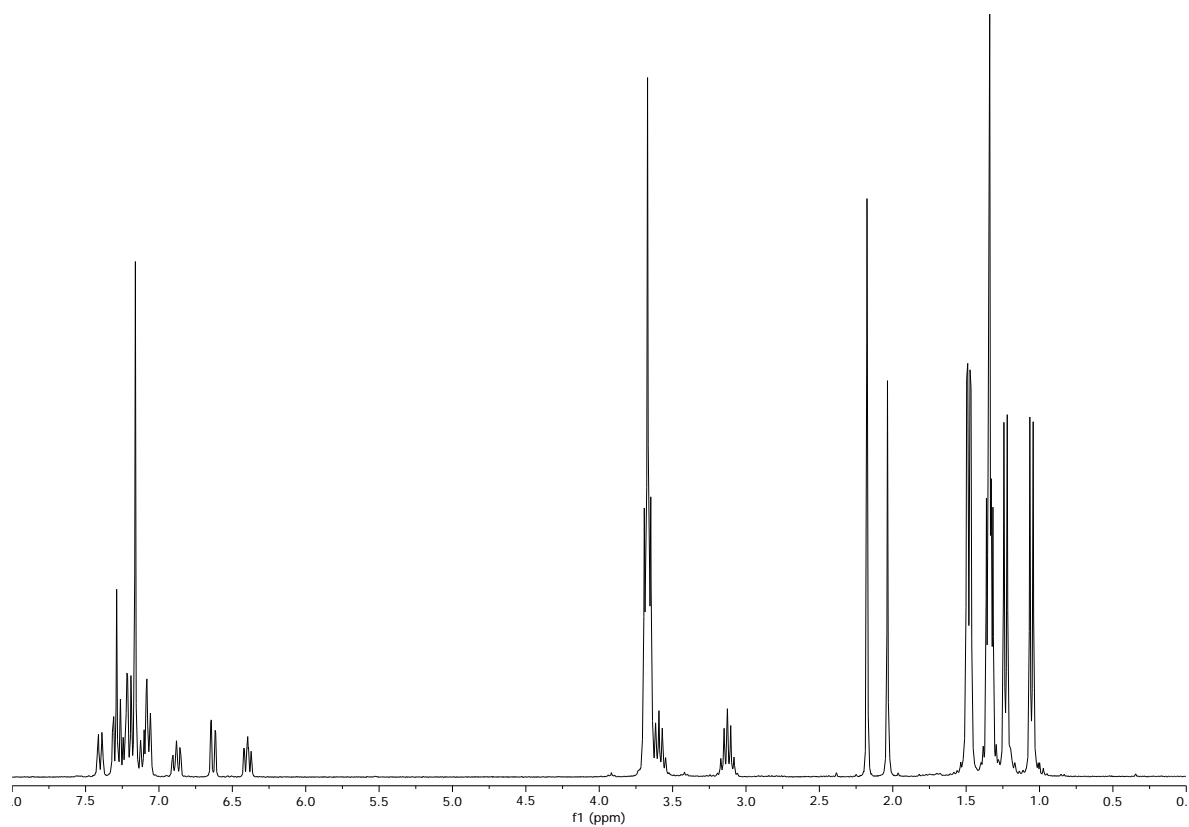


$^1\text{H}$  NMR (299.74 MHz  $\text{C}_6\text{D}_6$ , 298 K) and  $^{31}\text{P}$  NMR (121.32 MHz  $\text{C}_6\text{D}_6$ , 298 K) spectra of  $[\text{BDI}_{\text{Dipp}}\text{CdPCy}_2]$  **2** with toluene and  $[\text{BDI}_{\text{Dipp}}\text{-H}]$  impurity

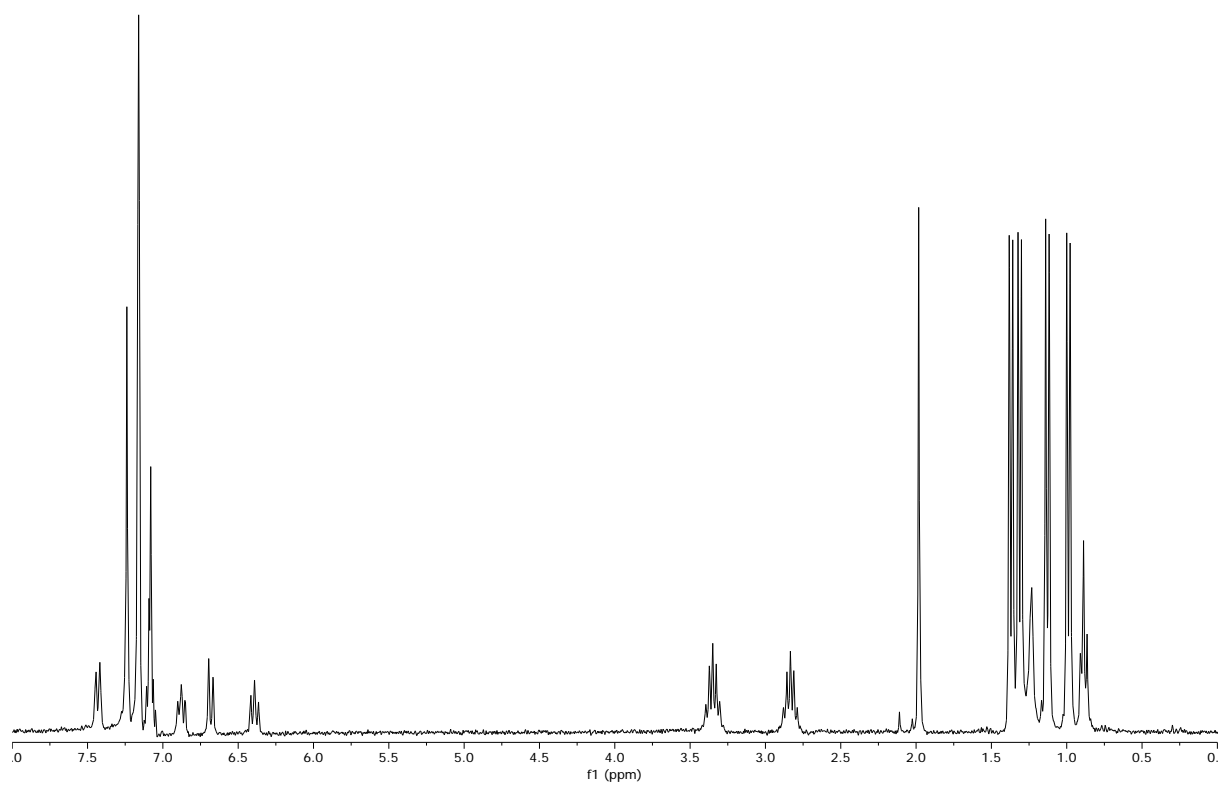




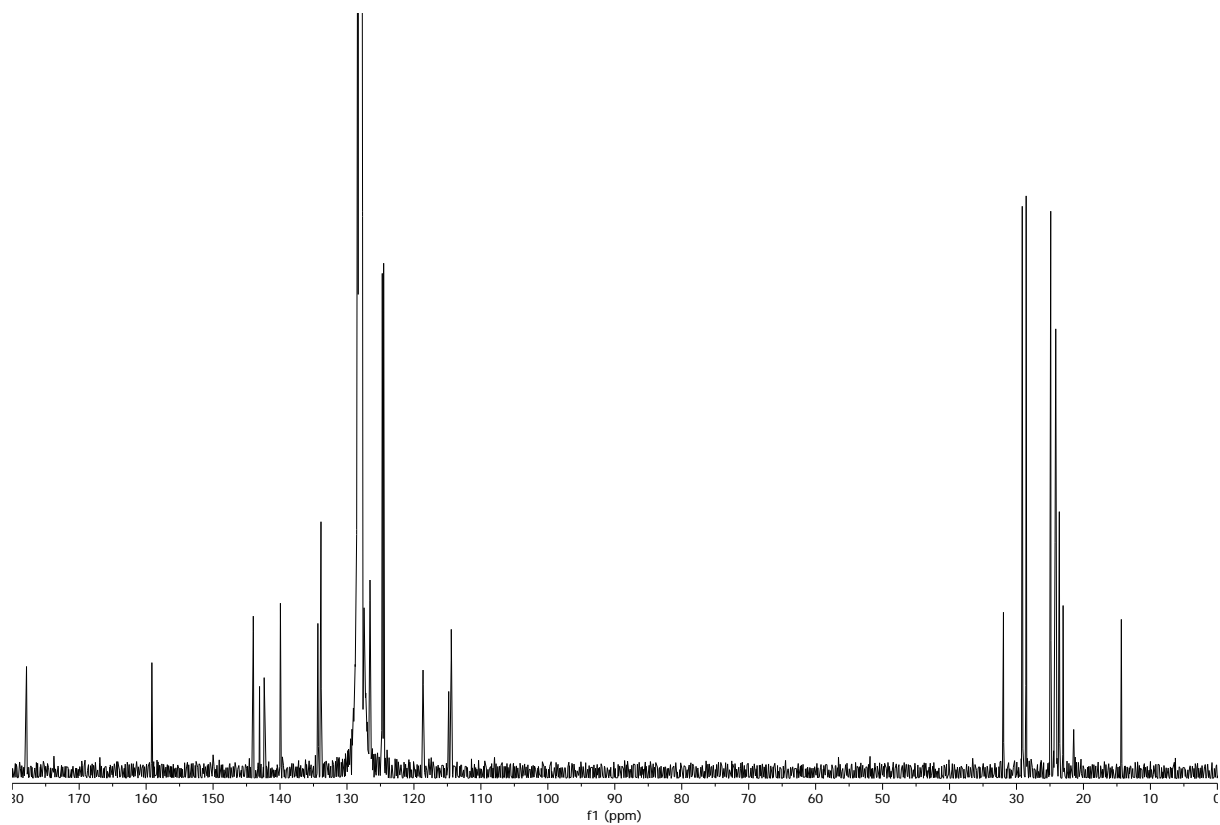
$^1\text{H}$  NMR spectrum of  $[\text{Ar-BDl}_{\text{Dipp}}\text{ZnBr}_2\text{Li}(\text{THF})_4]$  **9** (299.74 MHz,  $\text{C}_6\text{D}_6$ , 298 K) with toluene



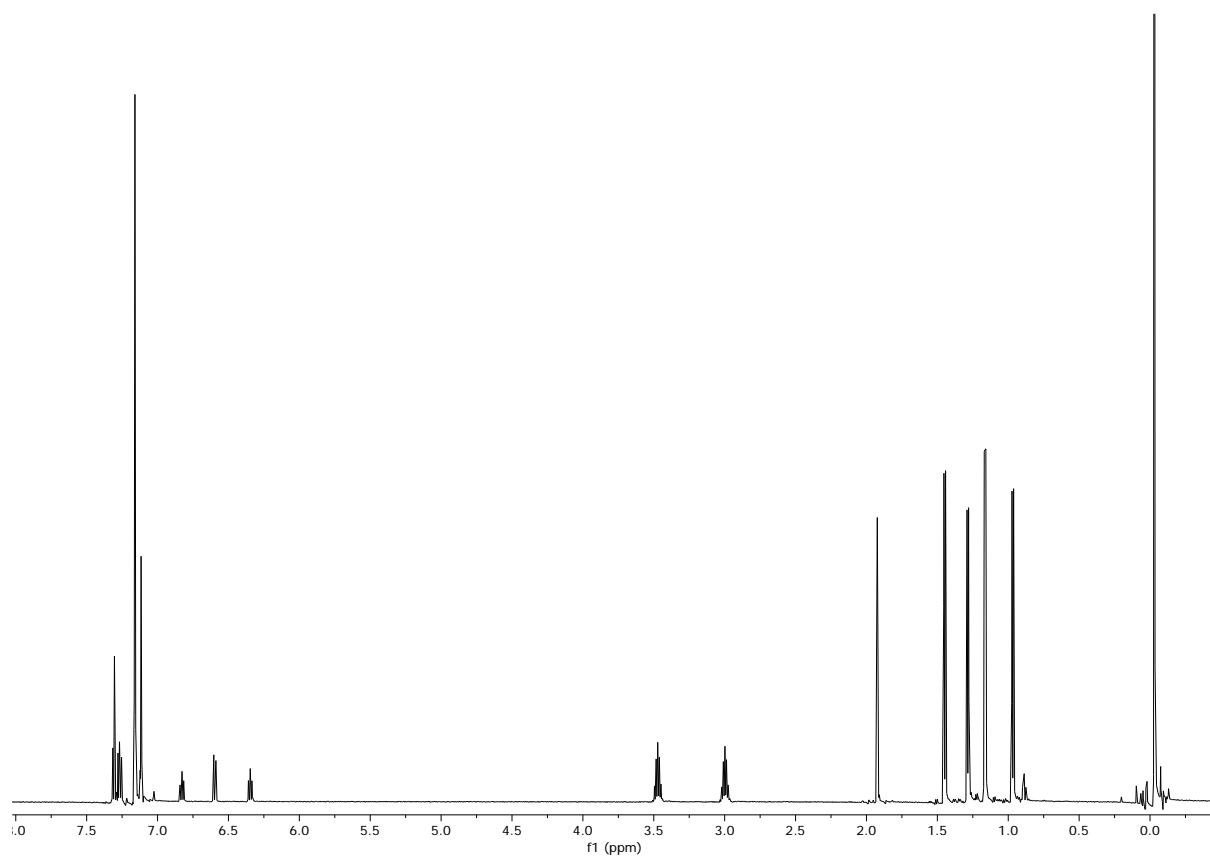
$^1\text{H}$  NMR spectrum of  $[\text{Ar-BDI}_{\text{Dipp}}\text{ZnBr}]$  **10** (299.74 MHz,  $\text{C}_6\text{D}_6$ , 298 K) with hexane



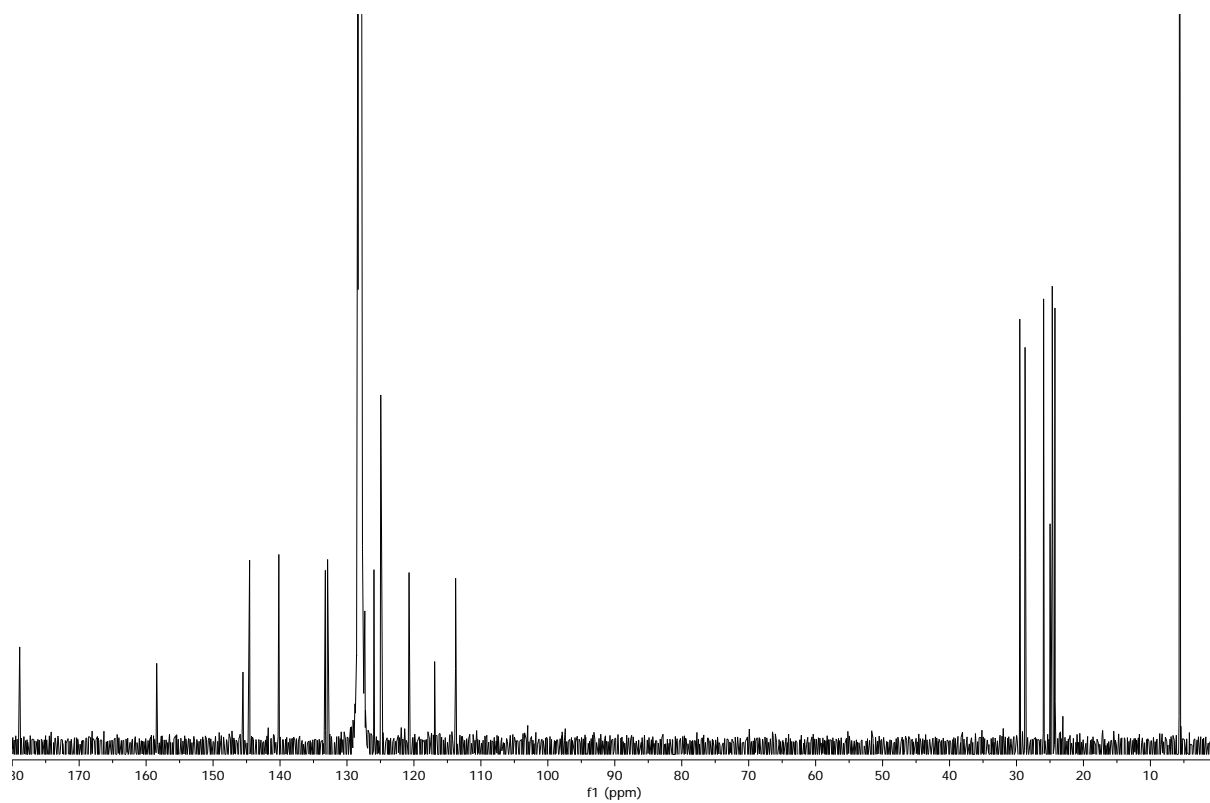
$^{13}\text{C}$  NMR spectrum of  $[\text{Ar-BDI}_{\text{Dipp}}\text{ZnBr}]$  **10** (150.76 MHz,  $\text{C}_6\text{D}_6$ , 298 K) with hexane



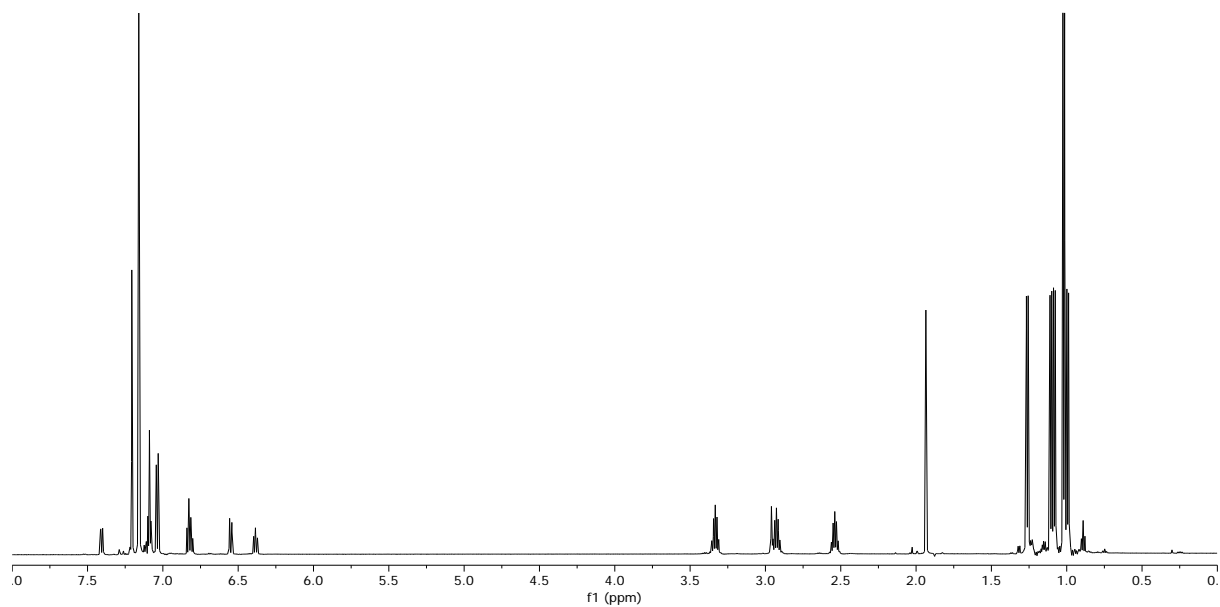
$^1\text{H}$  NMR spectrum of  $[\text{Ar-BDl}_{\text{Dipp}}\text{ZnHMDS}]$  **11** (599.48 MHz,  $\text{C}_6\text{D}_6$ , 298 K)



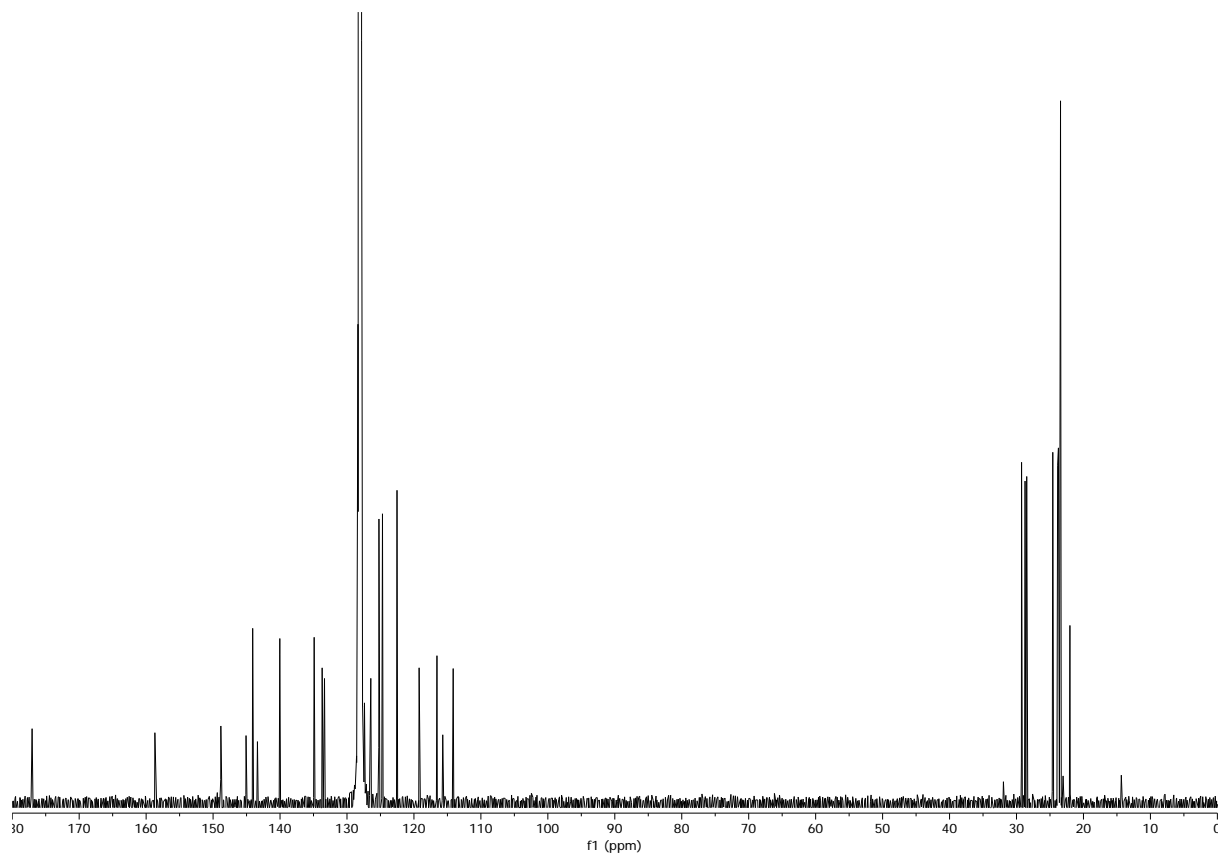
$^{13}\text{C}$  NMR spectrum of  $[\text{Ar-BDl}_{\text{Dipp}}\text{ZnHMDS}]$  **11** (150.76 MHz,  $\text{C}_6\text{D}_6$ , 298 K)



$^1\text{H}$  NMR spectrum of  $[\text{Ar-BDl}_{\text{Dipp}}\text{ZnNH}(\text{Dipp})]$  **12** (599.48 MHz,  $\text{C}_6\text{D}_6$ , 298 K)

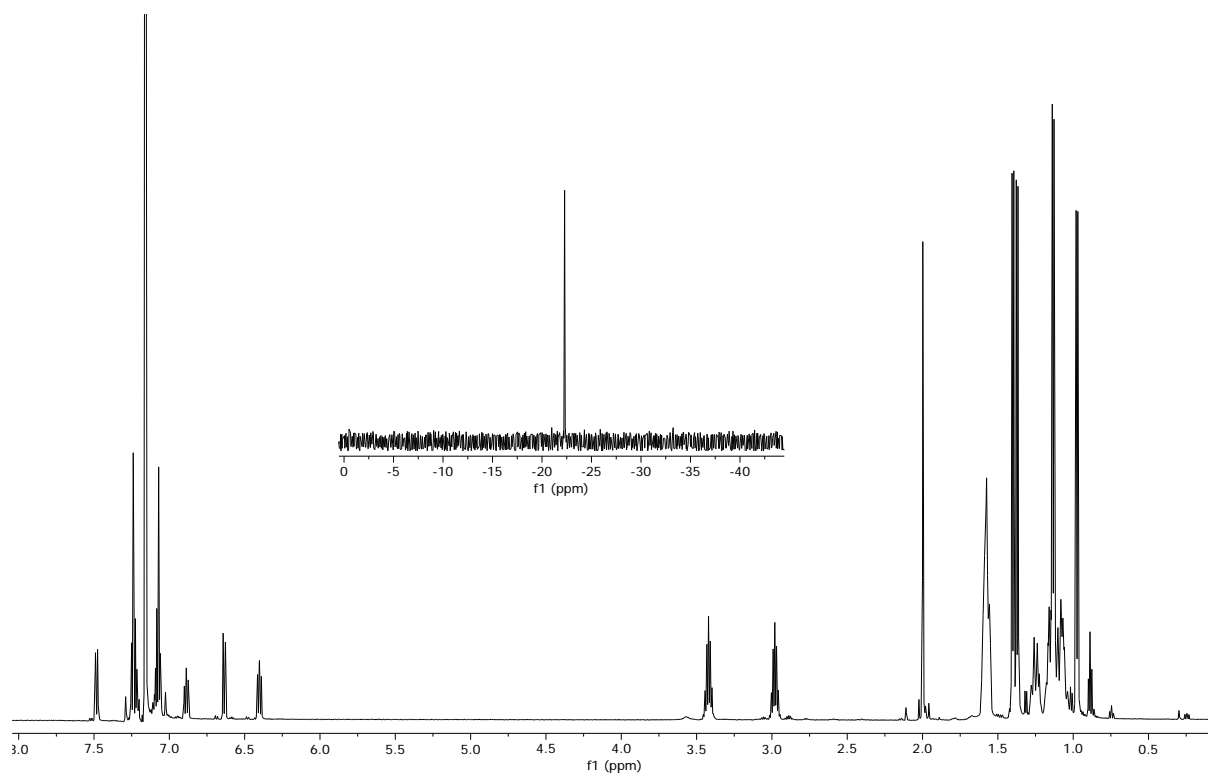


$^{13}\text{C}$  NMR spectrum of  $[\text{Ar-BDl}_{\text{Dipp}}\text{ZnNH}(\text{Dipp})]$  **12** (150.76 MHz,  $\text{C}_6\text{D}_6$ , 298 K) with hexane

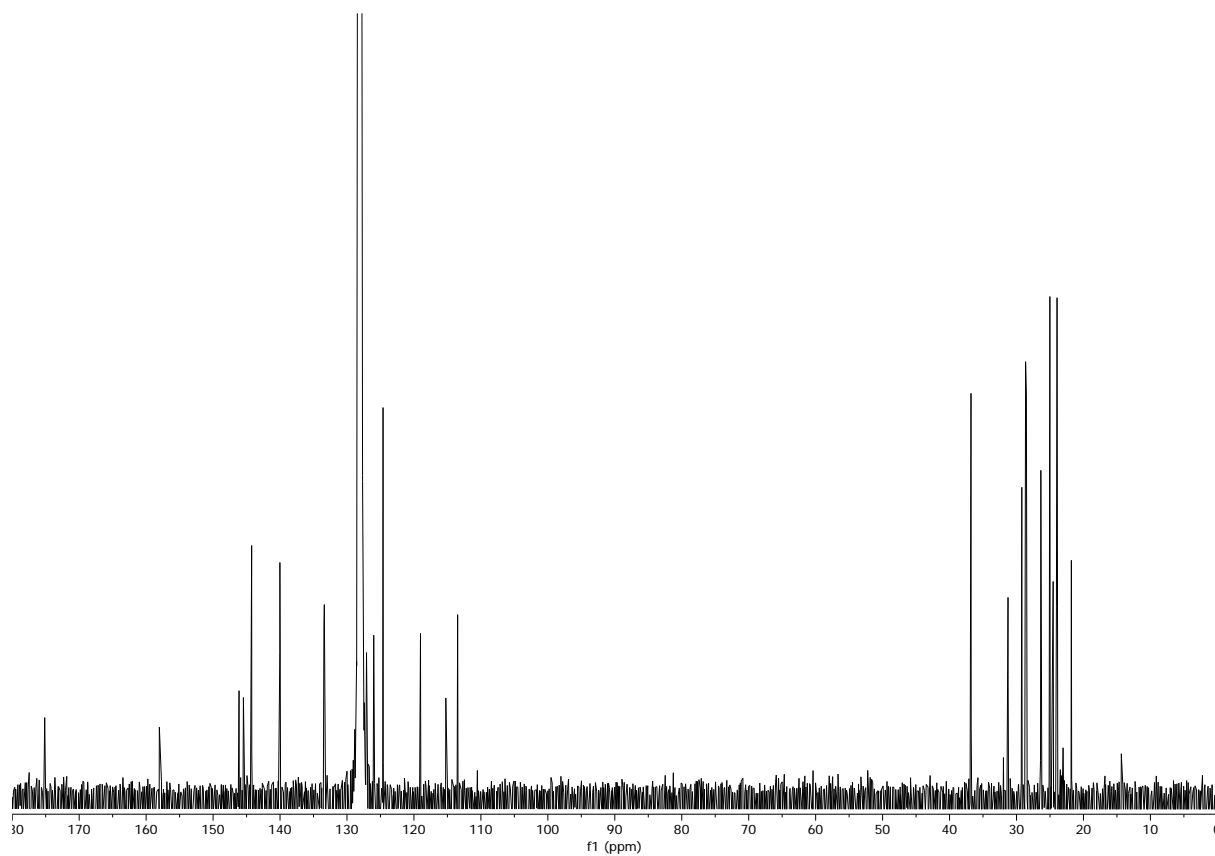


$^1\text{H}$  NMR (599.48 MHz) and  $^{31}\text{P}$  NMR (121.32 MHz  $\text{C}_6\text{D}_6$ , 298 K) spectra of  $[\text{Ar-BDl}_{\text{Dipp}}\text{ZnPCy}_2]$

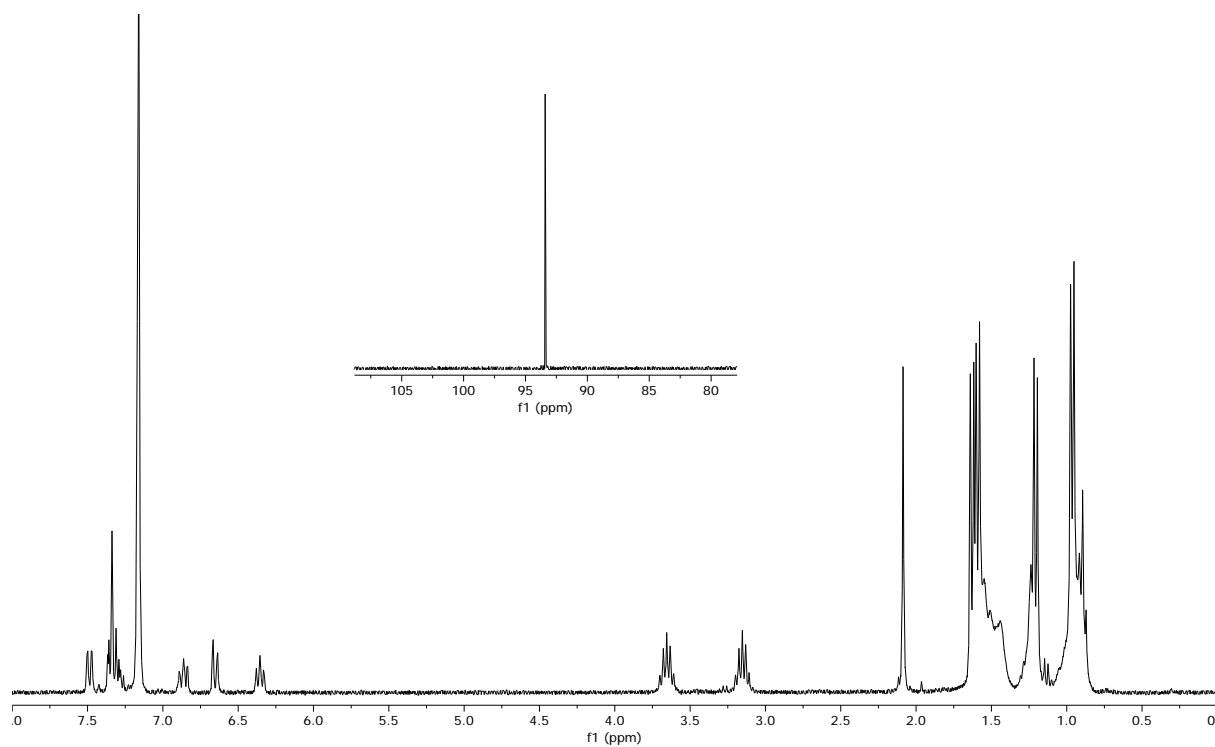
**13** with hexane



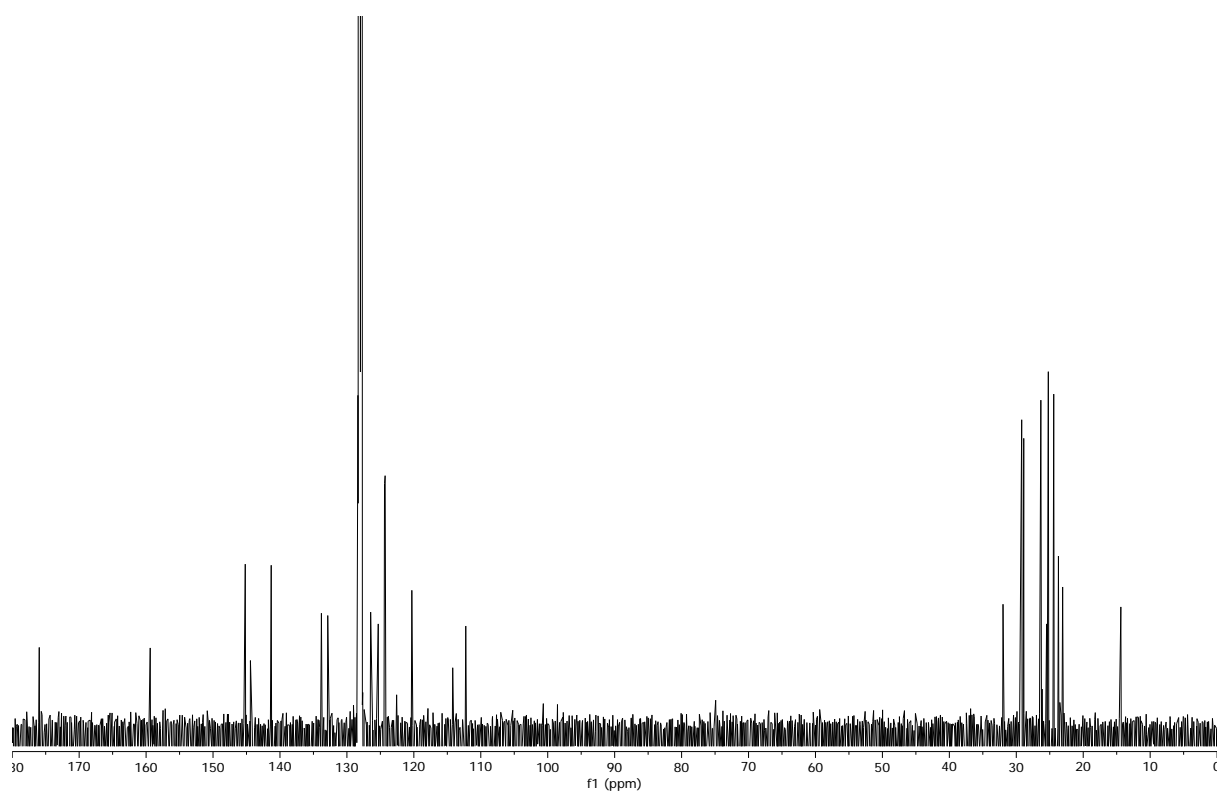
$^{13}\text{C}$  NMR spectrum of  $[\text{Ar-BDl}_{\text{Dipp}}\text{ZnPCy}_2]$  **13** (150.76 MHz,  $\text{C}_6\text{D}_6$ , 298 K) with hexane



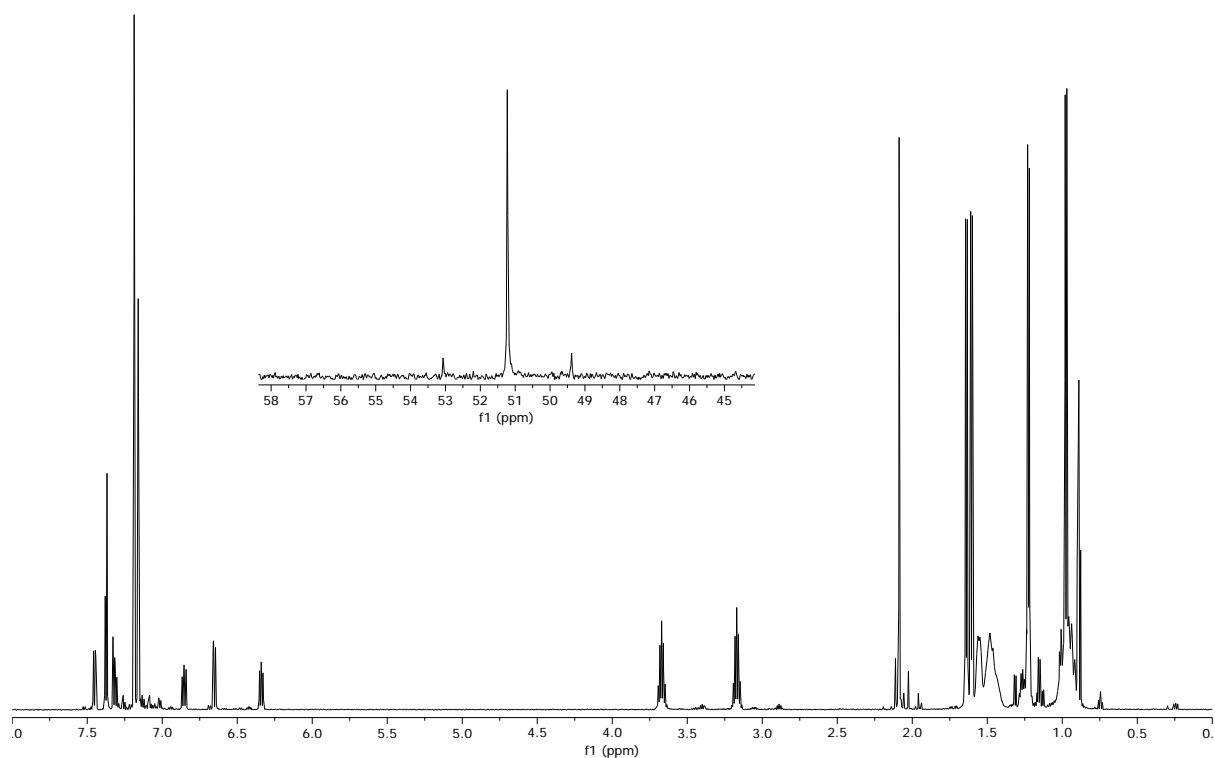
$^1\text{H}$  NMR (299.74 MHz,  $\text{C}_6\text{D}_6$ , 298 K) and  $^{31}\text{P}$  NMR (121.32 MHz,  $\text{C}_6\text{D}_6$ , 298 K) spectra of [*Ar*-BDI<sub>Dipp</sub>Zn(S)<sub>2</sub>PCy<sub>2</sub>] **15** with hexane



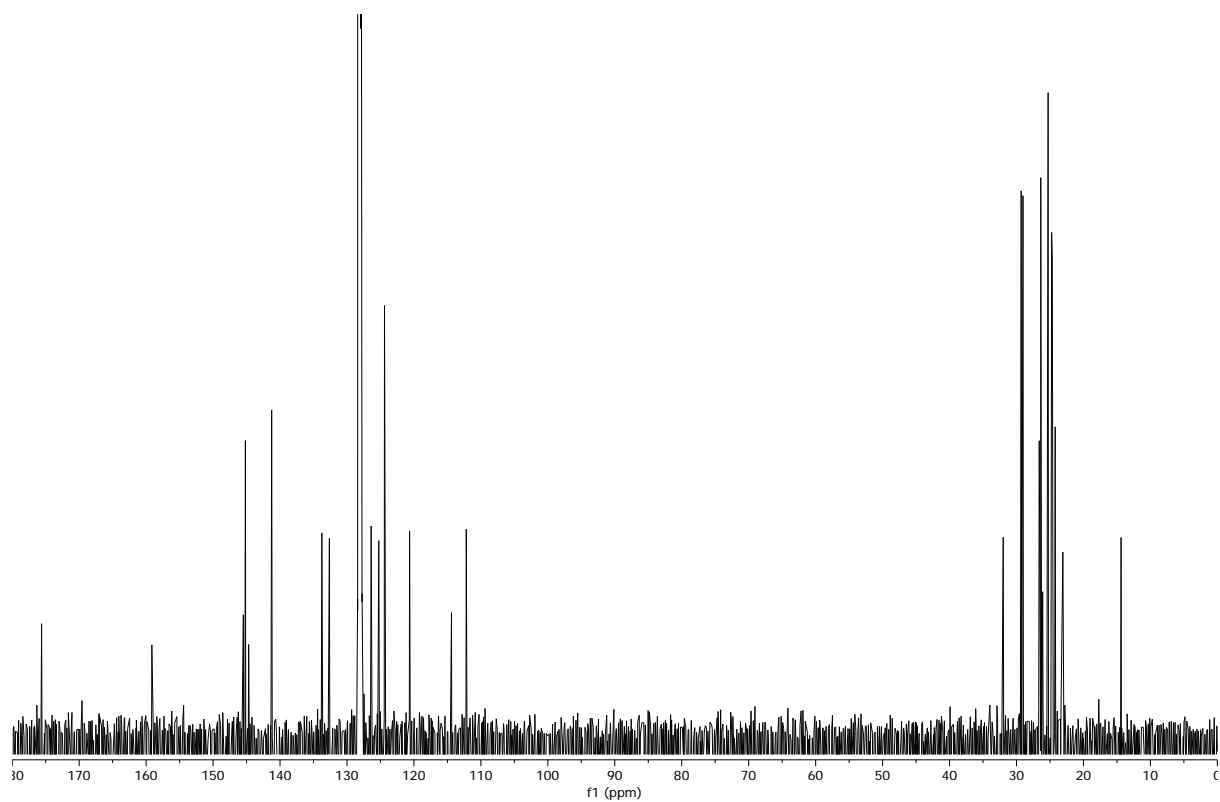
$^{13}\text{C}$  NMR spectrum of [*Ar*-BDI<sub>Dipp</sub>Zn(S)<sub>2</sub>PCy<sub>2</sub>] **15** (150.76 MHz,  $\text{C}_6\text{D}_6$ , 298 K) with hexane



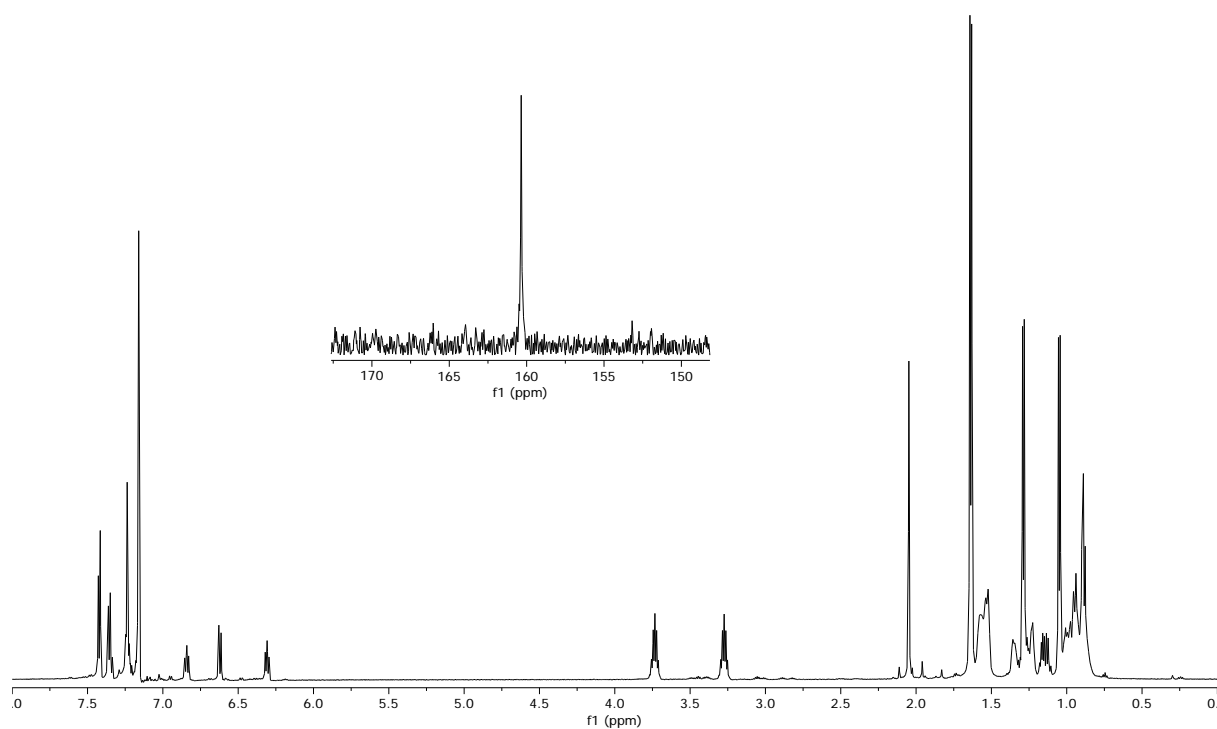
$^1\text{H}$  NMR (599.48 MHz,  $\text{C}_6\text{D}_6$ , 298 K) and  $^{31}\text{P}$  NMR (121.32 MHz,  $\text{C}_6\text{D}_6$ , 298 K) spectra of  $[\text{Ar-BDl}_{\text{Dipp}}\text{Zn}(\text{Se})_2\text{PCy}_2]$  **16** with unreacted  $[\text{Ar-BDl}_{\text{Dipp}}\text{ZnPCy}_2]$



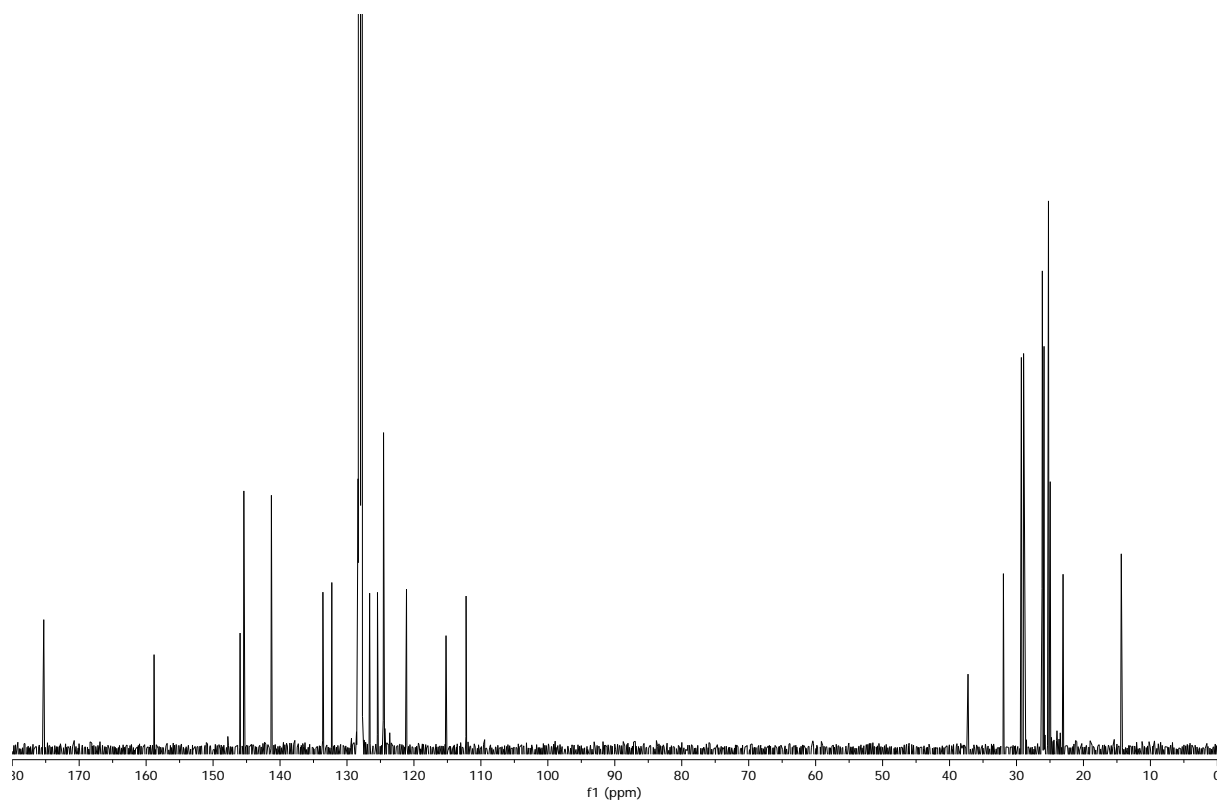
$^{13}\text{C}$  NMR spectrum of  $[\text{Ar-BDl}_{\text{Dipp}}\text{Zn}(\text{Se})_2\text{PCy}_2]$  **16** (150.76 MHz,  $\text{C}_6\text{D}_6$ , 298 K) with hexane



$^1\text{H}$  NMR (599.48 MHz) and  $^{31}\text{P}$  NMR (121.32 MHz,  $\text{C}_6\text{D}_6$ , 298 K) spectra of  $[\text{Ar-BDl}_{\text{Dipp}}\text{Zn}(\text{Te})_2\text{PCy}_2]$  **17**

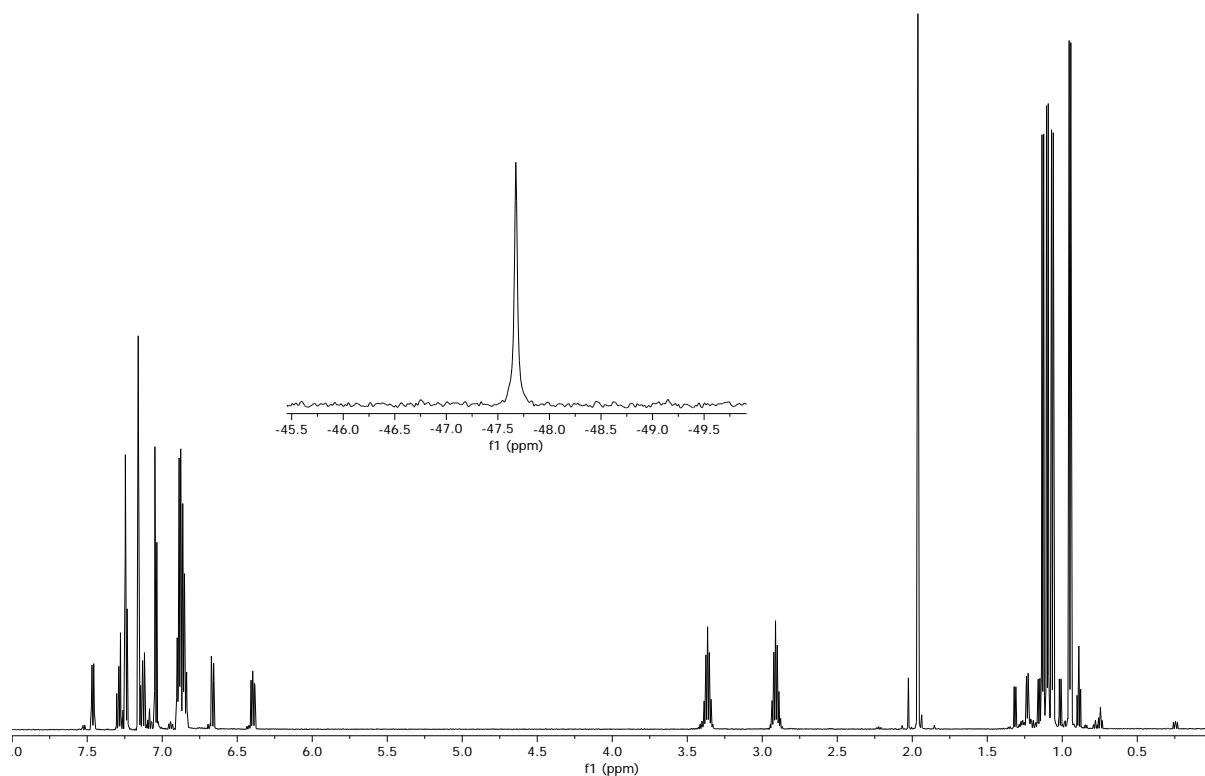


$^{13}\text{C}$  NMR spectrum of  $[\text{Ar-BDl}_{\text{Dipp}}\text{Zn}(\text{Te})_2\text{PCy}_2]$  **17** (150.74 MHz,  $\text{C}_6\text{D}_6$ , 298 K) with hexane

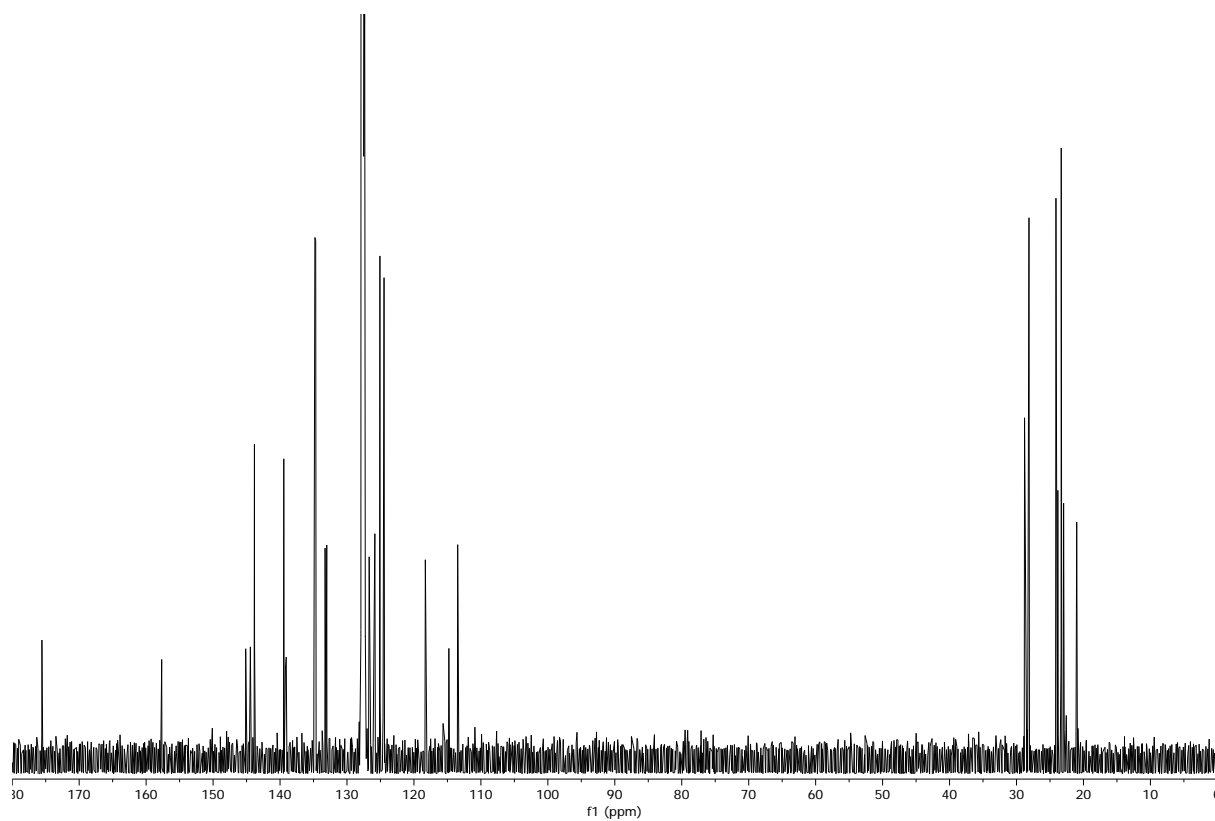




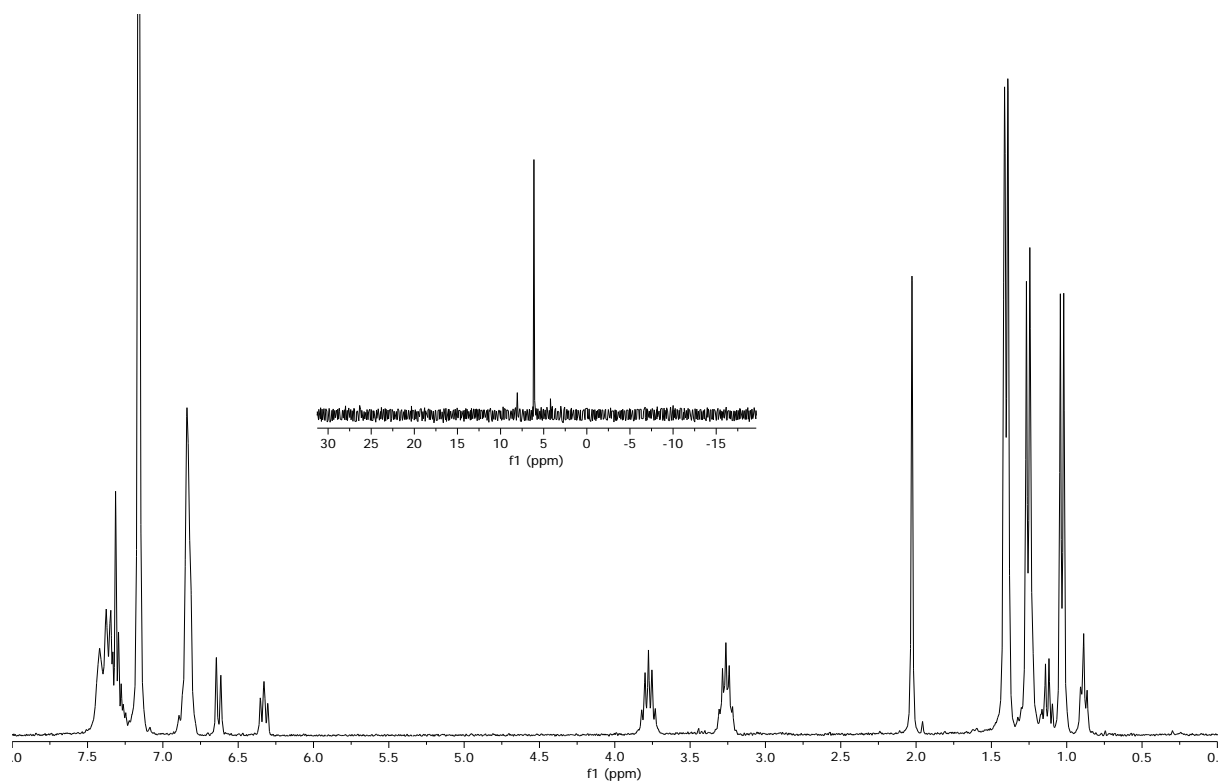
$^1\text{H}$  NMR (599.48 MHz,  $\text{C}_6\text{D}_6$ , 298 K) and  $^{31}\text{P}$  NMR (121.32 MHz,  $\text{C}_6\text{D}_6$ , 298 K) spectra of  $[\text{Ar-BDI}_{\text{Dipp}}\text{ZnPPh}_2]$  **14** with unreacted  $[\text{Ar-BDI}_{\text{Dipp}}\text{ZnBr}]$



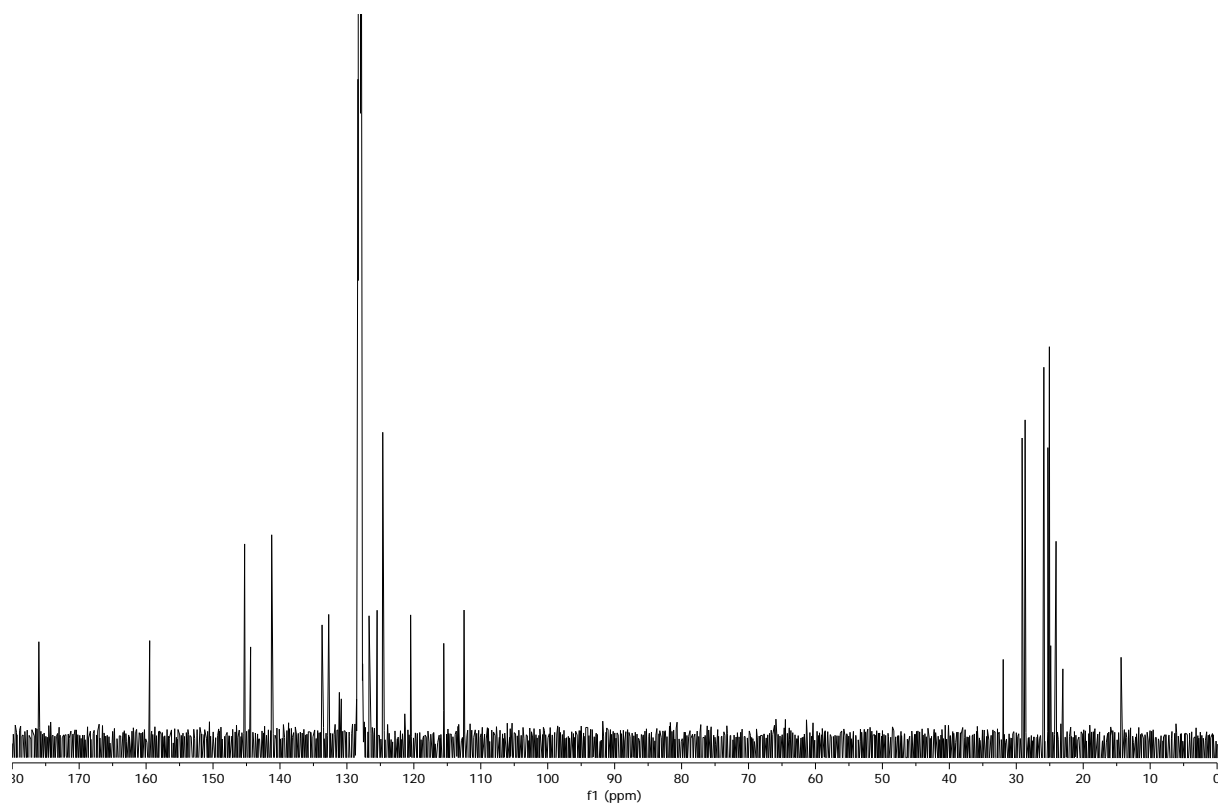
$^{13}\text{C}$  NMR spectrum of  $[\text{Ar-BDI}_{\text{Dipp}}\text{ZnPPh}_2]$  **14** (150.74 MHz,  $\text{C}_6\text{D}_6$ , 298 K)



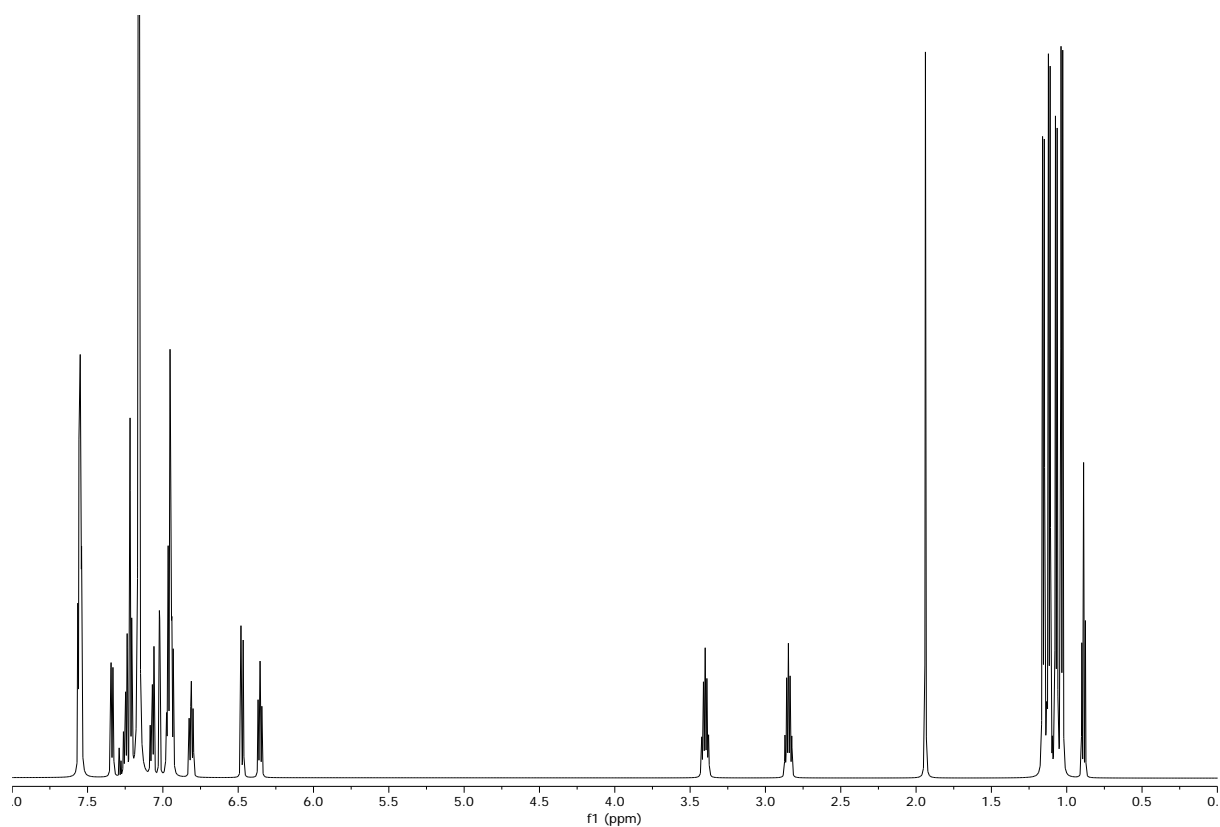
$^1\text{H}$  NMR (299.74 MHz,  $\text{C}_6\text{D}_6$ , 298 K) and  $^{31}\text{P}$  NMR (121.32 MHz,  $\text{C}_6\text{D}_6$ , 298 K) spectra of  $[\text{Ar-BDl}_{\text{Dipp}}\text{Zn}(\text{Se})_2\text{PPh}_2]$  **18**



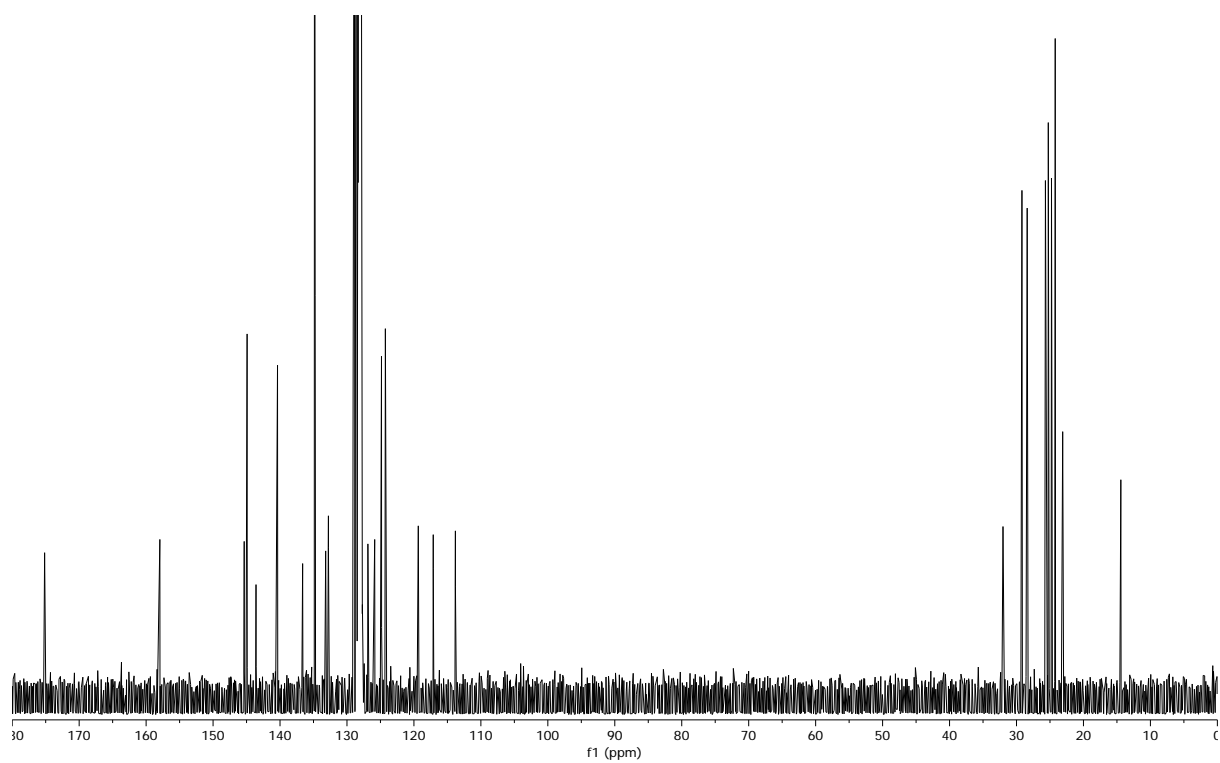
$^{13}\text{C}$  NMR spectrum of  $[\text{Ar-BDl}_{\text{Dipp}}\text{Zn}(\text{Se})_2\text{PCy}_2]$  **18** (150.76 MHz,  $\text{C}_6\text{D}_6$ , 298 K) with hexane



$^1\text{H}$  NMR spectrum of  $[\text{Ar-BDl}_{\text{Dipp}}\text{Zn}]_2\text{Te}$  **19** (599.48 MHz,  $\text{C}_6\text{D}_6$ , 298 K) with hexane and  $(\text{Ph}_2\text{P})_2$



$^{13}\text{C}$  NMR spectrum of  $[\text{Ar-BDl}_{\text{Dipp}}\text{Zn}]_2\text{Te}$  **19** (150.76 MHz,  $\text{C}_6\text{D}_6$ , 298 K) with hexane and  $[(\text{Ph}_2\text{P})_2]$



## 4.2 Appendix B: Crystal Data Tables

Crystal data and structure refinement for 55rf12. (XXX)

Identification code	55rf12
Empirical formula	C <sub>41</sub> H <sub>63</sub> N <sub>2</sub> PZn
Formula weight	680.27
Temperature/K	120.01(10)
Crystal system	monoclinic
Space group	P2 <sub>1</sub>
a/Å	11.11426(14)
b/Å	13.34770(17)
c/Å	13.06175(18)
α/°	90
β/°	93.1257(11)
γ/°	90
Volume/Å <sup>3</sup>	1934.83(4)
Z	2
ρ <sub>calc</sub> /g/cm <sup>3</sup>	1.168
μ/mm <sup>-1</sup>	1.472
F(000)	736.0
Crystal size/mm <sup>3</sup>	0.37 × 0.21 × 0.15
Radiation	CuKα (λ = 1.54184)
2θ range for data collection/°	6.778 to 153.588
Index ranges	-8 ≤ h ≤ 13, -16 ≤ k ≤ 16, -16 ≤ l ≤ 15
Reflections collected	20492
Independent reflections	8037 [R <sub>int</sub> = 0.0382, R <sub>sigma</sub> = 0.0379]
Data/restraints/parameters	8037/13/492
Goodness-of-fit on F <sup>2</sup>	1.064
Final R indexes [I >= 2σ (I)]	R <sub>1</sub> = 0.0481, wR <sub>2</sub> = 0.1174
Final R indexes [all data]	R <sub>1</sub> = 0.0505, wR <sub>2</sub> = 0.1193
Largest diff. peak/hole / e Å <sup>-3</sup>	1.01/-0.90
Flack parameter	-0.011(15)

The crystal structure has disorder in the phosphanide and the cyclohexyl groups which lay in two directions, 81% in one direction and 19% in the other. This was modelled, although the carbon atoms of the lower occupancy component were left isotropic.

Crystal data and structure refinement for 55RF13. (XXXII)

Identification code	55RF13
Empirical formula	C <sub>37</sub> H <sub>61</sub> Br <sub>2</sub> LiN <sub>2</sub> O <sub>2</sub> Zn
Formula weight	798.00
Temperature/K	286.38(10)
Crystal system	monoclinic
Space group	P2 <sub>1</sub> /n
a/Å	12.0250(3)
b/Å	21.1779(6)
c/Å	15.7842(4)
α/°	90
β/°	99.159(3)
γ/°	90
Volume/Å <sup>3</sup>	3968.42(18)
Z	4
ρ <sub>calc</sub> /g/cm <sup>3</sup>	1.336
μ/mm <sup>-1</sup>	2.664
F(000)	1664.0
Crystal size/mm <sup>3</sup>	0.41 × 0.4 × 0.31
Radiation	MoKα (λ = 0.71073)
2θ range for data collection/°	5.154 to 49.998
Index ranges	-14 ≤ h ≤ 14, -25 ≤ k ≤ 25, -18 ≤ l ≤ 18
Reflections collected	72044
Independent reflections	6987 [R <sub>int</sub> = 0.1163, R <sub>sigma</sub> = 0.0505]
Data/restraints/parameters	6987/0/420
Goodness-of-fit on F <sup>2</sup>	0.959
Final R indexes [I ≥ 2σ (I)]	R <sub>1</sub> = 0.0318, wR <sub>2</sub> = 0.0755
Final R indexes [all data]	R <sub>1</sub> = 0.0475, wR <sub>2</sub> = 0.0786
Largest diff. peak/hole / e Å <sup>-3</sup>	0.60/-0.60

Crystal data and structure refinement for 55RF11. (XXXIII)

Identification code	55RF11
Empirical formula	C <sub>45</sub> H <sub>73</sub> N <sub>2</sub> OPSe <sub>2</sub> Zn
Formula weight	912.31
Temperature/K	120.01(10)
Crystal system	monoclinic
Space group	P2 <sub>1</sub> /c
a/Å	10.40514(14)
b/Å	22.3222(3)
c/Å	19.9339(2)
α/°	90
β/°	90.9448(11)
γ/°	90
Volume/Å <sup>3</sup>	4629.32(11)
Z	4
ρ <sub>calc</sub> /g/cm <sup>3</sup>	1.309
μ/mm <sup>-1</sup>	2.171
F(000)	1912.0
Crystal size/mm <sup>3</sup>	0.48 × 0.41 × 0.36
Radiation	MoKα (λ = 0.71073)
2θ range for data collection/°	5.352 to 82.456
Index ranges	-19 ≤ h ≤ 18, -39 ≤ k ≤ 41, -36 ≤ l ≤ 36
Reflections collected	109730
Independent reflections	30070 [R <sub>int</sub> = 0.0498, R <sub>sigma</sub> = 0.0573]
Data/restraints/parameters	30070/0/481
Goodness-of-fit on F <sup>2</sup>	1.038
Final R indexes [I ≥ 2σ (I)]	R <sub>1</sub> = 0.0421, wR <sub>2</sub> = 0.0763
Final R indexes [all data]	R <sub>1</sub> = 0.0893, wR <sub>2</sub> = 0.0905
Largest diff. peak/hole / e Å <sup>-3</sup>	0.98/-1.05

Crystal data and structure refinement for 55rf10. (XXXIV)

Identification code	55rf10
Empirical formula	C <sub>41</sub> H <sub>51</sub> N <sub>2</sub> PSe <sub>2</sub> Zn
Formula weight	826.09
Temperature/K	120.01(10)
Crystal system	monoclinic
Space group	P2 <sub>1</sub> /c
a/Å	10.9760(2)
b/Å	26.8524(4)
c/Å	13.8894(3)
α/°	90
β/°	110.583(2)
γ/°	90
Volume/Å <sup>3</sup>	3832.33(14)
Z	4
ρ <sub>calc</sub> /g/cm <sup>3</sup>	1.432
μ/mm <sup>-1</sup>	2.613
F(000)	1696.0
Crystal size/mm <sup>3</sup>	0.48 × 0.47 × 0.39
Radiation	MoKα (λ = 0.71073)
2θ range for data collection/°	5.526 to 65
Index ranges	-16 ≤ h ≤ 16, -40 ≤ k ≤ 40, -20 ≤ l ≤ 20
Reflections collected	56742
Independent reflections	13867 [R <sub>int</sub> = 0.0456, R <sub>sigma</sub> = 0.0429]
Data/restraints/parameters	13867/0/434
Goodness-of-fit on F <sup>2</sup>	1.099
Final R indexes [I ≥ 2σ (I)]	R <sub>1</sub> = 0.0309, wR <sub>2</sub> = 0.0690
Final R indexes [all data]	R <sub>1</sub> = 0.0387, wR <sub>2</sub> = 0.0733
Largest diff. peak/hole / e Å <sup>-3</sup>	0.64/-0.60

Crystal data and structure refinement for exp\_60\_b. (1)

Identification code	exp_60_b
Empirical formula	C <sub>32</sub> H <sub>41</sub> ClHgN <sub>2</sub>
Formula weight	689.71
Temperature/K	120.01(10)
Crystal system	monoclinic
Space group	P2 <sub>1</sub> /n
a/Å	11.1840(3)
b/Å	22.9242(5)
c/Å	11.5002(3)
α/°	90
β/°	90.650(2)
γ/°	90
Volume/Å <sup>3</sup>	2948.27(13)
Z	4
ρ <sub>calc</sub> /cm <sup>3</sup>	1.554
μ/mm <sup>-1</sup>	5.333
F(000)	1376.0
Crystal size/mm <sup>3</sup>	0.2913 × 0.228 × 0.1402
Radiation	MoKα (λ = 0.71073)
2θ range for data collection/°	7.086 to 59.056
Index ranges	-15 ≤ h ≤ 15, -31 ≤ k ≤ 31, -15 ≤ l ≤ 13
Reflections collected	25541
Independent reflections	7199 [R <sub>int</sub> = 0.0388, R <sub>sigma</sub> = 0.0348]
Data/restraints/parameters	7199/0/334
Goodness-of-fit on F <sup>2</sup>	1.051
Final R indexes [I ≥ 2σ (I)]	R <sub>1</sub> = 0.0228, wR <sub>2</sub> = 0.0482
Final R indexes [all data]	R <sub>1</sub> = 0.0274, wR <sub>2</sub> = 0.0502
Largest diff. peak/hole / e Å <sup>-3</sup>	1.29/-1.08



Crystal data and structure refinement for 55rf15. (3)

Identification code	55rf15
Empirical formula	C <sub>29</sub> H <sub>42</sub> CdN <sub>2</sub>
Formula weight	531.04
Temperature/K	120.01(10)
Crystal system	monoclinic
Space group	P2 <sub>1</sub> /n
a/Å	12.5364(4)
b/Å	15.9813(3)
c/Å	14.0907(4)
α/°	90
β/°	105.609(3)
γ/°	90
Volume/Å <sup>3</sup>	2718.94(12)
Z	4
ρ <sub>calc</sub> /g/cm <sup>3</sup>	1.297
μ/mm <sup>-1</sup>	0.821
F(000)	1112.0
Crystal size/mm <sup>3</sup>	0.23 × 0.2 × 0.04
Radiation	MoKα (λ = 0.71073)
2θ range for data collection/°	5.688 to 70.548
Index ranges	-19 ≤ h ≤ 19, -25 ≤ k ≤ 24, -21 ≤ l ≤ 22
Reflections collected	35828
Independent reflections	11367 [R <sub>int</sub> = 0.0347, R <sub>sigma</sub> = 0.0389]
Data/restraints/parameters	11367/0/303
Goodness-of-fit on F <sup>2</sup>	1.079
Final R indexes [I ≥ 2σ (I)]	R <sub>1</sub> = 0.0330, wR <sub>2</sub> = 0.0772
Final R indexes [all data]	R <sub>1</sub> = 0.0489, wR <sub>2</sub> = 0.0874
Largest diff. peak/hole / e Å <sup>-3</sup>	1.17/-0.81

Crystal data and structure refinement for 55rf21. (4)

Identification code	55rf21
Empirical formula	C <sub>58</sub> H <sub>82</sub> Cd <sub>2</sub> N <sub>4</sub>
Formula weight	1060.07
Temperature/K	278.07(10)
Crystal system	monoclinic
Space group	P2 <sub>1</sub> /c
a/Å	14.4118(4)
b/Å	14.2417(4)
c/Å	26.8111(8)
α/°	90
β/°	94.817(3)
γ/°	90
Volume/Å <sup>3</sup>	5483.5(3)
Z	4
ρ <sub>calc</sub> /g/cm <sup>3</sup>	1.284
μ/mm <sup>-1</sup>	0.814
F(000)	2216.0
Crystal size/mm <sup>3</sup>	0.20 × 0.21 × 0.05
Radiation	MoKα (λ = 0.71073)
2θ range for data collection/°	5.396 to 54.998
Index ranges	-18 ≤ h ≤ 18, -18 ≤ k ≤ 18, -34 ≤ l ≤ 34
Reflections collected	60496
Independent reflections	12588 [R <sub>int</sub> = 0.0470, R <sub>sigma</sub> = 0.0364]
Data/restraints/parameters	12588/0/597
Goodness-of-fit on F <sup>2</sup>	1.117
Final R indexes [I ≥ 2σ (I)]	R <sub>1</sub> = 0.0352, wR <sub>2</sub> = 0.0746
Final R indexes [all data]	R <sub>1</sub> = 0.0471, wR <sub>2</sub> = 0.0812
Largest diff. peak/hole / e Å <sup>-3</sup>	0.89/-0.71

# Crystal data and structure refinement for exp\_82. (10)

Identification code	exp_82
Empirical formula	C <sub>32</sub> H <sub>41</sub> BrN <sub>2</sub> Zn
Formula weight	598.95
Temperature/K	291.24(10)
Crystal system	trigonal
Space group	R-3
a/Å	34.4281(6)
b/Å	34.4281(6)
c/Å	14.1576(3)
α/°	90
β/°	90
γ/°	120
Volume/Å <sup>3</sup>	14532.6(6)
Z	18
ρ <sub>calc</sub> /g/cm <sup>3</sup>	1.232
μ/mm <sup>-1</sup>	2.643
F(000)	5616.0
Crystal size/mm <sup>3</sup>	0.2868 × 0.2433 × 0.1644
Radiation	CuKα (λ = 1.54184)
2θ range for data collection/°	8.614 to 143.53
Index ranges	-41 ≤ h ≤ 42, -31 ≤ k ≤ 38, -17 ≤ l ≤ 16
Reflections collected	16028
Independent reflections	6236 [R <sub>int</sub> = 0.0214, R <sub>sigma</sub> = 0.0235]
Data/restraints/parameters	6236/0/356
Goodness-of-fit on F <sup>2</sup>	1.050
Final R indexes [I ≥ 2σ (I)]	R <sub>1</sub> = 0.0249, wR <sub>2</sub> = 0.0613
Final R indexes [all data]	R <sub>1</sub> = 0.0270, wR <sub>2</sub> = 0.0624
Largest diff. peak/hole / e Å <sup>-3</sup>	0.31/-0.28

The crystal structure has disorder in the BDI backbone which lay in two directions, 75% in one direction and 25% in the other. This was modelled, although the carbon atoms of the lower occupancy component were left isotropic.

Table 1 Crystal data and structure refinement for exp\_75. (11)

Identification code	exp_75
Empirical formula	C <sub>76</sub> H <sub>118</sub> N <sub>6</sub> Si <sub>4</sub> Zn <sub>2</sub>
Formula weight	1358.86
Temperature/K	120.01(10)
Crystal system	orthorhombic
Space group	Pca2 <sub>1</sub>
a/Å	18.1072(2)
b/Å	19.7437(3)
c/Å	21.5080(3)
α/°	90
β/°	90
γ/°	90
Volume/Å <sup>3</sup>	7689.20(17)
Z	4
ρ <sub>calc</sub> /cm <sup>3</sup>	1.174
μ/mm <sup>-1</sup>	1.686
F(000)	2928.0
Crystal size/mm <sup>3</sup>	0.1931 × 0.1713 × 0.0946
Radiation	CuKα (λ = 1.54184)
2θ range for data collection/°	9.364 to 143.538
Index ranges	-22 ≤ h ≤ 20, -24 ≤ k ≤ 19, -26 ≤ l ≤ 26
Reflections collected	34922
Independent reflections	13699 [R <sub>int</sub> = 0.0205, R <sub>sigma</sub> = 0.0237]
Data/restraints/parameters	13699/1/803
Goodness-of-fit on F <sup>2</sup>	1.033
Final R indexes [I ≥ 2σ (I)]	R <sub>1</sub> = 0.0329, wR <sub>2</sub> = 0.0833
Final R indexes [all data]	R <sub>1</sub> = 0.0344, wR <sub>2</sub> = 0.0846
Largest diff. peak/hole / e Å <sup>-3</sup>	0.94/-0.97
Flack parameter	-0.007(7)

Table 1 Crystal data and structure refinement for exp\_79. (13)

Identification code	exp_79
Empirical formula	C <sub>44</sub> H <sub>63</sub> N <sub>2</sub> PZn
Formula weight	716.3
Temperature/K	120.01(10)
Crystal system	monoclinic
Space group	P2 <sub>1</sub> /n
a/Å	10.88553(12)
b/Å	16.51628(19)
c/Å	22.0120(2)
$\alpha$ /°	90
$\beta$ /°	91.6596(10)
$\gamma$ /°	90
Volume/Å <sup>3</sup>	3955.84(8)
Z	4
$\rho_{\text{calc}}$ /cm <sup>3</sup>	1.203
$\mu$ /mm <sup>-1</sup>	1.464
F(000)	1544.0
Crystal size/mm <sup>3</sup>	0.2118 × 0.1523 × 0.0757
Radiation	Cu K $\alpha$ ( $\lambda$ = 1.54184)
2 $\theta$ range for data collection/°	8.9616 to 143.6478
Index ranges	-13 ≤ h ≤ 13, -19 ≤ k ≤ 20, -27 ≤ l ≤ 27
Reflections collected	28122
Independent reflections	7730 [ $R_{\text{int}}$ = 0.0334, $R_{\text{sigma}}$ = 0.0407]
Data/restraints/parameters	7730/0/482
Goodness-of-fit on F <sup>2</sup>	1.099
Final R indexes [ $I \geq 2\sigma(I)$ ]	$R_1$ = 0.0611, $wR_2$ = 0.1593
Final R indexes [all data]	$R_1$ = 0.0658, $wR_2$ = 0.1632
Largest diff. peak/hole / e Å <sup>-3</sup>	1.23/-0.70

The crystal structure has disorder in one of the cyclohexyl groups which lay in two directions, 40% in one direction and 60% in the other. The crystal structure has disorder in one of the isopropyl groups which lay in two directions, 42% in one direction and 58% in the other. Both were modelled, although the carbon atoms of the lower occupancy component were left isotropic.

Crystal data and structure refinement for exp\_84. (14)

Identification code	exp_84
Empirical formula	C <sub>44</sub> H <sub>51</sub> N <sub>2</sub> PZn
Formula weight	704.20
Temperature/K	291.24(10)
Crystal system	triclinic
Space group	P-1
a/Å	10.9460(3)
b/Å	13.4527(3)
c/Å	13.6087(4)
α/°	97.5890(19)
β/°	104.346(2)
γ/°	98.2482(19)
Volume/Å <sup>3</sup>	1891.77(8)
Z	2
ρ <sub>calc</sub> /g/cm <sup>3</sup>	1.236
μ/mm <sup>-1</sup>	1.533
F(000)	748.0
Crystal size/mm <sup>3</sup>	0.1862 × 0.1787 × 0.1364
Radiation	CuKα (λ = 1.54184)
2θ range for data collection/°	8.708 to 143.41
Index ranges	-13 ≤ h ≤ 13, -13 ≤ k ≤ 16, -16 ≤ l ≤ 14
Reflections collected	12976
Independent reflections	7215 [R <sub>int</sub> = 0.0182, R <sub>sigma</sub> = 0.0283]
Data/restraints/parameters	7215/7/442
Goodness-of-fit on F <sup>2</sup>	1.041
Final R indexes [I ≥ 2σ (I)]	R <sub>1</sub> = 0.0319, wR <sub>2</sub> = 0.0819
Final R indexes [all data]	R <sub>1</sub> = 0.0342, wR <sub>2</sub> = 0.0836
Largest diff. peak/hole / e Å <sup>-3</sup>	0.40/-0.29

Crystal data and structure refinement for exp\_86. (16)

Identification code	exp_86
Empirical formula	C <sub>47</sub> H <sub>70</sub> N <sub>2</sub> PSe <sub>2</sub> Zn
Formula weight	917.31
Temperature/K	120.01(10)
Crystal system	monoclinic
Space group	P2 <sub>1</sub> /n
a/Å	19.06601(16)
b/Å	10.35149(8)
c/Å	24.6114(3)
α/°	90
β/°	112.7016(11)
γ/°	90
Volume/Å <sup>3</sup>	4481.04(8)
Z	4
ρ <sub>calc</sub> /g/cm <sup>3</sup>	1.360
μ/mm <sup>-1</sup>	3.195
F(000)	1916.0
Crystal size/mm <sup>3</sup>	0.2631 × 0.1445 × 0.1012
Radiation	CuKα (λ = 1.54184)
2θ range for data collection/°	9.914 to 143.32
Index ranges	-14 ≤ h ≤ 23, -12 ≤ k ≤ 12, -30 ≤ l ≤ 25
Reflections collected	31720
Independent reflections	8690 [R <sub>int</sub> = 0.0133, R <sub>sigma</sub> = 0.0104]
Data/restraints/parameters	8690/3/473
Goodness-of-fit on F <sup>2</sup>	1.147
Final R indexes [I ≥ 2σ (I)]	R <sub>1</sub> = 0.0423, wR <sub>2</sub> = 0.1282
Final R indexes [all data]	R <sub>1</sub> = 0.0430, wR <sub>2</sub> = 0.1287
Largest diff. peak/hole / e Å <sup>-3</sup>	2.08/-0.46

Crystal data and structure refinement for exp\_90. (17)

Identification code	exp_90
Empirical formula	C <sub>44</sub> H <sub>63</sub> N <sub>2</sub> PZnTe <sub>2</sub>
Formula weight	971.50
Temperature/K	120.01(10)
Crystal system	monoclinic
Space group	P2 <sub>1</sub> /n
a/Å	19.1598(6)
b/Å	10.5401(3)
c/Å	24.5244(9)
α/°	90
β/°	112.768(4)
γ/°	90
Volume/Å <sup>3</sup>	4566.7(3)
Z	10
ρ <sub>calc</sub> /g/cm <sup>3</sup>	3.533
μ/mm <sup>-1</sup>	4.637
F(000)	4900.0
Crystal size/mm <sup>3</sup>	0.2506 × 0.2012 × 0.0946
Radiation	MoKα (λ = 0.71073)
2θ range for data collection/°	6.646 to 59.032
Index ranges	-25 ≤ h ≤ 15, -12 ≤ k ≤ 14, -31 ≤ l ≤ 33
Reflections collected	24889
Independent reflections	10777 [R <sub>int</sub> = 0.0305, R <sub>sigma</sub> = 0.0439]
Data/restraints/parameters	10777/0/472
Goodness-of-fit on F <sup>2</sup>	1.134
Final R indexes [I ≥ 2σ (I)]	R <sub>1</sub> = 0.0466, wR <sub>2</sub> = 0.1568
Final R indexes [all data]	R <sub>1</sub> = 0.0589, wR <sub>2</sub> = 0.1677
Largest diff. peak/hole / e Å <sup>-3</sup>	2.26/-0.87



Crystal data and structure refinement for exp\_94b. (19)

Identification code	exp_94b
Empirical formula	C <sub>67</sub> H <sub>89</sub> N <sub>4</sub> TeZn <sub>2</sub>
Formula weight	1208.76
Temperature/K	120.00(10)
Crystal system	triclinic
Space group	P-1
a/Å	12.1052(5)
b/Å	12.8767(5)
c/Å	22.5863(11)
α/°	85.696(3)
β/°	78.852(4)
γ/°	63.031(4)
Volume/Å <sup>3</sup>	3078.3(2)
Z	2
ρ <sub>calc</sub> /g/cm <sup>3</sup>	1.304
μ/mm <sup>-1</sup>	4.928
F(000)	1262.0
Crystal size/mm <sup>3</sup>	0.1726 × 0.112 × 0.0541
Radiation	CuKα (λ = 1.54184)
2θ range for data collection/°	8.33 to 144.242
Index ranges	-14 ≤ h ≤ 14, -15 ≤ k ≤ 15, -17 ≤ l ≤ 27
Reflections collected	22600
Independent reflections	11772 [R <sub>int</sub> = 0.0312, R <sub>sigma</sub> = 0.0462]
Data/restraints/parameters	11772/0/684
Goodness-of-fit on F <sup>2</sup>	1.196
Final R indexes [I ≥ 2σ (I)]	R <sub>1</sub> = 0.0406, wR <sub>2</sub> = 0.1127
Final R indexes [all data]	R <sub>1</sub> = 0.0468, wR <sub>2</sub> = 0.1153
Largest diff. peak/hole / e Å <sup>-3</sup>	1.40/-1.19

## 4.3 Appendix C: Bibliography

1. Eichler, R.; Aksenov, N. V.; Belozerov, A. V.; Bozhikov, G. A.; Chepigin, V. I.; Dmitriev, S. N.; Dressler, R.; Gaggeler, H. W.; Gorshkov, V. A.; Haenssler, F.; Itkis, M. G.; Laube, A.; Lebedev, V. Y.; Malyshev, O. N.; Oganessian, Y. T.; Petrushkin, O. V.; Piguet, D.; Rasmussen, P.; Shishkin, S. V.; Shutov, A. V.; Svirikhin, A. I.; Tereshatov, E. E.; Vostokin, G. K.; Wegrzecki, M.; Yereimin, A. V., Chemical characterization of element 112. *Nature* **2007**, *447* (7140), 72-75.
2. Hans Wedepohl, K., The composition of the continental crust. *Geochimica et Cosmochimica Acta* **1995**, *59* (7), 1217-1232.
3. Broadley, M. R.; White, P. J.; Hammond, J. P.; Zelko, I.; Lux, A., Zinc in plants. *New Phytologist* **2007**, *173* (4), 677-702.
4. Vesely, C. J.; Langer, D. W., Electronic Core Levels of the IIB and VIA Compounds. *Physical Review B* **1971**, *4* (2), 451-462.
5. Wang, X.; Andrews, L.; Riedel, S.; Kaupp, M., Mercury Is a Transition Metal: The First Experimental Evidence for HgF<sub>4</sub>. *Angewandte Chemie* **2007**, *119* (44), 8523-8527.
6. Blackman, A.; Gahan, L., *Aylward and Findlay's SI Chemical Data*. 7th Revised edition ed.; John Wiley & Sons Australia Ltd: Milton, QLD, Australia 2013.
7. Fluck, E., New notations in the periodic table. In *Pure and Applied Chemistry*, 1988; Vol. 60, p 431.
8. Jensen, W. B., The Place of Zinc, Cadmium, and Mercury in the Periodic Table. *Journal of Chemical Education* **2003**, *80* (8), 952.
9. Bourget-Merle, L.; Lappert, M. F.; Severn, J. R., The Chemistry of  $\beta$ -Diketiminatometal Complexes. *Chemical Reviews* **2002**, *102* (9), 3031-3066.
10. Spencer, D. J. E.; Aboelella, N. W.; Reynolds, A. M.; Holland, P. L.; Tolman, W. B.,  $\beta$ -Diketiminate Ligand Backbone Structural Effects on Cu(I)/O<sub>2</sub> Reactivity: Unique Copper-Superoxo and Bis( $\mu$ -oxo) Complexes. *Journal of the American Chemical Society* **2002**, *124* (10), 2108-2109.
11. Spencer, D. J. E.; Reynolds, A. M.; Holland, P. L.; Jazdzewski, B. A.; Duboc-Toia, C.; Le Pape, L.; Yokota, S.; Tachi, Y.; Itoh, S.; Tolman, W. B., Copper Chemistry of  $\beta$ -Diketiminate Ligands: Monomer/Dimer Equilibria and a New Class of Bis( $\mu$ -oxo)dicopper Compounds. *Inorganic Chemistry* **2002**, *41* (24), 6307-6321.
12. Yokota, S.; Tachi, Y.; Itoh, S., Oxidative Degradation of  $\beta$ -Diketiminate Ligand in Copper(II) and Zinc(II) Complexes. *Inorganic Chemistry* **2002**, *41* (6), 1342-1344.
13. Randall, D. W.; George, S. D.; Holland, P. L.; Hedman, B.; Hodgson, K. O.; Tolman, W. B.; Solomon, E. I., *Journal of American Chemical Society* **2000**, *122* (47), 11632-11648.
14. Gold, V.; Pure, I. U. o.; Chemistry, A., *Compendium of Chemical Terminology: IUPAC Recommendations*. Blackwell Scientific Publications: 1987.
15. Hartley, F. R.; Patai, S., *The Nature and cleavage of metal carbon bonds*. J. Wiley: 1985.

16. McCall, K. A.; Huang, C.; Fierke, C. A., Function and mechanism of zinc metalloenzymes. *Journal of Nutrition* **2000**, *130* (5S Suppl), 1437s-46s.
17. Greenwood, N. N.; Earnshaw, A., *Chemistry of the Elements 2nd edition*. Oxford: Butterworth-Heinemann: 1997.
18. Dedieu, A., *Transition Metal Hydrides 1st edition*. Wiley-VCH: 1991.
19. Brown, I. D.; Gillespie, R. J.; Morgan, K. R.; Tun, Z.; Ummat, P. K., Preparation and crystal structure of mercury hexafluoronioabate (Hg<sub>3</sub>NbF<sub>6</sub>) and mercury hexafluorotantalate (Hg<sub>3</sub>TaF<sub>6</sub>): mercury layer compounds. *Inorganic Chemistry* **1984**, *23* (26), 4506-4508.
20. Jolly, W. L., *Modern Inorganic Chemistry*. McGraw-Hill College: 1984.
21. Rogalski, A., *Infrared Detectors*. Taylor & Francis: 2000.
22. Council, N. R., *Toxicological Effects of Methylmercury*. The National Academies Press: Washington, DC, 2000; p 368.
23. Beletskaya, I. P.; Butin, K. P.; Ryabtsev, A. N.; Reutov, O. A., Stability of organo-mercury, -thallium, -tin and -lead complexes with anionic and neutral ligands. *Journal of Organometallic Chemistry* **1973**, *59*, 1-44.
24. Schwerdtfeger, P.; Boyd, P. D. W.; Brienne, S.; McFeaters, J. S.; Dolg, M.; Liao, M. S.; Eugen Schwarz, W. H., The mercury-mercury bond in inorganic and organometallic compounds. A theoretical study. *Inorganica Chimica Acta* **1993**, *213* (1), 233-246.
25. Kaupp, M.; von Schnering, H. G., Dominance of Linear 2-Coordination in Mercury Chemistry: Quasirelativistic and Nonrelativistic ab Initio Pseudopotential Study of (HgX<sub>2</sub>)<sub>2</sub> (X = F, Cl, Br, I, H). *Inorganic Chemistry* **1994**, *33* (12), 2555-2564.
26. Mozaffarian, D.; Rimm, E. B., Fish intake, contaminants, and human health: Evaluating the risks and the benefits. *JAMA* **2006**, *296* (15), 1885-1899.
27. Cheng, M.; Moore, D. R.; Reczek, J. J.; Chamberlain, B. M.; Lobkovsky, E. B.; Coates, G. W., Single-Site  $\beta$ -Diiminate Zinc Catalysts for the Alternating Copolymerization of CO<sub>2</sub> and Epoxides: Catalyst Synthesis and Unprecedented Polymerization Activity. *Journal of the American Chemical Society* **2001**, *123* (36), 8738-8749.
28. Liu, J.; Vieille-Petit, L.; Linden, A.; Luan, X.; Dorta, R., Synthesis and structural characterization of LiI, ZnII, CdII, and HgII complexes containing a fluorinated  $\beta$ -diketiminato ligand. *Journal of Organometallic Chemistry* **2012**, *719*, 80-86.
29. Ferro, L.; Coles, M.; Day, I.; Fulton, R., Taking Advantage of Hg-C Bonds: Synthesis of the First Homoleptic Bis- $\beta$ -diketiminato Complex Bound through the  $\gamma$ -Carbons. *Organometallics* **2010**, *29*, 2911-2915.
30. Farwell, J. D.; Fernandes, M. A.; Hitchcock, P. B.; Lappert, M. F.; Layh, M.; Omondi, B., Synthesis, crystal structures and reactions of sila- and germa-[small beta]-diketiminates. *Dalton Transactions* **2003**, (9), 1719-1729.
31. Jazdzewski, B. A.; Holland, P. L.; Pink, M.; Young, V. G.; Spencer, D. J. E.; Tolman, W. B., Three-Coordinate Copper(II)-Phenolate Complexes. *Inorganic Chemistry* **2001**, *40* (24), 6097-6107.

32. Brown, E. C.; Aboeella, N. W.; Reynolds, A. M.; Aullón, G.; Alvarez, S.; Tolman, W. B., A New Class of ( $\mu$ - $\eta^2$ : $\eta^2$ -Disulfido)dicopper Complexes: Synthesis, Characterization, and Disulfido Exchange. *Inorganic Chemistry* **2004**, 43 (11), 3335-3337.
33. Benidar, A.; Montero-Campillo, M. M.; Lamsabhi, A. M.; Yáñez, M.; Bouilloud, M.; Guillemin, J.-C.; Mó, O., On the Structures, Lifetimes, and Infrared Spectra of Alkylmercury Hydrides. *ChemPhysChem* **2014**, 15 (3), 530-541.
34. Gade, L. H.; Johnson, B. F. G.; Lewis, J.; McPartlin, M.; Scowen, I. J., Removing a second mercury atom from [Os18Hg3C2(CO)42]2-: synthesis of [Os18HgC2(CO)42]4- and crystal structure of [PPh3H]3[Os18HgHC2(CO)42]. *Journal of the Chemical Society, Dalton Transactions* **1996**, (5), 597-601.
35. Zhu, Z.; Brynda, M.; Wright, R. J.; Fischer, R. C.; Merrill, W. A.; Rivard, E.; Wolf, R.; Fetting, J. C.; Olmstead, M. M.; Power, P. P., Synthesis and Characterization of the Homologous M-M Bonded Series Ar'MMAr' (M = Zn, Cd, or Hg; Ar' = C6H3-2,6-(C6H3-2,6-Pri2)2) and Related Arylmetal Halides and Hydride Species. *Journal of the American Chemical Society* **2007**, 129 (35), 10847-10857.
36. Nakamura, E.; Yu, Y.; Mori, S.; Yamago, S., Unusually Stable Organomercury Hydrides and Radicals. *Angewandte Chemie International Edition* **1997**, 36 (4), 374-376.
37. Holloway, C. E.; Melník, M., Mercury organometallic compounds. Classification and analysis of crystallographic and structural data. *Journal of organometallic chemistry* **1995**, 495 (1), 1-31.
38. Bravo-Zhivotovskii, D.; Yuzefovich, M.; Bendikov, M.; Klinkhammer, K.; Apeloig, Y., The Synthesis and Molecular Structure of the First Two-Coordinate, Dinuclear  $\sigma$ -Bonded Mercury(II) RHgHgR Compound. *Angewandte Chemie International Edition* **1999**, 38 (8), 1100-1102.
39. Pauling, L., *The Nature of the Chemical Bond and the Structure of Molecules and Crystals: An Introduction to Modern Structural Chemistry*. Cornell University Press: 1960.
40. Hicks, J.; Underhill, E. J.; Kefalidis, C. E.; Maron, L.; Jones, C., A Mixed-Valence Tri-Zinc Complex, [LZnZnZnL] (L=Bulky Amide), Bearing a Linear Chain of Two-Coordinate Zinc Atoms. *Angewandte Chemie International Edition* **2015**, 54 (34), 10000-10004.
41. Cecconi, F.; Ghilardi, C. A.; Midollini, S.; Moneti, S., Synthesis of novel mercury(II) complexes containing a linear chain Co-Hg-Hg-Co. X-Ray crystal structure of the complex [{Co[N(CH2CH2PPh2)3]}2([small micro]-Hg2)][middle dot]thf. *Journal of the Chemical Society, Dalton Transactions* **1983**, (2), 349-352.
42. Sikirica, M.; Grdenic, D., The crystal structure of mercury(II) trifluoroacetate. *Acta Crystallographica Section B* **1974**, 30 (1), 144-146.
43. Scoullou, M., *Mercury — Cadmium — Lead Handbook for Sustainable Heavy Metals Policy and Regulation: Handbook for Sustainable Heavy Metals Policy and Regulation*. Springer Netherlands: 2001.
44. Haug, H.; Koch, S. W., *Quantum Theory of the Optical and Electronic Properties of Semiconductors*. World Scientific: 1994; p 473.

45. Buhro, W. E.; Colvin, V. L., Semiconductor Nanocrystals: Shape Matters. *Nature Materials* **2003**, 2, 138.
46. Carballo, R.; Castiñeiras, A.; Domínguez-Martín, A.; García-Santos, I.; Niclós-Gutiérrez, J., Solid State Structures of Cadmium Complexes with Relevance for Biological Systems. In *Cadmium: From Toxicity to Essentiality*, Sigel, A.; Sigel, H.; Sigel, K. O. R., Eds. Springer Netherlands: Dordrecht, 2013; pp 145-189.
47. Pang, K.; Rong, Y.; Parkin, G., Molecular structures of three coordinate zinc and cadmium complexes that feature  $\beta$ -diketiminato and anilido-imine ligands. *Polyhedron* **2010**, 29 (8), 1881-1890.
48. Borren, E. I. Synthesis and Reactivity of Novel  $\beta$ -Diketiminato-cadmium Complexes II. Synthesis of Lead Selenide Nanoparticles for Use in Solar Cells. Victoria University of Wellington, Wellington, 2014.
49. Webb, D., Victoria Summer Research 2014-2015. 2015.
50. Borren, E. S.; Fitchett, C. M.; Fulton, J. R., ( $\beta$ -Diketiminato)cadmium Bis(trimethylsilyl)amide: Facile Access to Low-Coordinate Cadmium Complexes. *European Journal of Inorganic Chemistry* **2016**, 2016 (18), 3024-3029.
51. Reger, D. L.; Mason, S. S.; Rheingold, A. L., Syntheses of the first molecular complexes containing a cadmium-cadmium bond and a cadmium-hydrogen bond. *Journal of the American Chemical Society* **1993**, 115 (22), 10406-10407.
52. Zhu, Z.; Fettingner, J. C.; Olmstead, M. M.; Power, P. P., *Organometallics* **2009**, 28, 2091-2095.
53. Lobbia, G. G.; Bonati, F.; Cecchi, P.; Pettinari, C., Metal Polypyrazolyborates. IV, Mercury Derivatives. *Gazzetta Chimica Italiana* **1991**, 121 (7), 355-358.
54. Medicine, I. o., *Dietary Reference Intakes for Vitamin A, Vitamin K, Arsenic, Boron, Chromium, Copper, Iodine, Iron, Manganese, Molybdenum, Nickel, Silicon, Vanadium, and Zinc*. The National Academies Press: Washington, DC, 2001; p 800.
55. Jiang, P.; Guo, Z., Fluorescent detection of zinc in biological systems: recent development on the design of chemosensors and biosensors. *Coordination Chemistry Reviews* **2004**, 248 (1-2), 205-229.
56. Greenwood, N.; Earnshaw, A., *Chemistry of the Elements 2nd Edition*. Butterworth-Heinemann: 1997.
57. Housecroft C. E.; Sharpe A. G., *Inorganic Chemistry 3rd Edition*. Prentice Hall: 2008.
58. Langer, D. W.; Vesely, C. J., Electronic Core Levels of Zinc Chalcogenides. *Physical Review B* **1970**, 2 (12), 4885-4892.
59. Panchal, C. J.; Opanasyuk, A. S.; Kosyak, V. V.; Desai, M. S.; Protsenko, I. Y., Structural and Substructural Properties of the Zinc and Cadmium Chalcogenides Thin Films (a Review). *Journal of Nano- and Electronic Physics* **2011**, 3 (1), 274.
60. Jia, G.; Banin, U., A General Strategy for Synthesizing Colloidal Semiconductor Zinc Chalcogenide Quantum Rods. *Journal of the American Chemical Society* **2014**, 136 (31), 11121-11127.

61. Herrmann, W. A., *Synthetic Methods of Organometallic and Inorganic Chemistry: Catalysis*. Georg Thieme Verlag: 1996.
62. Knochel, P.; Jones, P., *Organozinc Reagents: A Practical Approach*. Oxford University Press: 1999.
63. Overman, L. E.; Carpenter, N. E., The Allylic Trihaloacetimidate Rearrangement. In *Organic Reactions*, John Wiley & Sons, Inc.: 2004.
64. Rappoport, Z.; Marek, I., *The Chemistry of Organozinc Compounds: R-Zn*. Wiley: 2007.
65. Łowicki, D.; Baś, S.; Mlynarski, J., Chiral zinc catalysts for asymmetric synthesis. *Tetrahedron* **2015**, *71* (9), 1339-1394.
66. Dove, A. P.; Gibson, V. C.; Marshall, E. L.; White, A. J. P.; Williams, D. J., Magnesium and zinc complexes of a potentially tridentate [small beta]-diketiminato ligand. *Dalton Transactions* **2004**, (4), 570-578.
67. Wang, C.-H.; Li, C.-Y.; Huang, B.-H.; Lin, C.-C.; Ko, B.-T., Synthesis and structural determination of zinc complexes based on an anilido-alimine ligand containing an O-donor pendant arm: zinc alkoxide derivative as an efficient initiator for ring-opening polymerization of cyclic esters. *Dalton Transactions* **2013**, *42* (30), 10875-10884.
68. Liu, Y.-C.; Lin, C.-H.; Ko, B.-T.; Ho, R.-M., Ring-opening polymerization of  $\beta$ -butyrolactone catalyzed by efficient magnesium and zinc complexes derived from tridentate anilido-alimine ligand. *Journal of Polymer Science Part A: Polymer Chemistry* **2010**, *48* (23), 5339-5347.
69. Chisholm, M. H.; Gallucci, J.; Phomphrai, K., Coordination Chemistry and Reactivity of Monomeric Alkoxides and Amides of Magnesium and Zinc Supported by the Diiminato Ligand CH(CMeNC<sub>6</sub>H<sub>3</sub>-2,6-iPr<sub>2</sub>)<sub>2</sub>. A Comparative Study. *Inorganic Chemistry* **2002**, *41* (10), 2785-2794.
70. Wang, Y.; Quillian, B.; Wei, P.; Wang, H.; Yang, X.-J.; Xie, Y.; King, R. B.; Schleyer, P. v. R.; Schaefer, H. F.; Robinson, G. H., On the Chemistry of Zn-Zn Bonds, RZn-ZnR (R = [{(2,6-Pri<sub>2</sub>C<sub>6</sub>H<sub>3</sub>)N(Me)C}CH<sub>2</sub>]): Synthesis, Structure, and Computations. *Journal of the American Chemical Society* **2005**, *127* (34), 11944-11945.
71. Blake, M. P.; Kaltsoyannis, N.; Mountford, P., Synthesis, molecular and electronic structure, and reactions of a Zn-Hg-Zn bonded complex. *Chemical communications* **2015**, *51* (26), 5743-5746.
72. Schulz, S.; Schuchmann, D.; Westphal, U.; Bolte, M., Dizincocene as a Building Block for Novel Zn-Zn-Bonded Compounds? *Organometallics* **2009**, *28* (5), 1590-1592.
73. Prust, J.; Hohmeister, H.; Stasch, A.; Roesky, Herbert W.; Magull, J.; Alexopoulos, E.; Usón, I.; Schmidt, H.-G.; Noltemeyer, M., Synthesis and Structural Characterization of  $\beta$ -Diketoiminate Complexes Containing Three-Coordinate Zinc and Copper Atoms. *European Journal of Inorganic Chemistry* **2002**, *2002* (8), 2156-2162.
74. Drouin, F.; Oguadinma, P. O.; Whitehorne, T. J. J.; Prud'homme, R. E.; Schaper, F., Lactide Polymerization with Chiral  $\beta$ -Diketiminato Zinc Complexes. *Organometallics* **2010**, *29* (9), 2139-2147.

75. Sarish, S. P.; Schaffner, D.; Sun, Y.; Thiel, W. R., Evidence for the formation of a metal alkyl intermediate in the zinc mediated intramolecular hydroamination. *Chemical communications* **2013**, 49 (83), 9672-9674.
76. Biyikal, M.; Löhnwitz, K.; Meyer, N.; Dochnahl, M.; Roesky, P. W.; Blechert, S.,  $\beta$ -Diketiminato Zinc Complexes for the Hydroamination of Alkynes. *European Journal of Inorganic Chemistry* **2010**, 2010 (7), 1070-1081.
77. Vaughan, B. A.; Arsenault, E. M.; Chan, S. M.; Waterman, R., Synthesis and characterization of zinc complexes and reactivity with primary phosphines. *Journal of Organometallic Chemistry* **2012**, 696 (26), 4327-4331.
78. Chen, H.-Y.; Peng, Y.-L.; Huang, T.-H.; Sutar, A. K.; Miller, S. A.; Lin, C.-C., Comparative study of lactide polymerization by zinc alkoxide complexes with a  $\beta$ -diketiminato ligand bearing different substituents. *Journal of Molecular Catalysis A: Chemical* **2011**, 339 (1-2), 61-71.
79. Ayala, C. N.; Chisholm, M. H.; Gallucci, J. C.; Krempner, C., Chemistry of BDI<sup>\*</sup>M(2+) complexes (M = Mg, Zn) and their role in lactide polymerization where BDI<sup>\*</sup> is the anion derived from methylenebis(C-tBu, N-2,6-diisopropylphenyl)imine BDI<sup>\*</sup>H. *Dalton Transactions* **2009**, (42), 9237-9245.
80. Prust, J.; Stasch, A.; Zheng, W.; Roesky, H. W.; Alexopoulos, E.; Usón, I.; Böhrer, D.; Schuchardt, T., Synthesis and Structural Characterization of Monomeric Three-Coordinated  $\beta$ -Diketoiminate Organozinc Derivatives. *Organometallics* **2001**, 20 (17), 3825-3828.
81. Wang, C.-H.; Li, C.-Y.; Lin, C.-H.; Liu, Y.-C.; Ko, B.-T., Reactions of (E)-N-[2-(benzyliminomethyl)phenyl]-2,6-diisopropylaniline with diethylzinc: Synthesis, characterization and catalytic studies for ring-opening polymerization of  $\epsilon$ -caprolactone. *Inorganic Chemistry Communications* **2011**, 14 (9), 1456-1460.
82. Whitehorne, T. J. J.; Vabre, B.; Schaper, F., Lactide polymerization catalyzed by Mg and Zn diketiminato complexes with flexible ligand frameworks. *Dalton Transactions* **2014**, 43 (17), 6339-6352.
83. Spielmann, J.; Piesik, D.; Wittkamp, B.; Jansen, G.; Harder, S., Convenient synthesis and crystal structure of a monomeric zinc hydride complex with a three-coordinate metal center. *Chemical communications* **2009**, (23), 3455-3456.
84. Nako, A. E.; Tan, Q. W.; White, A. J. P.; Crimmin, M. R., Weakly Coordinated Zinc and Aluminum  $\sigma$ -Complexes of Copper(I). *Organometallics* **2014**, 33 (11), 2685-2688.
85. Bonello, O.; Jones, C.; Stasch, A.; Woodul, W. D., Group 2 and 12 Metal Gallyl Complexes Containing Unsupported Ga-M Covalent Bonds (M = Mg, Ca, Sr, Ba, Zn, Cd). *Organometallics* **2010**, 29 (21), 4914-4922.
86. Ekkert, O.; White, A. J. P.; Toms, H.; Crimmin, M. R., Addition of aluminium, zinc and magnesium hydrides to rhodium(iii). *Chemical Science* **2015**, 6 (10), 5617-5622.
87. Mazzacano, T. J.; Mankad, N. P., Base Metal Catalysts for Photochemical C-H Borylation That Utilize Metal-Metal Cooperativity. *Journal of the American Chemical Society* **2013**, 135 (46), 17258-17261.

88. Sapelza, G.; Mayer, P.; Westerhausen, M., Synthesis and Characterization of Methylzinc Tri(tert-butyl)silylphosphanide as well as Related Sodium and Potassium Phosphanylzincates. *Zeitschrift für anorganische und allgemeine Chemie* **2005**, 631 (15), 3087-3091.
89. Dickie, D. A.; Ulibarri-Sanchez Iii, R. P.; Jarman, P. J.; Kemp, R. A., Activation of CO<sub>2</sub> and CS<sub>2</sub> by (Me<sub>3</sub>Si)(i-Pr<sub>2</sub>P)NH and its zinc complex. *Polyhedron* **2013**, 58, 92-98.
90. Godfrey, S. M.; McAuliffe, C. A.; Pritchard, R. G.; Sheffield, J. M., The reaction of triorganophosphorus diiodides, R<sub>3</sub>PI<sub>2</sub>, with zinc metal powder; dependency of product on R; the X-ray crystal structures of dimeric {ZnI<sub>2</sub>[P(NMe<sub>2</sub>)<sub>3</sub>]}<sub>2</sub> and monomeric ZnI<sub>2</sub>(PPh<sub>2</sub>Me)<sub>2</sub>. *Inorganica Chimica Acta* **1999**, 292 (2), 213-219.
91. Kornev, A. N.; Belina, N. V.; Sushev, V. V.; Panova, J. S.; Lukyanova, O. V.; Ketkov, S. Y.; Fukin, G. K.; Lopatin, M. A.; Abakumov, G. A., Chemistry of the Phosphorus–Nitrogen Ligands. Multiple Isomeric Transformations of the Diphosphinohydrazine Bearing 8-Quinolyl Substituent: P→C, P→N, and P→P Migrations Caused by Different Factors. *Inorganic Chemistry* **2010**, 49 (20), 9677-9682.
92. McGrew, G. I.; Khatri, P. A.; Geiger, W. E.; Kemp, R. A.; Waterman, R., Unexpected formal insertion of CO<sub>2</sub> into the C-Si bonds of a zinc compound. *Chemical communications* **2015**, 51 (87), 15804-15807.
93. Murso, A.; Stalke, D., Electronic response of a (P,N)-based ligand on metal coordination. *Dalton Transactions* **2004**, (16), 2563-2569.
94. Goel, S. C.; Chiang, M. Y.; Buhro, W. E., Synthesis of homoleptic silylphosphido complexes (M[P(SiMe<sub>3</sub>)<sub>2</sub>][μ-P(SiMe<sub>3</sub>)<sub>2</sub>])<sub>2</sub>, where M = zinc and cadmium, and their use in metalloorganic routes to Cd<sub>3</sub>P<sub>2</sub> and MGeP<sub>2</sub>. *Journal of the American Chemical Society* **1990**, 112 (14), 5636-5637.
95. Fuhr, O.; Fenske, D., Reaktionen von Zink- und Cadmiumhalogeniden mit Tris(trimethylsilyl)phosphan und Tris(trimethylsilyl)arsan. *Zeitschrift für anorganische und allgemeine Chemie* **1999**, 625 (7), 1229-1236.
96. Kahnes, M.; Görls, H.; Westerhausen, M., Synthesis and crystal structures of dinuclear zinc complexes with the 1,3-bis(2-pyridylmethyl)acetamidinato ligand. *Journal of Organometallic Chemistry* **2011**, 696 (8), 1618-1625.
97. Hansen, K.; Szilvási, T.; Blom, B.; Irran, E.; Driess, M., A Donor-Stabilized Zwitterionic “Half-Parent” Phosphasilene and Its Unusual Reactivity towards Small Molecules. *Chemistry – A European Journal* **2014**, 20 (7), 1947-1956.
98. D'Auria, I.; Lamberti, M.; Mazzeo, M.; Milione, S.; Roviello, G.; Pellicchia, C., Coordination Chemistry and Reactivity of Zinc Complexes Supported by a Phosphido Pincer Ligand. *Chemistry – A European Journal* **2012**, 18 (8), 2349-2360.
99. Society, C.; Chemistry, R. S. o., *Photochemistry*. Royal Society of Chemistry: 1981.
100. Kimball, G. M.; Müller, A. M.; Lewis, N. S.; Atwater, H. A., Photoluminescence-based measurements of the energy gap and diffusion length of Zn<sub>3</sub>P<sub>2</sub>. *Applied Physics Letters* **2009**, 95 (11), 112103.



101. Köhl, O., *Phosphorus-31 NMR Spectroscopy: A Concise Introduction for the Synthetic Organic and Organometallic Chemist*. Springer Berlin Heidelberg: 2008.
102. DeGroot, M. W.; Taylor, N. J.; Corrigan, J. F., Molecular nanocluster analogues of CdSe/ZnSe and CdTe/ZnTe core/shell nanoparticles. *Journal of Materials Chemistry* **2004**, *14* (4), 654-660.
103. Eichhöfer, A.; Fenske, D.; Pfister, H.; Wunder, M., Zinkselenid- und Zinktelluridcluster mit Phenylselenolat- und Phenyltellurolatliganden. Die Kristallstrukturen von [NEt<sub>4</sub>]<sub>2</sub>[Zn<sub>4</sub>Cl<sub>4</sub>(SePh)<sub>6</sub>], [NEt<sub>4</sub>]<sub>2</sub>[Zn<sub>8</sub>Cl<sub>4</sub>Se(SePh)<sub>12</sub>], [Zn<sub>8</sub>Se(SePh)<sub>14</sub>(PnPr<sub>3</sub>)<sub>2</sub>], [HPnPr<sub>2</sub>R]<sub>2</sub>[Zn<sub>8</sub>Cl<sub>4</sub>Te(TePh)<sub>12</sub>] (R = nPr, Ph) und [Zn<sub>10</sub>Te<sub>4</sub>(TePh)<sub>12</sub>(PR<sub>3</sub>)<sub>2</sub>] (R = nPr, Ph). *Zeitschrift für anorganische und allgemeine Chemie* **1998**, *624* (11), 1909-1914.
104. Liu, C. W.; Lobana, T. S.; Santra, B. K.; Hung, C.-M.; Liu, H.-Y.; Liaw, B.-J.; Wang, J.-C., Coordination chemistry of Group 12 metals with phosphorodiselenoates: syntheses, structures and VT <sup>31</sup>P NMR study of monomer-dimer exchange equilibrium. *Dalton Transactions* **2006**, (4), 560-570.
105. Olmstead, M. M.; Power, P. P.; Shoner, S. C., Synthesis and characterization of novel quasiaromatic zinc-sulfur aggregates and related zinc-oxygen complexes. *Journal of the American Chemical Society* **1991**, *113* (9), 3379-3385.
106. Bochmann, M.; Bwembya, G.; Grinter, R.; Lu, J.; Webb, K. J.; Williamson, D. J.; Hursthouse, M. B.; Mazid, M., Three-coordinate thiolato complexes of zinc: solution and solid-state structures and EHMO analysis of the bonding pattern of [Zn(S-tert-Bu<sub>3</sub>C<sub>6</sub>H<sub>2</sub>-2,4,6)<sub>2</sub>]<sub>2</sub>. *Inorganic Chemistry* **1993**, *32* (5), 532-537.
107. Bonasia, P. J.; Arnold, J., Zinc, cadmium, and mercury tellurolates: hydrocarbon solubility and low coordination numbers enforced by sterically encumbered silyltellurolate ligands. *Inorganic Chemistry* **1992**, *31* (12), 2508-2514.
108. Hursthouse, M. B.; Malik, M. A.; Motevalli, M.; O'Brien, P., Synthesis and characterization of some mixed alkyl selenocarbamates of zinc and cadmium: novel precursors for II/VI materials. *Journal of Materials Chemistry* **1992**, *2* (9), 949-955.
109. Malik, M. A.; Motevalli, M.; Walsh, J. R.; O'Brien, P.; Jones, A. C., Adducts of methylzinc tert-butylthiolate and nitrogenous bases: implications for the use of adducts in MOCVD. *Journal of Materials Chemistry* **1995**, *5* (5), 731-736.
110. Ruhlandt-Senge, K.; Power, P. P., Compounds with M<sub>3</sub>Se<sub>3</sub> (M = lithium, zinc) rings: synthesis and characterization of [Zn(CH<sub>2</sub>SiMe<sub>3</sub>)Se-2,4,6-tert-Bu<sub>3</sub>C<sub>6</sub>H<sub>2</sub>]<sub>3</sub>.cntdot.0.5C<sub>6</sub>H<sub>14</sub> and [Li(THF)Se-2,4,6-tert-Bu<sub>3</sub>C<sub>6</sub>H<sub>2</sub>]<sub>3</sub>.cntdot.PhMe. *Inorganic Chemistry* **1993**, *32* (21), 4505-4508.
111. Afzaal, M.; Crouch, D.; Malik, Mohammad A.; Motevalli, M.; O'Brien, P.; Park, J.-H.; Woollins, J. D., Deposition of II-VI Thin Films by LP-MOCVD Using Novel Single-Source Precursors. *European Journal of Inorganic Chemistry* **2004**, *2004* (1), 171-177.
112. Bochmann, M.; Bwembya, G. C.; Powell, A. K.; Song, X., Zinc(II) arene tellurolato complexes as precursors to zinc telluride. The crystal and molecular structure of [Zn(TeC<sub>6</sub>H<sub>2</sub>Me<sub>3</sub>-2,4,6)(pyridine)<sub>2</sub>]. *Polyhedron* **1995**, *14* (23), 3495-3500.
113. Chivers, T.; Eisler, D. J.; Ritch, J. S., Synthesis and structures of M[N(TePPri)<sub>2</sub>-Te,Te[prime or minute]]<sub>n</sub> (n = 2, M = Zn, Cd, Hg; n = 3, M = Sb, Bi): the first

ditelluroimidodiphosphinato p- and d-block metal complexes. *Dalton Transactions* **2005**, (16), 2675-2677.

114. DeGroot, M. W.; Corrigan, J. F., Coordination Complexes of Zinc with Reactive ESiMe<sub>3</sub> (E = S, Se, Te) Ligands. *Organometallics* **2005**, 24 (14), 3378-3385.

115. Ellison, J. J.; Ruhlandt-Senge, K.; Hope, H. H.; Power, P. P., Synthesis and Characterization of the New Selenolate Ligand -SeC<sub>6</sub>H<sub>3</sub>-2,6-Mes<sub>2</sub> (Mes = C<sub>6</sub>H<sub>2</sub>-2,4,6-Me<sub>3</sub>) and Its Two-Coordinate Zinc and Manganese Derivatives: Factors Affecting Bending in Two-Coordinate Metal Complexes with Aryl-Substituted Ligands. *Inorganic Chemistry* **1995**, 34 (1), 49-54.

116. Melnick, J. G.; Docrat, A.; Parkin, G., Methyl, hydrochalcogenido, and phenylchalcogenolate complexes of zinc in a sulfur rich coordination environment: syntheses and structural characterization of the tris(2-mercapto-1-tert-butylimidazolyl)hydroboratozinc complexes [TmBut]ZnMe, [TmBut]ZnEH (E = S, Se) and [TmBut]ZnEPh (E = O, S, Se, Te). *Chemical communications* **2004**, (24), 2870-2871.

117. Minoura, M.; Landry, V. K.; Melnick, J. G.; Pang, K.; Marchio, L.; Parkin, G., Synthesis and structural characterization of tris(2-seleno-1-mesitylimidazolyl) hydroborato complexes: A new type of strongly electron donating tripodal selenium ligand. *Chemical communications* **2006**, (38), 3990-3992.

118. Trost, B. M., The Atom Economy--A Search for Synthetic Efficiency. *Science* **1991**, 254 (5037), 1471.

119. Wender, P. A.; Croatt, M. P.; Witulski, B., New reactions and step economy: the total synthesis of (±)-salsolene oxide based on the type II transition metal-catalyzed intramolecular [4+4] cycloaddition. *Tetrahedron* **2006**, 62 (32), 7505-7511.

120. Kasap, S.; Capper, P., *Springer Handbook of Electronic and Photonic Materials*. Springer: 2006.

121. Varonka, M. S.; Warren, T. H., S-nitrosothiol and nitric oxide reactivity at β-diketiminato zinc thiolates. *Inorganica Chimica Acta* **2007**, 360 (1), 317-328.

122. Gondzik, S.; Schulz, S.; Blaser, D.; Wolper, C., Reaction of L<sub>2</sub>Zn<sub>2</sub> with Ph<sub>2</sub>E<sub>2</sub> - synthesis of LZnEPh and reactions with oxygen and H-acidic substrates. *Chemical communications* **2014**, 50 (10), 1189-1191.

123. Chai, C.; Armarego, W. L. F., *Purification of Laboratory Chemicals*. Elsevier Science: 2003.

124. Calligaris, M., Structural inorganic chemistry by A. F. Wells. *Acta Crystallographica Section B* **1985**, 41 (3), 208.

125. Tam, E. C. Y. Synthesis and Reactions of beta-Diketiminato Heavy Group 14 Metal Alkoxides and Phosphanides. University of Sussex, 2012.

126. Reynolds, A. M.; Gherman, B. F.; Cramer, C. J.; Tolman, W. B., Characterization of a 1:1 Cu-O<sub>2</sub> Adduct Supported by an Anilido Imine Ligand. *Inorganic Chemistry* **2005**, 44 (20), 6989-6997.

127. Lobana, T. S.; Sánchez, A.; Casas, J. S.; Castiñeiras, A.; Sordo, J.; García-Tasende, M. S., Synthesis of [2-(pyridin-2'-yl)phenyl]-mercury(II) arylthiosemicarbazones: An unusual

coordination mode of a deprotonated 2-formyl-(2-hydroxy-benzene)-thiosemicarbazone. *Polyhedron* **1998**, *17* (21), 3701-3709.

128. Melnick, J. G.; Parkin, G., Cleaving mercury-alkyl bonds: a functional model for mercury detoxification by MerB. *Science* **2007**, *317* (5835), 225-227.

129. Melnick, J. G.; Yurkerwich, K.; Parkin, G., Synthesis, Structure, and Reactivity of Two-Coordinate Mercury Alkyl Compounds with Sulfur Ligands: Relevance to Mercury Detoxification. *Inorganic Chemistry* **2009**, *48* (14), 6763-6772.

130. Darensbourg, D. J.; Rainey, P.; Larkins, D. L.; Reibenspies, J. H., Solution <sup>31</sup>P and <sup>113</sup>Cd NMR Studies of Phosphine Adducts of Monomeric Cadmium (Bisphenoxide) Complexes and the Solid-State Structures of (2,6-Di-tert-butylphenoxide)<sub>2</sub>Cd(PCy<sub>3</sub>) and (2,6-Di-tert-butylphenoxide)<sub>2</sub>Cd(PMe<sub>3</sub>)<sub>2</sub>. *Inorganic Chemistry* **2000**, *39* (3), 473-479.

131. Darensbourg, D. J.; Wildeson, J. R.; Yarbrough, J. C.; Taylor, R. E., Tricyclohexylphosphine Derivatives of Bis(2,6-difluorophenoxide)cadmium: A Solution and Solid-State NMR Study. *Inorganic Chemistry* **2001**, *40* (14), 3639-3642.

132. Matchett, M. A.; Chiang, M. Y.; Buhro, W. E., Disilylphosphido complexes M[P(SiPh<sub>3</sub>)<sub>2</sub>]<sub>2</sub>, Where M = Zn, Cd, Hg, and Sn: Effective Steric Equivalency of P(SiPh<sub>3</sub>)<sub>2</sub> and N(SiMe<sub>3</sub>)<sub>2</sub> Ligands. *Inorganic Chemistry* **1994**, *33* (6), 1109-1114.

133. Jana, A.; Roesky, H. W.; Schulzke, C.; Döring, A., Reactions of Tin(II) Hydride Species with Unsaturated Molecules. *Angewandte Chemie International Edition* **2009**, *48* (6), 1106-1109.

134. Schulz, S.; Eisenmann, T.; Schmidt, S.; Blaser, D.; Westphal, U.; Boese, R., Reactions of a [small beta]-diketiminato zinc hydride complex with heterocumulenes. *Chemical communications* **2010**, *46* (38), 7226-7228.

135. Zhang, Y.; Reeder, E. K.; Keaton, R. J.; Sita, L. R., Goldilocks Effect of a Distal Substituent on Living Ziegler–Natta Polymerization Activity and Stereoselectivity within a Class of Zirconium Amidinate-Based Initiators. *Organometallics* **2004**, *23* (14), 3512-3520.

136. Dunsford, J. J.; Tromp, D. S.; Cavell, K. J.; Elsevier, C. J.; Kariuki, B. M., N-alkyl functionalised expanded ring N-heterocyclic carbene complexes of rhodium(i) and iridium(i): structural investigations and preliminary catalytic evaluation. *Dalton Transactions* **2013**, *42* (20), 7318-7329.

137. Taylor, E. C.; Ehrhart, W. A., A Convenient Synthesis of N,N'-Disubstituted Formamidines and Acetamidines. *The Journal of Organic Chemistry* **1963**, *28* (4), 1108-1112.

138. Abbina, S.; Du, G., Chiral Amido-Oxazolinato Zinc Complexes for Asymmetric Alternating Copolymerization of CO<sub>2</sub> and Cyclohexene Oxide. *Organometallics* **2012**, *31* (21), 7394-7403.

139. DeGroot, M. W.; Corrigan, J. F., Imine-Stabilized Zinc Trimethylsilylchalcogenolates: Powerful Reagents for the Synthesis of II-II'-VI Nanocluster Materials. *Angewandte Chemie International Edition* **2004**, *43* (40), 5355-5357.

140. Aime, S.; Harris, R. K.; McVicker, E. M.; Fild, M., Multinuclear magnetic resonance studies. Part 2. Diphosphanes and dithioxodi-[small lambda]5-phosphanes. *Journal of the Chemical Society, Dalton Transactions* **1976**, (21), 2144-2153.
141. de Silva, A. P.; de Silva, S. A., Fluorescent signalling crown ethers; 'switching on' of fluorescence by alkali metal ion recognition and binding in situ. *Journal of the Chemical Society, Chemical Communications* **1986**, (23), 1709-1710.
142. Franzen, S.; Ni, W.; Wang, B., Study of the Mechanism of Electron-Transfer Quenching by Boron–Nitrogen Adducts in Fluorescent Sensors. *The Journal of Physical Chemistry B* **2003**, 107 (47), 12942-12948.
143. Huston, M. E.; Haider, K. W.; Czarnik, A. W., Chelation enhanced fluorescence in 9,10-bis[[2-(dimethylamino)ethyl]methylamino]methyl]anthracene. *Journal of the American Chemical Society* **1988**, 110 (13), 4460-4462.
144. Konopelski, J. P.; Kotzyba-Hibert, F.; Lehn, J.-M.; Desvergne, J.-P.; Fagès, F.; Castellan, A.; Bouas-Laurent, H., Synthesis, cation binding, and photophysical properties of macrobicyclic anthraceno-cryptands. *Journal of the Chemical Society, Chemical Communications* **1985**, (7), 433-436.
145. Wang, H.-W.; Cheng, Y.-J.; Chen, C.-H.; Lim, T.-S.; Fann, W.; Lin, C.-L.; Chang, Y.-P.; Lin, K.-C.; Luh, T.-Y., Photoinduced Electron Transfer in Silylene-Spaced Copolymers Having Alternating Donor–Acceptor Chromophores. *Macromolecules* **2007**, 40 (8), 2666-2671.
146. Dey, D.; Kaur, G.; Patra, M.; Choudhury, A. R.; Kole, N.; Biswas, B., A perfectly linear trinuclear zinc–Schiff base complex: Synthesis, luminescence property and photocatalytic activity of zinc oxide nanoparticle. *Inorganica Chimica Acta* **2014**, 421, 335-341.
147. Cai, L.-Z.; Chen, W.-T.; Wang, M.-S.; Guo, G.-C.; Huang, J.-S., Syntheses, structures and luminescent properties of four new 1D lanthanide complexes with 2-thiopheneacetic acid ligand. *Inorganic Chemistry Communications* **2004**, 7 (5), 611-613.
148. Konar, S.; Jana, A.; Das, K.; Ray, S.; Chatterjee, S.; Golen, J. A.; Rheingold, A. L.; Kar, S. K., Synthesis, crystal structure, spectroscopic and photoluminescence studies of manganese(II), cobalt(II), cadmium(II), zinc(II) and copper(II) complexes with a pyrazole derived Schiff base ligand. *Polyhedron* **2011**, 30 (17), 2801-2808.
149. Ingle Jr, J. D.; Crouch, S. R., Spectrochemical analysis. **1988**.
150. Sjöback, R.; Nygren, J.; Kubista, M., Absorption and fluorescence properties of fluorescein. *Spectrochimica Acta Part A: Molecular and Biomolecular Spectroscopy* **1995**, 51 (6), L7-L21.
151. Lakowicz, J., Principles of Fluorescence. Kluwer Academic, New York: 1999; p 10.
152. Pandey, R.; Kumar, P.; Singh, A. K.; Shahid, M.; Li, P.-z.; Singh, S. K.; Xu, Q.; Misra, A.; Pandey, D. S., Fluorescent Zinc(II) Complex Exhibiting “On-Off-On” Switching Toward Cu<sup>2+</sup> and Ag<sup>+</sup> Ions. *Inorganic Chemistry* **2011**, 50 (8), 3189-3197.
153. Meng, Q.-h.; Zhou, P.; Song, F.; Wang, Y.-b.; Liu, G.-l.; Li, H., Controlled fluorescent properties of Zn(ii) salen-type complex based on ligand design. *CrystEngComm* **2013**, 15 (15), 2786-2790.

154. Zhou, P.; Li, H., Chirality delivery from a chiral copper(ii) nucleotide complex molecule to its supramolecular architecture. *Dalton Transactions* **2011**, 40 (18), 4834-4837.
155. Majumder, A.; Rosair, G. M.; Mallick, A.; Chattopadhyay, N.; Mitra, S., Synthesis, structures and fluorescence of nickel, zinc and cadmium complexes with the N,N,O-tridentate Schiff base N-2-pyridylmethylidene-2-hydroxy-phenylamine. *Polyhedron* **2006**, 25 (8), 1753-1762.
156. Splan, Kathryn E.; Massari, Aaron M.; Morris, Gregory A.; Sun, S.-S.; Reina, E.; Nguyen, SonBinh T.; Hupp, Joseph T., Photophysical and Energy-Transfer Properties of (Salen)zinc Complexes and Supramolecular Assemblies. *European Journal of Inorganic Chemistry* **2003**, 2003 (12), 2348-2351.
157. Mizukami, S.; Houjou, H.; Sugaya, K.; Koyama, E.; Tokuhisa, H.; Sasaki, T.; Kanesato, M., Fluorescence Color Modulation by Intramolecular and Intermolecular  $\pi$ - $\pi$  Interactions in a Helical Zinc(II) Complex. *Chemistry of Materials* **2005**, 17 (1), 50-56.